THE APPLICATION OF TETRAKIS(DIMETHYLAMINO)ETHYLENE CHEMILUMINESCENCE IN CHARACTERIZATION OF THE SURFACE PROPERTIES OF METAL OXIDES AND REVERSED MICROEMULSION SYSTEMS

by

CHIEN-CHANG HUANG

B.S., I-Shou University, 1996
M.S., Feng Chia University, 1998

AN ABSTRACT OF A DISSERTATION

submitted in partial fulfillment of the requirements for the degree

DOCTOR OF PHILOSOPHY

Department of Chemical Engineering
College of Engineering

KANSAS STATE UNIVERSITY
Manhattan, Kansas

2009

Abstract

To characterize surface properties by current techniques, metal oxides typically have to be pre-treated at high temperature to remove surface absorbents. Therefore, a new low temperature method which can provide information on the surface chemistry is desired. In this work, the surface properties of metal oxide samples were studied by tetrakis(dimethylamino)ethylene (TDE) chemiluminescence (CL). This chemiluminescent method was also employed in probing the properties of reversed microemulsions.

It was found that the emission intensity vs. reaction time curve (I_t) of catalyzed TDE CL on MgO was affected by the distributions and types of surface hydroxyl groups. Isolated hydroxyls with lower coordination were found to have higher catalytic reactivity for the emission of TDE CL. Although hydrogen bonded hydroxyls also catalyze the TDE oxidation reaction, the influence on the light emission was negative. Because the properties of surface hydroxyls are associated with specific orientations of adjacent ions, information on surface hydroxyls can provide information about some general surface characteristics of a metal oxide.

When characterizing surface hydroxyls on Al_2O_3 by TDE CL, it was found that the catalytic reactivity of isolated hydroxyl groups is strongly associated with the stretching frequency of isolated hydroxyl. The stretching frequency (ω) of an isolated hydroxyl group is related to the modification of the adjacent ions and the coordination of the isolated hydroxyl. The results showed that the blue-shifts in the stretching frequencies of isolated hydroxyls led to increases in the catalytic reactivity of Al_2O_3 surfaces for the emission of TDE CL.

TDE CL was further applied in characterizing the surfaces of other metal oxides and chemically grafted Al_2O_3. The results indicated that the isolated hydroxyl groups with fewer adjacent ions likely have higher affinity for the binding of grafting agents. Higher emission intensities were obtained from catalyzed TDE CL on metal oxides featuring higher percentages of isolated hydroxyls.

The determination of a surfactant's critical micellar concentration was accomplished by measuring the decay rate of the emission of TDE CL in a reversed microemulsion system. In this study, the CMC values of non-ionic and ionic surfactants were measured in different non-polar solvents.

THE APPLICATION OF TETRAKIS(DIMETHYLAMINO)ETHYLENE CHEMILUMINESCENCE IN CHARACTERIZATION OF THE SURFACE PROPERTIES OF METAL OXIDES AND REVERSED MICROEMULSION SYSTEMS

by

CHIEN-CHANG HUANG

B.S., I-Shou University, 1996
M.S., Feng Chia University, 1998

A DISSERTATION

submitted in partial fulfillment of the requirements for the degree

DOCTOR OF PHILOSOPHY

Department of Chemical Engineering
College of Engineering

KANSAS STATE UNIVERSITY
Manhattan, Kansas

2009

Approved by:

Major Professor
Dr. Keith L. Hohn

Abstract

To characterize surface properties by current techniques, metal oxides typically have to be pre-treated at high temperature to remove surface absorbents. Therefore, a new low temperature method which can provide information on the surface chemistry is desired. In this work, the surface properties of metal oxide samples were studied by tetrakis(dimethylamino)ethylene (TDE) chemiluminescence (CL). This chemiluminescent method was also employed in probing the properties of reversed microemulsions.

It was found that the emission intensity vs. reaction time curve (I_t) of catalyzed TDE CL on MgO was affected by the distributions and types of surface hydroxyl groups. Isolated hydroxyls with lower coordination were found to have higher catalytic reactivity for the emission of TDE CL. Although hydrogen bonded hydroxyls also catalyze the TDE oxidation reaction, the influence on the light emission was negative. Because the properties of surface hydroxyls are associated with specific orientations of adjacent ions, information on surface hydroxyls can provide information about some general surface characteristics of a metal oxide.

When characterizing surface hydroxyls on Al_2O_3 by TDE CL, it was found that the catalytic reactivity of isolated hydroxyl groups is strongly associated with the stretching frequency of isolated hydroxyl. The stretching frequency (ω) of an isolated hydroxyl group is related to the modification of the adjacent ions and the coordination of the isolated hydroxyl. The results showed that the blue-shifts in the stretching frequencies of isolated hydroxyls led to increases in the catalytic reactivity of Al_2O_3 surfaces for the emission of TDE CL.

TDE CL was further applied in characterizing the surfaces of other metal oxides and chemically grafted Al_2O_3. The results indicated that the isolated hydroxyl groups with fewer adjacent ions likely have higher affinity for the binding of grafting agents. Higher emission intensities were obtained from catalyzed TDE CL on metal oxides featuring higher percentages of isolated hydroxyls.

The determination of a surfactant's critical micellar concentration was accomplished by measuring the decay rate of the emission of TDE CL in a reversed microemulsion system. In this study, the CMC values of non-ionic and ionic surfactants were measured in different non-polar solvents.

Table of Contents

List of Figures

List of Tables

Acknowledgements

This work would not have been possible without the help and encouragement given from many people. It is impossible to overstate my gratitude to all of them.

Foremost, I would like to thank my major advisor, Dr. Keith L. Hohn, who shared with me a lot of his precious experiences inside in the fields of catalysis, nano-technology and reaction engineering during the past six years. His great effort and enthusiasm gave me a sense of direction for my studies in K-State, and his patience and encouragement enabled me to finish this work.

I am indebted to Dr. John Schlup for sharing his abounding knowledge in the technique of FT-IR with me, and for providing many valuable comments on my papers and thesis. His efforts and thoughtful advice helped me to solve many doubtful questions and troubles that I faced during this work. I also like to express my gratitude to my committee members, Dr. Larry Erickson, Dr. Kenneth Kabunde, Dr. Steven Eckels and Dr. Charles W. Rice for the time and insights they contributed to my thesis. My sincere thanks also go to Dr. James Edgar and Dr. L. T. Fan for their guidance and help when I studied at K-State, and to the staff members in the Chemical Engineering Department including Florence Sperman, Alison Hodges, David Threewit and Cindy Barnhart.

I also wish to thank my fellow lab-mates in my research group: Myles Ikenberry, Chundi Cao, Abdennour Bourane and Juan Salazar, for their assistance and stimulating discussions, and for all the fun we have had. Also, I would like to thank my friends who I met during my stay at K-State: Hui-Ju Pai, Shu-Ping Yang, Hui-Chun Huang, Chun-Fang Chiang and Yun-Ju Chen, and other friends for their encouragement when I was preparing my thesis. I am also grateful to the senior scientific glassblower Jim Hodgson for assisting me in building all the glass equipment used in my research.

Lastly and most importantly, I would like to thank my parents, Ming-Hua Huang and Jui-Hsia Shen, and the rest of my family for their support, endless patience and encouragement while I study abroad.

This research was funded by the U.S. Marine Corps. Foundation is acknowledged with gratitude.

Dedication

This thesis is dedicated to my parents, Ming-Hua Huang and Jui-Hsia Shen, who have selflessly supported and encouraged me throughout the course of this thesis.

CHAPTER 1 - Introduction

1.1 TDE chemiluminescence (TDE CL)

Tetrakis(dimethylamino)ethylene (TDE) chemiluminescence (CL) was observed in 1950 by Pruett *et. al.*[1] Several reports related to this chemiluminescent compound have been published that detail the reaction mechanism and application of this chemiluminescent compound in semiconductors as a reducing agent or as an auxiliary light source for emergency situations. However, studies on applying TDE as a probe either in chemical or biochemical reactions have not been done.

The oxidation reaction of TDE under aerobic condition is spontaneous, producing light emission. It was shown in early studies that the excited energy for light emission is liberated from the proportional or disproportional decomposition of the intermediate produced from the oxidation reaction of TDE, tetrakis-dimethylamino-1,2-dioxetane (TDMD), as seen in Figure 1.1. Rewick *et. al.* analyzed the composition of the products of TDE chemiluminescence (TDE CL) [2] and suggested that tetramethylurea (TMU) and tetramethyloxamide (TMO) were the two primary products, about 83 mole%. Rewick *et. al.* found that TMO and TMU were highly electron-affinity species. These two species act as quenchers for the emission of TDE CL. [3, 4, 5, 6]

TDE CL is considered as a chemical probe in this study because it features two unique properties. First of all, the polarity of TDE is different than its products. TDE is composed of four di-methyl amino groups symmetrically bonded to a vinyl center, so TDE is non-polar. The primary products of TDE oxidation, TMU and TMO, are both polar. This difference in polarity offers the potential for separating out the oxidation products and increasing emission intensity. We propose that this feature could be used to probe the properties of reversed micelles. When TDE is introduced into a system with a non-polar solvent and surfactant, because of the opposite polarity of TDE and it products, the products will be separated from the bulk phase, forming a secondary micellar phase. Second, it is well known that the reaction of TDE CL is enhanced if a protonic material, such as a hydroxyl group, is present. [7, 8, 9] The surfaces of metal oxides

abound in hydroxyl groups and the catalytic reactivity of surface hydroxyls with different configurations may affect TDE CL differently. The properties of surface hydroxyls depend on the adjacent surface ions (M^{n+} and O^{2-}) and interaction between neighboring hydroxyl groups. Therefore, TDE CL is expected to be a tool for detecting the surface properties of metal oxides via the catalysis of the surface hydroxyl groups for TDE CL.

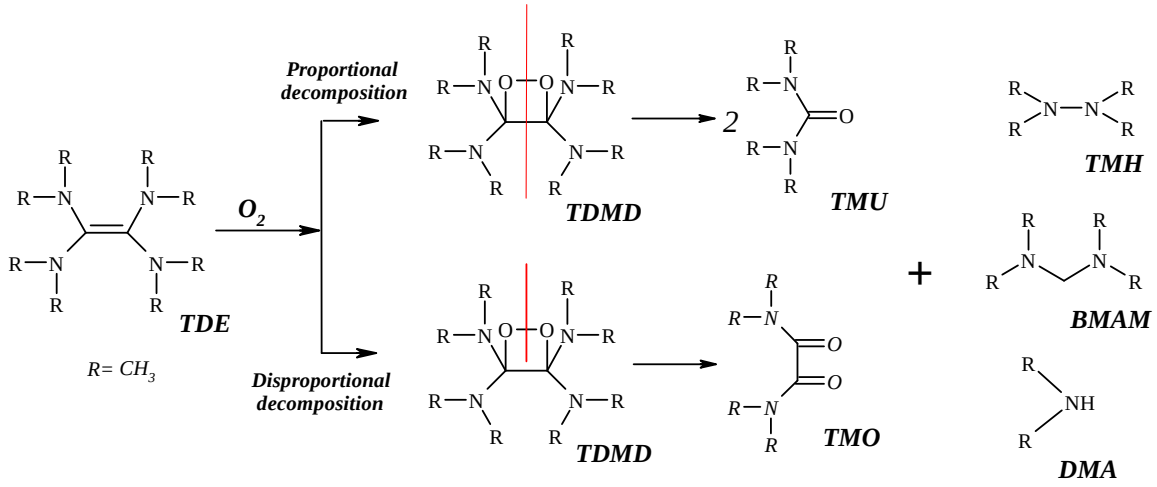

Figure 1.1 The molecular structures of the products produced from TDE oxidation reaction where TDMD, TMU, TMO, TMH BMAM and DMA represent tetrakis-dimethylamino-1,2-dioxetane, tetramethylurea, tetramethyloxamide, tetramethylhydrazine, bis(dimethylamino)methane, and dimethylamine respectively.

1.2 The Characterization of reversed microemulsion system by TDE CL

A reversed microemulsion micelle is constructed by the aggregation of amphipathic (surfactant) molecules with the polar heads attracted to interior of the micelles while the non-polar tails extend into the bulk non-polar solvent. For a microemulsion system, the CMC (critical micellar concentration) is the most important parameter since the system starts to feature the full functions when the concentration of surfactant is over the surfactant's CMC. Above the CMC, the surfactant monomers and micelles exist in a dynamic equilibrium. Further increasing the concentration in the system will result in the aggregation of the surfactants while the concentration of the free surfactant monomers remains virtually constant in the bulk phase.[10, 11]

The present technologies employed in measuring the CMC value of an oil-in-water (O/W) microemulsion typically are obtained from the abrupt change in the physical properties, such as surface tension, specific heat, conductivity, osmotic pressure, light scattering *et. al.*, as the concentration of surfactant is increased. In contrast, the change in the physical properties of reversed (water-in-oil, W/O) microemulsion typically is too slight to detect the abrupt change by present technologies. This leads the difficultly in the determination of the CMC of reversed microemulsions. Many early studies focused on the use of fluorescent probes along with spectroscopy, such as UV/Visible and fluorescent spectroscopy, to detect the CMC of W/O microemulsion. [12, 13, 14] TDE CL is different from the use of fluorescent probes in CMC determination. The most important difference is the absence of an external exciting source, such as a laser beam. This is a significant advantage for systems that are sensitive to laser irradiation.

The fundamental basis for using TDE to probe the CMC of reversed microemulsion systems is due to the different polarities of TDE and the quenching species, TMO and TMU. The collision between excited TDE and quenching species leads to the diminution in the emission intensity. It is hypothesized that the formation of an inter-layer assembled by surfactant molecules can extract the polar quenching species out of the non-polar TDE bulk phase when the concentration of surfactant is higher than its CMC in bulk solvent. Subsequently, the quenching species will be enclosed inside the water-pool of the reversed micelles. Therefore, the emission intensity of TDE CL can reflect the formation of reversed micelles. The decay of the emission intensity not only is related to the concentration of TDE, but also is associated with the number of micelles in the solution. In this study, the emission intensity vs. reaction time (I_t) curve were collected by fiber optic spectroscopy and used to analyze the CMC of few surfactants in alkanes, cyclohexane and mineral oil.

This research also demonstrated the potential of TDE CL to determine the viscosity of a system with a micro-volume. The emission intensity of TDE CL results from the kinetic competition between mechanical excitation and electronic excitation. Thereby, limiting the number of vibrational modes of excited TDE will limit the dissipation of the excited energy in intra-molecular vibration and rotation. This idea has been discussed by Haidekker *et. al.*.

Haidekker *et. al* illustrated that the emission can be enhanced if the intra-molecular rotation of the fluorescent molecules with unique structures is restricted via steric hindrance in a viscous media. [15, 16, 17] These specific fluorescers can be employed as molecular rotors in determining the viscosity of a system. TDE is constructed by four dimethylamino groups bound to a vinyl center. Therefore, it is proposed that emission will be enhanced by restricting the rotation of dimethylamino groups in a viscous media. The results show that the emission intensity of TDE CL is proportional to the viscosity of media, suggestings that TDE CL can be a tool to evaluate the viscosity of a system. This method is attractive for determing viscosity because it has no limitation in sample volume and sample type (non-Newtonian vs. Newtonian fluid). This feature overcomes the intrinsic disadvantages in present mechanical methods.

1.3 The characterization of surface properties on metal oxides by TDE CL

The surface chemistry of metal oxides has always attracted much attention because metal oxides are used as catalysts for different reactions and as a carrier for additional materials. However, quantitative studies of surface chemistry by present spectroscopic techniques are difficult due to the intrinsic complexity of the oxide surface and the limitations of the present techniques.

The outermost surface of metal oxide is covered by adsorbed species, such as hydroxyl groups and molecular water. Hydroxyl groups are left on the surface after molecular water is removed by outgassing at 200^{o}C. Because of the difference in the interaction between surface hydroxyl groups and the adjacent surface ion (M^{n+} or O^{2-}), the properties of hydroxyl groups, including reactivity, acid-base property and perturbation (stretching frequency), vary with the surface structure of the metal oxide. Therefore, surface hydroxyl groups can act as finger prints that reflect the surface morphology and properties of the metal oxide.

It had been proven in earlier studies that protonic materials, such as water and alcohols, act as catalysts for the reaction of TDE CL. [18, 19, 20] This study attempts to use TDE CL to characterize the surface properties of metal oxide since the surface hydroxyl group on metal oxide may play the same role as protonic material for the reaction of TDE CL. The catalytic reactivity of surface hydroxyls for the emission of TDE CL varies with the liberation magnitude

of surface hydroxyl groups. Through the variation in the emission intensity, the surface properties of metal oxide can be probed. Indeed, the emission intensity of TDE CL is associated with the production of TDMD. TDMD is the product of the oxidation reaction of TDE. With the presence of specific surface hydroxyl groups, the product of TDMD is thought to be enhanced and subsequently more photons will be released after the decomposition of TDMD, as the sketch shows in **Figure 1.2** .

Understanding the distribution of surface hydroxyls in different configurations is crucial and important before employing TDE CL in characterizing surface properties of metal oxide. The perturbation of hydroxyl group is decreased as two neighboring hydroxyl groups are bridged by hydrogen bonding. Surface hydroxyl groups can be divided into two major categories: hydrogen bonded hydroxyls and isolated hydroxyls. Klabunde *et. al.* suggested that isolated hydroxyl groups are adsorbed on edge and corner sites rather than on extend planes. [21] As will be shown, TDE CL is influenced by the amount and types of surface hydroxyls present on a metal oxide surface, so measuring the I_t (emission intensity vs. reaction time) curve can provide information on the surface properties of metal oxides.

1.4 Characterizing surface grafting by TDE CL

Surface grafting enables the metal oxide to feature different functions by changing its surface properties. For example, grafting hexamethyldisiloxane (HMDS) on the surface of a metal oxide causes the surface to become more hydrophobic. This grafting reaction is termed as silation. [22] The grafted HMDS helps the metal oxide to be dispersed in non-polar media easily. It was found in earlier studies that surface hydroxyl groups on metal oxide were the binding sites for grafted organic compounds. Therefore, the binding reactivity and binding position of a grafted compound on the metal oxide can be explored through TDE CL. In this study, three grafting agents, (2-chloroethyl)ethyl sulfide (2-CEES), HMDS and acetic acid (AA), were studied with Al_2O_3 and TDE CL to understand the effect of surface structure for the binding ability of metal oxide.

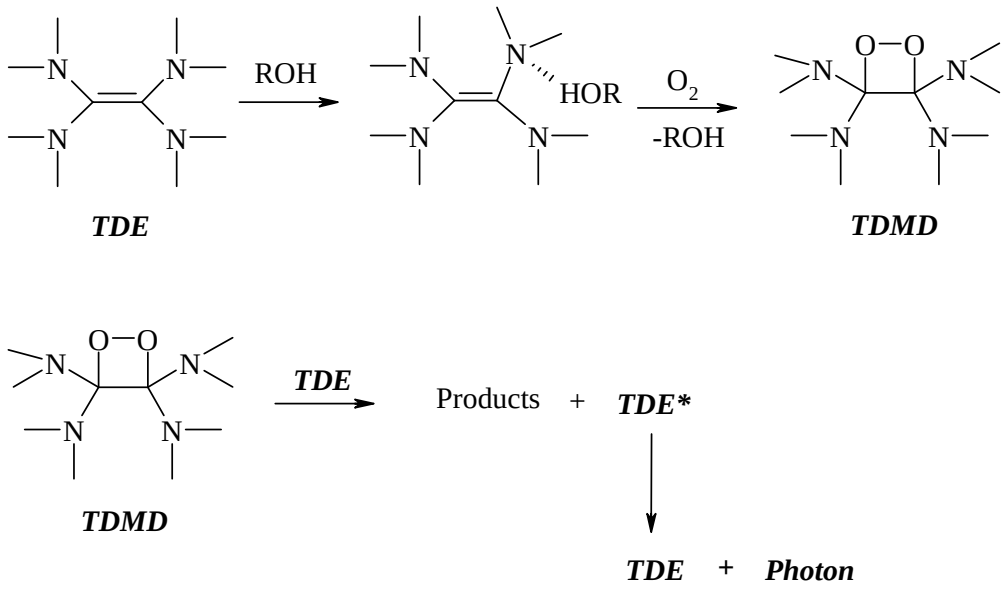

Figure 1.2 Sketch of the catalysis of surface hydroxyl group for the oxidation reaction of TDE and the emission of TDE CL.

1.5 References

1 Pruett, R. L.; Barr, J. T.; Rapp, K. E.; Bahner, C. T.; Gibson, J. D. and Lafferty, R. H., *J. Am. Chem. Soc.* , **1950** 72, 3646.

2 Rewick, R. T.; Schumacher, M. L.; Shapiro, S. L.; Weber, T. B.; and Cavalli-Sforza, M., *Anal. Chem.*, **1988**, 60, 2095.

3 Winberg. H. E.; Downing, J. R. and Coffman, D. D., *J. Am. Chem. Soc.*, **1965**, 87, 2054.

4 Winberg, H. E.; Carnahan, J. E.; Coffman, D. D. and Brown, M., *J. Am. Chem. Soc.*, **1965**, 87, 2054.

5 Winberg, W. E., *US. Paten 3,264,221*, **1960.**

6 Heller, C. A. and Fletcher, A., *J. Phys. Chem.*, **1965**, 69, 3313.

7 Fletcher, A. N., *J. Phys. Chem.*, **1969**, 73, 3686

8 Fletcher, A. N. and Heller, C. A., *J. Catal.*, **1966**, 6, 263.

9 Fletcher, A. N. and Heller, C. A., *J. Photochem. Photobiol.*, **1965**, 4, 1051.

10 Domìnguez, A.; Fernández, A.; González, N.; Iglesias, E. and Montenegro, L., *Journal of Chemical Education*, **1997**, 74, 1227.

11 Fendler, J. H., *Accounts of Chemical Research*, **1976**, 9, 153.

12 Behera G. B.; Mishra, B. K.; Behera, P. K. and Panda, M., *Advances in Colloid and Interface Science*, **1999**, 82, 1.

13 Olesik, S. V., and Miller, C. J., *Langmuir*, **1990**, 6, 183.

14 Rodenas, E., and Perez-Benito, E., *J. Phys. Chem.*, **1991**, 95, 4552.

15 Law, K. Y., *Chem. Phys. Lett.*, **1980**, 75, 545.

16 Haidekker, M. A. and Theodorakis, E. A., *Org. Biomol. Chem.*, **2007**, 5 1669.

17 Haidekker, M. A.; Akers, W.; Lichlyter, D.; Brady, T. P. and Theodorakis, E. A., *Sensor Lett.*, **2005**, 3, 42.

18 Fletcher, A. N., *Journal of Physical Chemistry*, **1969**, 73, 3686

19 Fletcher, A. N. and Heller, C. A., *Journal of Catalysis*, **1966**, 6, 263

20 Toby, S. T.; Astheimer, P. A. and Toby, F. S., *J. Photochem. Photobiol. A: Chem.*, **1992**, 67, 1.

21 Klabunde, K. J.; Stark, J.; Koper, O.; Mohs, C.; Park, D. G.; Decker, S.; Jiang, Y.; Lagadic, I. and Zhang, D., *J. Phys. Chem.*, **1996**, 100, 12142.

22 Slavov, S. V.; Sanger, A. R. and Chung, K. T., *J. Phys. Chem. B*, **1998**, 102, 5475.

CHAPTER 2 - Literature Review

2.1 Principles of Chemiluminescence

Light emission can result from incandescence or luminescence. Incandescence is an energy conversion procedure from vibrational energy to radiant energy. Luminescence, in contrast, is an energy transition from thermal or chemical energy to electronically excited energy. Chemiluminescence (CL) is a sub-category under luminescence. The energy source for the light emission in chemiluminescence is specifically liberated from a chemical reaction. Highly exothermic reactions are more like to result in the formation of an excited state in a CL procedure.

In the past half century, CL has been frequently investigated and used as an analytical tool in the fields of chemistry [1, 2] and biochemistry [3, 4, 5, 6, 7]. For example, 1,2-dioxetante and α-peroxylactones are two labile intermediates produced from the autoxidation of β-bromohydroperoxides [8, 9] and ketene [10, 11] and also are the energy source in CL processes. The breakdown of these two energy-rich compounds are catalyzed by acid/base-catalization and nucleophilic/electrophilic attack. These two chemiluminescent molecules are typically utilized to detect transition-metal ions in solution. [12] The distinct advantage using CL as an analytical tool is due to the absence of externally excited sources, which means that the analytically relevant emission can be measured against a completely dark background. Therefore, interference from light scattering can be ignored.

Numerous chemical reactions have been found that can emit a photon. The best known of those involve luminol, luciginen, and oxalate esters. The reactions can be broken down into three stages: preliminary reaction, excitation, and fluorescence emission. [13] The intermediate produced from the preliminary reaction is the source of the necessary excited energy that is then transferred to an emissive product or a fluorescent acceptor. The conversion of chemical energy liberated from the key intermediate to electronic excitation energy is the excitation step. Finally, the photon is released from excited reaction product as the excited reaction product falls back to

ground state in the step of fluorescence emission. Therefore, if a chemical reaction is to be chemiluminescence, the reaction has to have three essential features.

1. The reaction should be an exothermic reaction and the excited energy liberated from the key intermediate is sufficient to excite an energy acceptor to its excited state.
2. The structure of excited energy acceptor is stiff to prevent the consumption of excited energy in intra-molecular torsional vibrations. [14]
3. The loss of excited energy is via a radiative process.

2.1.1 Chemiluminescence: Preliminary Reaction

Two general mechanisms possessing the ability to generate photons have been found: peroxyoxalate chemiluminescence and electrogenerated chemiluminescence (ECL). [15, 16] For peroxyoxalate CL, the high-energy molecules, 1,2-dioxetane and its carbonyl derivatives, are converted through a thermal reaction to an electronically excited state. In contrast, the electronically excited energy liberated from charge annihilation results in ECL.

2.1.1.1 Unimolecular Fragmentation (Peroxide Chemiluminescence)

The unimolecular fragmentation of peroxides and it derivatives, 1,2-dioxetants α-peroxylactones and 1,2-dioxetandiones (as seen in **Figure 2.1**), are extremely exothermic reactions. They also are commonly found in organic chemiluminescence and bioluminescence. [17] Peroxides are synthesized normally via two procedures: hydroperoxide cyclization and singlet oxygen cycloaddition. The starting reagents for producing peroxyoxalates can be oxalic reagents, such as aryl oxalates [18, 19], oxalyl chloride [20] and oxalic anhydrides [27], ketenes [21], allylic hydroperoxide [22], α-hydroperoxy acids [23], flavins [24], olefins [25, 26] *et. al.*. Because these four-membered ring peroxides involve high strain energy, the electronically excited energy is produced from bond energy. Both O-O and C-C bonds cleave simultaneously and liberate much energy. Two carbonyl fragments, both containing a C=O bond, are produced from the decomposition of the peroxide molecule. If the photon is emitted from the excited products of the reaction directly, the CL reaction is termed direct chemiluminescence. Alternatively, the excited energy can be transferred to a fluorescent molecule; the subsequent emission from this excited fluorescent molecule is called indirect chemiluminescence.

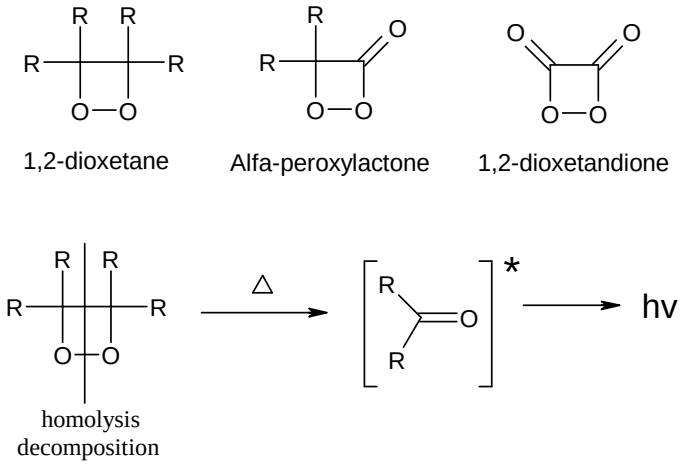

Figure 2.1 Energy-rich molecules for chemiluminescence (referenced from [17, 28]).

2.1.1.2 Charge Annihilation

The second general mechanism of luminescence is charge annihilation, also called electrogenerated chemiluminescence (ECL). ECL involves a bimolecular reaction with two radical ions with opposite charge. The photon is librated by an electrochemical reaction. Undergoing the electron transfer from radical anion ($D^{-\cdot}$) to a radical cation ($A^{+\cdot}$), the donor is excited to an excited state [29]. ECL occurs usually by suitable aromatic hydrocarbons [30, 31], polyaromatic hydrocarbons [32] and some inorganic complexes, such as tri(2,2'-bipyridyl)ruthenium(II) [33, 34]. A systematic report on ECL was published by Schuster *et. al.* [35, 36]

2.1.1.3 Chemically Initiated Electron Exchange Luminescence (CIEEL)

Chemically initiated electron exchange luminescence (CIEEL) features the characteristics of peroxyoxalate chemiluminescence and ECL. A fluorescer acts as the activator and the electron donor in CIEEL reaction. Initially, an electron is transferred from a fluorescer to a peroxide molecule which contains high energy and acts as an electron acceptor in CIEEL. The electron transfer is concomitant with the formation of a radical-ion pair and O-O bond cleavage. An electronically excited fluorescer is formed when an electron is transferred backward (backward electron transfer, BET). The early studies relating to the reaction mechanisms of CIEEL and the

correlation between peroxyoxalates and fluorescer had been reported by Matsumoto [37, 38] and Catherall [39, 40, 41, 42, 43].

2-1-2 Chemiluminescence: Excitation Stage

2-1-2-1 Excited Energy

In 1864, Maxwell proposed that light possesses both magnetic and electrical components and is an electromagnetic wave. Thus, the velocity of light (C) equals the product of wave frequency (υ) and wavelength (λ).

$$C = \upsilon \times \lambda \qquad (2\text{- }1)$$

Until the 19th century, Planck and Einstein illustrated the concept of photon and combined two theories of light, electromagnetic and quantum theories. [44] Therefore, energy of photon (E, ergs/molecule) is calculated by **Equation 2- 2**:

$$E = h\upsilon = hC / \lambda = hC\bar{\upsilon} \qquad (2\text{- }2)$$

where h is the Planck constant (6.63×10^{-34} J s), C is the velocity of light (3×10^{8} ms^{-1}) and $\bar{\upsilon}$ is wave number (cm^{-1}). **Figure 2.2** shows the relationships between energy and wavelength of light emission.

By Planck's equation, exciting a visible fluorescer, in theory, requires 177 KJ/mole (λ_{em}=700 nm) to 309 KJ/mole (λ_{em}=400nm). However, this critical energy can be lost among the vibrational modes of the produced molecules in the excitation process in radiationless transitions that are accompanied by heat release and photochemical reactions. The chemical energy is not completely transferred to electronically excited energy. For this reason, the adsorption wavelength usually is lower then the emission wavelength when a fluorescer is excited by external light source. The excited energy liberated from an exothermic reaction in chemiluminescence has to be higher than the theorially excited energy for the fluorescer in the reaction.

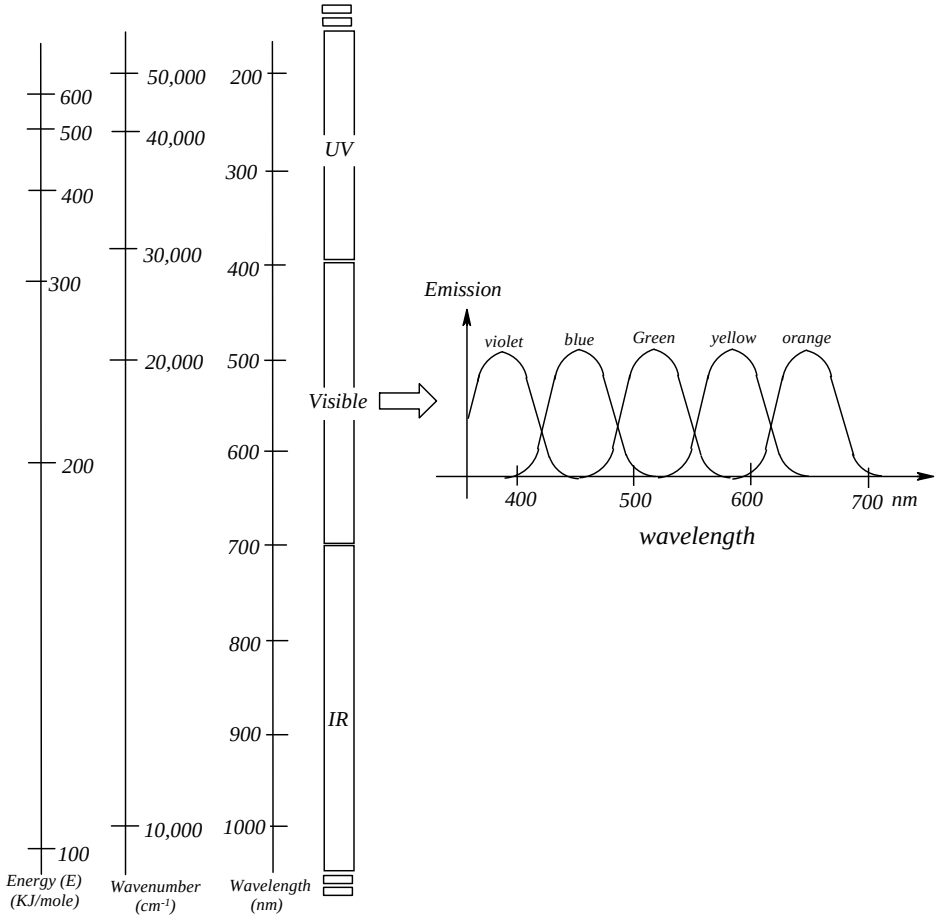

Figure 2.2 The relationship between emission energy, color, wavelength and wavenumber.

2.1.2.2 Characteristics of Excitation Stage

For most fluorescers, the absorption spectra appear as diffuse structureless bands with several primary maxima and secondary maxima in visible and UV regions. The primary bands are representative of the energy transition from ground state to excited states while the secondary maxima represent the vibrational and rotational motions of the whole molecule or its parts. [48] Since molecular rotation and vibration will cause the dissipation of excited energy, the wavelength of light emission spectra always is red-shifted from that of excited radiation. The emission spectrum is mirror-symmetric to the adsorption spectrum adsorption, and, usually, overlaps with adsorption spectrum in the range from 50-70 nm (Stockes' law). The range will be extended to 150-250 nm according to the molecular structure of fluorescer if the fluorescer molecule has a more planar and rigid configuration or intramolecular hydrogen bonds. These features minimize the loss of energy from the excited state by intramolecular thermal motions.

2.1.2.3 Transition of Electronically Excited Energy

A singlet state (S) has electrons with antiparallel spins (↓↑) while the triplet state (T) has electrons with a parallel arrangement (↑↑). The energy transition in CL involves not only singlet-singlet and triplet-triplet energy transitions but also inter-system crossing (singlet-triplet). When the fluorecer molecule is in the ground state (S_0), the electrons occupy the same orbital with antiparallel spins. After the adsorption of excited energy, the electrons are excited to a higher electronic state (S_n, n=1, 2, 3….). Subsequently, both singlet-singlet and singlet-triplet transitions may occur. The light emission due to the singlet-singlet transition ($S_n \rightarrow S_0$) is termed fluorescence. On the other hand, phosphorescence occurs when light emission is due to the transition of triplet-singlet ($T_n \rightarrow S_0$) (as seen in **Figure 2.3**). Inter-system crossing is carried out by spin orbital coupling which is induced by intra- or inter-molecular heavy atom, [7, 45, 46, 47] and will extend the lifetime of the excited state. For example, the lifetime of a singlet state typically is 1 to 100 ns. However, it will be extended to 100 ns- 10 s for a triplet-excited state. [48, 49]

Deactivation is carried out by a non-radiative process including inter- and intra-molecular deactivation. Intra-molecular deactivation involves a thermal relaxation by molecular rotation and vibration and inter-system crossing from single (S) to triple (T) state (displayed in **Figure 2.3**). Due to the long lifetime of the triplet-excited state, inter-system crossing has to be inhibited if high emission intensity is desired. The magnitude of thermal relaxation is dependent on the molecular structure of fluorescer. Higher quantum states result from more rigid molecular structures. This will be further discussed in section 2-1-3-1. Inter-molecular deactivation typically is caused by a quenching effect. Many processes can result in quenching deactivation. They include molecular collision, static quenching, excited state reactions, electron transfer and energy transfer. [50, 51, 52, 53, 54, 55, 56]

Currently 9,10-diphenylanthracene (DPA) and 9,10-dibromoanthracene (DBA) are widely used to evaluate the excited state (single or triple state) occurring in a CL reaction through an indirect chemiluminescence. Because it lacks heavy atoms, DPA is a singlet-singlet energy transformation. [46, 57] In practice, the singlet-singlet energy transfer efficiency from an

excited carbonyl product created from a CL to DPA is set as one. Therefore, the singlet quantum yield (Φ^S) can be calculated easily [7, 46, 58]. In contrast, DBA is a triplet-singlet energy transformation. [59, 60] The spin-orbital coupling is caused by the bromine atoms of DBA.

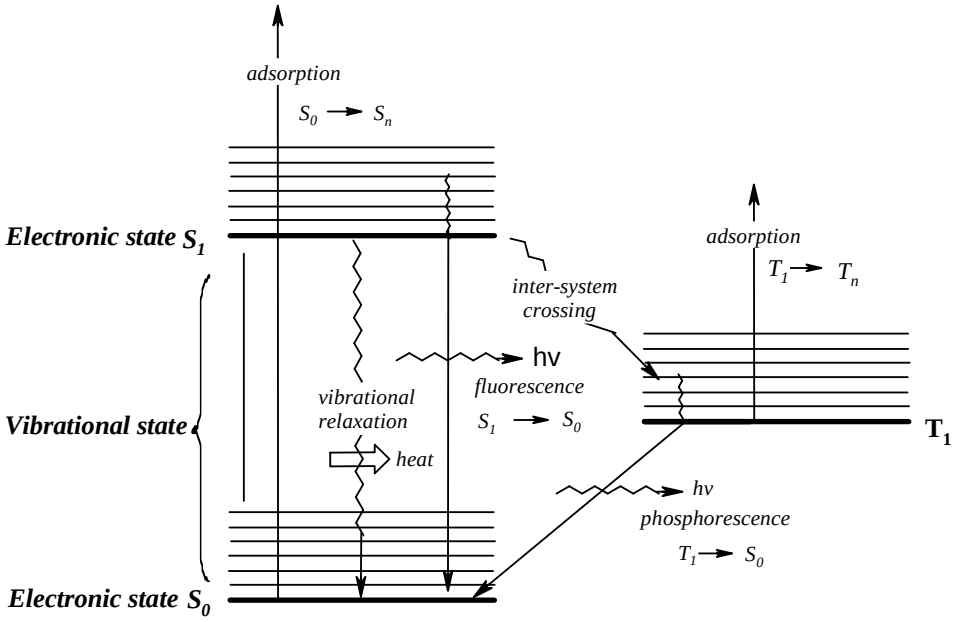

Figure 2.3 Diagram of energy levels and excited energy transitions occurring in organic molecule. Please note that vibrational relaxation is non-radiating transitions.

2.1.3 Chemiluminescence: Emission

The efficiency of a luminescent reaction is defined as the number photons generated from the reaction per reactant molecule. [13] The quantum yield (Φ_{CL}) is given by **Equation 2- 3**.

$$\Phi_{CL} = \Phi_{CE} \times \Phi_{ET} \times \Phi_{EM} \qquad (2\text{- }3)$$

where Φ_{ET}, energy transfer efficiency, is an additional term for indirect chemiluminescence reaction. The factors Φ_{CE} and Φ_{EM} present the efficiencies of chemical reaction and emission, respectively.

Φ_{CE} is related to the productive efficiency of the energy-rich intermediate or complex produced from a chemical reaction and, further, associated with the equilibrium and control of chemical reaction. The factors which affect Φ_{ET} and Φ_{EM} are fairly well understood and can be roughly separated into two categories: interior and exterior.

2-1-3-1 Internal-Factor : Molecular Structure of Fluorescer

Two basic criteria are available for fluorescer design, conjugated and rigid molecular structure. The fluorescent molecules typically are extended conjugated system, containing a number of fused aromatic rings or unsaturated double bonds to pool electronically excited energy together. By Hückel's rule, the total number of π electrons in a conjugated ring system equal to 4n+2, where n=1, 2, 3….. The increase of aromatic ring number (n) will enhance the activity of π or n electron and, therefore, cause a decrease of activation energy and a shift the emission spectrum to longer wavelengths. [44] For instance, the emission of benzene and naphthalene is in the UV region. Bathochromic shift (red-shift) occurs when the conjugated system become larger, such as anthracene (in the visible region) and violanthrone(in the IR region). [61, 62] (**Figure 2.4**)

The quantum yield of a fluorecer is influenced by many factors. However, a rigid plane structure is the most important feature for an efficient fluorescent emitter. The example shown in **Figure 2.5** is classic and is used frequently. Fluorescein is a highly fluorescent emitter. Although phenolphthalein has similar structure to fluorescein, it is a non-fluorescent molecule because too much excited energy is lost by vibrational and rotational motions after phenolphthalein is excited.

The last factor to cause the batho- and hyperchromic shift of flurescer is the substitution effect. It is assumed that the addition of an auxochrome (electron donor, such as $–NR_2$, -NHR, -OH and -NHAr) and an antiaucochrome (electron acceptor, such as $-SO_2CHF_2$ and $–NO_2$) to a chromophore (conjugated system) will cause the extension of the numbers of resonance structure and, therefore, lead to an easier excitability of electron in the molecular orbital of fluorescer. [14, 48, 69]

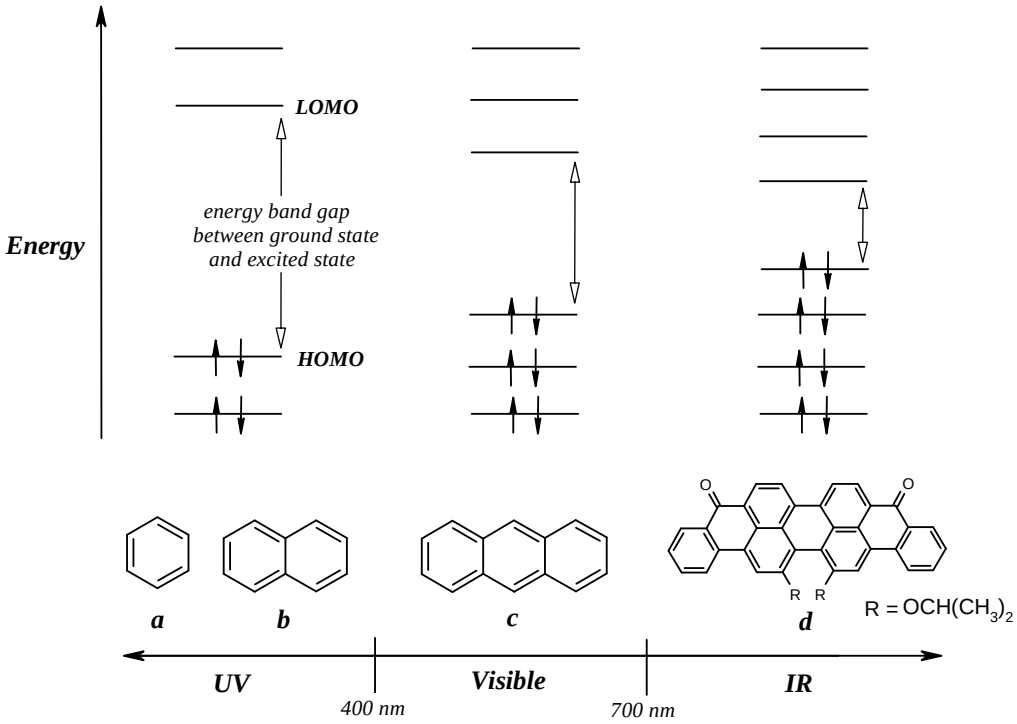

Figure 2.4 The emission wavelength of aromatic compounds. a. benzene; b. naphthalene; c. anthracene; d. 16,17-diisopropoxyviolanthrone.

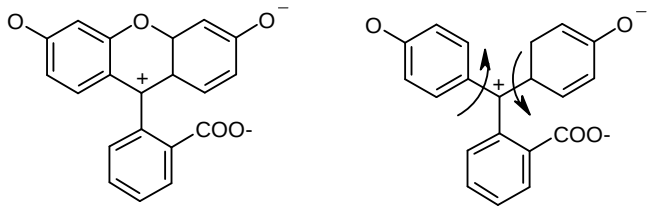

Fluorescein ***Phenolphthalein***

Figure 2.5 Because the rotational and vibrational moving of the substitution groups of phenolphthalein leads the radiationless consumption of excited energy, phenolphthalein is not a fluorescer. [14]

2.1.3.2 External-Factor: Solvent Effect

Besides the molecular structure of the fluorescer, the emission intensity and wavelength are associated with the properties of external solvent also. Typically hyperchromic (enhancement) or hypochromic (diminution) shifts result from the change of viscosity, hydrogen

bond formation and the solubility of fluorescer while bathochromic (red) and hypsochromic (blue) shifts are usually due to the various forms of solvent polarity.

It is well known that the non-radiative consumption of excited energy via vibrational or rotational motions or dynamic collision quenching can be inhibited when the fluorescer is dissolved in the solvent with high viscosity [48, 50, 63, 64]. Therefore, fluorescers with specific molecular structures possess the potential to be molecular rotors in measuring the viscosity of solution. [65, 66, 67, 68] In practical application, those fluorescent probes mainly were used in situations when common mechanical manners failed in viscosity measurement, such as the system with very small volumes or with non-Newtonian fluids.

2.2 Tetrakis(dimethylamino)ethylene (TDE) chemiluminescence

Tetrakis(dimethylamino)ethylene (TDE) is constructed of four dialkylamino groups bonding to a vinyl center. [70] It is well known that dialkylamino groups have strong electron donating properties. Because of these groups, TDE has an extremely low ionization potential, about 6.13 eV, leading to the spontaneous chemiluminescence of TDE upon exposure to oxygen or air. Furthermore, TDE had been noted as an organic reducing agent. [71, 72] The oxidation potential of TDE is almost comparable to that of zinc. [73, 74] These unique properties of TDE have led to patent applications for use as a marker in military and road services, in polymerization as initiator, and in aviation as an emergency light source. [75, 76, 77, 78, 79]

Since TDE was observed by Pruett *et. al.* [80] in 1950, a large number of papers dealing with TDE have appeared that detail the reaction mechanism, characterize the reaction by spectroscopy, and identify the reaction products. The structure of TDE is shown in **Figure 2.6**. The structure of TDE is expected to be quasi planer with a deviation by 28^{o} from planarity due to the repulsion of the bulky adjacent CH_3 groups. TDE has two π electrons in the central part of the molecule. [81, 82, 83] Therefore, TDE has two of the required features for a fluorescer: a planar molecular structure and a conjugated configuration. TDE chemiluminescence is achieved by inter-molecular energy transfer. It had been proven that the emitting species in TDE CL is electronically excited TDE (TDE*) because the known oxidation products do not fluoresce under

these conditions. [84, 96] The emission spectrum of TDE chemiluminescence is a structureless band with a maximum at 500 nm.

During TDE CL in solution, energy transfer can occur by collisions between the energy donor and accepter. Therefore, the hyperchromic and hypsochromic shifts of the emission from TDE CL are associated with the solvent property, such as viscosity and polarity. [85, 86, 87, 89] Fletcher *et. al.* indicated that the photoluminescence peaks of TDE in n-decane, neat TDE, dioxetane, 75% TDE/25% TMU mixture are at 487 nm, 505 nm, 550 nm and 565 nm respectively. [89]

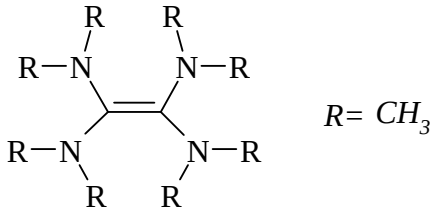

Figure 2.6 Molecular structure of TDE.

2.2.1 Reaction Mechanism of TDE Chemiluminescence

The reaction mechanism of TDE chemiluminescence in liquid phase and gas phase were studied by Urry *et. al.* [85, 88, 89, 90, 91] and Toby *et. al.* [92]. Both indicated that the energy-rich peroxide, tetrakis-dimethylamino-1,2-dioxetane (TDMD), is the energy source to create electronically excited state. [93] TDMD is converted from the autoxidation reaction between TDE and oxygen. Fletcher *et. al.* indicated that the autoxidation reaction is catalyzed by protonic material, such as alcohols or water (ROH). [90, 91, 94] Hydroxylic additives act as an activator for the autoxidation reaction. Indeed, pure TDE in the absence of protonic activators will not react with oxygen. [85, 88, 96] The published data show that the autoxidation reaction is first order in TDE and oxygen while the chemiluminescence is second order with respect to TDE. [85, 88] The reaction mechanism of TDE chemiluminescence is shown in **Figure 2.7**.

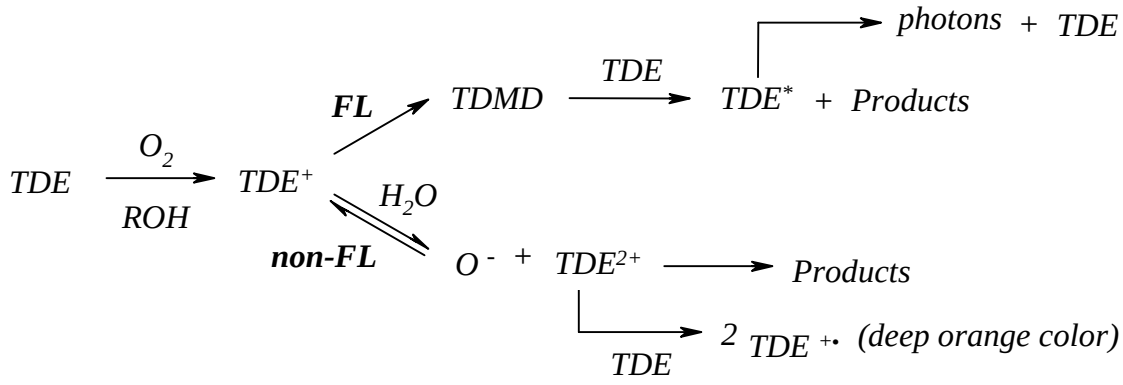

Figure 2.7 The reaction mechanism of TDE chemiluminescence

Looking at the reaction mechanism of TDE chemiluminescence (shown in Figure 2.7), TDE^+ is produced from the autoxidation reaction of TDE in the solvents containing non-polar solvent with little water or protonic material (ROH). [95] TDE^+ subsequently is converted to the energy-rich compound, TDMD. A TDE molecule is excited to an excited state by the energy transfer from cleaved TDMD to TDE in the ground state. Alternatively, the hydrolysis of TDE^+ occurs to give TDE di-cation (TDE^{2+}) [72, 95] if excess protonic material is added into the solution. For example, if the solvent contains more than 67% water, the reaction mixture is bright red. This color is predicted due to the formation of TDE cation radical ($TDE^{+\cdot}$) which is converted from TDE^{2+}. As excess hydroxylic compound is added, the formation of TDMD competes with the formation of TDE^{2+} and decreases the emission intensity. [85]

2-2-2 The Products of TDE Chemiluminescence

The composition of the products generated from TDE chemiluminescence has been analyzed by gas chromatography, mass and nuclear magnetic resonance spectrometry techniques. [85, 97] Urry *et. al.* and Schumacher *et. al.* [85, 97] stated that the composition of the products produced from TDE CL is constant in various solvents: tetramethylurea (TMU, 65 mole%), tetramethyloxamide (TMO, 18 mole%), tetramethylhydrazine (TMH, 12 mole%), bis(dimethylamino)methane (BMAM, 2 mole%), and dimethylamine (DMA, trace amounts). The structures of these products are shown in **Figure 2.8**.

TMO and TMU are the major oxidation products. Shapiro *et. al.* investigated the oxidation products by electron capture detector to determine the relative electron affinity. [97] Electron capture analysis of the major TDE CL products suggested that TMO and TMU have relatively high electron capture cross section compared with oxygen. On the other hand, TDE is a good electron donor. The high electron donor strength of TDE had been identified by Hammond *et. al.* via the inter-molecular charge-transfer between TDE and π electron acceptors. [98, 99] Therefore, the electronically excited energy not only is transferred to unoxidized TDE but also is transferred to TMO and TMU by molecular collision. It was concluded from earlier studies that the emission intensity decreases with increasing the concentration of TMO and TMU [96, 100, 101] and high emission intensity from TDE CL can be expected if the oxidation products are removed continuously.

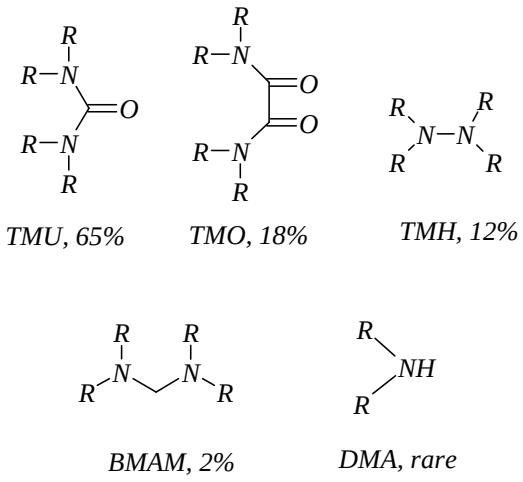

Figure 2.8 The molecular structures of the products of TDE chemiluminescence.

2-2-3 TDE Characterization

Raman and infrared spectra proved that the TDE molecule in the ground state is a centrosymmetric structure. The central C=C bond stretching frequency was identified by Raman at 1630 cm^{-1}. [96, 102] The electron donor properties of TDE are associated with the stabilization by dimethylamino groups. When TDE is in a mono-cation (TDE^{+}) or di-cation (TDE^{2+}) state, the positive charge is stabilized by sharing the weakly bonded electron pairs of dimethylamino with the central carbon. [103] The charge-states of TDE were recognized by Hori

et. al. using electronic absorption spectroscopy. [99] The vibrational frequency of C-N stretching is an indicator for analysis of TDE by IR spectroscopy. Pokhodnia *et. al.* indicated that the stretching and bending of C-N bonds in the central $N_2C=CN_2$ fragment are in the region 1450-1050 cm^{-1}. The broad band in the region 1420-1490 cm^{-1} is assigned to the approximately 20 bending modes of CH_3 fragments. The ionization will cause a blue-shift and intensity gain since the $N_2C=CN_2$ fragment in TDE^+ or TDE^{2+} is no longer planar. [103] In particular the angle between two N-C-N planes increase with the charge-states of TDE. The angle for the di-cation is more than double that of the neutral TDE.

2-3 Reversed Microemulsion Systems (RMS)

Reversed microemulsion systems (RMS) have attracted more and more attention because they increase the mutual solubility between aqueous phase and oil phase by amphiphile, surfactant. Therefore, RMS has been used extensively as extraction and reaction selection medias. In the application of RMS, the water pool entrapped in the reversed micelle acts as a micro-reactor for chemical or biochemical reactions and as a cage for nano-particle production. [104] For instance, using RMS as the media in polymerization and metal catalyst synthesis, RMS enables one to control the yield of reaction and, further, to adjust the crystal structure and size of synthesized particle. [105, 106, 107, 108, 109, 110, 111, 112, 113, 114] The interaction of amphiphile molecules with oil and aqueous phases has been extensively investigated and published in several articles and books that address the properties, characterization methods, and application of RMS. [115, 117, 118, 119, 123, 120, 121, 122]

Fluorescent probes have extensively been used as a tool for investigating the properties of reversed microemulsions; however, there have been no published studies using chemiluminescence to characterize RMS. Fluorescent probes in conjunction with UV-Visible and fluorescent spectrometers are the most common methods to characterize the micellar structure (shape and size), aggregation number (N_{agg}), phase equilibrium, critical micelle concentration (CMC) and water-to-surfactant ratio (W_0) of RMS. [50, 124, 125, 126, 127, 128] Otherwise, FT-IR [129, 130], NMR [130, 131], light scattering, small angle neutron scattering

[132, 133], calorimeter [134], small angle X-ray scattering [135], and X-ray diffraction [136] are also employed in the study of RMS.

2.3.1 Amphiphiles (Surfactants)

Amphiphiles are organic molecules that consists of a hydrophilic head group and an oleophilic tail group. Amphiphiles can, thus, dissolve into both aqueous and oil substances and offer an interface between two immiscible components. Surfactants can be classified into ionic surfactants (including cation, anion ionic and zwitterionic) and non-ionic surfactants. Examples of non-ionic and ionic surfactants are listed in **Figure 2.9**.

Ionic surfactants, e.g. DTAB and NaDDBS, stabilize a microemulsion by electrostatic repulsion while non-ionic surfactants, e.g. Triton®X-100, mainly stabilize a microemulsion through steric stabilization. Zwitterionic surfactants, such as AIPS and EDAB (as seen in **Figure 2.9**), [137, 138] feature cationic behavior near or below the isoelectric point and anionic behavior at higher pH. Some studies found that the stability of RMS can be further enhanced when an alcohol, such as 1-butanol, is added into the system. [139, 140, 141, 142, 143] The alcohol acts as co-surfactant. The schematically molecular structure of RMS with co-surfactant is shown in **Figure 2.10**.

Ionic Surfactant:

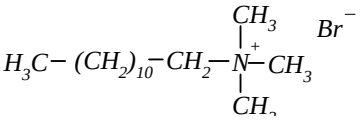

DTAB *(cationic surfactant)*

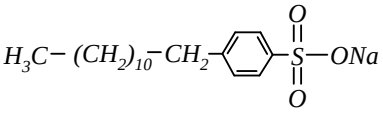

NaDDBS *(anionic surfactant)*

Zwitterionic Surfactant:

AIPS

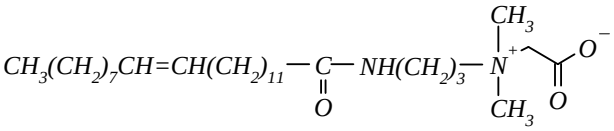

EDAB

Non-ionic Surfactant:

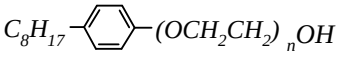

Triton ® ***X-100***

Figure 2.9 The molecular structures of ionic and non-ionic surfactants. DTAB, NaDDBS, AIPS and EDAB represent n-dodecyl trimethylammonium bromide, sodium dodecylbenzenesulfonate, 3-((11-acryloyloxyundecyl)imidazolyl) propyl sulfonate, and erucyl dimethyl amidopropyl betaine, respectively.

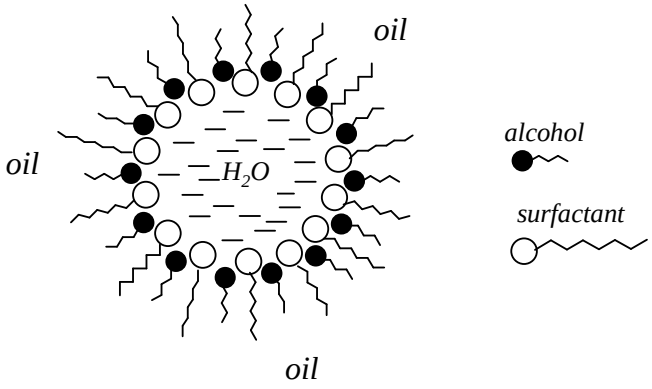

Figure 2.10 The molecular structure of reversed microemulsion with alcohols as co-surfactant.

2.3.1.1 Surfactant Aggregate

At low surfactant concentration, surfactant molecules exist in the interface of two immiscible compounds. Over a narrow concentration range, surfactant molecules dynamically associate to form a big molecular aggregation. [144] This narrow concentration range is termed the critical micelle concentration (CMC). For O/W (oil in water) microemulsion, it is well known that the aggregation of the amphiphile in the interface strongly decreases the surface tension of the solution and dramatically changes some physicochemical properties, such as surface tension, conductivity, light scattering, and osmotic pressure. The determination of the CMC value in an O/W microemulsion is due to the abrupt changes of theses physicochemical properties with increasing concentration of surfactant (as seen in **Figure 2.11**).

For O/W microemulsion, several techniques have been developed and some of them have become standard methods for determining the CMC. The techniques include conductometry [145], fluorescent probe [146, 147], cyclic voltammetry [148], UV-VIS, fluorescence spectrometer [149], capillary electrophoresis [150, 151, 152], and surface tension [153]. The influences of temperature and pressure on the CMC of surfactants in aqueous media have been systemtically investigated and reported. [122] However, there is much less information on the CMC of RMS. This is due to the difference in the micellar structures between O/W (oil in water or normal) and W/O (water in oil or reversed) micelle. The methods typically employed in determining the CMC value of O/W microemulsion are not suitable to be used in that of RMS. Only few methods have been reported. The methods employed to measure the CMC of RMS are further described in **Section 2.3.3**.

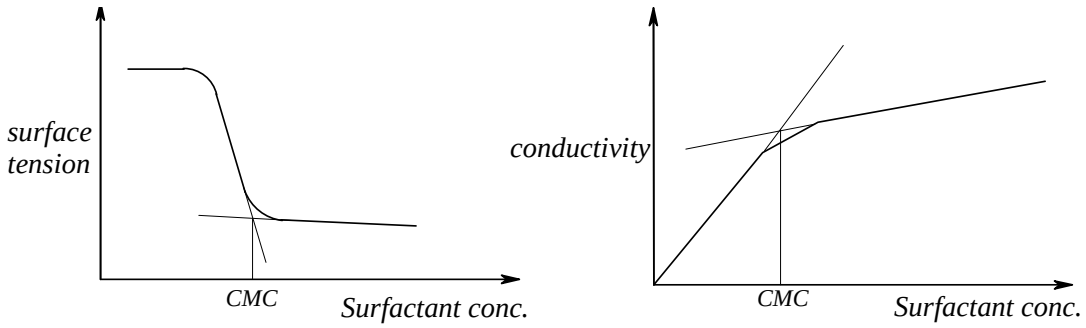

Figure 2.11 Determination of CMC value by surface tension and conductivity

2.3.1.2 Aggregation Number (N_{agg})

Reversed micelles have the opposite structure as O/W micelles. For reversed micelle, the hydrophilic head of surfactant bonds to the interior aqueous component of the microemulsion via hydrogen bonds and the hydrophobic tail extends into the bulk oil phase in order to escape from aqueous core of micelle. [154] Bcause of the differences in the micellar structure, the number of surfactant monomers involved in a reversed micelle is relatively small compared to that in a normal micelle. [155, 156, 157] According to published data, RMS's micelles typically consists about 10-100 surfactant monomers (aggregation number, N_{agg}) depending on the surrounding organic media, type of surfactant, temperature and water-to-surfactant ratio (W_0). [115, 116]

RMS features a sponge-like structure. A large amount of aqueous materials can be dissolved into the water pool of reversed micelle. Increasing the value W_0 of RMS increases both the water pool radii and N_{agg}. For a W/O micelle system, a few models based on the nature of surfactant and CMC value had been developed to calculated the expected N_{agg} value. [50, 146, 158, 159, 160, 161, 121, 122] However, a model for estimating the N_{agg} of reversed micelles is absent. The N_{agg} value of a RMS can be derived experimentally via several techniques, such as steady-state fluorescence quenching [163], fluorescent probe [50], and FT-IR [162].

2.3.1.3 Packing Parameter of Surfactant (S)

The surfactant can be characterized by a packing parameter (S). This concept was first elucidated by Israelachvili *et. al.*. [164]. In a solution, the parcking parameter of surfactant

determines that the surfactant monomers tend to form a reversed or normal micelle. The packing parameter is derived from **Equation 2- 4**. V_{tail}, A_{head}, and L_{tail} represent the effective tail length, tail volume and head surface, respectively. A depiction of the effective tail length, tail volume and head surface of a surfactant is shown in **Figure 2.12**. For a spherical micelle with a core radius r, the volume (V_{core}) and surface area (A_{core}) of the core are equal to $4\pi r^3/3$ and $4\pi r^2$,respectively, and, therefore, $r = 3V_{core}/A_{core} = 3V_{tail}/A_{head}$. Because r can not exceed the length of the tail, L_{tail}, in an aqueous media, the *S* value for the micelle with spherical structure should be in the range from 0-1/3. [165] Depending on this theory, the correlation between the type of micelle (O/W or revered micelle) and S can be deduced. **Table 2 -1** relates the connection between the type and the shape of micelle and the *S* value. [122, 165, 166]

$$S = \frac{V_{tail}}{A_{head} L_{tail}} \qquad (2\text{- }4)$$

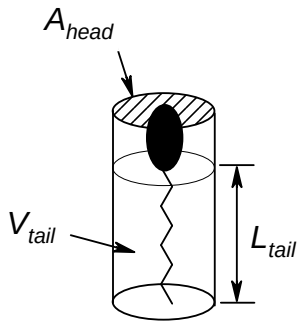

Figure 2.12 Schematic representation of effective tail length (L_{tail}), tail volume (V_{tail}) and head surface (A_{head}) for surfactant.

S value	Type of micelle	Micelle structure
$0 \le S \le 1/3$	**Oil-in-water (O/W)**	**Sphere**
$1/3 \le S \le 1/2$	**Oil-in-water (O/W)**	**Sylinder**
$1/2 \le S \le 1$	**Oil-in-water**	**Bilayer**
$1 < S$	**Water-in-oil (W/O)**	**-**

Table 2-1. The relationship between the value of the packing parameter (S), and the type and structure of micelles.

2.3.1.4 Surfactants for RMS and Water-in-scCO$_2$ Microemulsion

When selecting a suitable surfactant for an O/W or reversed microemulsion system, the surfactant's packing parameter, electronic properties and solubility are the most important parameters to consider. **Figure 2.13** shows a few surfactants usually employed in RMS. They include AOT, DDAB [179, 172], CTAB [140, 180], SDS [141, 175] and X-100 [181]. Super critical CO_2 (sc-CO_2) reversed micelle is a special case in the category of RMS. The surfactant which can be used in W/sc-CO2 RMS usually features fluorinated tails, such as ammonium or phosphate carboxylate perfluoropolyether (PFPE-NH_4 and PFPE-PO_4) [183, 197, 198, 199, 200, 201, 202, 203, 204, 207, 205] (molecular structures showed in **Figure 2.13**).

Sodium bis(2-ethylhexyl) sulphosuccinate (Aerosol OT, or AOT) is a commercial surfactant that is used in RMS most frequently. AOT features a high packing parameter (about 7 [177]) and a high solubility for aqueous phase in most non-polar solvents. Petit *et. al.* indicated that the water-to-surfactant ratio (W_0) of AOT micelle can reach 60 at moderate temperature and in suitable oil media. [178] AOT consists of double hydrophobic tails with a tail length about 8 Å, and a hydrophilic head with an effective area of ~51 Å^2. [167] The diameter of the micelle constructed by AOT monomers in alkanes is about 5-50 nm. [175] Numerous articles have addressed the physical properties, applications, and the phase equilibrium of AOT-oil-aqueous material reversed microemulsion in the past two decades. [106, 142, 143, 167, 168, 169, 170, 171, 172, 173, 174, 175, 176, 191]

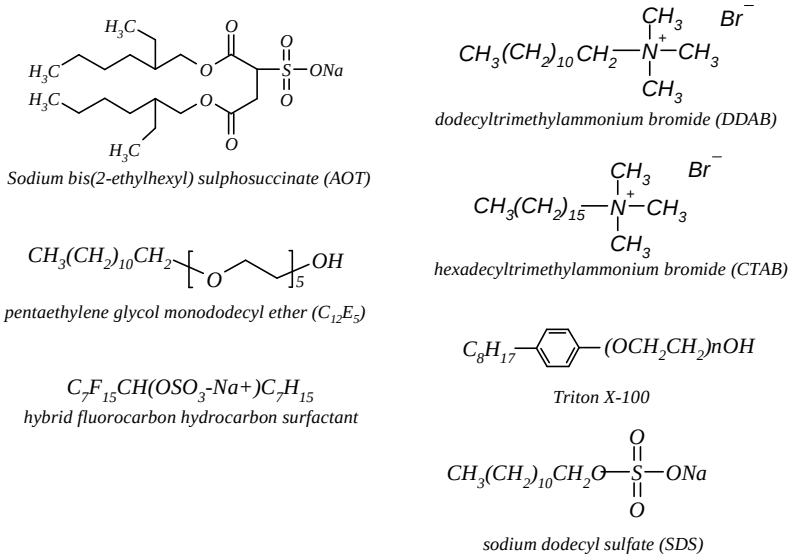

Figure 2.13 The molecular structures usually used in RMS or W/sc-CO_2 RMS.

2.3.2 Important Factors for Surfactant Aggregation

The aggregation of surfactant monomers is influenced by W_0, temperature [120, 201], surfactant concentration [196], the presence of an additional salt and co-surfactant [139, 140, 141, 142, 143, 206]. These influences are mainly reflected in the curvature of the micelle [104, 186, 206] (as shown in **Figure 2.14**) and the phase transition [185, 187, 188 189, 190, 191] (as shown in **Figure 2.15**). They also determine the type of microemulsion formed: O/W or reversed microemulsion. Eastoe *et. al.* found that the type of microemulsion can be tuned by changing temperature. [192, 193, 194, 195] A systematical study in the phase transition of surfactant-oil-water system (SOW) under various temperatures and compositions has been done by Kahlweit *et. al.* [196] and Winsor *et. al.*. [208]

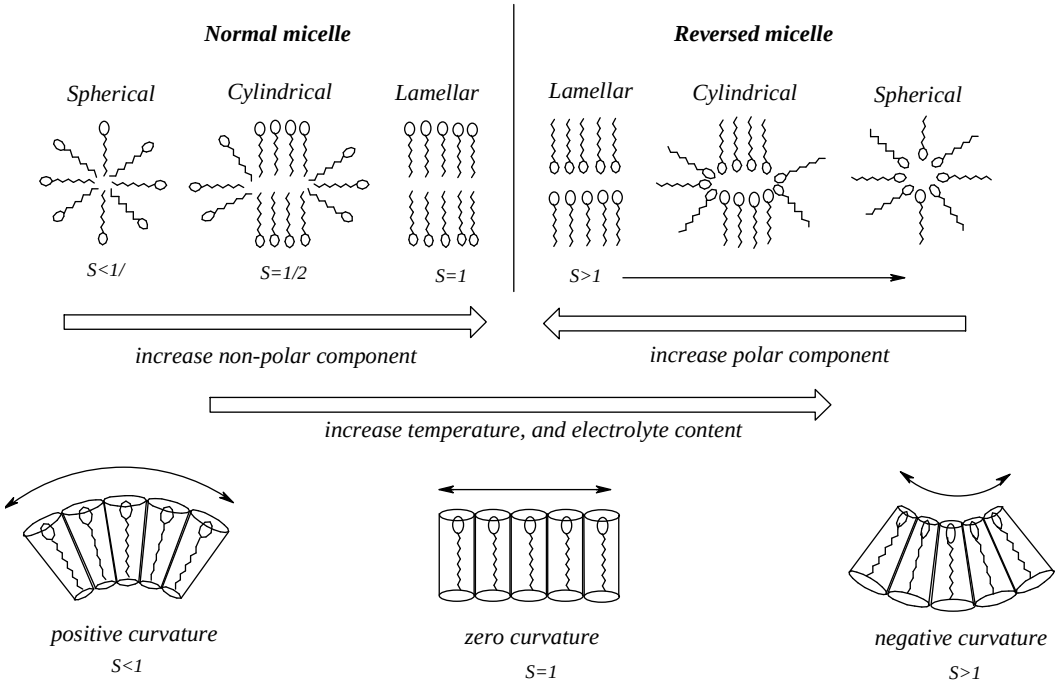

Figure 2.14 The influences of temperature, additional chemicals and the composition for the curvature of surfactant aggregation and micelle structure.

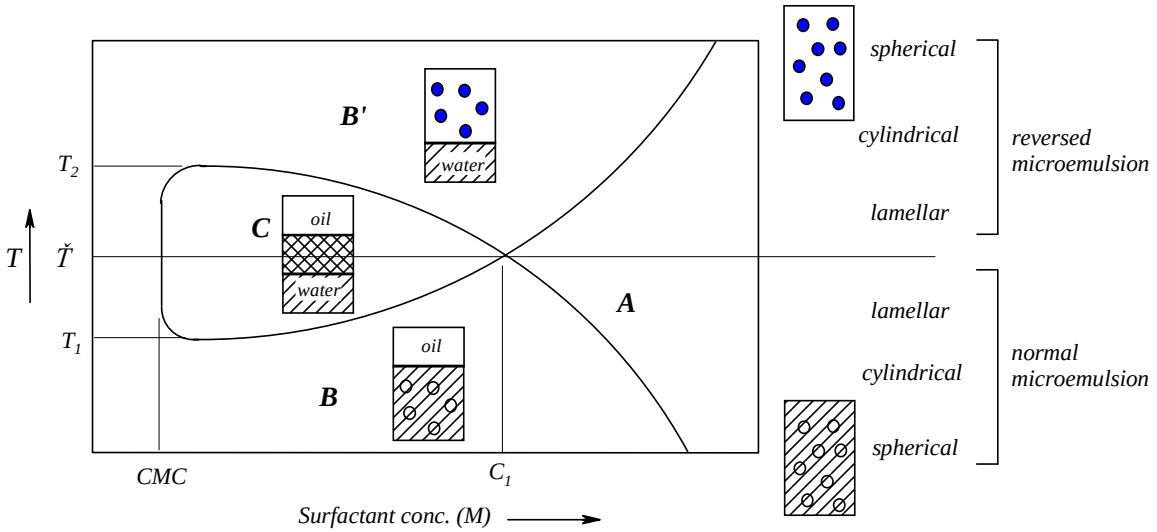

Figure 2.15 A fish-like phase diagram is observed when water and oil are mixed at a 1:1 ratio. After CMC, the phase transition is dominated by temperature and surfactant concentration effects. [196] Region A: Winsor IV system; there is no excess oil and water present. Region B and B': Winsor I and II systems; two phases exist in the system. O/W or reversed micelles exist in water-rich (B) and oil-rich (B') phase, respectively. Region C: Winsor III system; the system includes three phases. The ternary phase containing a water- and oil-continuous phase is formed between water- and oil-rich phase.

2.3.3 Determination of the CMC of a RMS

The CMC value of RMS mainly varies with the type of surfactant, the properties of the hydrocarbon media, and temperature. The CMC values of a normal microemulsion is determined based on the abrupt change of some physicochemical properties, such as surface tension or conductivity. However, those determination methods usually fail in measuring the CMC value of a RMS since the change of the physicochemical properties typically is slight when the concentration of surfactant approaches the CMC. Moreover, reverse micelles usually are much smaller than normal micelles. This also increases the difficulty in CMC determination for a RMS. In earlier studies, several techniques have been found for determining the CMC value of RMS.

Spectroscopic methods are the most widely employed in the CMC determination for a RMS. The techniques include ^{1}H and ^{13}C NRM [211, 212, 213], IR spectroscopy [213, 214], Raman Scatter fluorescence [213], microcalorimetry [209, 215, 216], fluorometry [209] use of a fluorescent probe in conjunction with a UV-VIS spectrophotometer [213, 214, 216, 218, 220, 221], small angle neutron scattering [219, 222, 223], light scattering [224], controlled partial pressure-vapor pressure osmometry [225], photon correlation spectroscopy [226], and positron annihilation techniques [227]. Reviewing the present methods which had been utilized in the CMC determination of RMS, fluorescent probe plays a most important role not only in probing the CMC value of RMS, but also in studying the micellar structure and aggregation number and the surfactant's behavior in non-polar media. Behera *et al.* published a systemic study on the use of fluorescent probes in RMS and O/W microemulsions. [50, 115, 228]

2.4. Physicochemical Properties of Metal Oxide Surfaces (MgO and Al_2O_3)

Metal oxide nano-particles attract attention because metal oxides have been widely used as catalysts [229, 230, 231, 232], support for other catalysts [231, 233, 234] and organic functional groups [235, 236, 237, 238, 239], and adsorbents for waste chemicals [248, 263, 269]. The characteristics of metal oxide nano-particles which include the crystal structure, surface morphology, electric, and acid-base properties have been investigated qualitatively by several methods. The methods include FT-IR [239, 240, 241, 242], UV-visible [245, 246, 247], photoluminescent spectroscopy [249, 251, 252], electron paramagnetic resonance (EPR) [253], XRD [240], scanning electron microscopy (SEM) [249], scanning photoelectron microscopy (SPEM) [250], X-ray photoelectron spectroscopy (XPS) [239, 243, 244], electron spin resonance [262], chemical probes [242, 254, 255, 256, 257, 258, 260, 261], BET [256], mass spectroscopy [258, 295], ERS [259] and NMR [291, 292]. However, quantitative studies relating to metal oxide nano-particles are relatively rare due to their complex surface structure. For example, infrared spectroscopy has been widely employed in qualitatively characterizing surface structure for metal oxides through the identification of surface chemisorbed species. The difficulty of using IR spectroscopy in quantitatively analyzing surface chemisorbed species is due to the difficulty of determining the IR adsorption coefficients at each relaxation for the adsorbed species. [296]

The surface properties of metal oxides play the most important role as metal oxides are used industrially in various reactions. [231] More theoretical and fundamental studies have been done on MgO and Al_2O_3 than on other metal oxides. Reviewing previous studies on MgO and Al_2O_3, it is well known that the surface structure is strongly associated with the acid-base, electronic, and reactive properties of these metal oxides. In the case of MgO and Al_2O_3, the outmost layer anions (O^{2-}) and cations (M^{n+}, n= 2 for Mg and 3 for Al) are coordinatively unsaturated. Therefore, the outmost layer of the metal oxide is covered by various species when exposed to the atmosphere. Water is the most abundant component adsorbed on the surface. When there is adsorption of water on MgO or Al_2O_3, water may be present in its undissociated form (H_2O), existing in multiple adsorption layers, or dissociated forms (hydroxyl (OH^-) and proton (H^+)), adsorbing on lattically unsaturated sites, M^{n+} and O^{2-}. Goodman *et. al.* indicated that the IR band near 1645 cm^{-1} is associated with molecular water on the surface and the IR bands in the range from 3000 to 3800 cm^{-1} are contributed by dissociated water (hydroxyl groups) with different coordination on MgO and Al_2O_3. [264, 265]

In the IR spectra of MgO and Al_2O_3, the IR bands in the range from 3000 to 3800 cm^{-1} are due to two hydroxyl groups with different configurations. The sharp bands at higher frequency are assigned to isolated hydroxyl groups. Due to the formation of hydrogen bonds between two hydroxyl groups, the IR band of hydrogen bonded hydroxyl group is a broad band at a lower frequency (H-OH). [266, 267, 268, 270, 271] On the other hand, the perturbation of the isolated hydroxyl group is related to the coordination of adsorbed lattice ion. Consequentially the stretching frequency of isolated OH reflects the surface structure of metal oxide and is a spectral fingerprint of the surface structure. [272] In other words, surface hydroxyl groups are the markers presenting the surface morphology and surface reactivity on MgO and Al_2O_3.

2.4.1 Magnesium Oxide (MgO)

2.4.1.1 The Present Models of Surface Hydroxyl Groups on MgO

The correlation between O-H stretching frequencies and the their locations on MgO have been determined by several experimental [249, 270, 271, 273, 275, 276] and theoretical models

[279, 280, 281, 283, 282]. Anderson *et. al.* first elucidated that there are two proposed types of surface hydroxyls formed on MgO surface when water decomposes, as shown in **Figure 2.16**. [268, 271] Knözinger *et. al.* refined previous models by introducing the consideration of the hydrogen bond between hydroxyl groups and the coordination of surface cation and anion for the stretching frequencies of O-H groups. [276, 273] According to the coordination number of surface cations and anions, the categories of surface hydroxyl groups can be classified into 1-coordinated OH (type A) as well as 3-, 4- and 5-coordinated OH (type B), as seen in **Figure 2.17**. Hydrogen bonds form between neighbouring type A and type B hydroxyl groups under certain conditions. The formation of a hydrogen bond will lead type A and type B hydroxyls to become hydrogen bond acceptors (type C) and hydrogen bond donors (type D), respectively. In the IR spectrum, the sharp bands in a narrow frequency range from 3690 to 3750 cm^{-1} are assigned to isolated hydroxyl groups (type A and type B). The broad band in the interval from 3200 to 3650 cm^{-1} is assigned to hydrogen bonded hydroxyls.

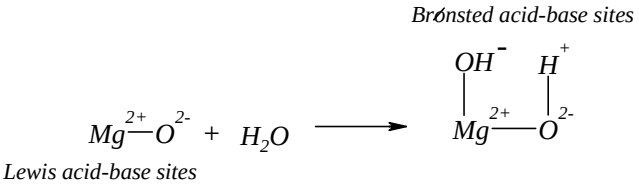

Figure 2.16 Two types of surface hydroxyls form on metal oxide after the decomposition of molecular water.

Investigating the stretching frequencies of isolated hydroxyls adsorbed on different locations, both electronic properties of the ions and the distance between lattice cations and anions have to be considered. Type A OH has the highest stretching frequency (appearing at 3750 cm^{-1}) because the cooridination of the cation weakens the OH bond. The stretching frequency will be reduced with increasing the coordination of the cation bonded with type A hydroxyl. [268, 273, 276] Type B hydroxyls, appearing at 3730-3450 cm^{-1}, are composed of a lattice oxygen ion and a proton. [270, 276, 279] Increasing the coordination number of the lattice ion shortens the distance between ions (O^{2-} and Mg^{2+}). Therefore, the type B OH with higher coordination number have a lower stretching frequency due to the positive charge of neighbouring Mg^{2+} and the Coulomb interaction between the cations and OH. [276, 279]

According to previous studies, the stretching frequency of type B hydroxyls can be concluded to be in the order shown in **Equation 2- 5** and the stretching frequencies of different hydroxyl groups are shown in **Figure 2.18**. [86, 268, 273, 275, 276, 277, 279, 285]

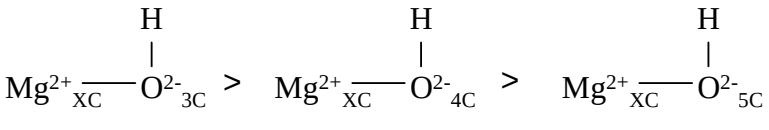

(2- 5)

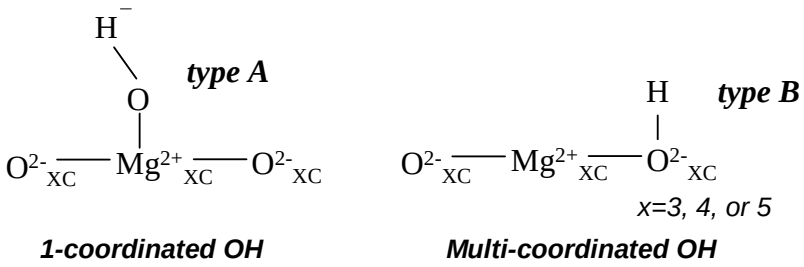

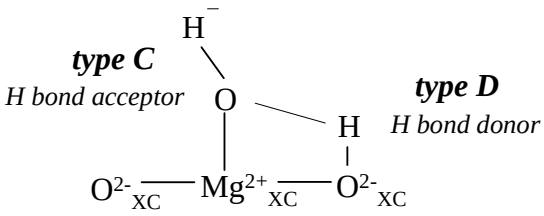

Figure 2.17 Types of surface hydroxyl groups. Type C and type D hydroxyl groups result from the formation of a hydrogen bond between type A and type B hydroxyl groups. The 3, 4 and 5 coordinated ions are due to the location of ions on corner, edge, and extended planes, respectively.

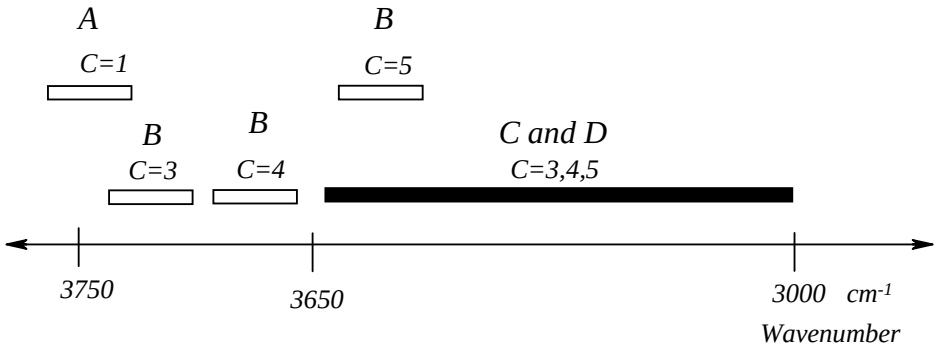

Figure 2.18 The proposed wavenumbers of hydroxyl groups in the IR spectrum. Type A and B isolated OH are indicated by empty bars and type C and D hydrogen bonded OH are shown by a solid bar. The values shown above the bar are the coordination number of hydroxyls.

2.4.1.2 The Location and Thermal Stability of Hydroxyl Groups

2.4.1.2.1 Location of Surface Hydroxyls on MgO

On an MgO surface, 3-, 4-, and 5-coordinated hydroxyls are located on corners, edges and, extended planes, respectively. It was proposed by Klabunde *et. al.* [277] that the OH groups concentrated on edge and corner sites are more isolated. Consequently the ratio of isolated OH to total OH decreases when the surface of MgO is more flat. [278] On a nearly perfect MgO surface, the hydroxyls with lower coordination numbers are much less abundant [284], and their concentration increases with increasing surface defect concentration. Zecchina *et. al.* indicated that treating MgO surface by water vapor causes surface erosion and considerably increases the concentration of the hydroxyl groups with lower coordination numbers. [245, 249, 274, 275, 284] The increase of surface hydroxyl groups with lower coordination is associated with the creation of edge and corner sites (lower coordination sites). This also enhances the surface reactivity of a dehydrated surface. The relationship between surface morphology and the surface reactivity of MgO was studied by Ahmed *et. al.*. [291, 293, 301] Ahmed *et. al.* suggested that the surface reactivity is related to the surface roughness or the number of intrinsic sites with lower coordination (e.g. M^{2+}_{LC} and O^{2-}_{LC}). The more rough MgO surfaces containing more intrinsic sites with lower coordination numbers have higher reactivity. [274, 294]

2.4.1.2.2 Quantitative Determination of Surface Hydroxyl Group

Although surface hydroxyls can be studied by several chemical and physical techniques, only a few of them can be used to quantify the surface hydroxyls. Bermudez first pointed out the use of NMR in the analysis of surface hydroxyl content on hydrated silica gel in 1970. [295]. Furthermore, Morimoto *et. al.* used weight loss upon ignition to measure surface hydroxyl concentration on ZnO. [297] Hoq *et. al.* approached the surface hydroxyl content by D_2 exchange reaction over thermally activated MgO and, subsequently, determined the ratio of HD^+ to D_2^+ by mass spectrometry. [298] McCafferty *et. al.* determined the concentration of surface hydroxyl group on MgO films by XPS. [244] Even though the total hydroxyl adsorbed on metal oxide can be evaluated accurately, to quantitatively identify the different types of hydroxyl groups (i.e. isolated vs. hydrogen bonded) is difficult. To measure surface isolated and hydrogen bonded hydroxyl, respectively, Sato *et. al.* reported a chemical characterizion method. By Sato's method, the amount of isolated and hydrogen bonded hydroxyl groups are determined by **Equation 2-6**, **2-7** and **2-8** based on the exchange reaction between the ethyl group of triethylaluminum ($AlEt_3$) and the proton of hydroxyl groups. [299] An extension of this method was reported recently by Grieken *et. al.* [300] for determining surface hydroxyl groups on silica and Itoh *et. al.* [277, 278] in measuring hydroxyl groups on MgO.

$$3N = E_1 + E_2 \qquad (2\text{-}6)$$

$$E_1 = n_L + 2n_B \qquad (2\text{-}7)$$

$$E_2 = 2n_L + n_B \qquad (2\text{-}8)$$

where N is the moles of $AlEt_3$ chemisorbed on metal oxide. E_1 and E_2 are the moles of evolved ethane during $AlEt_3$ and 1-pentanol addition. n_L and n_B represent the moles of $AlEt_3$ adsorbed on metal oxide in linear and bridged form, respectively.

2.4.1.2.3 Thermal Stability of Hydroxyl Groups on MgO

It is well known that increasing temperature leads to desorption of surface hydroxyl groups. The desorption temperature of the hydroxyl groups are associated with the locations (coordination number) of the hydroxyl groups. Experimental data showed that the lower coordination hydroxyl groups ($O_{LC}H$, L=3, or 4) have stronger interaction with MgO surface.

[276, 277, 278] This result is in agreement with the theoretical calculations reported by Chizallet *et. al.* [280, 285, 286, 287, 288, 289] In the IR spectrum of MgO, the broad band (3650-3000 cm^{-1}) is contributed by the hydrogen bonded hydroxyls (type C and D hydroxyl groups). Experimentally, this band starts to decrease at lower temperature than the sharp band between 3750-3650 cm^{-1} and almost disappears at 773K. [285] Because the shape of this band changes as temperature increases, this broad band is a multicomponent band. [285] The thermal stabilities of the hydroxyl groups contained in with this broad band are difficult to distinguish by simply raising the temperature and measuring the IR spectra.

From early studies, it was found that 1-coordinated OH has a lower thermal stability compared with 3-coordinated OH. Chizallet *et. al.* [279] stated that the sharp band shift from 3750 to 3725 cm^{-1} occurs above 573K and can be proposed as the desorption of 1-coordination OH. The thermal stability of lower coordinated isolated hydroxyl had been investigated by Bailly *et. al.*. [302] Bailly *et. al.* found that the O^{2-}_{4C} and O^{2-}_{3C} sites start to be released at 673 and 1073 K, respectively. Klabunde *et. al.* [277] reported that 4- and 3-coordinated isolated hydroxyl groups are thermal unstable at 673 and 1073 K, respectively. The thermal stability of 5-coordinated isolated hydroxyl group is much lower than 3- and 4-coordinated isolated hydroxyl groups. This assumption was reported by Chizallet and Huang *et. al.*. [86, 285] They found that the right shift (from high to low frequency) of the broad band occurs at low temperature (~473^{o}C). In contrast with the relative stretching frequency of hydroxyl groups shown in **Figure 2.18**, the band of 5-coordinated isolated hydroxyl group overlaps with the band of hydrogen bonded hydroxyl, and, therefore, the band shift as increasing temperature can be explained by the removal of 5-coordination isolated hydroxyl groups. The removal temperature of 5-coordinated isolated hydroxyl groups can be assumed to be 473 K. From these studies, the relative desorption temperature of surface hydroxyl groups can be summarized as shown in **Figure 2.19**.

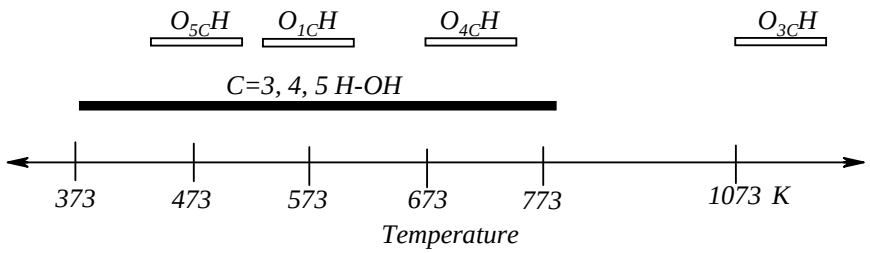

Figure 2.19 The desorption temperature of surface hydroxyl groups on MgO. The solid and hollow bars indicate the desorption temperatures of hydrogen bonded hydroxyls (*H-OH*) and isolated hydroxyls (*$O_{1C}H$, $O_{3C}H$, $O_{4C}H$, and $O_{5C}H$*) respectively.

2-4-1-3 Surface Acid-Base Properties of MgO

The characterization of surface acid-base properties on catalyst surface is crucial since acid-base properties are key for the potential catalytic properties of metal oxides. On a metal oxide surface, the adsorption of external compound may be in molecular form or dissociated form depending on it acid-base properties. [303] Therefore, the acid-base properties of an acid or base catalyst is associated with its reactivity and chemisorption ability and, further, reflects the population of the active sites on the surface.

2.4.1.3.1 Determination Methods

The surface acid-base properties associated with catalyst activity and selectivity are typically characterized by the topography on metal oxides. It had been mentioned in **Sections 2.4.1.1** and **2.4.1.2** that the stretching frequencies of isolated hydroxyl groups in IR spectrum are unique on the specific sites. Indeed, isolated hydroxyl groups are outstanding marker reflecting the acid or basic sites on metal oxide surface. However, it also is well known that the quantitative determination of surface isolated hydroxyl groups is difficult. Only very few techniques can be employed.

Recently the characterization of surface acid-base properties in most studies is based on the adsorption of a probing molecule and the ability to react along a basic reagent complemented by NMR, FT-IR, XPS, XRD, UV-Visible, TPD (temperature programmed desorption-mass

spectroscopes). Otherwise, luminescent emission data collected by photoluminescence also have been used to analyze the surface acid-base properties on several metal oxide surfaces. [242, 254, 256, 258, 260, 285, 304, 305, 306, 307, 308, 309, 310, 312, 311] Reviewing at those methods, the step of high temperature treatment is required to get clean surface before the addition of probe molecule or the detection (~1073 K). [256] Since high temperature treatment will lead to the change of surface morphology and, subsequently, cause the variation of surface acid-base properties, a deviation existing in experimental result from actual situation usually occurs. Therefore, a low-temperature examination method is desired.

2.4.1.3.2 Acid and Base Sites on MgO

The strong base character of MgO is well known. In several base-catalyzed reactions, [230, 231, 314, 315] the strong base character of MgO plays an important role. On clean MgO surface, the electron rich lattice oxygen anion (O_{LC}^{2-}) acts as a strong Brønsted base (electron donating site) and the electron deficient lattice magnesium (Mg_{LC}^{2+}) act as a weak Brønsted acid (electron accepting site). [282, 316] On a hydrated MgO surface, $O_{1C}H$ and $O_{LC}H$ (L=3,4 or 5) form on Mg_{LC}^{2+} and O_{LC}^{2-} after the decomposition of water. The surface hydroxyl group is thought of as a weak Brønsted base and is more active than O^{2-} ion (evaluated by the conversion of 2-methyl-but-3-yn-2-ol, MBOH). [260, 282, 285, 298, 313]

The interaction between a hydroxyl group and surface ion reflects the acid or base strength of surface ions. The basic strength of a metal oxide surface is defined as the ability to donate an electron pair to an acid molecule (such as CO_2) (Lewis base) or to accept a proton (Brønsted base). [260, 312, 317, 318] As discussed above, it was found that the dehydration temperature increases with decreasing coordination number. Therefore, the basicity of lattice oxygen ions can be assumed as the following order: $O_{3C}^{2-} > O_{4C}^{2-} > O_{5C}^{2-}$. This proposition is in agreement with the studies on the surface acid-base properties on MgO. Chizallet *et. al.* [285] studied the surface acid-base property by the deprotonation ability for methanol and propyne and conversion ability for MBOH on MgO. They found that the deprotonation or conversion ability is associated with the concentration of surface basic anion sites with lower coordination, O_{LC}^{2-}. Aramendía *et. al.* [260, 317] used CO_2 as a probe molecule and classified the basic sites by the interaction strength between O_{LC}^{2-} and probe molecule. Aramendía *et. al.* found five peaks in the

temperature-programmed desorption (TPD) spectrum at 402, 535, 732, 863, and 1017 K. Lower desorption temperature corresponds to site with lower basic strength. It is stated by Stone *et. al.* that lower coordination anion sites exhibit stronger basicity and can react with weaker acid. [247, 256, 260]

2.4.2 Aluminum Oxide

Aluminum oxide is frequently used as a catalyst support because of its high surface area, superior chemical and thermal stability. [319, 320, 321, 322, 323, 324] The dispersion of a supported metal on aluminum oxide is related to the concentration of surface hydroxyls. Heemeier *et. al.* [325] stated that the metal dispersion on a support increases with increasing concentration of surface hydroxyl since surface hydroxyls act as nucleation sites for initiation of metal particle growth. For the application of aluminum oxide in the automobile industry, γ-Al_2O_3 is typically used as support for BaO or K_2O in traditional automotive exhaust control catalysts to treat NO_X. [323] In the chemical industry, aluminum oxide also can be used as adsorbent [269] and catalyst [326, 327, 328, 329] in several reactions. Due to its widespread use in different fields, the properties of aluminum oxide, including surface acid-base properties, reactivity, structure, hydroxyl configurations and crystal phases, have been well studied and reported in the past few decades. [321, 326, 330, 331, 346, 348, 350, 351]

2.4.2.1 The Crystal Phases of Al_2O_3

Various precursors of aluminum oxide, aluminum hydroxides (including gibbsite ($Al(OH)_3$), bayerite ($Al(OH)_3$), nordstrandite ($Al(OH)_3$), diaspore (AlOOH) and boehmite (AlOOH)), have been discussed in the literature. [330, 337, 338] Aluminum oxides with different lattice phases are produced from the thermal dehydration of aluminum hydroxides under evacuation. The crystal phase of aluminum oxide is temperature-dependent. [330] It changes with dehydration temperature, which further causes variations in the configuration of chemisorptional species, particularly for hydroxyl groups. [341] The characteristic of aluminum oxide is dependent on the crystal structure. In previous research, the change in the surface properties caused by the variation of crystal phase usually is monitored by FT-IR since the

stretching frequencies of surface hydroxyls shift with the change of surface structure. The details have been addressed by Knözinger *et. al.*. [326, 326, 330, 331]

Knözinger suggested that the change in the lattice phase is due to the migration of surface ions under high temperature. [326, 326, 330, 331]. α-Al_2O_3 is a thermodynamically stable phase and is the final result upon thermally dehydrating aluminum hydroxide under evacuation. Before the formation of α-Al_2O_3, a series of meta-stable oxide phases (termed transition phases) with highly porous surfaces are formed. Depending on the difference in the precursors, the formation temperatures for each transition aluminum oxides may be different. Typically, the creation of each transition aluminum oxides follows the order shown in **Equation 2- 9** with increased dehydration temperature. [332]

$$AlOOH \rightarrow \gamma\text{-} \rightarrow \delta\text{-} \rightarrow \theta\text{-} \rightarrow \alpha\text{-}Al_2O_3 \qquad (2\text{-}9)$$

α-Al_2O_3 is generally considered to be the most inert of all the aluminum oxides. [330] In contrast to thermally stable α-Al_2O_3, meta-stable aluminum oxides have higher activity and are studied more frequently. Based on the dehydration temperature, transition aluminum oxide can be classified into two families:

1. Low temperature transition phases: such as γ-Al_2O_3 and η-Al_2O_3
   Dehydration temperature < 600^oC
2. High temperature transition phases: such as δ-Al_2O_3 and θ-Al_2O_3
   Dehydration temperature > 600 - 1150^oC

The structural difference in each transitional phase is ascribed to the arrangement of cations in an approximately cubic close-packed oxygen array. [332] The dehydration temperature affects how many close-packed oxygen lattice with aluminum ions in the octahedral (Al^{VI}) and tetrahedral (Al^{IV}) interactions are formed during dehydration. [330] It has been found that more aluminum ions in the octahedral interaction are formed if dehydrating the precursor at higher temperature. The surface activity is influenced by the number of cations in tetrahedral and octahedral positions. Previous research has shown that tetrahedrally coordinated Al^{3+} (cation vacancy) possesses higher activity than octahedrally coordinated Al^{3+}. [321, 327, 349, 349] Moreover, Morterra *et. al.* [331] indicated that the high-temperature transition phases are definitely less active than the low-temperature phase. Wilson *et. al.* reported that the cation

vacancies on δ-Al_2O_3 are essentially located in octahedral sites. [332] It is reasonable to assume that there is a smaller fraction of tetrahedrally coordinated Al^{3+} ions existing in high-temperature transition alumina than in low-temperature transition alumina.

2.4.2.2 Surface Activity

An Al_2O_3 surface has a high population of surface impurities (including hydroxyls, water, carbonates and organics with alkyl groups) as well as surface defect sites. Under moderate temperature, the defect sites (active sites) are de-activated by the covering of impurities. [333] Thermally treating aluminum oxide typically is accompanied by weight loss. The weight loss implies the removal of chemisorbed or physisorbed impurities on aluminum surface. The IR bands of surface impurities on aluminu oxide had been reported by Costa *et. al.*. [340, 342, 352, 355] The bands with higher frequency, 3800-3000 cm^{-1}, are attributed to surface hydroxyl groups. Two small bands between 1600-1400 cm^{-1} are due to carboxylate species, including CO_2, CO, CO_3^{2-} or HCO_3^-. The band between 2960-2860 cm^{-1} corresponds to H-C stretching. Weight loss during thermal treatment is mostly associated with the removal of water and hydroxyl groups. [333, 335]

Knözinger *et. al.* studied the dehydration temperature of surface hydroxyl groups and found that 90.4% of surface hydroxyl content is eliminated at 670^oC. [321, 326] For the removal of the hydroxyl with multi-coordination, the removal of surface hydroxyl creates an oxygen ion in the outermost layer and an aluminum ion in next lower layer. The exposed cation is thought of as a “hole” (vacancy, or surface defect) and acts as a Lewis acid site. It was suggested by Cauwelaert *et. al.* [333] that the surface reactivity is developed right after the removal of surface species and is associated with the population and type of coordinately unsaturated ions on the aluminum oxide surface. Further dehydration at higher temperature leads to the migration of ions. The high temperature transition aluminum oxide phase is formed slowly. In contrast with low temperature transition phase, e.g. γ-Al_2O_3, the aluminum oxide with high temperature transition phase, e.g. δ-Al_2O_3, has less activity due its higher order lattice structure. [331]

Concluding from previous studies, it was found that the stretching frequencies of hydroxyl groups vary with the adjacent surface sites. The variation in the stretching frequency of

surface hydroxyl is due to the interactional strength between hydroxyl and adjacent sites and reflects the perturbation of the hydroxyl group. Type I hydroxyl is considered as the most perturbation group since the restriction from neighboring cations is less in contrast with type II and III hydroxyls. Therefore, it is reasonable to suppose that type I isolated hydroxyl possesses higher catalytic reactivity and the catalytic reactivity of surface hydroxyl is in the order: type I > type II > type III. This hypothesis is in agreement with the study of Rinaldi and his co-workers. [327]

2.4.2.3 Surface Hydroxyl Groups

The surface of aluminum oxide abounds in hydroxyl groups and water. Peri and Cantrell indicated respectively that the densities of water and surface hydroxyl groups and on aluminum oxide are 1.25×10^{19} OH/m^2 and 13 $H_2O/Å^2$. [334, 335, 336] Surface hydroxyls result from the dissociation of water on coordinatively unsaturated surface sites (Al^{3+} and O^{2-}). In the IR spectrum, surface hydroxyl and molecular water appear at high (3800-3000 cm^{-1}) and low (~1630 cm^{-1}) frequencies. Costa supposed that the band at 1630 cm^{-1} in the IR spectrum of aluminum oxide is due to the bending of molecular water. [340] This band disappears after dehydrating at 200^oC. [344] Further thermal dehydration from 200^oC under vacuum leads to the decomposition of the associated OH to evolve water and is accompanied by the formation of isolated OH and unsaturated active sites (Al^{3+} and O^{2-}). [354] The bands appearing in the interval from 3800-3000 cm^{-1} are due to surface hydroxyl groups. Busca *et. al.* elucidated that the stretching frequencies of surface hydroxyl groups are associated with the surface structure and the modifications of alumina. [337] Indeed, the surface acid-base properties, reactivity and topography can be assumed after the surface hydroxyls are identified. A few models have described a correlation between hydroxyl configurations and the surface structure of alumina. [321, 346, 348, 349, 351] Knözinger's model is used more frequently, because Knözinger's model completes the previous models by adding the considerations of the coordination of surface hydroxyl, the number of nearest neighbor cations, and the coordination of the surface cation (including Al^{IV} and Al^{VI}). [321]

2.4.2.3.1 Knözinger's Model

In the IR spectrum of alumina, the IR bands in the interval from 3800 to 3000 cm^{-1} are ascribed to hydroxyl groups. The interaction between neighbor hydroxyls is increased with the formation of hydrogen bonds and causes the difference both in band shape and band location (frequency). [339] The broad band whose stretching frequency is in the interval 3600-3000 cm^{-1} and centered at 3580 cm^{-1} is assigned to hydrogen bonded hydroxyls. [340, 343] The sharp bands at 3800-3600 cm^{-1} are attributed to isolated hydroxyl groups. [326, 350] Knözinger *et. al.* proposed that the (100), (110) and (111) faces are covered by hydroxyl and there are five different types of hydroxyl groups (type I_a, I_b,II_a, II_b and III) on alumina. [321, 326] The difference between each type is associated with the net charge (σ) and the configuration of the hydroxyl group. (as seen in **Figure 2.20**) Net charge is calculated from the strength of the electrostatic bond between cation and anion, as shown in **Equation 2-10**. For example, the charge and the coordination number of the Al cation which bonds to type I_a hydroxyl group are +3 and 4, respectively. Subsequently, the net charge of I_a hydroxyl groups is 1-2+3/4= -0.25.

$$C_{Net} = C_{hydrogen} + C_{oxygen} + \frac{C_{cation}}{n_{anion}} \qquad (2\text{-}10)$$

where C_{net} is the net charge of a hydroxyl group. For the hydroxyl group on aluminum oxides surface, $C_{hydrogen}$, C_{oxygen}, C_{cation} are the charges of hydrogen, oxygen and aluminum and equal +1, -2 and +3 respectively. n_{anion} represents the number of adjacent anions for the cation (coordination number). [321, 331]

On well crystallized sample surfaces, the band at 3775 cm^{-1} has a relatively high intensity and is sensitive to various probe molecules. It was suggested by Nortier *et. al.* [347] that the hydroxyl group with a stretching frequency of 3775 cm^{-1} is a type I isolated hydroxyl, possibly formed on edges or on (100) faces. Costa *et. al.* used FT-IR to study nanocrystalline γ-Al_2O_3 and demonstrated that type I, II and III isolated hydroxyls give IR features at 3790-3770, 3730-3720, and 3680-3590 cm^{-1}. [331, 340, 352, 353] The large band between 1000-400 cm^{-1} is a characteristic adsorption band of transition alumina. Al^{IV} and Al^{VI} are two general transformations. The terminal hydroxyl group over one tetrahedrally coordinated aluminum ion (type I_b) is assumed to have a lower frequency than that over one octahedrally coordinated aluminum ion (type I_a). [331] The difference in their frequencies is about 60 [321] – 20 [331,

349] cm^{-1}. Therefore, it can be assumed that the stretching frequency of type II_a isolated hydroxyl group is higher than that of type II_b isolated hydroxyl groups. The relative stretching frequencies of the surface hydroxyl groups in various configurations are shown in **Figure 2.21**.

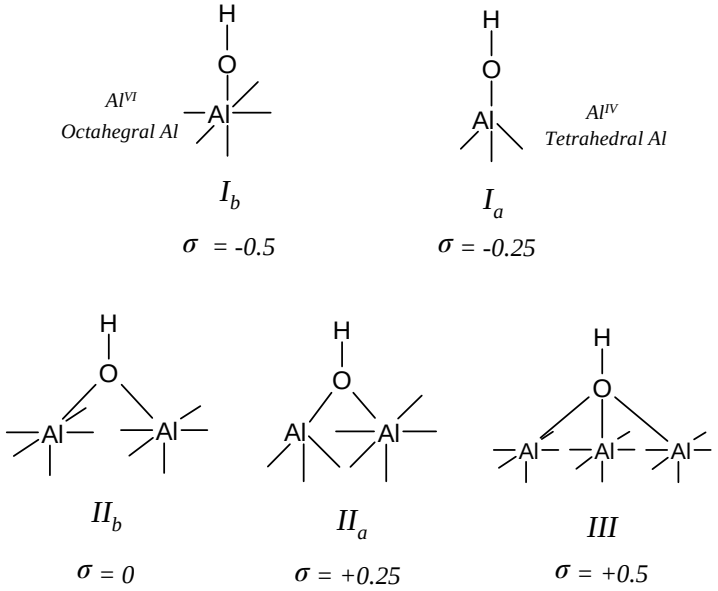

Figure 2.20 The configurations and net charges of surface hydroxyl groups on aluminum oxide.

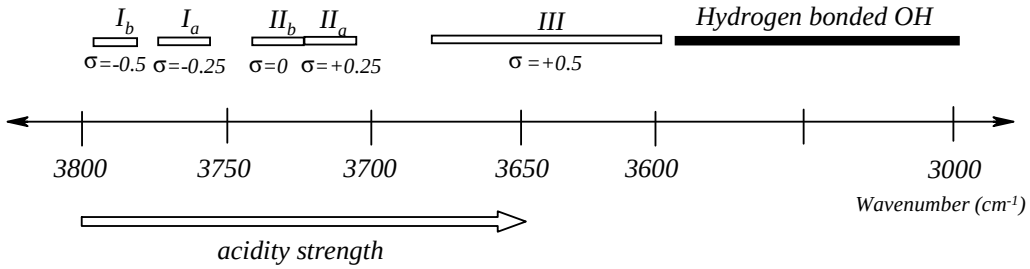

Figure 2.21 The stretching frequencies and acid-base properties of surface hydroxyl groups on γ-Al_2O_3.

2.4.2.3.2 Thermal Stability of Surface Hydroxyls and Activities of the Corresponding Ions

It was demonstrated by Gadzhieva *et. al.* that thermally treating Al_2O_3 at T=973 K under vacuum ($P=10^{-5}$ Pa) for 8 hours can remove most impurities, such as hydroxyls, water and carbonates, from the surface. [355] In contrast with isolated hydroxyl groups, hydrogen bonded hydroxyls are less thermally stable. Borello *et. al.* found the interaction between neighboring

hydroxyl groups (hydrogen bond) decreases when treating aluminum oxide samples at 470^{o}C under evacuation. [344, 345] When thermally treating Al_2O_3, the hydrogen bonded hydroxyls are initially removed or converted to isolated hydroxyl companied by the breakdown of hydrogen bond. For the thermal stability of isolated hydroxyls, type III isolated hydroxyl has lowest thermal stability by comparison with type II and type I isolated hydroxyl. The thermal stability of isolated hydroxyl groups in different configurations follows the order shown in **Equation 2-11**. [344] Upon heating to 800 K, all hydrogen bonded hydroxyls are removed; isolated hydroxyls are removed at 1200 K. [354]

$$\textit{Type III} < \textit{Type I} < \textit{Type II} \qquad (2\text{-}11)$$

Surface hydroxyl groups can be acidic, basic or neutral depending on their location on the surface of aluminum oxide. The comparison between the acid-base character and stretching frequency of hydroxyl groups in different types is shown in **Figure 2.21**.

2.4.2.3 Acid-Base Properties

It is well known that the acid-base and catalytic properties on aluminum oxide surface can be modified by the presence of unsaturated ions (Al^{3+} and O^{2-}) and impurities, e.g. hydroxyls. In earlier research, the surface acid-base properties of aluminum oxide usually were detected by using probe molecules cooperating with infrared spectroscopy. For example, the acid-base properties of surface OH and active sites had been detected by using organic compounds, such as benzene, toluene, acetonitrile, pyrazine and pyridine, and CO. [354, 358]

Hydroxyl groups on aluminum oxide have been assumed to supply protons, either directly or indirectly in certain reactions. [356, 327, 328, 329] Surface hydroxyl groups on aluminum oxide are considered to be a Bønsted acid site. [327] According to Knözinger's study [321], the acidic strength of surface hydroxyl is associated with the net charge (δ). The hydroxyl with type III configuration ($\delta_{\text{type III}}$=+0.5) is the most acidic group and hydroxyls with terminal configurations (type I_a and I_b, $\delta_{\text{type Ib}}$=-0.5 and $\delta_{\text{type Ib}}$=-0.25) are less acidic and more labile groups. (as seen in **Figure 2.21**). Hiemstra *et. al.* reported that the difference between the acid strength of type I_a and III is of the order of 10^8. [359]

On the other hand, the exposed aluminum cations and oxygen anions act as Lewis-acidic and Lewis-basic centers. At low temperature, the Lewis-acid and -base sites are blocked by hydroxyl groups. The active sites are created during the thermal dehydration procedure. Hiemstra *et. al.* found that the Lewis-acid sites double as temperature is increased from 150 to 500^{o}C. [360] For the acid-base strength of the active sites, Vigué *et. al.* [321, 331, 352, 353] suggested that the aluminum ion monocoordinated to type I_a hydroxyl group (Al^{IV}, tetrahedral aluminum) is the most basic sites and active site with respect to chlorination reaction. The acidity strength of surface ions is associated with their coordination; the higher coordination, the more acidity.

2.5 Chemical Surface Modifications

Surface modification is an efficient means to improve the dispersion [361, 362], surface behavior [363] as well as to modify surface acid-base properties for metal oxide particles. In early studies, chemical grafting has been widely used to change the surface properties of metal oxides [364, 365] and has been utilized to evaluate the surface reactivity of metal oxides [296]. (2-chloroethyl)ethyl sulfide (2-CEES), hexamethyldisiloxane (HMDS) and acetic acid (AA) have been found to selectively react with hydroxyl groups on metal oxide surfaces. During reaction, the grafting species substitute for the adsorbed hydroxyl groups, adsorb on the surface, and block the active sites (M^{n+} and O^{2-}).

2.5.1 (2-chloroethyl)ethyl sulfide (2-CEES)

2-CEES contains a sulfur and a chlorine functional group. Both functional groups are capable of interacting with the active sites on metal oxides. The hydrolysis reaction of 2-CEES first had been reported by Yang *et. al.* [366, 367] Mawhinney *et. al.* investigated the reaction mechanisms of 2-CEES on aluminum oxide [368, 369] and indicated that the hydrolysis reaction of 2-CEES on aluminum oxide is temperature-dependent.

At moderate temperatures (303-473 K), the chlorine moiety of 2-CEES selectively binds to isolated hydroxyl groups on aluminum oxide and converts isolated hydroxyl groups to associated hydroxyl group (hydrogen bonded hydroxyl). [368] The conversion of isolated hydroxyl group has been shown through infrared spectroscopy. Narske *et. al.* reported a

diminution of the band at 3750-3700 cm^{-1} [370] on MgO, at 3800-3678 cm^{-1} [369, 371, 372] on Al_2O_3 and at 3720-3640 cm^{-1} on TiO_2 [373, 374] upon interaction with 2-CEES. These decreases in bands associated with isolated hydroxyls were accompanied by an increase in intensity of bands associated with hydrogen bonded hydroxyl. [371]

The hydrolysis reaction of 2-CEES on aluminum oxide occurs above 473 K. At high temperature, adsorbed 2-CEES is converted into adsorbed alkoxy species, liberating HCl. This is shown in **Figure 2.22 A**. Mawhinnery *et. al.* stated that the hydrolysis of 2-CEES can be characterized by a carbon-oxygen stretching mode in the IR spectrum with a peak at 1100 cm^{-1} or by the released HCl which appears as several weak peaks in the range of 2880-2700 cm^{-1}. [369] The hydrolysis reaction of 2-CEES can also be characterized by the variation of the intensity ratio of $\upsilon(CH_2)$ to $\upsilon(CH_3)$ in the IR spectrum. Thompson *et. al.* investigated the reaction of 2-CEES on TiO_2 and pointed out that the bands at 2978 and 2943 cm^{-1} are due to the asymmetric $\upsilon(CH_2)$ and $\upsilon(CH_3)$ modes respectively. [373] The band at 2887 cm^{-1} is due to overtones of the $\delta(CH_2)$ and $\delta(CH_3)$ modes which are intensified by Fermi resonance. [373] They found that the increases in the peak intensities of asymmetric $\upsilon(CH_3)$ and two overtones $\delta(CH_2)$ and $\delta(CH_3)$ modes is accompanied by the decrease of asymmetric $\upsilon(CH_2)$ as temperature was increased from 255-514 K. The change in adsorption ratio in this case is due to structural and configurational changes of 2-CEES and is irrespective for the increase of 2-CEES coverage.

Besides isolated hydroxyl groups, Lewis acid and base sites (Al^{3+} and O^{2-} pair) also are involved in the conversion reaction of 2-CEES. Especially for highly dehydrated aluminum oxide, the conversion reaction of 2-CEES is dominated by nucleophilic attack ,as seen in **Figure 2.22 B**. Both $C_2H_5SCH_2CH_2$-O^{2-} and Cl-Al^{3+} remain on the aluminum oxide surface after the reaction. [369, 375] Mawhinnery *et. al.* reported that this nucleophilic attack is inhibited as the Lewis acid-base sites are blocked by other adsorbed molecules, such as pyrindine. [369] Therefore, the adsorption of 2-CEES on aluminum oxide occurs mainly through the hydrolysis reaction when the surface abounds in hydroxyl groups.

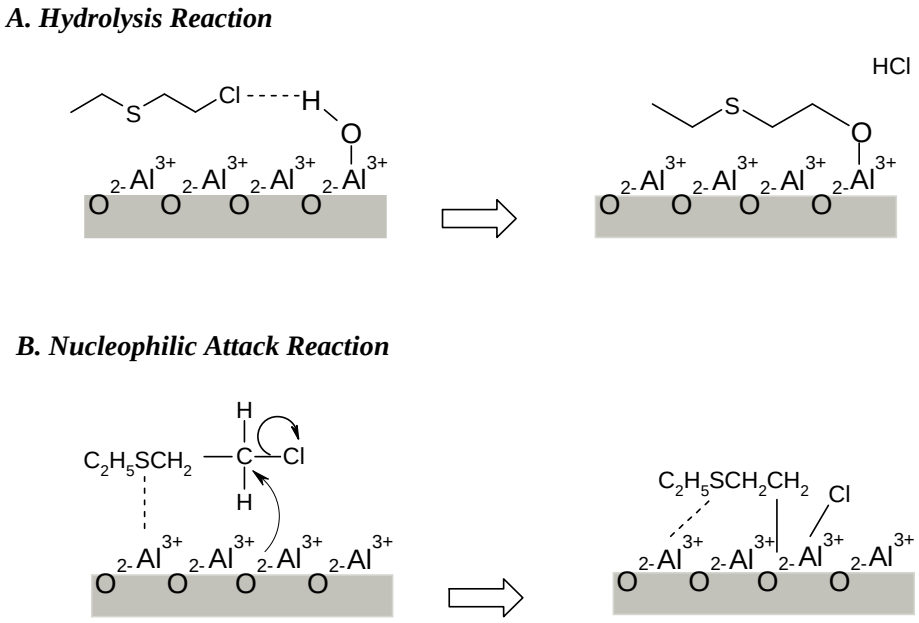

Figure 2.22 Hydrolysis and nucleophilic attack pathways for 2-CEES on Al_2O_3.

2.5.2 Hexamethyldisiloxane (HMDS)

Chemically replacing surface Brønsted (hydroxyl groups) sites [376, 377, 378] or removing Lewis (coordinatively unsaturated cations and anions) sites [364] by silyl ether groups (-O-$SiMe_3$) is termed as silation. Silation is frequently used to modify the surface of oxides in analytical, separations and catalytic processes. For example, since the outmost layer of an oxide is covered by silyl ether groups after siliation, the metal oxide surface becomes less hydrophilic. [379, 380, 381] This helps the dispersion ability of metal oxide particles in non-polar solvents. Paul *et. al.* reported that the degradation of catalyst is prevented when the isolated Al-OH groups on Rh/Al_2O_3 are replaced by silyl ether groups under the conditions where CO adsorption occurs. [380] Rosenthal *et. al.* reported that the Brønsted sites (hydroxyl groups) are the active sites on silica-alumina catalyst for the conversion of cumene. The poisoning of the catalyst for cumene cracking occurred with the elimination of Brønsted sites by attachment of silyl ether fragments after the treatment of HMDS. [296] Matsumiya *et. al.* evaluated the catalytic activity of platinum by poisoning the active site using HMDS. [382]

HMDS has been used as silating agent for more than forty years. HMDS attacks Brønsted sites (hydroxyl groups) on a metal oxide, leaving a silyl ether group (-O-$SiMe_3$) after the reaction (see **Equation 2-12**). [364, 376, 377, 378] Hertl *et. al.* [376, 377, 379] indicated that HMDS selectively reacts with isolated hydroxyl groups on metal oxides. Hydrogen bonded hydroxyls are essentially nonreactive toward HMDS. On a dehydrated metal oxide surface, Slavov *et. al.* [364] proposed that the reaction of HMDS with aluminum oxide is initially a dissociative process from reaction with coordinatively unsaturated sites (Al^{3+} and O^{2-}). This is shown in **Equation 2-13**. Ammonia is liberated from the further dissociative reaction after the transfer of two hydrogen atoms to the nitrogen center of the $-NMSiMe_3$ group.

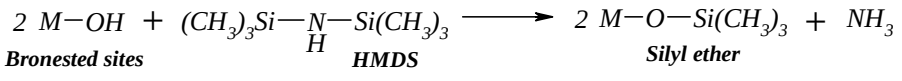

(2-12)

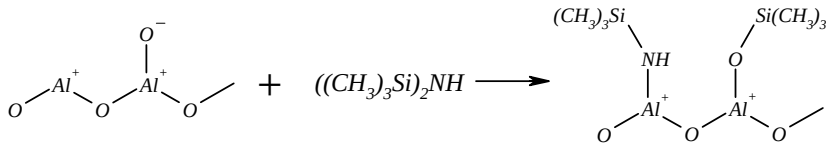

(2-13)

The dissociative chemisorption of HMDS either on hydrated or dehydrated metal oxides typically is characterized by FT-IR. Paul *et. al.* found that the attachment of –O-$Si(Me)_3$ group on Al_2O_3 leads to the disappearance of isolated OH modes at 3716 and 3670 cm^{-1} with concomitant formation of the characteristic $\upsilon(CH_3)$ and $\delta(CH_3)$ vibrational modes at 2958 ($\upsilon_{as}(CH_3)$), 2907 ($\upsilon_s(CH_3)$), 1446 ($\delta_{as}(CH_3)$), 1414 ($\delta_{as}(CH_3)$) and 1261 ($\delta_s(CH_3)$) cm^{-1}. [380] Slavov *et. al.* reported that the dissociation chemisorption of HMDS on dehydrated Al_2O_3 is temperature-dependent. They noted an increase in relative intensity of the Si-O band in the region of 1100 cm^{-1} as temperature increased. [364]

2.5.3 Acetic Acid (AA)

Similar to the dissociated chemisorption of 2-CEES and HMDS on metal oxides, the chemisorption of acetic acid is irreversible. [385] Evans *et. al.* noted that acetate species in

different configurations are formed after the chemisorption of acetic acid on metal oxide surfaces, as seen in **Figure 2.23**. [383, 384]

Characterizing the chemisorption of acetic acid on MgO and Al_2O_3, FT-IR spectroscopy is frequently employed. Hasan *et. al.* indicated that the isolated hydroxyl groups on aluminum oxide are involved in the reaction of acetic acid. They observed a negative adsorption in the region 3800-3680 cm^{-1} after aluminum oxide was treated with acetic acid. [385] Symmetric carboxylate (CO_2^-) in the region from 1480-1390 cm^{-1} (two bands) and asymmetric carboxylate at 1608 cm^{-1} appear following the bonding of acetate on oxidized alumina. [386, 387] The symmetric and asymmetric CH_3 stretching vibrations were observed at 2937 cm^{-1} and 1337 cm^{-1}. [386]

The IR spectrum of the chemisorption of acetic acid on MgO have been reported by Xu *et. al.*. [384, 388, 389, 390] The peaks in the region 1655-1630 cm^{-1} and 1360-1300 cm^{-1} are correlated with symmetric and asymmetric carboxylate vibration respectively. The peaks in the region 2975-2920 cm^{-1} and the peaks at 1416 and 1432 cm^{-1} are due to the C-H stretching of acetate group. [384, 388, 389, 390]

Foster *et. al.* observed severe topographical change accompany the reaction between MgO (100) and water or acetic acid through atomic force microscopy (AFM). [388] **Figure 2.24** shows these changes. Zecchina *et. al.* indicated that surface erosion occurs upon vapor treating the MgO surface. [245, 249, 274, 275, 284] Therefore, the change in the topography on MgO caused by the surface treatment of acetic acid is likely due to surface erosion.

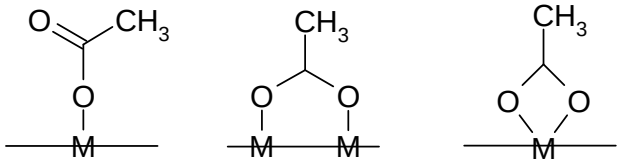

Monodentate *Bidentate Bridging* *Bindentate Chelating*

Figure 2.23 The possible binding configurations of acetate species on metal oxides.

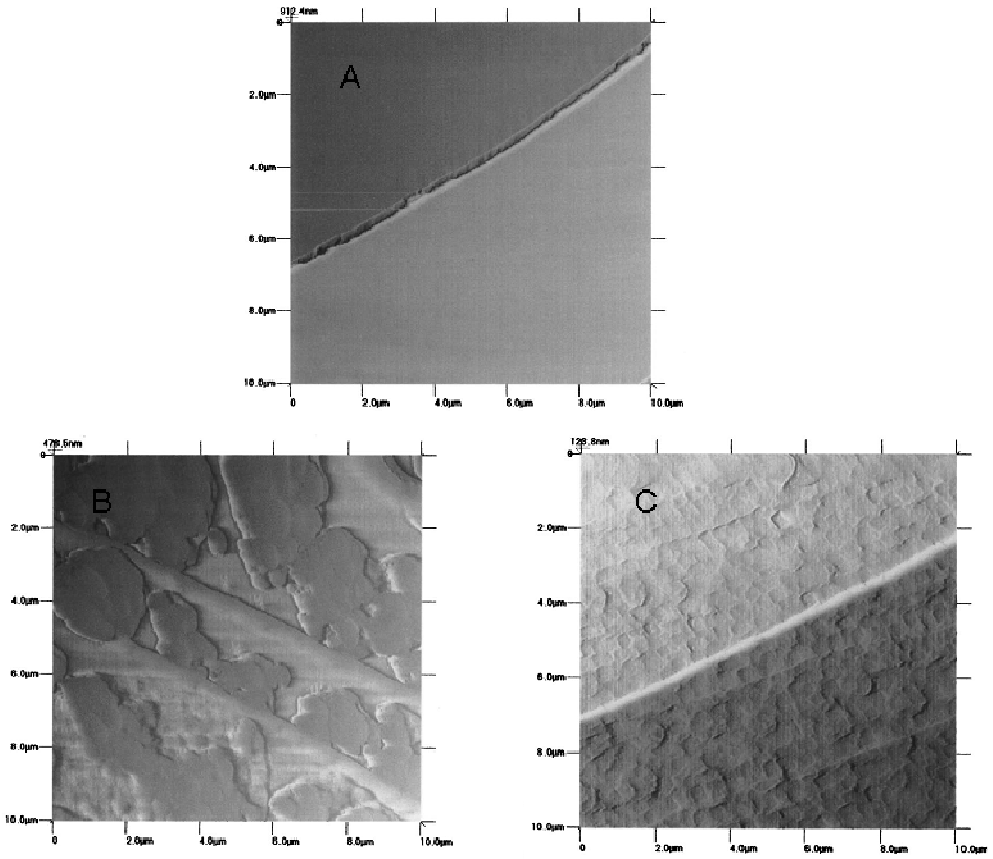

Figure 2.24 AFM images taken from (A) clean MgO (100). (B) MgO (100) exposed to 19 Torr of H_2O for 100 hours. (C) MgO (100) exposed to 12 Torr of acetic acid for 1 hour. [388]

2.6 References

1 Montano, L. A. and Ingle, J. D., *Anal. Chem.*, **1979**, 51, 926.

2 Marino, D. F.; Wolff, F., and Ingle, D. J., *Anal. Chem.*, **1979**, 51, 2051.

3 Mendenhall, G. D., *Angew. Chem. Int. Ed. Engl.*, **1977**, 16, 225.

4 Williams, D. C. and Seite, W. R., *Anal. Chem.*, **1976**, 48, 1478.

5 Hummelen, J. C.; Luider, T. M., and Wynberg, H. in *Complementary Immunoassays*; Collins, W. P. ed.; John Wiley & Sons Ltd: New York, **1988**; Chapter 14.

6 Lakowicz, J. R.; Piszczek, G. and Kang, J. S., *Anal. Biochem.*, **2001**, 288, 62.

7 Adam, W and Cilento, G., *Angew. Chem. Int. Ed. Engl.*, **1983**, 22, 529.

8 Kopecky, K. P.; Lockwood, P. A.; Filby, J. E. and Reid, R. W., *Can. J. Chem.*, **1973**, 51, 468.

9 Kopecky, K. P.; Filby, J. E.; Mumford, C.; Lockwood, P. A., and Ding, J. Y., *Can. J. .Chem.*, **1975**, 53, 1103.

10 Turro, N. J.; Ito, Y.; Chow, M.-F.; Adam, W.; Rodriguez, O., and Yany, F., *J. Am. Chem. Soc.*, **1977**, 99, 5836.

11 Turro, N. J.; Chow, M.-F. and Ito, Y., *J. Am. Chem. Soc*., **1978**, 100, 5580.

12 Berger, A. W.; Driscoll, J. N. and Pirog, J. A., *Photochem. and Photobio.*, **1965**, 4, 1123.

13 Rauhut, M. M., *Acc. Chem. Res.*, **1969**, 2, 80.

14 Zollinger, H. in *Color Chemistry: Syntheses, Properties and applications of Organic Dyes and Pigments*; VCH: New York, **1987**.

15 Gold, V. and Bethell, D. in *Advance in Physical Organic Chemistry*; Academic Press: New York, **1982**; V 18.

16 Schuster, G. B.; Dixon, B.; Koo, J.-Y.; Schmidt, S. P. and Smith, J. P., *Photochem. and Photobiol.*, **1979**, 30, 17.

17 Adam, W., and Yany, F. in *The Chemistry of Heterocyclic Compounds*, Part 3; John Wiley and Sons: New York, **1983**.

18 Rauhut, M. M.; Bollyky, L. J.; Roberts, B. G.; Loy, M.; Whitman, R. H.; Iannotta, A. V.; Semsel, A. M. and Clarke, R. A., *J. Am. Chem. Soc.*,**1967**, 89, 6515.

19 Tseng, S.-S.; Mohan, A. G.; Haines, L. G.; Vizcarra, L. S. and Rauhut, M. M., *J. Org. Chem.*, **1979**, 44, 4113.

20 Rauhu, M. M.; Roberts, B. G. and Semsel, A. M., *J. Am. Chem. Soc.*, **1966**, 88, 3604.

21 Bollyky, L. J., *J. Am. Chem. Soc.*, **1970**, 92, 3230.

22 Adam, W. and Sakanishi, K., *J. Am. Chem. Soc.*, **1978**, 100, 3935.

23 Adam, W.; Alzerreca, A.; Liu, J.-C. and Yany, F., *J. Am. Chem. Soc.*, **1977**, 99, 5768.

24 Haun, M.; Durán, N. and Cilento, G., *Biochem. Biophys. Res. Commum.*, **1978**, 81, 779.

25 Fletcher, A. N. and Heller, C. A., *J. Phys. Chem.*, **1967**, 71, 1507.

26 Orf, H. W. and Dolphin, D., *Proc. Nat. Acad. Sci. USA*, **1974**, 71, 2649.

27 Bollyky, L. J.; Whitman, R. H.; Roberts, B. G. and Rauhut, M. M., *J. Am. Chem. Soc.*, **1967**, 89, 6523.

28 Gundermann, K.-D. and McCapra, F. in *Chemiluminescence in Organic Chemistry*; Springer-Verlag: New York, **1987**; Chapter VII.

29 Bard, A. J. in *Electrogenerated Chemiluminescence*; CRC press: New York, **2004**.

30 Vitt, J. E., Johnson, D. C., and Engstrom, R. C., *J. Electrochem. Soc.*, **1991**, 138, 1637.

31 Tokel-Takvoryan, N. E.; Hemingway, R. E. and Bard, A. J., *J. Am. Chem. Soc.*, **1973**, 95, 6582.

32 Faulkner, L. R. and Bard, A. J., *J. Am. Chem. Soc.*, **1968**, 90, 6284.

33 Rubinstein, I. and Bard, A. J., *J. Am. Chem. Soc.*, **1981**, 103, 512.

34 Lindino, C. A. and Bulhões, L. O. S., *J. Braz. Chem. Soc.*, **2004**, 15, 178.

35 Schuster, G. B. and Schmidt S. P. in *Advance in Physical Organic Chemistry*; Gold, V. and Bethell, D., Eds; Academic Press: New York, **1982**.

36 Adam, W., and Cilento, G. in *Chemical and Biological Generation of Excited States*; Academica Press.: New York, **1982**, Chapter 6.

37 Matsumoto, M, *J. Photochem. Photobio. C: Photochem. Rev.*, **2004**, 5, 27.

38 Blakey, I.; George, G. A. and Billingham, N. C., *Macromolecules*, **2001**, 34, 9130.

39 Catherall, C. L. R.; Palmer, T. F. and Cundall, R. B., *J. Chem. Soc., Faraday Trans. 2*, **1984**, 80, 837.

40 Sigvardson, K. W.; Kennish, J. M. and Birks, J. W., *Anal. Chem.*, **1984**, 56, 1096.

41 Motoyoshiya, J.; Sakai, N.; Imai, M.; Yamaguchi, Y.; Koike, R.; Takaguchi, Y. and Aoyama, H., *J. Org. Chem.*, **2002**, 67, 7314.

42 Koo, J.-Y. and Schuster, G. B., *J. Am. Chem. Soc.*, **1977**, 99, 6107.

43 Koo, J.-Y., and Schuster, G. B., *J. Am. Chem. Soc.*, **1978**, 100, 4496.

44 Campbell, A. K. in *Chemiluminescence: principles and Application in Biology and Medicine*; VCH: New York, **1988**; Chapter 1.

45 Solovyov, K. N. and Borisevich, E. A., *Physics-Uspekhi*, **2005**, 48, 231.

46 Turro, N. J.; Lechtken, P.; Schuster, G.; Orell, J. and Steinmetzer, H. C., *J. Am. Chem. Soc.*, **1974**, 96, 1627.

47 Turro, N. J. and Lechtken, P., *J. Am. Chem. Soc.*, **1973**, 95, 264.

48 Krasovitskii, B. M., and Bolotin, B. M. in *Organic Luminescent Materials*; VCH: New York, **1988**.

49 Campbell, A. K. in *Chemiluminescence: Principles and Applications in Biology and Medicine*; VCH: New York, **1988**; Chapter 9.

50 Behera G. B.; Mishra, B. K.; Behera, P. K. and Panda, M., *Adv. Coll. Int. Sci.*, **1999**, 82, 1.

51 Behera, P. K.; Mukherjee, T. and Mishra, A. K., *J. Luminescence*, **1995**, 65, 131.

52 Behera, P. K.; Mukherjee, T. and Mishra, A. K., *J. Luminescence*, **1995**, 65, 137.

53 Arnaut, L. G. and Formosinho, S. J., *J. Photochem. Photobio. A: Chem.*, **1993**, 75, 1.

54 Borsarelli, C. D.; Chesta, C. A.; Cosa, J. J.; Crystall, B. and Phillips, D., *Chem. Phys. Lett.*, **1995**, 232, 103.

55 Collin, J.-P.; Harriman, A.; Heitz, V.; Odobel, F. and Sauvage, J.-P., *J. Am. Chem. Soc.*, **1994**, 116, 5679.

56 Sirish, M. and Maiya, B. G., *J. Photochem. Photobio. A: Chem.*, **1995**, 85, 127.

57 Wilson, T, and Schaap, P, *J. Am. Chem. Soc.*, **1971**, 93, 4126.

58 Adam, W. and Cilento, G. in *Chemical and Biological Generation of Excited States; Academic Press.*: New York, **1982**; Chapter 4.

59 Belyakov, V. A. and Vassil'ev, R. F., *Photochem. Photobiol.*, **1970**, 11, 179.

60 Adam, W.; Rodriguez, O. and Zinner, K., *J. Org. Chem.*, **1978**, 43, 4495.

61 Campbell, A. K. in *Chemiluminescence: principles and Application in Biology and Medicine*; VCH: New York, **1988**; Chapter 2

62 Rauhut, M. M.; Roberts, B.G.; Maulding, D. R.; Bergmark, W. and Coleman, R., *J. Org. Chem.*, **1975**, 40, 330.

63 Loutfy, R. O. and Arnold, B. A., *J. Phys. Chem.*, **1982**, 86, 4205.

64 Adam, W.; Matsumoto, M. and Trofimov, V., *J. Am. Chem. Soc.*, **2000**, 122, 8631.

65 Haidekker, M. A.; Brady, T. P.; Lichlyter, D. and Theodorakis, E. A., *Bioorg. Chem.*, **2005**, 33, 415.

66 Akers, W. and Haidekker, M. A., *J. Biomech. Eng.*, **2004**, 126, 340.

67 Haidekker, M. A. and Theodorakis, E. A., *Org. Biomol. Chem.*, **2007**, 5, 1669.

68 Haidekker, M. A.; Akers, W.; Lichlyter, D.; Brady, T. P. and Theodorakis, E. A., *Sensor Lett.*, **2005**, 3, 42.

69 Gregory, P. in *High-Technology Applications of Organic Colorants*; Plenum Press: New York, **1991**.

70 Fleurat-Lessard, P. and Volatron, F., *J. Phys. Chem.* A, **1998**, 102, 10151.
71 Carpenter, W., *J. Org. Chem.*, **1965**, 30, 3082.
72 Burkholder, C. and Dolbier, W. R., *J. Org. Chem.*, **1998**, 63, 5385.
73 Kuroboshi, M.; Waki, Y. and Tanaka, H., *J. Org. Chem.*, **2003**, 68, 3938.
74 Hammond, P. R. and Knipe, R. H., *J. Am. Chem. Soc.*, **1967**, 89, 6063.
75 Freeman, T. M. and Seitz, W. R., *Anal. Chem.*, **1981**, 53, 98.
76 Shefler, S.; Little, S. M.; Mills, J. H.; Mex., N. and Humiston, L. E., *U.S. Patent 3,732,413*, **1973**.
77 Viehbeck, A.; Buchwalter, S. L.; Goldberg, M. J.; Kovac, C. A. and Tisdale S. L., *U.S. Patent 5,135,779*, **1992**.
78 Shefler, S., *U.S. Patent 3,697,434*, **1972**.
79 Heller, C. A.; Richter, H. R. and McEwan, W. S., *U.S. Patent 3,729,425*, **1973**.
80 Pruett, R. L.; Barr, J. T.; Rapp, K. E.; Bahner, C. T.; Gibson, J. D. and Lafferty, R. H., *J. Am. Chem. Soc.* , **1950**, 72, 3646.
81 Bock, H.; Borrmann, H.; Havlas, Z.; Oberhammer, H.; Ruppert, K. and Simon, A., *Angew. Chem. Int. Ed. Engl.*, **1991**, 30, 1678.
82 Soep, B.; Mestdagh, J. M.; Sorgues, S. and Visticot, J. P., *Eur. Phys., J. D.*, **2001**, 14, 191.
83 Nakato, Y.; Ozaki, M. and Tsubomura, H., *Bull. Chem. Soc. Japan*, **1972**, 45, 1299.
84 Waring, C. E. and Berard, R. A., *J. Phys. Chem.*, **1976**, 80, 1025.
85 Urry, W. H. and Sheeto, J., *Photochem. Photobiol.*, **1965**, 4, 1067.
86 Huang, C.-C.; Hohn, K. L. and Schlup, J. R., submitted to *J. Physic. Chem. C*, **2009**, 113 (25), 11050.
87 Huang, C.-C. Hohn, K. L., submitted to *Langmuir*, January **2009**.
88 Paris, J. P., *Photochem. Photobiol.*, **1965**, 4, 1059.
89 Fletcher, A. N. and Heller, C. A., *J. Phys. Chem.*, **1967**, 71, 1057.
90 Fletcher, A. N., *J. Phys. Chem.*, **1969**, 73, 3686.
91 Fletcher, A. N. and Heller, C. A., *J. Catal.*, **1966**, 6, 263.
92 Toby, S. T.; Astheimer, P. A. and Toby, F. S., *J. Photochem. Photobiol. A: Chem.*, **1992**, 67, 1.
93 Orf, H. W. and Dolphin, D., *Proc. Nat. Acad. Sci. USA*, **1974**, 71, 2646.
94 Fletcher, A. N. and Heller, C. A., *Photochem. Photobiol.*, **1965**, 4, 1051.
95 Kuwata, K. and Geske, D. H., *J. Am. Chem. Soc.*, **1964**, 86, 2101.
96 Winberg, H. E.; Carnahan, J. E. and Coffman, D. D., *J. Am. Chem. Soc.*, **1965**, 87, 2054.
97 Rewick, R. T.; Schumacher, M. L.; Shapiro, S. L.; Weber, T. B. and Cavalli-Sforza, M., *Anal. Chem.*, **1988**, 60, 2095.
98 Hammond, P. R. and Knipe, R. H., *J. Am. Chem. Soc.*, **1967**, 89, 6063.
99 Hori, M.; Kimura, K. and Tsubomura, H., *Spectrochimica Acta*, **1968**, 24A, 1397.
100 Winberg, W. E., *US. Paten 3,264,221*, **1960**.
101 Heller, C. A. and Fletcher, A., *J. Phys. Chem.*, **1965**, 69, 3313.
102 Tanaka, K.; Sato, T. and Yamabe, T., *J. Phys. Chem.*, **1996**, 100, 3980.

103 Pokhodnia, K. I.; Papavassiliou, J.; Umek, P.; Omerzu, A. and Mihailovič, D., *J. Chem. Phys.*, **1999**, 110, 3606.
104 Fendler, J. H., *Acc. Chem. Res.*, **1976**, 9, 153.
105 Price, K. E. and McQuade, D. T., *Chem. Commun.*, **2005**, 1714.
106 Yoon, B.; Kim, H. and Wai, C. M., *Chem. Commun.*, **2003**, 1040.
107 Chew, C. H. and Gan, L. M., *J. Disp. Sci. Technol.*, **1990**, 11, 593.
108 Eriksson, S.; Nylén U.; Rojas, S. and Boutonnet, M., *Appl. Catal. A: Gen.*, **2004**, 265, 207.
109 Natarajan, U.; Handique, K.; Mehra, A.; Bellare, J. R. and Khilar, K. C., *Langmuir*, **1996**, 12, 2670.
110 Chhabra, V.; Pillai, V.; Mishra, B. K.; Morrone, A. and Shah, D. O., *Langmuir*, **1995**, 11, 3307.
111 Hao, J., *J. Polym. Sci. Part A: Polym. Chem.*, **2001**, 39, 3320.
112 Stathatos, E. and Lianos, P., *Langmuir*, **1997**, 13, 4295.
113 Eastoe, J.; Hollamby, M. J. and Hudson, L., *Adv. Coll. Int. Sci.*, **2006**, 128, 5.
114 Fendler, J. H., *Chem. Rev.*, **1987**, 87, 877.
115 Silber, J. J.; Biasutti, A.; Abuin, E. and Lissi, E., *Chem. Rev.*, **1999**, 82, 189.
116 Ruckenstein, E. and Nagarajan, *J. Phys. Chem.*, **1980**, 84, 1349.
117 Fendler, J. H., and Fendler, E. J. in *Catalysis in Micellar and Macromolecular System*; Academic Press: New York, **1975**.
118 Barzykin, A. V. and Tachiya, M., *Heter. Chem. Rev.*, **1996**, 3, 105.
119 Paul, B. K. and Moulik, S. P., *Current Sci.*, **2001**, 80, 990.
120 Nagarajan, R. and Ruckenstein, E., *Langmuir*, **2000**, 16, 6400.
121 Tanford, C. in *The Hydrophobic Effect*; Wiley: New York, 2nd ed., **1980**.
122 Rosen, M. J. in *Surfactants and Interfacial Phenomena*; Wiley: New York, third ed., **2004**.
123 Paul, B. K. and Moulik, S. P., *J. Disp. Sci. Technol.*, **1997**, 18, 301.
124 Menger, F. M. and Saito, G., *J. Am. Chem. Soc.*, **1978**, 100, 4376.
125 Olesik, S. V. and Miller, C. J., *Langmuir*, **1990**, 6, 183.
126 Rodenas, E. and Perez-Benito, E., *J. Phys. Chem.*, **1991**, 95, 4552.
127 Brenneck, J. F. and Eckert, C. A., *ACS Symp. Ser.*, **1989**, 406, 14
128 Tomasko, D. L.; Knutson, B. L.; Coppom, J. M.; Windsor, W.; West, B. and Eckert, C. A., *ACS Symp. Ser.*, **1993**, 514, 220.
129 MacDonald, H.; Bedwell, B. and Gulari, E., *Langmuir*, **1986**, 2, 704.
130 Thompson, K. F. and Gierasch, L. M., *J. Am. Chem. Soc.*, **1984**, 106, 3648.
131 Giddings, L. D. and Olesik, V., *Langmuir*, **1994**, 10, 2877.
132 Kotlarchyk, M.; Chen, S.-H.; Huang, J. S. and Kim, M. W., *Phys. Rev. A*, **1984**, 29, 2054.
133 Eastoe, J.; Cazelles, B. M. H.; Steytler, D. C.; Holmes, J. D.; Pitt, A. R.; Wear, T. J. and Heenan, R. K., *Langmuir*, **1997**, 13, 6980.
134 Ray, S. and Moulik, S. P., *Langmuir*, **1994**, 10, 2511.
135 Assih, T.; Larché, F. and Delord, P., *J. Coll. Int. Sci.*, **1982**, 89, 35.

136 Fontell, K., *J. Coll. Int. Sci.*, **1973**, 44, 318.
137 Gan, L. M.; Chow, P. Y.; Liu, Z.; Han, M. and Quek, C. H., *J. Chem. Soc., Chem. Commun.*, **2005**, 4459.
138 Kumar, R.; Kalur, G. C.; Ziserman, L.; Danino, D. and Raghavan, S. R., *Langmuir*, **2007**, 23, 12849.
139 Farago, B. and Richter, D., *Phys. Rev. Lett.*, **1990**, 65, 3348.
140 Palazzo, G.; Lopez, F.; Giustini, M.; Colafemmina, G. and Ceglie, A, *J. Phys. Chem. B*, **2003**, 107, 1924.
141 Lianos, P.; Modes, S.; Staikos, G. and Brown, W., *Langmuir*, **1992**, 8, 1054.
142 Sakai, H.; Kawahara, H.; Shimazaki, M. and Abe, M., *Langmuir*, **1998**, 14, 2208.
143 Farago, B. and Richter, D., *Phys. Rev. Lett.*, **1990**, 65, 3348.
144 Fendler, J. H., *Acc. Chem. Res.*, **1976**, 9, 153.
145 García-Mateos, I.; Velázquez, M. M. and Rodríguez, L. J., *Langmuir*, **1990**, 6, 1078.
146 Stam, J. V.; Depaemelaere, S. and Schryver, C. D., *J. Chem. Edu.*, **1998**, 75, 93.
147 Huang, X.; Yang, J.; Zhang, W.; Zhang, Z. and An, Z., *J. Chem. Edu.*, **1999**, 76, 93.
148 Mandal, A. B.; Nair, B. U. and Ramaswamy, D., *Langmuir*, **1988**, 4, 736.
149 Domínguez, A.; Fernández, A.; González, N.; Iglesias, E. and Montenegro, L., *J. Chem. Edu.*, **1997**, 74, 1227.
150 Nagamine, N. and Nakamura, H., *Anal. Sci.*, **1998**, 14, 405.
151 Lin, C.-E., *J. Chromatogr. A*, **2004**, 1037, 467.
152 Mora, M. F.; Felhofer, J.; Ayon, A. and Garcia, C. D., *Anal. Lett.*, **2008**, 41, 312.
153 López-Fontán, J. L.; González-Pérez, A.; Costa, J.; Ruso, J. M.; Prieto, G.; Schulz, P. C. and Sarmiento, F., *J. Coll. Int. Sci.*, **2006**, 294, 458.
154 Kahlweit, M., *Science*, **1988**, 240, 617.
155 Fendler, E. J.; Constien, V. G. and Fendler, J. H., *J. Phys. Chem.*, **1975**, 79, 917.
156 EI Seoud, O. A.; Fendler, E. J.; Fendler, J. H. and Medary, R. T., *J. Phys. Chem.*, **1973**, 77, 1876.
157 Fendler, E. J.; Fendler, J. H.; Medary, R. T. and EI Seoud, O. A., *J. Phys. Chem.*, **1973**, 77, 1432.
158 Nagarajan, R. and Ruckenstein, E., *Langmuir*, **1991**, 7, 2934.
159 Tanford, C. in *The Hydrophobic Effect: Formation of Micelles and Biological Membranes*; John Wiley & Sons: New York, **1980**.
160 Turro, N. J. and Yekta, A., *J. Am. Chem. Soc.*, **1978**, 100, 5951.
161 Borbely, S.; Cser, L.; Ostanevich, Y. M. and Vass, S., *J. Phys. Chem.*, **1989**, 93, 7967.
162 Jain, T. K.; Varshney, M. and Maitra, A., *J. Phys. Chem.*, **1989**, 93, 7409.
163 Tummino, P. J. and Gafni, A., *Biophys. Soc.*, **1993**, 64, 1580.
164 Israelachvili, J. N.; Mitchell D. J. and Ninham, B. W., *J. Chem. Soc., Faraday Trans. 2*, **1976**, 72, 1525.
165 Nagarajan, R., *Langmuir*, **2002**, 18, 31.
166 Antonietti, M. and Förster, S., *Adv. Mater.*, **2003**, 15, 1323.
167 Holmberg, A.; Piculell, L. and Wesslén, B., *J. Phys. Chem.*, **1996**, 100, 462.
168 Gale, R. W.; Fulton, J. L. and Smith, R. D., *J. Am. Chem. Soc.*, **1987**, 109, 920.
169 Blitz, J. P.; Fulton, J. L. and Smith, R. D., *J. Phys. Chem.*, **1988**, 92, 2707.

170 Eastoe, J.; Young, W. K. and Robinson, B. H., *J. Chem. Soc. Faraday Trans.*, **1990**, 86, 2883.
171 Kaler, E. W.; Billman, J. F.; Fulton, J. L. and Smith, R. D., *J. Phys. Chem.*, **1991**, 95, 458.
172 Eastoe, J.; Steytler, D. C.; Robinson, B. H. and Heenan, R. K., *J. Chem. Soc. Faraday Trans.*, **1994**, 90, 3121.
173 Angelo, M. D'; Fioretto, D.; Onori, G. and Santucci, A., *Phys. Rev. E*, **1998**, 58, 7657.
174 Holmberg, A.; Piculell, L. and Wesslén, B., *J. Phys. Chem.*, **1996**, 100, 462.
175 Darab, J. G.; Pfund, D. M.; Fulton, J. L. and Linehan, J. C., *Langmuir*, **199**4, 10, 135.
176 Hirai, T.; Sato, H. and Komasawa, I., *Ind. Eng. Chem. Res.*, **1994**, 33, 3262.
177 Kotlarchyk, M. and Chen, S.-H., *Phys. Rev. Lett.*, **1984**, 53, 941.
178 Petit., C., Lixon, P., and Pileni, M. P., *Langmuir*, **1991**, 7, 2620.
179 Tingey, J. M.; Fulton, J. L.; Matson, D. W. and Smith, R. D., *J. Phys. Chem.*, **1991**, 95, 1445.
180 Dan, N. and grayeski, M. L., *Langmuir*, **1994**, 10, 447.
181 Wu, M.; Long, J.; Huang, A. and Luo, Y., *Langmuir*, **1999**, 15, 8822.
182 Eicke, H.-F.; Meier, W. and Hammerich, H., *Coll. Surf. A: Physicochem. Eng. Asp.*, **1996**, 118, 141.
183 Liu, J.; Ikushima, Y. and Shervani, Z., *Curr. Opin. Solid State Mat. Sci.*, **2003**, 7, 255.
184 Bharatwaj, B. and Rocha, S. R. P., *Braz. J. Chem. Eng.*, **2006**, 23, 183.
185 Aveyard, R.; Binks, B. P.; Lawless, T. A. and Mead, J., *J. Chem. Soc., Faraday Trans. 1*, **1985**, 81, 2155.
186 Bisceglia, M.; Acosta, E.; Kurlat, D. and Ginzberg, B., *Coll. Surf. A: Physicochem. Eng. Asp.*, **1996**, 108, 137.
187 Sottmann, T. and Strey, R., *J. Chem. Phys.*, **1997**, 106, 8606.
188 Saito, H., Shinoda, K., *J. Coll. Int. Sci.*, **1970**, 32, 647.
189 Leitao, S.; Somoza, A. M.; Telo da Gama, M. M.; Sottmann, T. and Strey, R., *J. Chem. Phys.*, **1996**, 105, 2875.
190 Strey, R., *Coll. Polym. Sci.*, **1994**, 272, 1005.
191 Eastoe, J. and Robinson, B. H., *J. Chem. Soc. Faraday Trans.*, **1990**, 86, 511.
192 Ray, S.; Paul, S. and Moulik, S. P., *J. Coll. Int. Sci.*, **1996**, 183, 6.
193 García-Río, L.; Godoy, A. and Rodríguez-Dafonte, P., *Eur. J. Org. Chem.*, **2006**, 3364.
194 Hou, M. J.; Kim, M. and Shah, D. O., *J. Coll. Int. Sci.*, **1988**, 123, 398.
195 Martln, C. A. and Magid, L. J., *J. Phys. Chem.*, **1981**, 85, 3938.
196 Kahlweit, M. and Strey, R., *Angew. Chem. Int. Ed. Engl.*, **1985**, 24, 654.
197 Johnston, K. P.; Harrison, K. L.; Clarke, M. J.; Howdle, S. M.; Heitz, M. P.; Bright, F. V.; Carlier, C. and Randolph, T. W., *Science*, **1996**, 271, 624.
198 Sagisaka, M.; Fujii, T.; Ozaki, Y.; Yoda, S.; Takebayashi, Y.; Konodo, Y.; Yoshino, N.; Sakai, H.; Abe, M. and Otake, K., *Langmuir*, **2004**, 20, 2560.
199 Ohde, H.; Hunt, F. and Wai, C. M., *Chem. Mater.*, **2001**, 13, 4130.
200 Harrison, K.; Goveas, J. and Johnston, K. P., *Langmuir*, **1994**, 10, 3536.
201 Lee, T. C.; Psathas, P. A. and Johnston, K. P., *Langmuir*, **1999**, 15, 6781.
202 Ohde, H.; Ohde, M.; Bailey, F.; Kim, H. and Wai, C. M., *Nano Lett.*, **2002**, 2, 721.

203 Johnston, K. P.; Harrison, K. L.; Clarke, M. J. and Howdle, S. M., *Science*, **1996**, 271, 624.
204 Holmes, J. D.; Bhargava, P. A.; Korgel, B. A. and Johonston, K. P., *Langmuir*, **1999**, 15, 6613.
205 Zielinski, R. G.; Kline, S. R.; Kaler, E. W. and Rosov, N., *Langmuir*, **1997**, 13, 3934.
206 Nishimi, T. and Miller, C. A., *Langmuir*, **2000**, 16, 9233.
207 Jacobson, G. B.; Lee, C. T. and Johnston, K. P., *J. Org. Chem.*, **1999**, 64, 1201.
208 Winsor, P. A., *Trans. Faraday Soc.*, **1948**, 44, 376.
209 Majhi, P. R.; Mukherjee, K. and Moulik, S. P., *Langmuir*, **1997**, 13, 3284.
210 Mukerjee, P., and Mysels, M. J. in *Critical Micelle Concentrations of Aqueous Surfactant Systems*; National Standard Reference Data System-NBS 36: Washington, DC, **1971**.
211 Fendler, J. H.; Fendler, E. J.; Medary, R. T. and EL Seoud, O. A., *J. Chem. Soc., Faraday Trans, 1*, **1973**, 69, 280.
212 Heatley, F., *J. Chem. Soc., Faraday Trans. 1*, **1987**, 83, 517.
213 Jayakumar, R.; Jeevan, R. G. and Mandal, A. B., *J. Chem. Soc., Faraday Trans.*, **1994**, 90, 2725.
214 Muto, S. and Meguro, K., *Bull. Chem. Soc. Japan*, **1973**, 46, 316.
215 Majhi, P. R. and Moulik, S. P., *J. Phys. Chem. B*, **1999**, 103, 5977.
216 Mukherjee, K. and Moulik, S. P., *Langmuir*, **1993**, 9, 1727.
217 Jayakumar, R.; Mandal, A. B. and Manoharan, P. T., *J. Chem. Soc., Chem. Commun.*, **1993**, 853.
218 Manoj, K. M.; Jayakumar, R. and Rakshit, S. K., *Langmuir*, **1996**, 12, 4068.
219 Gorski, N. and Ostanevich, Y. M., *Progr. Colloid Polym. Sci.*, **1993**, 93, 256.
220 Herrmann, U. and Schelly, Z. A., *J. Am. Chem. Soc.*, **1979**, 101, 2665.
221 Manoj, K. M.; Jayakumar, R. and Rakshit, S. K., *Langmuir*, **1996**, 12, 4068.
222 Kotlarchyk, M. and Huang, J. S., *J. Phys. Chem.*, **1985**, 89, 4382.
223 Wang, H.; Zhou, W.; Ho, D. L.; Winey, K. I.; Fischer, J. E.; Glinka, C. J. and Hobbie, E. K., *Nano Lett.*, **2004**, 4, 1789.
224 Kitahara, A.; Kobayashi, T. and Tachibana, T., *J. phys. Chem.*, **1962**, 66, 363.
225 Ueda, M. and Schelly, Z. A., *Langmuir*, **1988**, 4, 654.
226 Zulauf, M. and Eicke, H.-F., *J. Phys. Chem.*, **1979**, 83.
227 Jean, Y.-C. and Ache, H. J., *J. Am. Chem. Soc.*, **1978**, 100, 6320.
228 Miguel, M. da G., *Adv. Coll. Int. Sci.*, **2001**, 89, 1.
229 Menini, C.; Park, C.; Shin, E.-J.; Tavoularis, G. and Keane, M. A., *Catal. Today*, **2000**, 62, 355.
230 Hur, J. M.; Coh, B.-Y. and Lee, H.-I., *Catal. Today*, **2000**, 63, 189.
231 Tanabe, K. and Hölderich, W. F., *Appl. Catal. A: Gen.*, **1999**, 181, 399.
232 Hattori, H. in *Adsorption and Catalysis on Oxide Surfaces*; Elsevier Science Ltd, Edited by Che, M., and Bond, G. C.: New York, **1985**.
233 Giordano, L.; Goniakowski, J. and Pacchioni, G., *Phys. Rev. B*, **2001**, 64, 075417-1.
234 Kurkova, N. S.; Katsobashvili, Ya. R. and Bukhtenko, O. V., *Chem. Tech. Fuels Oils*, **1978**, 14, 9.
235 Busch, G.; Cai, X.; Jähne, E. and Adler, H.-J. P., *Eur. Cell. Mater.*, **2003**, 6, 64.

236 Kamat, P. V., *Chem. Rev.*, **1993**, 93, 267.
237 Jeevanandam, P. and Klabunde, K. J., *Langmuir*, **2003**, 19, 5491.
238 Hoffmann, M. R.; Martin, S. T.; Choi, W. and Bahnemann, D. W., *Chem. Rev.*, **1995**, 95, 69.
239 Kera, Y.; Kamada, M.; Hanada, Y. and Kominami, H., *Compos. Interface.*, **2001**, 8, 109.
240 Henderson, B. and Sibley, W. A., *J. Chem. Phys.*, **1971**, 55, 1276.
241 Yanagisawa, Y.; Kuramoto, K. and Yamabe, S., *J. Phys. Chem. B*, **1999**, 103, 11078.
242 Fouad, N. E.; Thomasson, P. and Knözinger, H., *Appl. Catal. A: Gen.*, **2000**, 194, 213.
243 Metson, J. B.; Hyland, M. M.; Gillespie, A. and Hemmingsen-Jensen, M., *Coll. Surf. A: Physicochem. Eng. Asp.*, **1994**, 93, 173.
244 McCafferty, E. and Wightman, J. P., *Surf. Inter. Anal.*, **1998**, 26, 549.
245 Zecchina, A.; Lofthouse, M. G. and Stone, F. S., *J. Chem. Soc., Faraday Trans. 1*, **1975**, 71, 1476.
246 Zecchina, A. and Stone, F. S., *J. Chem. Soc., Faraday Trans. 1*, **1976**, 72, 2364.
247 Stone, F. S.; Garrone, E.; Zecchina, A.; *Mater. Chem. Phys.*, **1985**, 13, 331.
248 Chang, C.-H., *U.S. Patent 5,186,727*, **1993**.
249 Coluccia, S. and Tench, A. J., *J. Chem. Soc., Faraday Trans. 1*, **1979**, 75, 1769.
250 Yl, Y.; Cho, S.; Noh, M.; Whang, C.-N.; Jeong, K. and Shin, H.-J., *Jpn. J. Appl. Phys.*, **2005**, 44, 861.
251 Anpo, M. and Che, M., *Adv. Catal.*, **2000**, 44, 119.
252 Bailly, M.-L.; Costenitin, G.; Krafft, J. M. and Che, M., *Catal. Lett.*, **2004**, 92, 101.
253 Che, M. and Tench, A. J., *Adv. Catal.*, **1982**, 31, 77.
254 Chayabutra, S.; Grady, B. V.O' and Larkins, F. P., *Silpakorn University international Journal*, **2003**, 3, 154.
255 Tsyganenko, A. A.; Storozheva, E. N.; Manoilova, O. V.; Lesage, T.; Daturi, M. and Lavalley, J. C., *Catal. Lett.*, **2000**, 70, 159.
256 Bailly, M.-L.; Chizallet, C.; Costentin, G.; Krafft, J.-M.; Lauron-Pernot, H. and Che, M., *J. Catalysis*, **2005**, 235, 413.
257 Spielbauer, D.; Mekhemer, G. A. H.; Riemer, T.; Zaki, M. I. and Knözinger, H., *J. Phys. Chem. B*, **1997**, 101, 4681.
258 Aramendía, M. A.; Borau, V.; Jiménez, C.; Marinas, A.; Marinas, J. M.; Ruiz, J. R. and Urbano, F. J., *J. Mol. Catal. A: Chem.*, **2004**, 218, 81.
259 Richards, R. M.; Volodin, A. M.; Bedilo, A. F. and Klabunde, K. J., *Phys. Chem. Chem. Phys.*, **2003**, 5, 4299.
260 Liu, Z.; Cortés-Concepción, J. A.; Mustian, M. and Amiridis, M. D., *Appl. Catal. A: Gen.*, **2006**, 302, 232.
261 Arena, F.; Dario, R. and Parmaliana, A., *Appl. Catal. A: Gen.*, **1998**, 170, 127.
262 Cordischi, D.; Indovina, V. and Occhiuzzi, M., *J. Chem. Soc., Faraday Trans. 1*, **1978**, 74, 883.
263 Pendergraft, P. T. and Okla, T., *U.S. Patent 4,871,521*, **1989**.
264 Goodman, A. L.; Bernard, E. T. and Grassian, V. H., *J. Phys. Chem. A*, **2001**, 105, 6443.
265 Li, C.; Li, G. and Xin, Q., *J. Phys. Chem.*, **1994**, 98, 1933.
266 Tretyakov, N. E. and Filimonov, V. N., *J. Appl. Spectr.*, **1970**, 11, 989.
267 Teramura, K.; Tanaka, T.; Ishikawa, H.; Kohno, Y. and Funabiki, T., *J. Phys. Chem. B*, **2004**, 108, 346.

268 Tsyganenko, A. A. and Filimonov, V. N., *J. Mol. Struct.*, **1973**, 19, 579.

269 Lucas, E.; Decker, S.; Khaleel, A.; Seitz, A.; Fultz, S.; Ponce, A.; Li, W.; Carnes, C. and Klabunde, K. J., *Chem. Eur. J.*, **2001**, 7, 2505.

270 Coluccia, S., Marchese, L., Lavagnino, S., and Anpo, M., *Spectrochim. Acta*, **1987**, 43A, 1573.

271 Anderson, P. J.; Horlock, R. F. and Oliver, J. F., *Trans. Faraday Soc.*, **1965**, 61, 2754.

272 Morterra, C. and Magnacca, G., *Catal. Today*, **1996**, 27, 497.

273 Shido, T.; Asakura, K. and Iwasawa, Y., *J. Chem. Soc., Faraday Trans. 1*, **1989**, 85, 441.

274 Coluccia, S.; Barton, A. and Tench, A. J., *J. Chem. Soc., Faraday Trans. 1*, **1981**, 77, 2203.

275 Coluccia, S.; Lavagnino, S. and Marchese, L., *Mater. Chem. Phys.*, **1988**, 18, 445.

276 Knözinger, E.; Jacob, K.-H.; Singh, S. and Hofmann, P., *Surf. Sci.*, **1993**, 290, 388.

277 Klabunde, K. J.; Stark, J.; Koper, O.; Mohs, C.; Park, D. G.; Decker, S.; Jiang, Y.; Lagadic, I. and Zhang, D., *J. Phys. Chem.*, **1996**, 100, 12142.

278 Itoh, H.; Utamapanya, S.; Stark, J. V.; Klabunde, K. J. and Schlup, J. R., *Chem. Mater.*, **1993**, 5, 71.

279 Chizalle, C.; Costenitin, G.; Che, M.; Delbecq, F. and Sautet, P., *J. Am. Chem. Soc.*, **2007**, 129, 6442.

280 Chizallet, C.; Costentin, G.; Che, M.; Delbecq, F. and Sautet, P., *J. Phys. Chem. B*, **2006**, 110, 15878.

281 Oviedo, J.; Calzado, C. J. and Sanz, J. F., *J. Chem. Phys.*, **1998**, 108, 4219.

282 Kawakami, H. and Yoshida, S., *J. Chem. Soc., Faraday Trans. 2*, **1984**, 80, 921.

283 Derouane, E. G.; Fripiat, J. G. and André, J. M., *Chem. Phys. Lett.*, **1975**, 35, 525.

284 Coluccia, S. and Tench, A. J., *J. Chem. Soc. Faraday Trans. 1*, **1979**, 75, 1769.

285 Chizallet, C.; Costentin, G.; Lauron-Pernot, H.; Krafft, J. M.; Bazin, P.; Saussey, J.; Delbecq, F.; Sautet, P. and Che, M., *Oil Gas Sci. Technol. –Rev. IFP*, **2006**, 61, 479.

286 Leeuw, N. H.; Watson, G. W. and Parker, S. C., *J. Phys. Chem.*, **1995**, 99, 17219.

287 Halim, W.S. A. and Shalabi, A. S., *Applied Surface Science*, **2004**, 221, 53.

288 Scamehorn, C. A.; Harrison, N. M. and McCarthy, M. I., *J. Chem. Phys.*, **1994**, 101, 1547.

289 Langel, W. and Parrinello, M., *J. Chem. Phys.*, **1995**, 103, 3240.

290 Tsygnenko, A. A. and Filimonov, V. N., J. *J. Mol. Struct.*, **1973**, 19, 579.

291 Ahmed, S. I.-U.; Perry, S. S. and El-Bjeirami, O., *J. Phys. Chem. B*, **2000**, 104, 3343.

292 Aramendía, M. A.; Benítez, J. A.; Borau, V.; Jiménez, C.; Marinas, J. M.; Ruiz, J. R. and Urbano, F., *Langmuir*, **1999**, 15, 1192.

293 Stirniman, M. J.; Huang, C.; Smith, R. S.; Joyce, S. A. and Day, B. D., *J. Chem. Phys.*, **1996**, 105, 1295.

294 Costa, D.; Chizallet, C.; Ealet, B.; Goniakowski, J. and Finocchi, F., *J. Chem. Phys.*, **2006**, 125, 054702-1.

295 Bermudez, V. M., *J. Phys. Chem.*, **1970**, 74, 4160.

296 Rosenthal, D. J.; White, M. G. and Parks, G. D., *AIChE Journal*, **1987**, 33, 336.

297 Morimoto, T. and Suda, Y., *Langmuir*, **1985**, 1, 239.

298 Hoq, M. F.; Nieves, I. and Klabunde, K. J., *J. Catalysis*, **1990**, 123, 349.

299 Sato, M.; Kanbayashi, T.; Kobayashi, N. and Shima, Y., *J. Catalysis*, **1967**, 7, 342.

300 Grieken, R. V.; Calleja, G.; Serrano, D.; Martos, C.; Melgares, A. and Suarez, I., *Polymer React. Eng.*, **2003**, 11, 17.

301 Mechanism, P.; Boccuzai, F.; Ghiotti, G. and Morterra, C., *J. Chem. Soc., Faraday Trans. 1*, **1982**, 78, 2111.

302 Bailly, M.-L.; Costentin, G.; Lauron-Pernot, H.; Krafft, J. M. and Che, M., *J. Phys. Chem. B*, **2005**, 109, 2404.

303 Markovits, A.; Ahdjoudj, J. and Minot, C., *Mol. Eng.*, **1997**, 7, 245.

304 Hattori, H., *Appl. Catal. A: Gen.*, **2001**, 222, 247.

305 Szöllösi, G. and Gartók, M., *J. Mol. Struct.*, **1999**, 482-483, 13.

306 Meyer, U. and Hoelderich, W. F., *J. Mol. Catal. A: Chem.*, **1999**, 142, 213.

307 Coluccia, S. and Tench, A. J., *J. Chem. Soc., Faraday Trans. 1*, **1983**, 79, 1881.

308 Díez, V. K.; Apesteguía, C. R. and Di Cosimo, J. I., *Catal. Today*, **2000**, 63, 53.

309 Anpo, M.; Yamada, Y.; Kubokawa, Y.; Coluccia, S.; Zecchina, A. and Che, M., *J. Chem. Soc., Faraday Trans. 1*, **1988**, 84, 751.

310 Peng, X. D. and Barteau, M. A., *Surf. Sci.*, **1989**, 224, 327.

311 Chiesa, M.; Paganini, M. C. and Giamello, E., *ChemPhysChem*, **2004**, 5, 1897.

312 Aramendía, M. A.; Borau, V.; Jiménez, C.; Lafont, F.; Marinas, J. M.; Porras, A. and Urbano, F. J., *Rapid Communications in Mass Spectrometry*, **1995**, 9, 193.

313 Di Cosimo, J. I.; Díez, V. K.; Xu, M.; Iglesia, E. and Apesteguía, C. R., *J. Catalysis*, **1998**, 178, 499.

314 Corma, A., Iborra, S., Primo, J., and Rey, F., *Applied Catalysis A: General*, **1994**, 114, 215.

315 Di Cosimo, J. I.; Díez, V. K. and Apesteguía, C. R., *Appl. Catal. A: Gen.*, **1996**, 137, 149.

316 Peng, X. D. and Barteau, M. A., *Langmuir*, **1991**, 7, 1426.

317 Lavalley, J. C., *Catal. Today*, **1996**, 27, 377.

318 Aramendía, M. A.; Borau, V.; Jiménez, C. and Marinas, A., *J. Catalysis*, **2002**, 211, 556.

319 Quigley, W. W. C.; Yamamoto, H. D.; Aegerter, P. A.; Simpson, G. J. and Busseell, M. E., *Langmuir*, **1996**, 12, 1500.

320 Ferri, D.; Diezi, S.; Maciejewski, M. and Baiker, A., *Appl. Catal. A: Gen.*, **2006**, 297, 165.

321 Knözinger, H. and Ratnasamy, P., *Catal. Rev. Sci. Eng.*, **1978**, 17, 31.

322 Ratnasamy, P. and Sivasanker, S., *Catal. Rev. Sci. Eng.*, **1980**, 22, 401.

323 Szanyi, J.; Kwak, J. H.; Chimentao, R. J. and Peden, C. H. F., *J. Phys. Chem. C*, **2007**, 111, 2661.

324 Abdel-Rehim, M. A.; dos Santos, A. C. B.; Camorim, V. L. L. and Faro, A. da C., *Appl. Catal. A: Gen.*, **2006**, 305, 211.

325 Heemeier, M.; Frank, M.; Libuda, J.; Wolter, K.; Kuhlenbeckm, H.; Bäumer, M. and Freund, H.-J., *Catal. Lett.*, **2000**, 68, 19.

326 Knözinger, H., *Adv. Catal.*, **1976**, 25, 184.

327 Rinaldi, R.; Fujiwara, F. Y.; Hölderich, W. and Schuchardt, U., *J. Catalysis*, **2006**, 244, 92.

328 van Vliet, M. C. A.; Mandelli, D.; Arends, W. C. E.; Schuchardt, U. and Sheldon, R. A., *Green Chem.*, **2001**, 3, 243.

329 Silba, J. M. de S; Vinhado, F. S.; Mandelli, D.; Schuchardt, U. and Rinaldi, R., *J. Mol. Catal. A: Chem.*, **2006**, 252, 186.

330 Lippens, B. C., and Steggerda, J. J. in *Physical and Chemical Aspects of Adsorbents and Catalysts*; Acadamic Press, Edited by Linsen, B. G., Fortuin, J. M. H., Okkerse, C., and Steggerda, J. J.: New York, **1970**.

331 Morterra, C. and Magnacca, G., *Catal. Today*, **1996**, 27, 497.

332 Wilson, S. J. and McConnell, J. D. C., *J. Solid State Chem.*, **1980**, 34, 315.

333 Cauwelaer, F. H. V. and Hall, W. K., *Trans. Faraday Soc.*, **1970**, 66, 454.

334 Peri, J. B., *J. Phys. Chem.*, **1965**, 69, 211

335 de Boerm, J. H.; Fortuin, J. M. H.; Lippens, B. C. and Meijs, W. H., *J. Catalysis*, **1963**, 2, 1.

336 Cantrell, J. H., *J. Appl. Phys.*, **2004**, 96, 3775.

337 Busca, G.; Lorenzelli, V.; Escribano, V. S. and Guidetti, R., *J. Catalysis*, **1991**, 131, 167.

338 Zecchina, A. and Areán, C. O., *Catal. Rev. Sci. Eng.*, **1993**, 35, 261.

339 Kim, S.; Sorescu, D. C. and Yates, J. T., *J. Phys. Chem. C*, **2007**, 111, 5416.

340 Costa, T. M. H.; Gallas, M. R.; Benvenutti, E. V. and da Jornada, J. A. H., *J. Phys. Chem. B*, **1999**, 103, 4278.

341 Nortier, P. and Fourre, P., *Appl. Catal.*, **1990**, 61, 141.

342 Peri, J. B., *J. Phys. Chem.*, **1965**, 69, 211.

343 Shirai, T.; Li, J. W.; Matsumaru, K.; Ishizaki, C. and Ishizaki, K., *Sci. Technol. Adv. Mater.*, **2005**, 6, 123.

344 Borello, E.; Gatta, G. D.; Fubini, B.; Morterra, C. and Venturello, G., *J. Catalysis*, **1974**, 35, 1.

345 Trokhimets, A. I.; Mardilovich, P. P.; Buslov, D. K. and Lysenko, G. N., *J. Appl. Spectr.*, **1979**, 31, 995.

346 Peri, J. B., *J. Phys. Chem.*, **1965**, 69, 220.

347 Nortier, P. and Fourre, P., *Appl. Catal.*, **1990**, 61. 141.

348 Tsyganenko, A. A. and Filimonov, V. N., *J. Mol. Struct.*, **1973**, 19, 579.

349 Busca, G.; Lorenzelli, V.; Escribano, V. S. and Guidetti, R., *J. Catalysis*, **1991**, 131, 167.

350 Peri, J. B. and Hannan, R. B., *J. Phys. Chem.*, **1960**, 64, 1526.

351 Morterra, C.; Ghiotti, G.; Garrone, E. and Boccuzzi, F., *J. Chem. Soc., Faraday Trans. 1*, **1976**, 72, 2722.

352 Vigué, H.; Quintard, P.; Merle-Méjean, T. and Lorenzelli, V., *J. Eur. Ceram. Soc.*, **1998**, 18, 305.

353 Busca, G.; Lorenzelli, V. and Escribano, V. S., *Chem. Mater.*, **1992**, 4, 595.

354 Ballinger, T. H. and Yates, J. T., *Langmuir*, **1991**, 7, 3041.

355 Gadzhieva, N. N. and Gribov, A. A., *J. Appl. Spectr.*, **1998**, 65, 32.

356 Peri, J. B. and Hannan, R. B., *J. Phys. Chem.*, **1960**, 64, 1526.

357 Borello, E.; Gatta, G. D.; Fubini, B.; Morterra, C. and Venturello, G., *J. Catalysis*, **1974**, 35, 1.

358 Layman, K. A. and Hemminger, J. C., *J. Catalysis*, **2004**, 222, 207.

359 Hiemstra, T.; van Riemsdijk, W. H. and Bolt, G. H., *J. Coll. Int. Sci.*, **1989**, 133, 91.

360 Sharanda, L. F.; Shimansky, A. P.; Kulikm, T. V. and Chuiko, A. A., *Coll. Surf. A: Physicochem. Eng. Asp.*, **1995**, 105, 167.

361 Li, H.; Yan, Y.; Liu, B.; Chen, W. and Chen, S., *Powder Technol.*, **2007**, 178, 203.

362 Jeevanandam, P. and Klabunde, K. J., *Langmuir*, **2003**, 19, 5491.

363 Alliot, C.; Bion, L.; Mercier, F. and Toulhoat, P., *J. Coll. Int. Sci.*, **2005**, 287, 444.
364 Slavov, S. V.; Sanger, A. R. and Chung, K. T., *J. Phys. Chem. B*, **1998**, 102, 5475.
365 Mottola, H. A. and Steinmetz, J. R. in *Chemically Modified Surfaces*; Elsevier: New York, **1992**.
366 Yang, Y.-C.; Szafraniec, L. L.; Beaudry, W. T. and Ward, J. R., *J. Org. Chem.*, **1988**, 53, 3293.
367 Yang, Y.-C.; Ward, R. and Luteran, T., *J. Org. Chem.*, **1986**, 51, 2756.
368 Mawhinney, D. B.; Rossin, J. A.; Gerhart, K. and Yates, J. T., *Langmuir*, **1999**, 15, 4617.
369 Mawhinney, D. B.; Rossin, J. A.; Gerhart, K. and Yates, J. T., *Langmuir*, **1999**, 15, 4789.
370 Narske, R. M.; Klabunde, K. J. and Fultz, S., *Langmuir*, **2002**, 18, 4819.
371 Kim, S.; Byl, O.; Liu, J.-C.; Johnson, J. K. and Yates, J. T., *J. Phys. Chem. B*, **2006**, 110, 9204.
372 Mawhinney, D. B.; Rossin, J. A.; Gerhart, K. and Yates, J. T., *Langmuir*, **2000**, 16, 2237.
373 Thompson, T. L.; Panayotov, D. A. and Yates, J. T., *J. Phys. Chem. B*, **2004**, 108, 16825.
374 Panayotov, D. and Yates, J. T., *J. Phys. Chem. B*, **2003**, 107, 10560.
375 Martin, M. E.; Narske, R. M. and Klabunde, K. J., *Micropor. Mesopor. Mater.*, **2005**, 83, 47.
376 Hertl, W. and Hair, M. L., *J. Phys. Chem.*, **1971**, 75, 2181.
377 Baraton, M.-I.; Chancel, F. and Merhari, L., *Nanostruct. Mater.*, **1997**, 9, 319.
378 Van Roosmalen, A. J. and Mol, J. C., *J. Phys. Chem.*, **1978**, 82, 2748.
379 Armistead, C. G. and Hockey, J. A., *Trans. Faraday Soc.*, **1967**, 63, 2549.
380 Paul, D. K. and Yates, J. T., *J. Phys. Chem.*, **1991**, 95, 1699.
381 Angst, D. L. and Simmons, G. W., *Langmuir*, **1991**, 7, 2236.
382 Matsumiya, M.; Shin, W.; Qiu, F.; Izu, N.; Matsubara, I. and Murayama, N., *Sens. Actuat. B*, **2002**, 96, 516.
383 Evans, H. E. and Weinberg, W. H., *J. Chem. Phys.*, **1979**, 71, 4789.
384 Xu, C. and Koel, B. E., *J. Chem. Phys.*, **1995**, 102, 8158.
385 Hasan, M. A.; Zaki, M. I. and Pasupulety, L., *Appl. Catal. A: Gen.*, **2003**, 243, 81.
386 Sondag, A. H. M.; Raas, M. C. and van Velzen, P. N. T., *Chem. Phys. Lett.*, **1989**, 155, 503.
387 Noto, Y.; Fukuda, K.; Onishi, T. and Tamaru, K., *Trans. Faraday Soc.*, **1967**, 63, 2300.
388 Foster, M.; Passno, D. and Rudberg, J., *J. Vac. Sci. Technol. A*, **2004**, 22, 1640.
389 Wang, W.; Qiao, X. and Chen, J., *J. Am. Ceram. Soc.*, **2008**, 91, 1697.
390 Petrie, W. T. and Vohs, J. M., *Surf. Sci. Lett.*, **1991**, 259, L750.

CHAPTER 3 - Experimental and Characterization Methods

3.1 TDE Synthesis

TDE was synthesized using a modification of the method published by Pruett *et. al.* [1] Chlorotrifluoroethylene (from SynQuest Laboratories Inc.) was employed directly without further purification. Dimethylamine (40% in water, from Alfa Aesar) was purified twice by distillation through a Vigreux column before use. After the dimethylamine was purified, 3.72 moles were sealed in a high pressure reaction vessel and cooled in liquid nitrogen as chlorotrifluoroethylene (0.52 moles) was introduced into the vessel from a gas cylinder. After loading the reagents, the reaction vessel was heated to 56^{o}C and kept at this temperature for 10 hours. Because this reaction is extremely exothermic, the excess reaction heat had to be removed by cooling water which flowed through a coil inside the reaction vessel. The product is a bright yellow solid at room temperature. Heating the solid product in a sealed flask placed in a water bath at 56^{o}C caused the solid product to melt and form two liquid layers. The upper layer (an oil phase containing TDE and byproducts) was further washed with deionized water to remove the polar impurities. A light yellow liquid (TDE) remained after the impurities were removed. Depending on the quality of the temperature control in the beginning of the reaction, the yield of TDE varies from 30 to 40%. The emission spectrum of TDE CL had been reported previously by Winberg *et. al.* [2] A similar emission spectrum with a peak at around 510 nm was given when TDE was exposed to atmosphere. The purity of TDE was checked by NMR spectroscopy. An NMR spectrum, as seen in **Figure 3.1**, showed a single sharp band at 2.519 ppm (with tetramethylsilane as a chemical shift reference) resulting from the protons of the methyl functional groups of TDE, proving that the product was TDE.

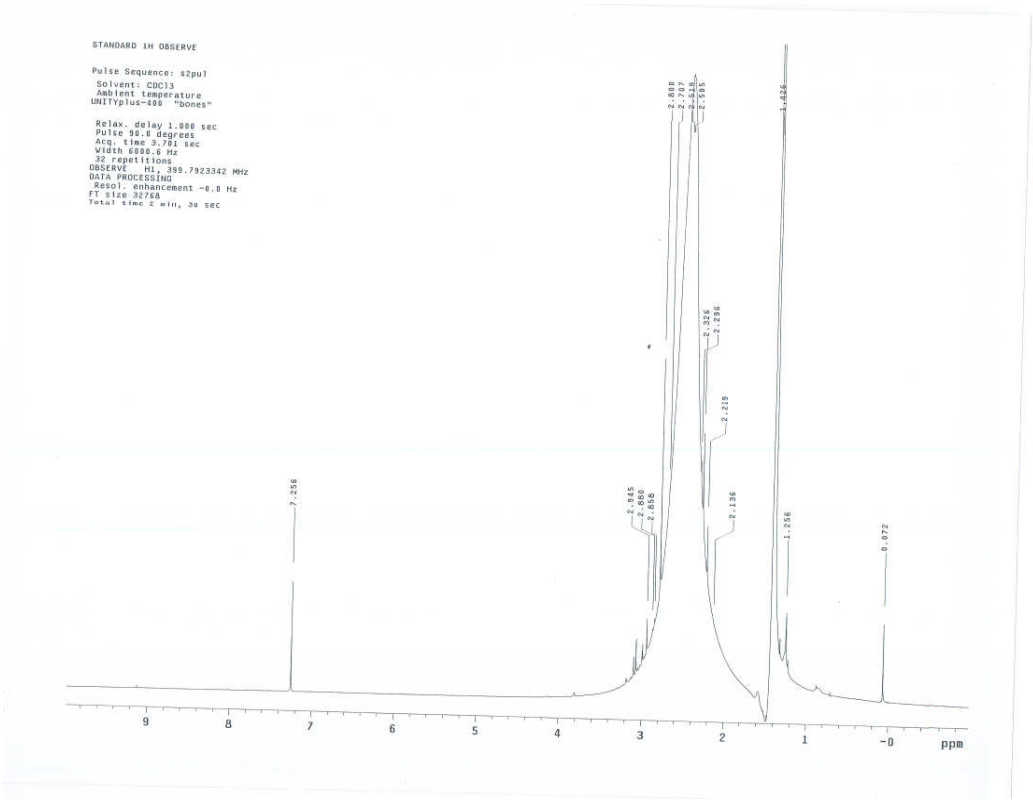

Figure 3.1 NMR spectrum of TDE with cyclohexane. The peaks at 7.256, 2.519, 1.426 and 0 ppm are assigned to $CDCl_3$, TDE, cyclohexane and TMS (Internal Std.) respectively.

3.2 Experimental Apparatus

The emission intensity vs. reaction time (I_t) curve of TDE CL was detected by a fiber optic spectrometer (StelarNet Inc. EPP2000) and recorded by SpectraWiz operating software at room temperature (~26^{o}C). An apparatus was constructed in which the sample could be monitored while a gas was flowing into the sample. This apparatus consisted of a sample holder, the fiber optic cable, and an outer glass chamber to which inlet and outlet tubes were connected, as sketched in **Figure 3.2**. The flexible fiber optic cable was positioned below the sample holder. The mixture of metal oxide sample with TDE or reversed microemulsion solution with TDE was loaded into the sample vial, which was then placed in the sample holder. The chamber was sealed with an O-ring and purged with dry air at 300 ml/min using a rotameter during the reaction. In order to avoid the influence caused by stray light from the surroundings, the outside wall of the glass chamber was covered by a layer of aluminum foil.

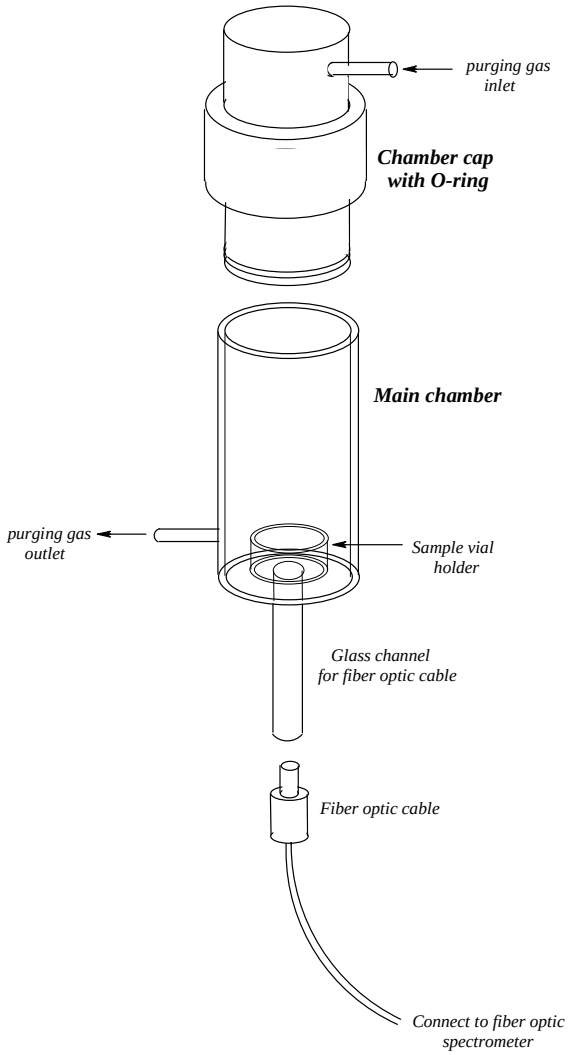

Figure 3.2 Sketch of the apparatus used to measure TDE chemiluminescence.

3.3 Characterization Methods

3.3.1 $AlEt_3$ Titration for Measuring the Content of Surface Hydroxyl Groups

The apparatus for measuring the number of surface hydroxyl groups on metal oxides was modified from the apparatus described by Sato and his coworkers [3]. This apparatus is shown in **Figure 3.3**. The whole system was contained inside a glove box that was pre-purged by nitrogen. The metal oxide sample size was approximately 0.4g. **Figure 3.4** shows the measuring procedure. The titrating agents, triethylaluminum and 1-pentanol, were both purchased from Alfa Aesar and were used without purification.

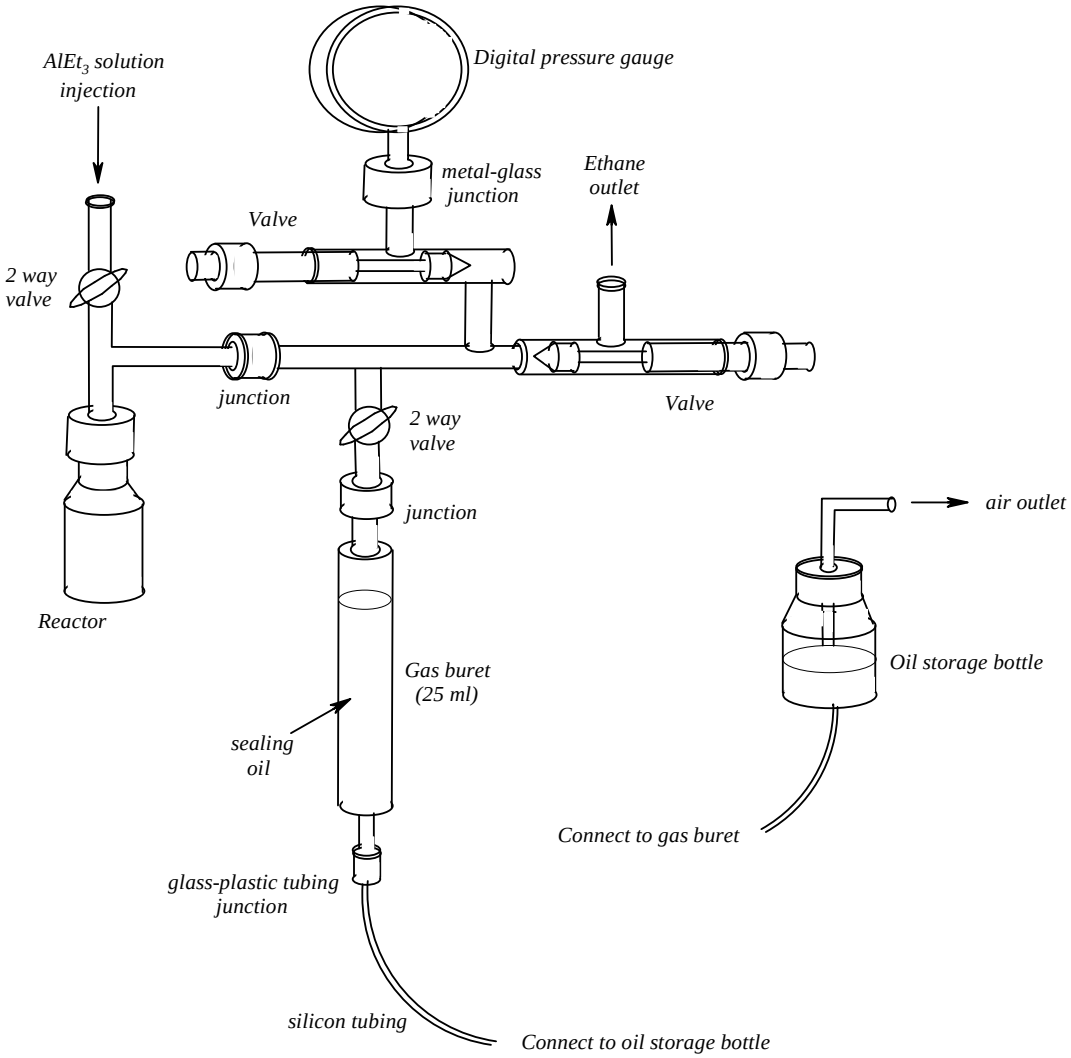

Figure 3.3 Apparatus for measuring the amount of surface hydroxyl groups on metal oxides.

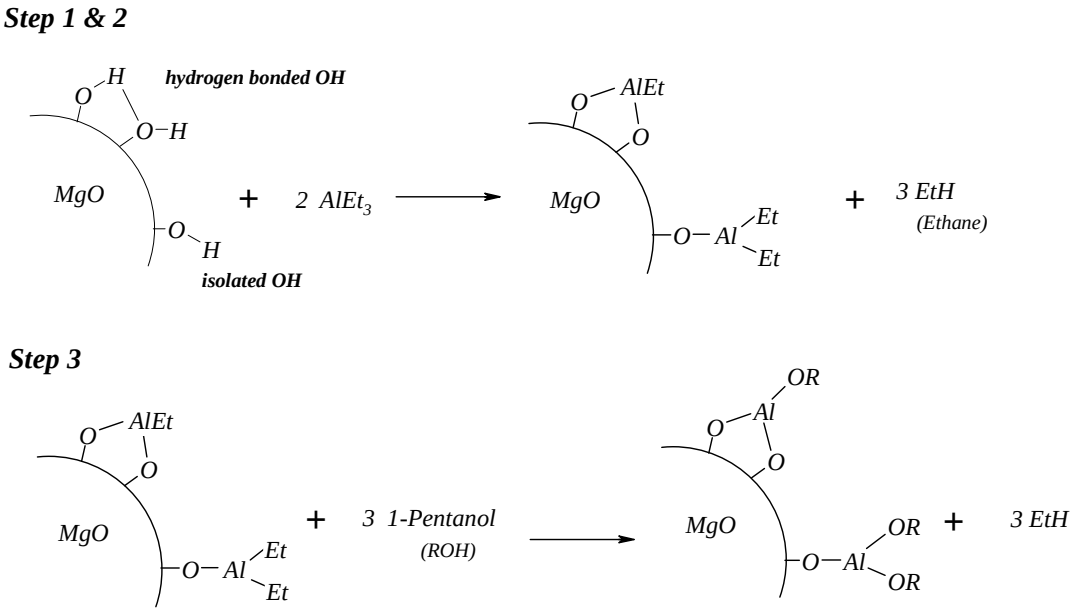

Figure 3.4 Process for measuring hydrogen bonded and isolated hydroxyls by $AlEt_3$ titration.

Triethylaluminum titration used in the measurement of surface hydroxyl groups on magnesium oxide is a substitution and reduction reaction. The determination of the hydroxyl group concentrations on the metal oxide samples was based on the amount of ethane released during the reaction between $AlEt_3$ and the hydroxyl groups. Monodetate ($OAlEt_2$) and bidentate (O_2AlEt_1) species were formed via reactions between the ethyl groups of $AlEt_3$ and the protons of adsorbed hydroxyl groups on metal oxides when $AlEt_3$ reacts with isolated OH and hydrogen-bonded OH, respectively (**Figure 3.4**) [4]. The remaining ethyl groups on $OAlEt_2$ and O_2AlEt_1 were further reduced by 1-pentanol and released in the final step. Because the density of surface isolated OH and hydrogen bonded OH varies with the pre-treating processes, excess $AlEt_3$ had to be added to make sure that the protons of the surface hydroxyl groups were completely substituted by $AlEt_3$. However, the ethane would be released either from $OAlEt_2$ / O_2AlEt_1 or excess $AlEt_3$ when 1-pentanol was added into the reaction. Thus, the amount of $AlEt_3$ added had to be adjusted depending on the densities of adsorbed hydroxyl groups on metal oxide surface. The first step was used to estimate the appropriate amount of $AlEt_3$ which would be added into the solution in the second step.

In the first step, an excess (4ml) of a 0.5M $AlEt_3$/decalin solution was added into the reactor and mixed with the metal oxide sample with a magnetic stir bar for 8-12 hours until no more ethane was evolved from the reaction. The ethane released from the reaction (n_{EG}, **Equation 3- 1**) was simply calculated by the ideal gas law. Based on the calculation of released ethane (n_{EG}, **Equation 3- 2**) in the first step and the supposition that all adsorbed hydroxyls are isolated OH, a stoichiometric amount of $AlEt_3$ was added. This procedure overestimated the amount of $AlEt_3$ required (**Equation 3- 3**), so $AlEt_3$ at a low concentration was left in solution after the reaction. The residual $AlEt_3$, thus, had to be removed before 1-pentanol was added. 4ml decalin was added into the reactor to extract out the residual $AlEt_3$. In the third step, 4 ml of 1-pentanol was added into the reactor.

$$n_{E_G} = \frac{P_{E_G} V_{E_G}}{RT} \qquad (3\text{- }1)$$

$$n_{E_G} = n_{iso-OH} + 2n_{H-OH} \qquad (3\text{- }2)$$

$$n_{AlEt_3} = \frac{1}{2} n_{H-OH} + n_{iso-OH} \qquad (3\text{- }3)$$

where P_{EG} and V_{EG} are the ethane pressure and volume of the measuring instrument. n_{EG} is the number of moles of ethane which is released from the reaction between the proton of hydroxyl on metal oxide surface and $AlEt_3$. $n_{iso\text{-}OH}$ is the number of moles of isolated OH on metal oxide, $n_{H\text{-}OH}$ is the number of moles of hydrogen bonded OH on metal oxide, and n_{ALEt3} is the required additional amount of $AlEt_3$ in step 2.

As $AlEt_3$ reacted with an isolated hydroxyl on the metal oxide surface, only one ethane molecule was released from the reaction, leaving monodentate $OAlEt_2$ on metal oxide surface. In contrast, two ethane molecules were released when $AlEt_3$ reacted with hydrogen bonded OH groups, leaving bidentate O_2AlEt_1 on metal oxide surface [5,6] (**Figure 3.4**). 1-pentanol (Alfa Aesar) was added to replace residual ethyl groups on monodentate or bidentate and reduce the ethyl group to ethane. The volume-pressure data was converted to a mole number through the ideal gas law. The number of moles of ethane released from step 2 was named E_1 while the number of moles of ethane released from step 3 was named E_2. The amount of isolated OH ($n_{iso\text{-}}$

$_{OH}$) and the amount of hydrogen bonded OH ($n_{H\text{-}OH}$) was, then, calculated via **Equations 3- 4** and **3- 5**:

$$n_{iso-OH} = \frac{1}{3}(2E_2 - E_1) \qquad (3\text{- }4)$$

$$n_{H-OH} = \frac{1}{3}(2E_1 - E_2) \qquad (3\text{- }5)$$

3.3.2 Surface IR Study

The apparatus employed for studying the surface hydroxyls and grafted groups on metal oxides, and the interaction between TDE and metal oxide surfaces is shown in **Figure 3.5**. All infrared spectra were obtained in a high temperature DRIFTS cell (SpectraTech). Metal oxide sample, about 30 mg, was loaded into the ceramic sample cup in the cell without dilution. The desired temperature for treating the metal oxide sample in the DRIFTS cell was controlled by a temperature controller (Thermo Electron Corp.) O_2 and inert gas cylinders were connected to the DRIFT cell by plastic tubing.

The flow rate of inlet gasses was controlled by mass flow controllers. A sealed flask with 20ml TDE was pre-purged by dry nitrogen and connected to the DRIFT cell with ¼" stainless tubes. The inert gas and oxygen were further dehydrated by a water trap before being introduced into the DRIFTS cell. To introduce TDE into the DRIFTS cell, the nitrogen and oxygen flows were bubbled through TDE and into the cell.

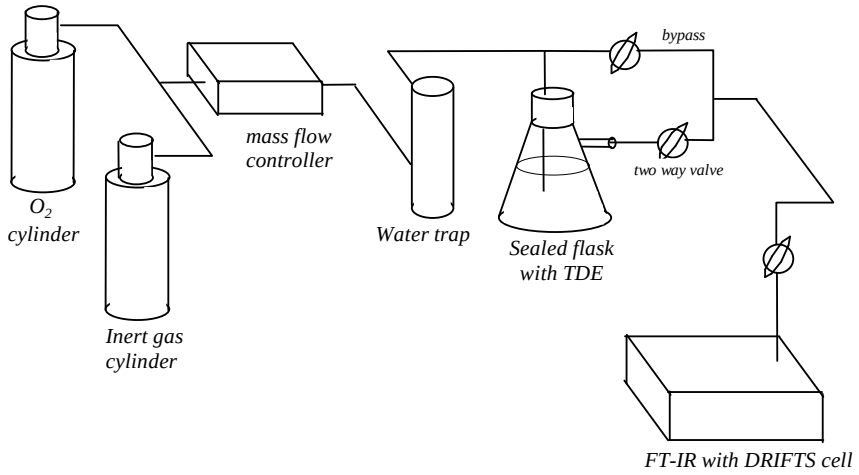

Figure 3.5 The scheme of the apparatus used to measure the IR spectra of metal oxide and catalyzed TDE CL reaction on metal oxide surface. The amount of TDE in sealed flask is 20 ml.

3.3.3 Measurement of Surface Area

The surface areas of metal oxides were determined by the BET dynamic method using a Quantachrome Autosorb-1. Nitrogen was used for the adsorption experiment at liquid nitrogen temperature.

3.3.4 X-ray Powder Diffraction Analyses

X-ray powder (XRD) traces of metal oxides were carried out using a Bruker D8 Advance X-ray diffractometer (40 kV, 40 mA) (Karlsruhe, Germany). The aluminum oxide samples were scanned starting from $2\theta=25\text{-}70^{o}$ with increment of 0.05^{o} and a scan speed of 1 degree/minute.

3.4 References

1 Pruett, R. L.; Barr, J. T.; Rapp, K. E.; Bahner, C. T.; Gibson, J. D.; Lafferty, R. H. *J. Am. Chem. Soc.* **1950** 72, 3646.

2 Winberg, H. E.; Carnahan, J. E.; Coffman, D. D.; Brown, M. *J. Am. Chem. Soc.* **1965**, 87, 2054.

3 Sato, M.; Kanbayashi, T.; Kobayashi, N.; Shima, Y. *J. Cat.* **1967**, 7, 342.

4 Klabunde, K. J.; Stark, J.; Koper, O.; Mohs, C.; Park, D. G.; Decker, S.; Jiang, Y.; Lagadic, I.; Zhang, D. *J. Phys. Chem.* **1996**, 100, 12142.

5 Fletcher, A. N. *J. Phys. Chem.* **1969**, 73, 3686.

6 Itoh, H.; Utamapanya, S.; Stark, J. V.; Klabunde, K. J.; Schlup, J. R. *Chem. Mater.* **1993**, 5, 71.

CHAPTER 4 - The Influence of Surface Hydroxyls on Catalyzed Tetrakis(dimethylamino)ethylene Chemiluminescence

4.1 Introduction

The surface morphology of alkaline earth metal oxides is associated with the acidity, basicity, adsorptive properties, and reactivity of the metal oxide.[1,2,3,4,5] Magnesium oxide (MgO) has been widely used as a solid base catalyst or as a catalyst support.[6,7,8] The electron transfer from magnesium to oxygen atoms in MgO leads to electron rich oxygen anions that act as strong base sites. In addition to oxide ions, hydroxyl groups also act as basic sites on MgO. [9,10]

The basicity of MgO is expected to greatly depend on the distribution of the oxide ions and the location of surface hydroxyl groups. On a clean MgO surface, there are lower coordinated (LC) oxide sites (O^{2-}_{LC}) including 5, 4 and 3-coordinated oxides (O^{2-}_{5C}, O^{2-}_{4C} and O^{2-}_{3C}) at extending planes, edges and corners, respectively. Brønsted basicity of O^{2-}_{LC} ions increases in the order: $O^{2-}_{5C} < O^{2-}_{4C} < O^{2-}_{3C}$. [11,12] Hydroxyl groups can be divided into two categories depending on the atom (metal or oxygen atom) on which the hydroxyl groups adsorbs. Hydroxylated magnesium cations and protonated oxide anions are usually referred to as mono-coordinated ($-O_{1C}H$) and multi-coordinated ($-O_{LC}H$, where L=3,4 and 5) hydroxyl groups (**Figure 4.1**).[13] Since the reactivity of surface hydroxyl groups varies with the specific surface species, the analysis of surface hydroxyl groups not only characterizes surface acid-base properties but also can provide information on the surface morphology of MgO.

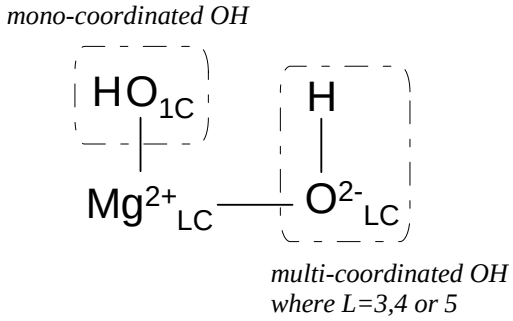

Figure 4.1 Mono-coordinated and multi-coordinated hydroxyl groups on MgO. Mono-coordinated OH is the OH on hydroxylated magnesium cation while multi-coordinated OH is a protonated oxide anion. [13]

Although solid bases have been applied industrially for more than forty years, the surface properties associated with solid base catalysts have been less well studied compared with solid acid catalysts. [6] Previously solid basic metal oxides have been characterized mainly with spectroscopic tools (such as UV-visible [14] and photoluminescence [9]) and a variety of adsorption experiments.[15,16,17] Determination of surface hydroxyl groups usually is accomplished via FT-IR spectroscopy [18,19,20,21,22] and by titration with molecular probes. [11,23] Few quantitative methods relating to measuring the content of surface hydroxyl groups on metal oxides had been published previously. [24,25,26,27] To detect basic sites on metal oxide surfaces either by spectroscopy or the adsorption/desorption of probe molecules (ex. CO_2 and phenol), thermal pre-treatment at high temperature is required to remove adsorbed species. For example, to remove hydroxyls and carbonates from MgO, the pre-treatment temperature has to exceed at least 800^{o}C. At this temperature, the distribution of surface oxide sites is expected to change significantly due to the change in the morphology. Another disadvantage of current techniques is that each provides a limited picture of surface hydroxyl chemistry; multiple techniques need to be used to fully characterize surface hydroxyls in terms of their quantity and type. Thus, characterization methods for metal oxides that can proceed at modest temperatures and simultaneously interpret the type and quantity of hydroxyl groups are desired.

This work proposes that a chemiluminescent reaction may provide a means to characterize active sites on metal oxides. Since tetrakis(dimethylamino)ethylene (TDE) was observed in 1950 by Pruett *et al*. [28], the reaction mechanism of TDE chemiluminescence (CL) and properties of TDE have been well studied; [29,30,31,32,33,34] However, research applying TDE as a probe in chemical and biochemical reactions is rare. As the reaction shown in **Figure 4.2**, TDE reacts spontaneously with oxygen to from the high energy intermediate, tetrakis-dimethylamino-1,2-dioxetane, TDMD. [34,35] The cleavage of the C-C and O-O bonds of the 1,2-dioxetane moiety provides the energy for emission of a photon. [36,37,38,39] In TDE CL, TDE itself is the emitter. [40]

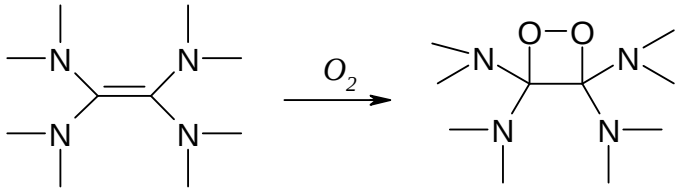

TDE *TDMD*

Figure 4.2 The molecular structures of tetrakis(dimethylamino)ethylene (TDE) and tetrakis-dimethylamino-1,2-dioxetane (TDMD).

TDE CL is unique from other chemiluminescent reactions because TDE is non-polar, while the products of TDE oxidation are polar. Five polar products are produced when TDE reacts with oxygen spontaneously: tetramethylurea (TMU, 65 mole%) and tetramethyloxamide (TMO, 18 mole%), tetramethylhydrazine (TMH, 12 mole%), bis(dimethylamino)methane (BMAM, 2mole%), and dimethylamine (DMA, trace amounts). [41] TMU and TMO are known to quench TDE CL. [34,40] These molecules collide with excited TDE, leading to reduced emission intensity and a red shift in emission wavelength. In addition, the transfer of the polar high energy intermediate of TDE CL, TDMD, from the TDE non-polar bulk phase into the products' polar disperse phase leads to a decrease in the emission intensity of TDE CL. [32,42,43]

TDE CL is enhanced by the addition of compounds with hydroxyl groups, such as alcohols. [44,45,46] For this reason, this work focuses on whether TDE CL could be used to analyze the distribution and density of adsorbed hydroxyl groups on metal oxide. MgO was

chosen in this study because more theoretical and fundamental studies have been done on MgO than other metal oxides. [21,54] A lot of papers relating to the surface properties have been published. Therefore, it is convenient for us to develop a new characterization method used in detecting surface properties of a metal oxide. Samples resulting from different pretreatment conditions were analyzed using established characterization techniques and subsequently were tested in TDE CL to examine how the variation in density and distribution of hydroxyl groups impacts TDE CL.

4.2 Experimental and Sample Preparation

4.2.1 Preparation of the MgO Samples

The MgO nanoparticles (MgO^{plus}) were purchased from NanoScale, Inc. (Manhattan, KS.). They feature an extremely high surface area ($270 m^2/g$), small crystal size (4nm) and rough surface morphology. The MgO was heat treated by sealing the MgO sample in a glass cell connected to a N_2 cylinder and vacuum line. A cylindrical electric furnace heated the MgO sample to the desired temperature while the cell was purged by dry nitrogen. The temperature was maintained at the desired temperature for 2.5 hours. In order to inhibit surface reconstruction during preparation, the temperature was increased from room temperature to the desired temperature at 3^oC/min. After that, the sample cell was purged by a vacuum line to evacuate the residual gas inside the cell at the desired temperature for 0.5 hours. The heat treated MgO sample was sealed inside the cell, cooled down in air, and then moved into a glove box for further study. Moisture-treated MgO was prepared by treating the MgO in an electric furnace at 700^oC for 3 hours to remove adsorbed species and then re-hydrating with steam at 85^oC for 2 hours. Before the use of the moist treated MgO, the sample was treated at 150^oC in a sealed cell which was purged by nitrogen to remove physisorbed water.

4.2.2 IR Spectroscopy

All infrared spectra were obtained in a DRIFTS cell (SpectraTech) using a Mattson FT-IR spectrometer (Model: Cygnus 25). The spectrometer is equipped with liquid nitrogen-cooled MCT detector, KBr beam splitter, and ceramic light source. The DRIFTS cell was connected to

both mass flow controller and a sealed flask with 20 ml TDE, as the sketch showed in Figure 3. 4. The flow rates of N_2 and O_2 going through the flask and DRIFTS cell were controlled by a mass flow controller.

4.2.3 Surface Hydroxyl and Surface Area Measurement

The surface area of pre-treated MgO samples were determined by BET dynamic method using Quantachrome Autosorb-1. Nitrogen was used for the adsorption experiment at liquid nitrogen temperature. The content of surface hydroxyls on each MgO sample were measured by the $AlEt_3$ titration. [44,47,48,49] The detail procedure of $AlEt_3$ titration was described in Chapter 3.

4.3 Results

4.3.1 Measurement of Surface Hydroxyls

In order to eliminate physisorbed water, the MgO samples were pretreated at 150^{o}C. The surface hydroxyl groups on heat-treated MgO or moisture-treated MgO were measured and the results are shown in **Figure 4.3**. **Figure 4.3** shows the concentrations of total hydroxyls, hydrogen-bonded hydroxyls, and isolated hydroxyls on pretreated MgO. The concentration of hydroxyl groups on MgO heat-treated at 150^{o}C is 1.72×10^{21} OH/g (2.87 OH / nm^2) and decreases with increasing pretreatment temperature. Both the densities of isolated and hydrogen-bonded hydroxyl groups decrease linearly with increasing pretreatment temperature for MgO. However, the decrease is much more significant for hydrogen-bonded hydroxyl groups. The decrease in hydroxyl density is due to the desorption of the hydroxyl groups with lower thermal stability and the loss of surface area when MgO was outgassed at high temperature. The loss of surface area was particularly significant when MgO was pre-treated using the moisture-treatment. For example, the surface area of heat-treated MgO at 150^{o}C was 270 m^2/g, but decreased to 78 and 82 m^2/g, respectively, when MgO was treated by heat-treatment at 700^{o}C and moisture-treatment. In moisture-treatment, MgO was heated at 700^{o}C for 3 hours to remove adsorbed hydroxyl groups. Although the surface of MgO was re-hydrated by steam, the total

hydroxyl group density on moist-treated MgO (55.84×10^{-5} mole/g) was less than that on heat-treated MgO (at 150, 200, 300 and 400^{o}C).

The heat-treated MgO samples have nearly the same ratio of isolated hydroxyl group to total hydroxyl group at all conditions, with a range 16.6-18.8%. However, this ratio jumps to 26.4% for moisture-treated MgO. Treating the samples with water vapor clearly changed the composition of surface hydroxyl groups and increased the ratio of isolated hydroxyl groups to total hydroxyl groups.

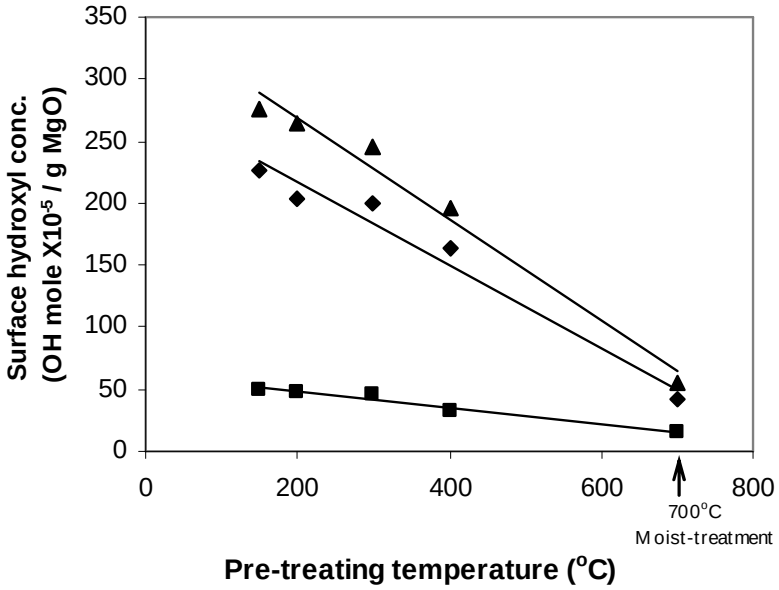

Figure 4.3 Densities of total OH(▲), hydrogen-bonded OH (♦) and isolated OH (■) on heat-treated and moisture-treated MgO surfaces.

4.3.2 Infrared spectra of MgO

The IR spectrum of MgO, shown in **Figure 4.4**, has two intense bands in the regions 3000-3800cm^{-1} and 1300-1700cm^{-1}. The bands in these two regions are attributed to hydroxyl groups and carbonates, respectively. The shoulder next to the band of carbonate at around 1645cm^{-1} is adsorbed water. This water could be removed completely by heating to 100^{o}C or higher,[22,50] as seen in **Figure 4.4**. The OH stretching region typically is employed in identifying two types of hydroxyl groups. The broad domain in the region of 3100 to 3660 cm^{-1}

is assigned to the stretching modes of the hydrogen-bonded OH groups, whereas the narrow bands at higher frequency in the region from 3660 to 3750 cm^{-1} are assigned to isolated OH stretching vibrations. The band intensity of hydrogen bonded OH decreases in intensity with increasing pre-treatment temperature between 100^{o}C to 700^{o}C, as seen in **Figure 4.5**. In contrast, the band intensities of isolated OH at 3695 and 3741 cm^{-1} did not noticeably change before the pretreatment temperature reached 300^{o}C and 600^{o}C, respectively. A peak shift occurs with the increase of pretreatment temperature, both in the sharp band at 3741 cm^{-1} and the broad band between 3100 and 3660 cm^{-1}.

The band at 3741 cm^{-1} appears as a shoulder on the band at 3695 cm^{-1} at lower temperatures (25-200^{o}C). The band of isolated OH splits into two equally intense bands at 3695 and 3741 cm^{-1} when the temperature increases to 300^{o}C. The band at 3695 cm^{-1} disappears following heating to 400^{o}C. The thermal stability of adsorbed OH was in the order of (from most to least stable): the shoulder at 3741 cm^{-1}, the sharp band at 3695 cm^{-1}, the broad band from 3100 to 3660 cm^{-1} (seen in **Figure 4.5**).

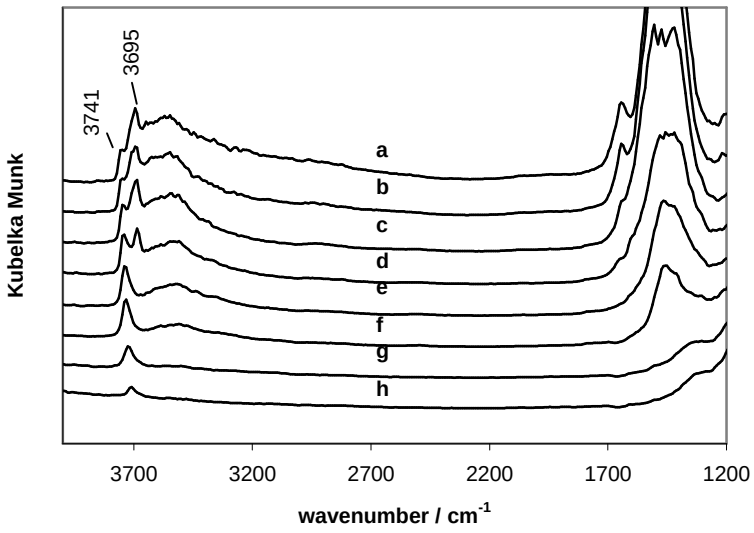

Figure 4.4 IR spectra of heat-treated MgO at elevated temperature: a. room temperature (25^{o}C); b. 100 ^{o}C; c. 200 ^{o}C; d. 300 ^{o}C; e. 400 ^{o}C; f. 500 ^{o}C; g. 600 ^{o}C; h. 700^{o}C.

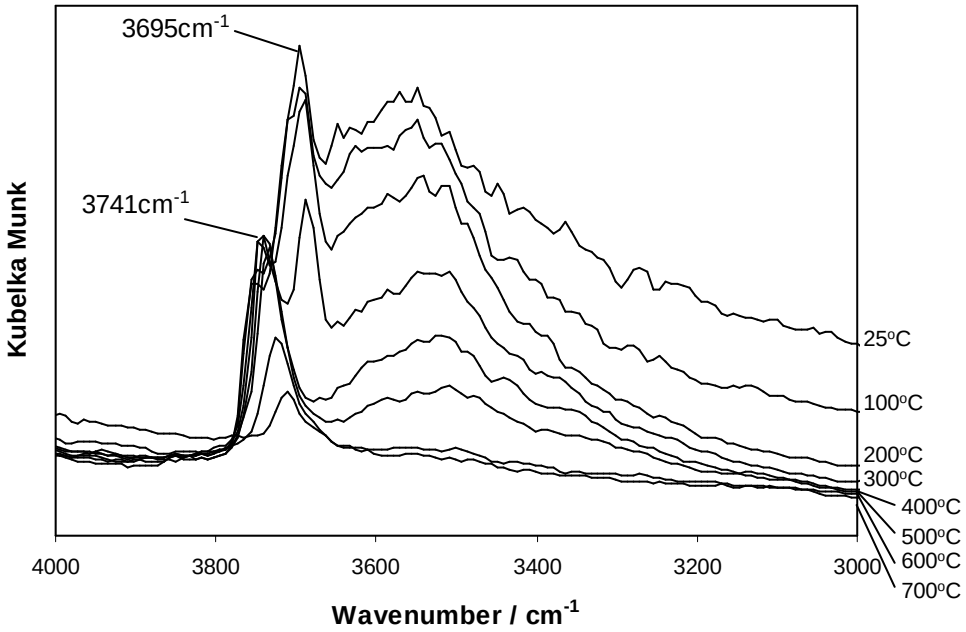

Figure 4.5 The IR bands of 3C, 4C isolated OH and hydrogen-bonded OH on the surface of MgO which was heat-treated at temperatures from 25 ^{o}C to 700 ^{o}C.

4.3.3 Decomposition of TDE on MgO

The interaction between TDE and pre-treated MgO (including heat- and moisture-treated MgO) were studied both with and without oxygen through IR spectroscopy. The results for the trials when no oxygen was fed are shown in **Figure 4.6** and **Figure 4.7**. The IR bands of TDE are noted in the region of 1000-1400 cm^{-1}, 1420-1490, and near 1650 cm^{-1}. The bands from 1000-1400 cm^{-1} can be assigned to C-N bond stretching or bending within the central $N_2C{=}CN_2$ or $N\text{-}CH_3$ fragments. The IR bands in the region 1420-1490 cm^{-1} are assigned to the approximately 20 bending modes of CH_3 groups. [51] The feature at 1650 cm^{-1} is consistent with a C=O bond stretch, which could come from the oxygen-containing products of TDE oxidation, likely TMU or TMO. It was also noted that the peak at 1650 cm^{-1} appeared after the moisture-treated MgO upon which TDE was pre-adsorbed was exposed to oxygen. It was found that this peak grew with time, consistent with the assignment of this peak to oxidation products. As seen in **Figure 4.6** and **Figure 4.7**, the band at 1650 cm^{-1} was observed on heat-treated MgO (at 700^{o}C) but not on moisture-treated MgO. On heat-treated MgO, the band at 1650 cm^{-1}

increases with time after TDE was introduced into the DRIFT cell from 0 to 40 minutes and stops increasing at 40 minutes, while the intensities of other bands (1049, 1095 and 1388 cm^{-1}) still increase with time from 40 to 80 minutes.

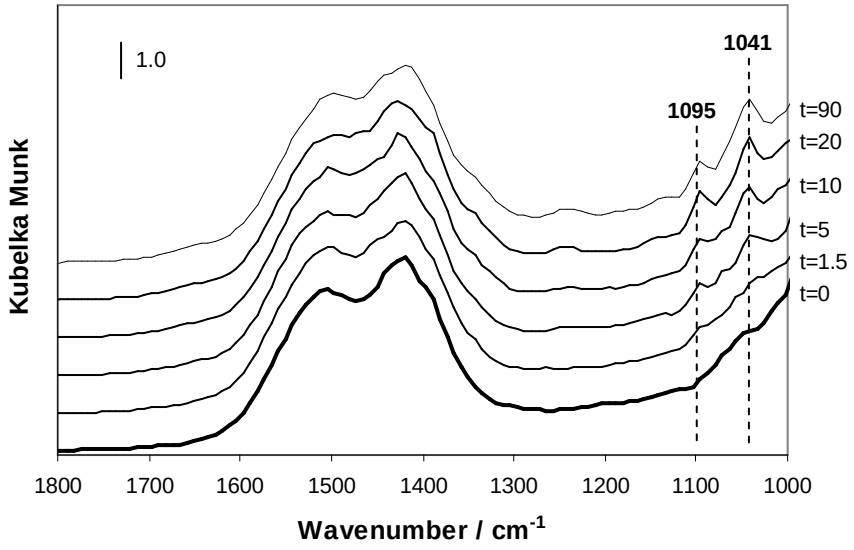

Figure 4.6 IR spectra of TDE on moisture-treated MgO. TDE was introduced into the DRIFT cell from 0 to 90 minutes.

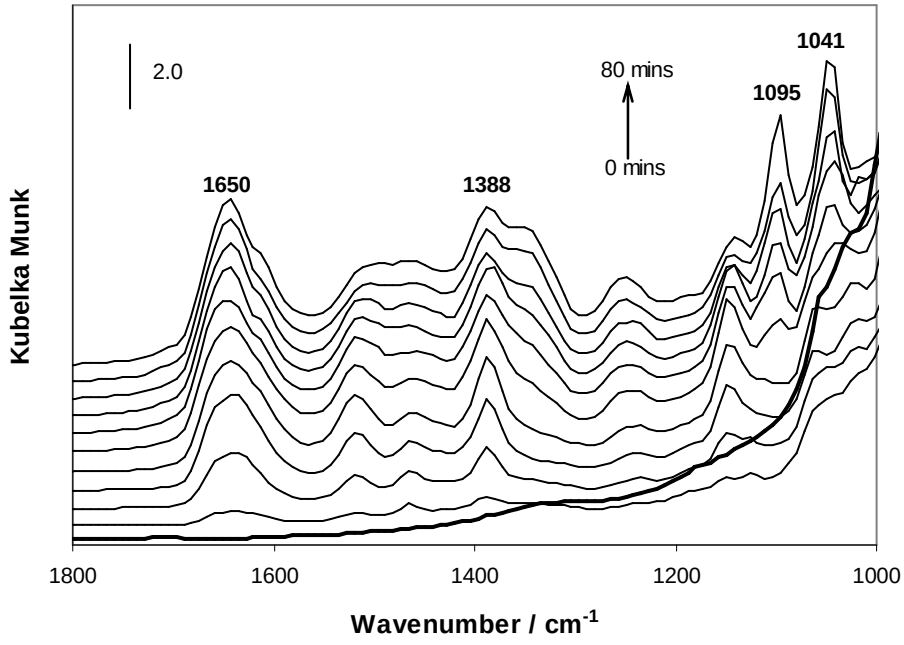

Figure 4.7 The decomposition of TDE on the active sites (Mg^{2+} or O^{2-} ions) of MgO which was pre-treated at 700^{o}C. TDE was introduced into the DRIFT cell from 0 to 80 minutes.

4.3.4 The I_t (emission intensity vs. reaction time) curves of catalyzed TDE CL

The I_t curves for TDE mixed with MgO which was heat-treated at 150, 200, 300 and 400^oC and also a moisture-treated sample are shown in **Figure 4.8**. It is clear that the I_t curve of TDE CL on moisture-treated MgO differs from the others, not only in the maximum emission intensity but also in the shape. The maximum intensity of the I_t curve of TDE CL on moisture-treated MgO was about four times that of the I_t curve of TDE CL on heat-treated (150^oC) MgO. The shape of the I_t curves of the TDE CL catalyzed by moisture-treated MgO, heat-treated MgO at 400^oC, and TDE CL without MgO have a similar exponential decay (**Figure 4.8**, curves **d**, **e** and **f**). The I_t curves of TDE CL on heat-treated MgO at 150, 200 and 300^oC (**Figure 4.8**, curves **a**, **b** and **c**) are quite different. After an initial decrease in emission intensity, there is a brief increase, followed by an exponentially decreasing trend. The maximum in the emission intensity occurs at longer reaction times with increasing pretreatment temperature.

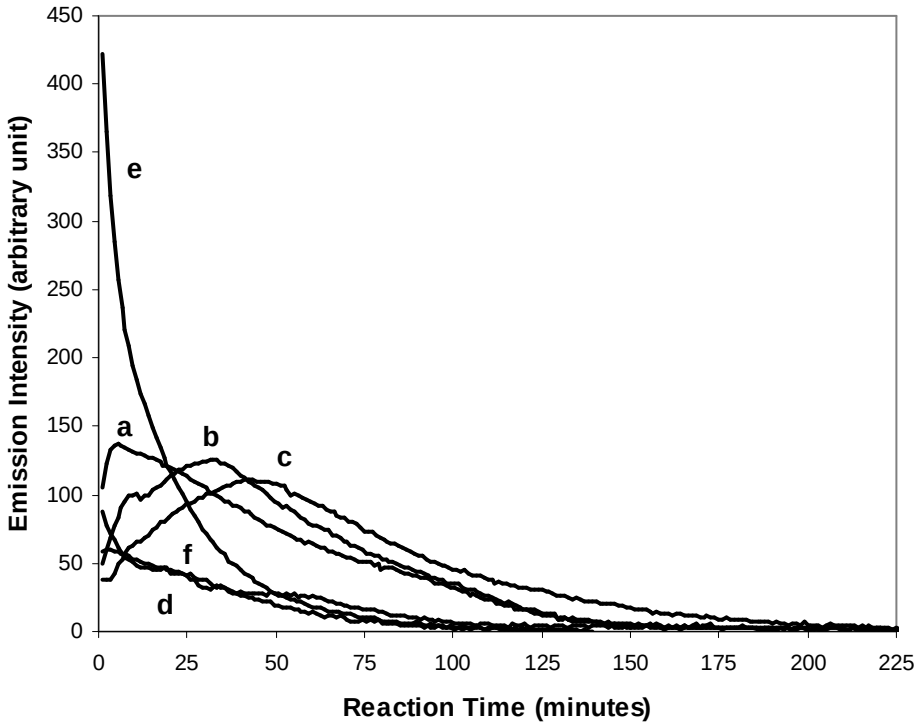

Figure 4.8 The I_t curves of catalyzed TDE CL on heat-treated MgO (curve a-curve d) and moisture-treated MgO (curve e). For the I_t curves of TDE on heat-treated MgO, MgO was pre-treated at a. 150°C; b. 200 °C; c. 300 °C; d. 400 °C before mixing with TDE. Curve f is the I_t curve of TDE CL without MgO.

4.4 Discussion

4.4.1 IR studies of adsorbed OH on MgO

On an MgO surface, the 3, 4 and 5-coordination (3C, 4C and 5C) active sites (uncovered Mg^{2+} and O^{2-} ions) are provided by (111), (110) and (100) crystallographic planes, respectively, usually denoted as $Mg^{2+}{}_{3C}O^{2-}{}_{3C}$, $Mg^{2+}{}_{4C}O^{2-}{}_{4C}$ and $Mg^{2+}{}_{5C}O^{2-}{}_{5C}$. [53] Knözinger *et al*. [21] indicated that the stretching frequency of OH was correlated with the degree of coordination of oxygen ions in OH. Increasing the number of metal ions adjacent to the oxygen ion of OH would cause an additional downward frequency shift. [21,52] For instance, when isolated OH was adsorbed on a lower coordination ion, the stretching frequency of this isolated OH would appear

at higher frequency in the IR spectra since OH on edges or corners (4C or 3C) are necessarily less perturbed by the reduced number of nearest neighbors compared with the hydroxyl groups on an extend plane (5C). [22] Chizallet *et al*. and Knözinger *et al*. summarize the surface isolated OH into two categories from the dissociation of water on MgO (**Figure 4.9**):

A. 1-coordinated OH groups (proton acceptor) - produced by the hydroxylation of magnesium ions
B. Multi-coordinated (3-, 4-, 5-coodinated) OH groups (proton donor) – created by the protonation of oxide ions.

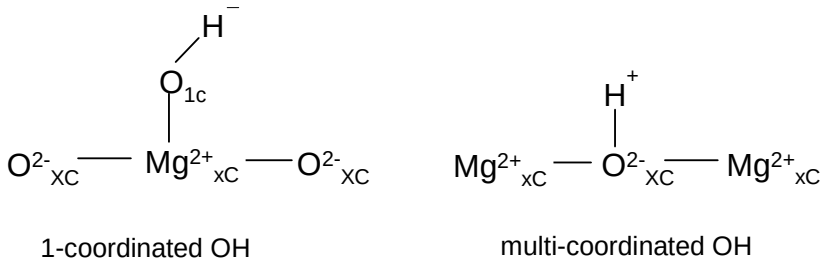

Figure 4.9 Types of surface hydroxyl groups on MgO, where X = 3, 4 and 5 when the ions locate on corner, edge and planes, respectively.

The stretching frequency of these two type OH groups in the IR spectrum is still in dispute. Some researchers argued that the sharper band at higher frequency (3740 cm^{-1}) is contributed by type A (1-coordinated OH) hydroxyl and the broad band at lower frequency (3650-3450 cm^{-1}) is assigned to B type hydroxyl (multi-coordinated OH) [53,54] while other researchers stated that type A OH appears at higher frequency (>3700 cm^{-1}) and type B OH appears both at a higher frequency (>3700 cm^{-1} for defect and lower coordinated OH) and the lower frequency (<3700cm^{-1} for higher coordinated OH). [10,21,22] However, it can be concluded from the former studies [9] that the thermal stability of isolated hydroxyl groups are inversely proportional to the coordination number of the oxide ion. The deprotonation temperatures for oxide ions are in the order of Mg_{LC}-$O^{2-}{}_{3C}H$ (deprotonated at 800^oC) > Mg_{LC}-$O^{2-}{}_{4C}H$ (deprotonated at 400^oC) > Mg_{LC}-$O^{2-}{}_{5C}H$ (deprotonated < 400^oC). Such results also infer that the basicity of oxide ions on MgO increases with the decrease in the coordination number of the oxide ion.

From our IR results and those described in the literatures, the following conclusions can be reached about the types and relative amounts of different types of hydroxyl groups on the surface of MgO following different pretreatment procedures. First of all, hydrogen-bonded hydroxyls are located in the region from 3100 to 3660 cm^{-1}, making it difficult to observe any contribution of 5-coordinated (5C) isolated OH ($OH_{isolated}$) [9,17] A shift in the peak of the broad band at 3660-3100 cm^{-1} was noted as temperature was increased (**Figure 4.5**): above 400^{o}C, the peak of the broad band shifts from 3556 to 3525 cm^{-1}. This may be explained by the disappearance of 5C isolated OH.

The features noted between 3660 and 3750 cm^{-1} are assigned to 3 and 4-coordinated isolated OH and 1-coordinated isolated OH. There are significant changes in this band as treating temperature increases, as noted above. The peak at 3741 cm^{-1} is more thermally stable than the peak at 3695 cm^{-1}. For this reason, and because of the known stability of 3 and 4-coordinated isolated OH, the peak at 3741 cm^{-1} can be assigned to the 3-coordinated isolated OH and 3695 cm^{-1} as 4-coordinated isolated OH. There also may be some contribution of 1-coordinated isolated OH in the peak at 3741 cm^{-1}. [55] The presence of this peak may explain why the feature at 3741 cm^{-1} decreases in intensity at moderate temperatures (500^{o}C) and shifts to 3718 cm^{-1}, characteristic of the 3-coordinated isolated OH group, at 700^{o}C. Previous research suggests that 3-coordinated isolated OH is stable up to temperatures of 800^{o}C. [9] The assignments associated with each hydroxyl group are presented in **Figure 4.10**.

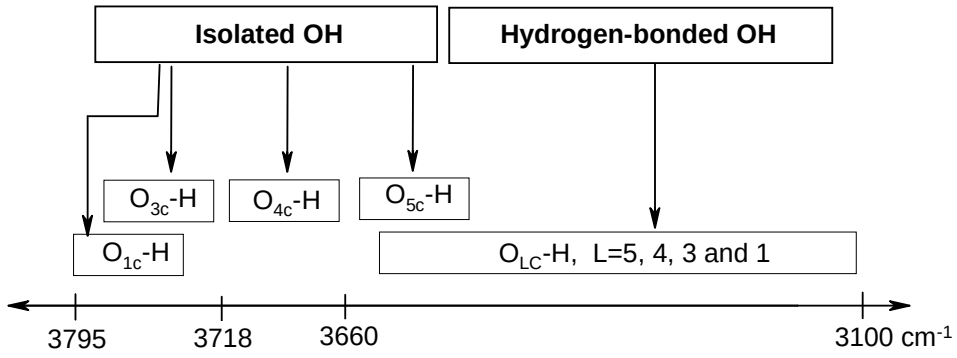

Figure 4.10 The stretching frequencies of different hydroxyl groups on MgO.

As seen in **Figure 4.11**, the moisture-treated MgO surface exhibits more 4 coordination isolated OH. The results of Bailly *et al*. [56], Coluccia *et al*. [57] and Zecchina *et al*. [58] noted that the cubic MgO particle was eroded by water vapor, leading to an increase in the lower coordinated sites (O^{2-}_{3C} and O^{2-}_{4C}) on the surface. **Figure 4.11** shows a relatively intense peak at 3695 cm^{-1} after MgO was re-hydrated by steam at 85^{o}C (moisture-treatment). The enhancement in the intensity of the peak at 3695 cm^{-1} indicates that more 4-coordinated isolated hydroxyls (or surface defects) were formed on the surface after moisture- treatment. The thermal stability of this intense band was studied in **Figure 4.12**. The intensity of the band at 3695 cm^{-1} was constant from 25 to 200^{o}C. However, it started to decrease at temperatures over 300^{o}C and disappeared by 400^{o}C. Thus, it is clear that the surface of moisture-treated MgO was dominated by 4-coordinated isolated OH groups, which disappear upon treatment at moderate temperatures (< 400°C).

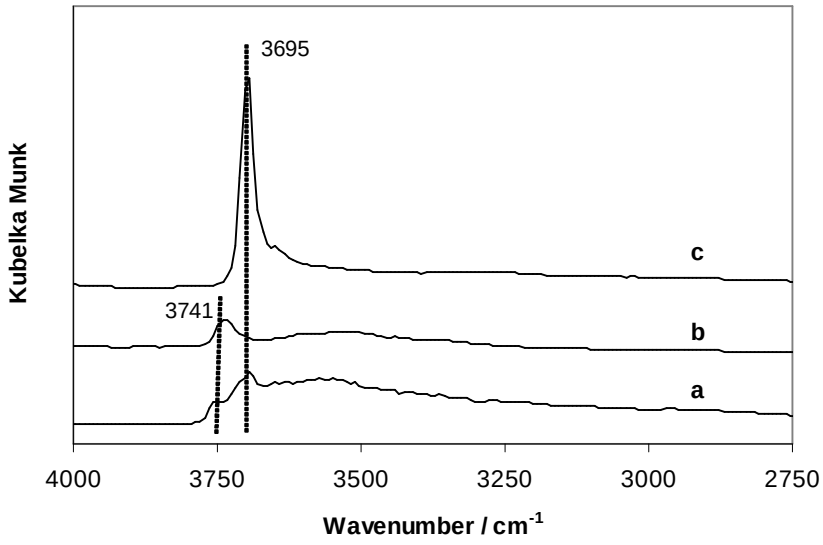

Figure 4.11 IR spectra of hydroxyl groups on MgO surface: a. the hydroxyl groups on heat-treated MgO at 150^{o}C; b. the residual hydroxyl groups on heat-treated MgO at 400^{o}C; c. the hydroxyl groups (4-coordinated isolated OH) on moisture-treated MgO.

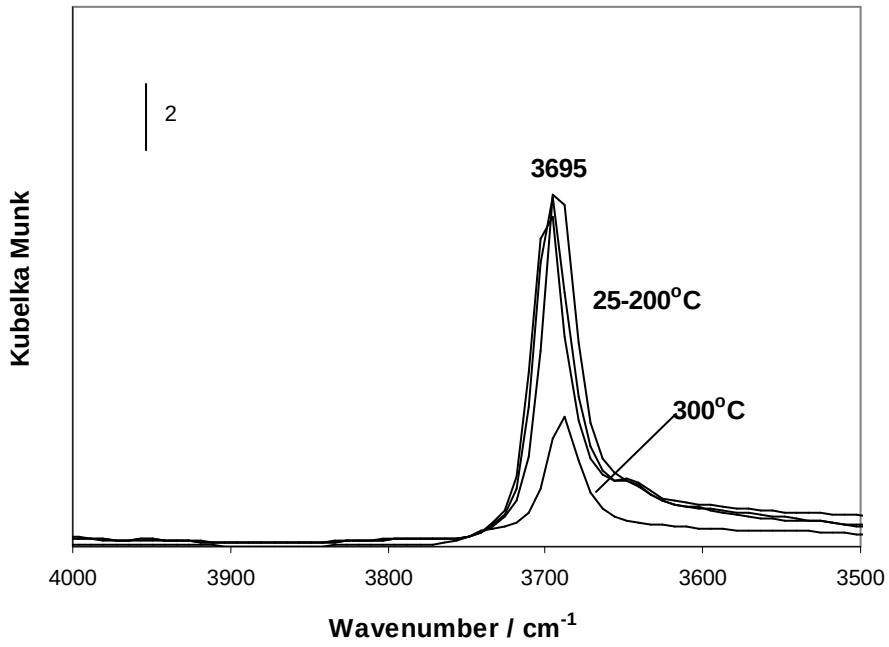

Figure 4.12 The thermal stability of isolated OH on moisture-treated MgO when moisture-treated MgO was treated by an elevated temperature from 25 to 300°C. The band at 3695cm^{-1} disappeared when the temperature was increased up to 400°C.

4.4.2 I_t curve of TDE CL

As seen in **Figure 4.8**, the I_t curve for catalyzed TDE CL on MgO varies dramatically for different pretreatments. For this reason, it infers information on the nature (surface area, morphology, and types of hydroxyl groups) of the MgO surface from the I_t curve. To do this, a number of trends in the I_t curves must be explained. First, the shape of the I_t curves varies dramatically for samples that have undergone different pretreatments. In some cases, the I_t curve displays a maximum in the emission intensity which is a function of the pre-treating temperature of the MgO (**Figure 4.8**, curve **a**, **b** and **c**). In addition, this maximum disappears, assuming an exponentially decreasing trend with moisture-treatment or heat-treatment at 400°C. These trends are hypothesized to be due to multiple factors, including the presence of quenching species, the types and surface concentrations of hydroxyl ions present on the MgO surface, and the ability of bare MgO sites to decompose TDE.

4.4.2.1 Quenching effect

The influence of the species which quench TDE CL is hypothesized to be responsible for the deformation of the I_t curves (the I_t curve with a local maximum). It is well known that the products (primarily TMU and TMO) which are produced from the TDE chemiluminescence reaction can act to quench the emission of light from the reaction of TDE with oxygen. [34,40] Prior results in our laboratory have shown that adding TMU into solution does, indeed, decrease the intensity of TDE CL [56]; however, the trend is not linear. Initially, intensity decreases linearly with TMU concentration. After a concentration of 0.383M, the intensity continues to decrease, but the slope is much smaller than at lower TMU concentrations. These results were interpreted based on the solubility of TMU in TDE. TMU is polar, while TDE is not. For this reason, TMU will form a second liquid phase within TDE once its concentration exceeds its modest solubility in TDE. Experimentally, a second liquid phase was observed at high TMU concentration. The point where the slope changed probably corresponded to the solubility of TMU in TDE. At concentrations beyond that point, TMU formed a second liquid phase, so additional TMU beyond that concentration had little effect on emission intensity.

The unusual shape of the I_t curves can be explained by the presence of quenching species, the relative rates of their formation, and their subsequent removal into a second liquid phase. This hypothesis was tested by using a surfactant (AOT, dioctyl sulfosuccinatesodium salt) to introduce a micellar phase. **Figure 4.13** shows the I_t curves of TDE CL in solutions with and without AOT reversed micelles. When AOT is added at a concentration less than its critical micelle concentration (CMC) (**Figure 4.13** curve **a**) [60,61,62,63], a maximum is observed in the emission intensity similar to that observed with numerous MgO-catalyzed TDE CL trials. These results suggest that the local maximum in TDE CL I_t curve is a consequence of the presence of quenching species in the TDE bulk phase. In the presence of AOT reversed micelles (**Figure 4.13** curve **b**, [AOT]=1.782 mM in iso-octane), the I_t curve progressively decreases with reaction time. When reversed micelles are present, the quenching species will be removed continuously by the migration from the non-polar TDE bulk phase to the hydrophilic water pools within the AOT reversed micelles. [59] In this way, the concentration of the quenching species is kept much lower than the saturation points of quenching species. The monotonically decreasing I_t curve is a consequence of the consumption of TDE. When reversed micelles are not present, the

quenchers accumulate in the bulk phase over time and aggregate together to form micro-drops when the concentration of quenchers reaches their saturation points in the solution. Thus, the local maximum on the I_t curve indicates the competition between the quenching reactions and TDE chemiluminescence.

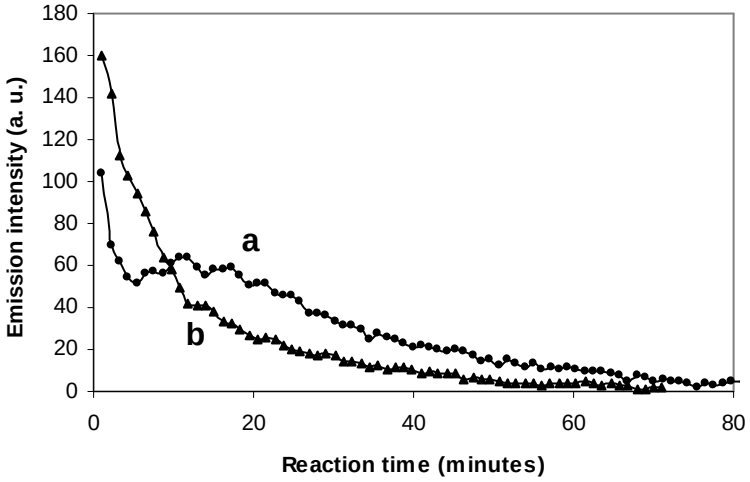

Figure 4.13 I_t curves of TDE CL in iso-octane with addition of AOT: a. below the critical micelle concentration of AOT ([AOT]=0.430 mM); b. above the critical micelle concentration of AOT ([AOT]=1.782 mM). The concentration of TDE in cyclohexane was fixed at 2.54M.

In the system of interest, the local maximum indicates the presence of TDE reaction products (as quenching species) in the non-polar TDE liquid phase. **Figure 4.14** depicts the proposed aggregation mechanism of TDE products in the non-polar TDE bulk phase. In region **a**, the emission intensity of TDE CL decreases gradually with increasing concentration of the dissolved TDE products until the concentration of TDE products reach the saturation points (point **1**). At the saturation point, the TDE products separate out from the bulk phase and coalesce together to form micro-drops suspended in the TDE bulk phase. After point **1**, because the aggregation rate of polar TDE products in the TDE non-polar bulk phase is higher than the production rate of the products, the curve goes up with reaction time (region **b**). The aggregation rate of TDE products is balanced by the production rate of TDE products at point **2**. After point **2**, a further increase in the concentration of TDE products leads to the formation of the second polar liquid layer that separates from the TDE phase. This second phase has been seen

experimentally as tiny drops sticking on the wall or bottom of the sample cuvette when the reaction time is in region **c** have been observed. The drops further combine together to form a second layer at the end of the reaction.

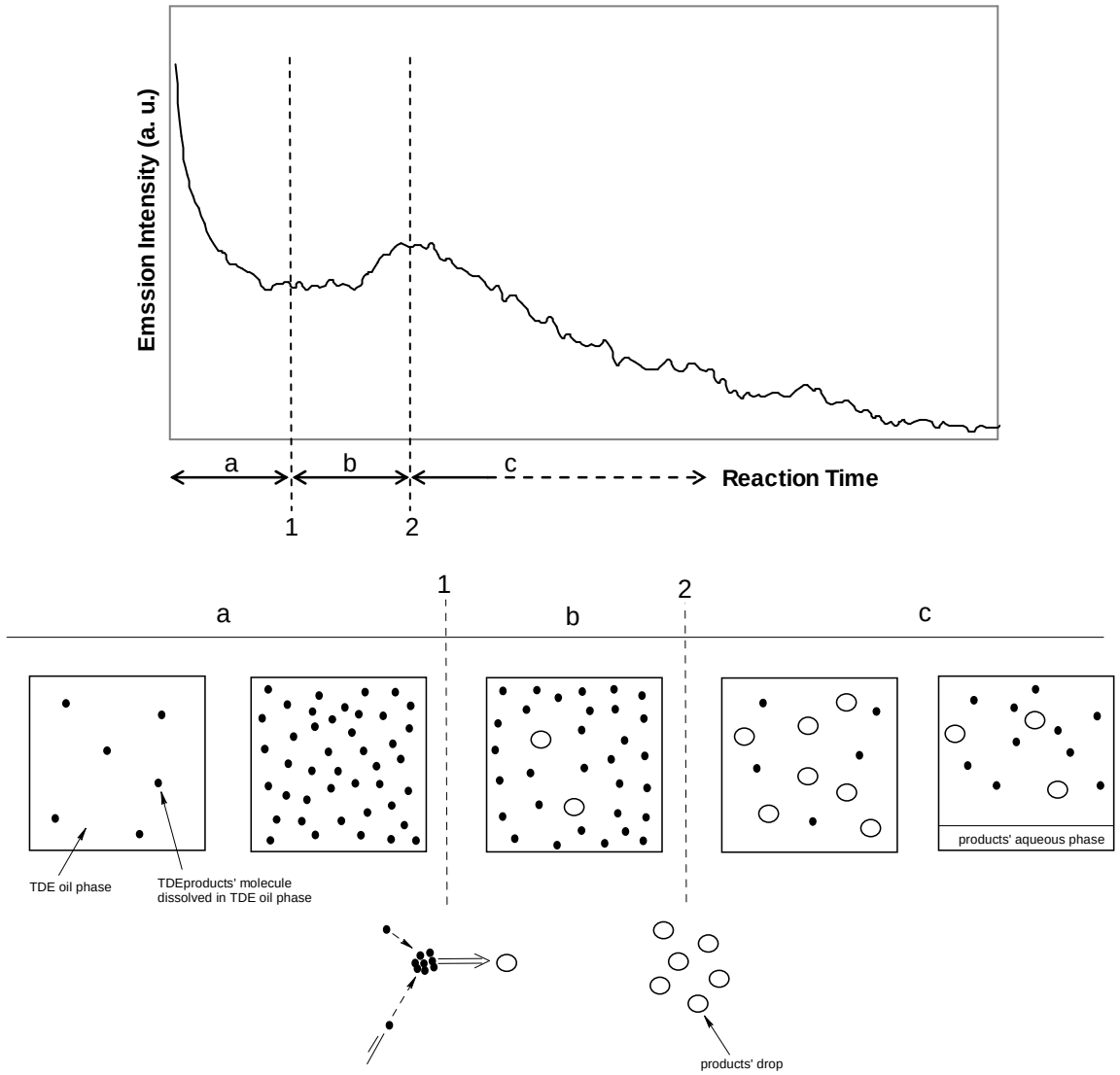

Figure 4.14 Aggregation mechanism of the polar TDE products in the TDE non-polar bulk phase.

If quenching species are responsible for the presence of the local maximum, then they would also affect the time at which the local maximum appeared. To investigate this, TMU was added in different amounts while TDE CL was monitored (see **Figure 4.15**). As seen in this figure, the local maximum in the I_t curves are observed for all concentrations of TMU; but, the time at which the local maximum occurs shifts to earlier reaction times with increasing TMU

concentration. This observation is consistent with the mechanism proposed in **Figure 4.15**. The presence of more quenchers at the start of reaction means that the saturation concentration is reached at earlier times, causing the local maximum to appear earlier.

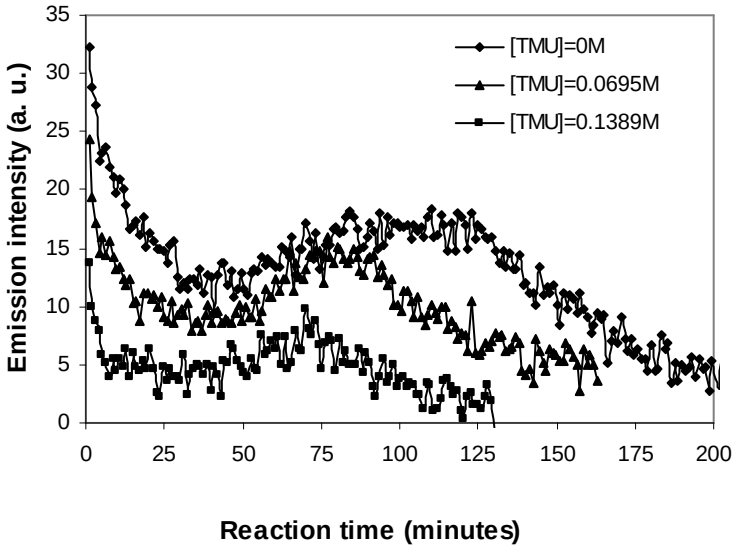

Figure 4.15 I_t curves when the addition of TMU in cyclohexane solution (with 2.8654 M TDE) was adjusted from 0 M to 0.1389 M.

With these ideas in mind, the results observed in **Figure 4.8** can be explained. The reaction time at which the local maximum appears is highly dependent on the pretreatment conditions. Higher pretreatment temperatures shift the local maxima to later reaction times; these pretreatment conditions also correspond to much lower surface hydroxyl group concentrations. Thus, it is hypothesized that surface hydroxyls catalyze the reaction of TDE with oxygen. Lower pretreatment temperatures result in materials with more hydroxyls, which enhance TDE oxidation. This results in faster reaction rates and faster production of quenching species. As noted above, the increasing concentration of quenching species causes the local maximum to occur at shorter times. For this reason, it was observed that samples with more hydroxyl groups (lower pretreatment temperatures) exhibit the local maximum at shorter times than samples with fewer hydroxyl groups. This hypothesis is further supported by experiments when different amounts of MgO were used to enhance TDE CL, shown in **Figure 4.16**. The additional MgO reduced the time at which the local maximum in emission intensity appeared,

again consistent with a larger number of hydroxyl groups increasing the reaction rate for TDE CL.

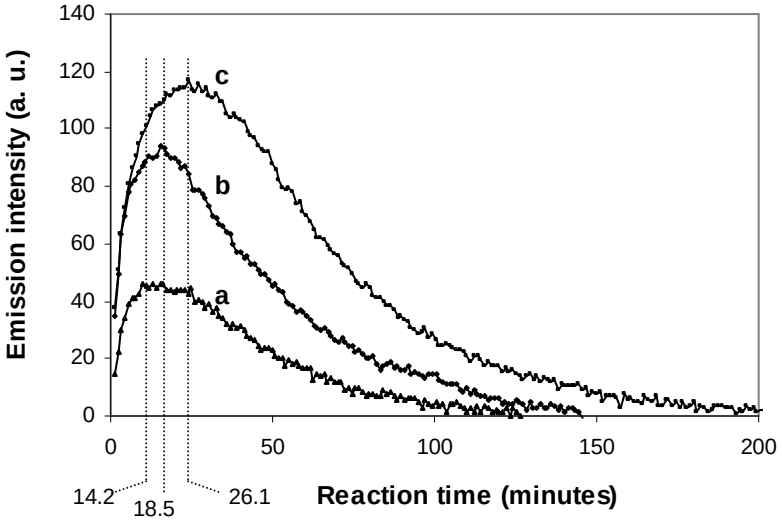

Figure 4.16 The shift of the local maxima on the I_t curves when a. 0.2g, b. 0.15g and c. 0.10g heat-treated MgO at 150^{o}C was added into the solution of 400 µl TDE and 200 µl cyclohexane. The dash line points out the peak position of the local maximum on the I_t curve.

4.4.2.2 Surface Hydroxyl effect

Although samples with more hydroxyl groups speed up TDE oxidation, this does not necessarily imply that those samples produce the highest chemiluminescence. Several different types of hydroxyl groups are present on all samples that may have very different roles in TDE CL.

4.4.2.2.1 Isolated hydroxyls

Isolated hydroxyls are believed to be the cause for enhanced chemiluminescence for some MgO samples. In particular, lower coordinated isolated OH, $O^{2-}{}_{3C}H$ (3C OH) and $O^{2-}{}_{4C}H$ (4C OH), are thought to significantly enhance TDE CL. These conclusions are based on the results shown in **Figure 4.8** and **Figure 4.11**. Moisture-treated MgO gave the most intense emissions of any of the MgO samples tested, as seen in **Figure 4.8**. If all hydroxyl groups were

equally active for catalyzing TDE CL, we would expect that moisture-treated MgO would have the highest concentration of hydroxyl groups. In fact, the opposite is the case: the total hydroxyl concentration is less than the other samples (55.84×10^{-5} mol/g compared to a range of 196.10-276.04×10^{-5} mol/g for other samples). An alternate interpretation is that only isolated hydroxyl groups are active in catalyzing TDE CL. This interpretation would suggest that moisture-treated MgO should have more isolated hydroxyl groups; again, this is not the case (moisture-treated MgO has an isolated hydroxyl concentration of 14.74×10^{-5} mol/g compared to a range from 32.50-49.17×10^{-5} mol/g for other MgO samples). Instead, the data suggest that 4C isolated OH are most active in TDE CL. As shown in **Figure 4.11**, the isolated hydroxyls on moisture-treated MgO are mostly 4C isolated OH.

Further support for the role of 4C isolated OH in catalyzed TDE CL can be seen in the trends for heat-treated MgO samples as the pretreatment temperature is increased. As seen in Figure 4.8, the emission intensity of TDE CL slightly decreases as pretreatment temperature is increased from 150 to 300^{o}C. Increasing pretreatment temperature up to 400^{o}C, the MgO surface loses the ability to enhance the emission intensity of TDE CL. The I_t curve of TDE CL on heat-treated MgO at 400^{o}C (curve **d**) almost overlaps with the I_t curve of TDE without MgO (curve **f**). As the pretreatment temperature is increased from 200 to 400^{o}C, both the total concentration of isolated hydroxyls and the amount of 4C isolated OH (**Figure 4.12**) decrease, again suggesting that isolated OH groups (particularly 4C isolated OH) are the active species for catalyzing TDE CL. It is particularly interesting to note that MgO treated at 400^{o}C has essentially no impact on TDE CL, since this sample is virtually free of 4C isolated OH. This interpretation is further supported by the chemiluminescence data in **Figure 4.8**.

The prior discussion ignored the possible role of 3C isolated OH for TDE CL. However, 3C isolated OH persists on the surface even at very high pretreatment temperatures as evidenced by the presence of the absorption band at 3741 cm^{-1} (see **Figure 4.4**). The reason that 3C isolated OH are not given a primary role in TDE CL is that 4C sites (edge sites) would be expected to be much more numerous than 3C sites (corner sites). Imaging a cubic particle constructed by Mg and O ions ($d_{Mg\text{-}O}$ = 2.107) with the same number of ions on each edge, the ratio of corner ions to edge ions would decrease rapidly with increasing particle size. For instance, the distance

between Mg^{2+} and O^{2-} ions is 2.107 Å. [18] For a MgO cubic with 0.6 nm on each edge, it can be calculated that the ratio of corner ions to edge ions is 33.33%. However this ratio decreases to 1.39% when the particle size of MgO cubic is increased to ~10.3 nm. The average crystallite size of the MgO that was used in this research was about 4 nm. Assuming an MgO particle forms a perfect cubic structure, the ratio of corner (3-coordination) ions to edge (4-coordination) ions is 3.7%. Obviously the MgO particles observed are not perfect cubes, thus the ratio should be lower than 3.7%. The possibility that 3C isolated OH catalyzed TDE CL cannot be excluded, particularly at high temperatures when these are the only hydroxyl species present; their impact, however, is expected to be much less than 4C isolated OH because of their lower concentration.

4.4.2.2.2 Hydrogen-Bonded Hydroxyls

As discussed above, emission intensity appears to be correlated with isolated hydroxyls, not total hydroxyls. Instead, hydrogen-bonded hydroxyls are believed to play a negative role in TDE CL. Like water and alcohols, [32] the participation of hydrogen-bonded hydroxyls in TDE CL could cause the transformation from a TDE mono-cation, TDE^+, to the TDE di-cation (TDE^{2+}) and TDE cation radical (TDE^{+}*), leading to the consumption of TDE through a non-fluorescent pathway. The color of TDE^{+}* is deep orange [32], thus, a color change from light yellow (the original color of TDE) to deep orange would be seen if a surface caused the transformation of TDE^+ to TDE^{+*}. Such a color change was observed at the instant that TDE was added to MgO surfaces that were rich in hydrogen-bonded hydroxyl groups. The color became lighter and lighter with reaction time as the TDE^{+*} underwent further decomposition.

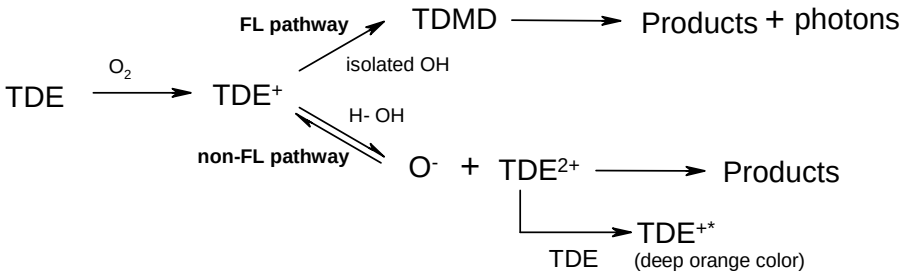

4.4.3 Interaction of TDE with MgO

Based upon the IR results shown in **Figure 4.7**, oxygen-containing products (TMU and/or TMO) are formed on heat-treated MgO even in the absence of oxygen in the feed. When a similar experiment was repeated on moisture-treated MgO, no evidence of TMU or TMO was found (no peak at 1650 cm^{-1} appeared for the 90 minutes of the experiment, **Figure 4.6**). This suggests that the heat-treated MgO surface could oxidize TDE, while the moisture-treated surface could not. We explain these results by pointing to the differences in the surfaces of these two materials. The moisture-treated sample has undergone surface reconstruction and adsorption of water. The adsorbed water is further decomposed into hydroxyl groups. The surface is likely saturated with hydroxyl groups, and few uncovered sites exist. For the heat-treated MgO, however, heating has removed many of the carbonate and hydroxyl groups adsorbed to the surface, so uncovered sites (Mg^{2+} and O^{2-} ions) are present at the surface. We hypothesize that these uncovered sites can react with TDE, producing TMU and TMO. Eventually, these sites become covered with products, explaining why the intensity of the peak at 1650 cm^{-1} ceases to increase after 40 minutes.

Decomposition of TDE on bare MgO sites may play some role in catalyzed TDE CL, but it is not expected to be a dominant role. Blocking of bare sites by products or adsorbed species will limit the influence of these sites. An exception may occur at the beginning of reaction. For example, the differences in the emission intensity in the beginning of the reaction for non-catalyzed TDE CL and TDE CL catalyzed by MgO pretreated at 400^{o}C noted in **Figure 4.8**. The decreased emission intensity noted for catalyzed TDE CL on pretreated MgO 400^{o}C may be caused by reaction of TDE with the bare sites on the MgO sample.

4.5 Conclusion

The potential for using TDE CL to probe surface hydroxyl distribution and, therefore, surface morphology and acid-base properties of MgO was studied. It was found that the TDE CL is extremely sensitive to the types of hydroxyl groups present on the surface of MgO. TDE CL intensity was enhanced by the presence of lower coordinated isolated hydroxyl groups,

particularly 4-coordinated isolated OH. Quenching species produced from TDE oxidation played a significant role in TDE CL and their production rate was affected by the amount of surface hydroxyls present. As quenching species (tetramethyl oxamide and tetramethyl urea) were formed, they began to aggregate and eventually formed a second liquid phase because they are polar while TDE is not. The aggregation caused a temporary increase in emission intensity after some time, as the quenching species were removed from the TDE bulk phase. The time at which this increase occurs is related to the number of hydroxyls on the MgO surface: more hydroxyls leads to a great production rate of quenchers and an earlier appearance of the slight increase in TDE CL intensity. Because of its sensitivity to surface hydroxyl groups, TDE CL can provide qualitative information on the surface chemistry of metal oxides like MgO.

4.6 References

1. Markovits, A.; Ahdjoudj, J.; Minot, C. *Molecular Engineering* **1997**, 7, 245.
2. Digne, M.; Sautet, P.; Raybaud, P.; Euzen, P.; Toulhoat, H. *J. Cat.* **2002**, 211, 1.
3. Digne, M.; Sautet, P.; Raybaud, P.; Euzen, P.; Toulhoat, H. *J. Cat.* **2004**, 226, 54.
4. Markovits, A.; Ahdjoudj, J.; Minot, C. *Molecular Engineering* **1997**, 7, 245.
5. Arrouvel, C.; Digne, M.; Breysse, M.; Touhoat, H.; Raybaud, P. *J. Cat.* **2004**, 222, 152.
6. Tanabe, K.; Hölderich, W. F. *Appl. Catal. A: General* **1999**, 181, 399.
7. Aramendía, M. A.; Benítez, J. A.; Borau, V.; Jiménez, C.; Marinas, J. M.; Ruiz, J. R.; Urbano, F. *Langmuir* **1999**, 15, 1192.
8. Hur, J. M.; Coh, B.-Y.; Lee, H.-I. *Catalysis Today* **2000**, 63, 189.
9. Bailly, M.-L. ; Costentin, G. ; Lauron-Pernot, H. ; Krafft, J. M.; Che, M. *J. Phys. Chem. B* **2005**, 109, 2404.
10. Chizallet, C.; Costentin, G.; Lauron-Pernot, H.; Krafft, J. M.; Bazin, P.; Saussey, J.; Delbecq, F.; Sautet, P.; Che, M. *Oil & Gas Science and Technology-Rev. IFP* **2006**, 61, 479.
11. Bailly, M.-L.; Chizallet, C.; Costentin, G.; Krafft, J.-M.; Lauron-Pernot, H.; Che, M. *J. Cat.* **2005**, 235, 413.
12. Peng, X. D.; Barteau, M. A. *Langmuir* **1991**, 7, 1426.
13. Chizallet, C. ; Costentin, G. ; Che, M. ; Delbecq, F. ; Sautet, P. *J. Phys. Chem. B* **2006**, 110, 15878.
14. Stone, F. S.; Garrone, E.; Zecchina, A.; *Mater. Chem. Phys.*, **1985**., 13, 331.
15. Fouad, N. E.; Thomasson, P.; Knözinger, H. *Appl. Catal. A: General* **2000**, 194-195, 213.
16. Liu, Z.; Cortés-Concepción, J. A.; Mustian, M.; Amiridis, M. D. *Appl. Catal. A: General* **2006**, 302, 232.
17. Benítez, J. J.; Díaz, A.; Laurent, Y.; Odriozola, J. A. *Catal. Lett.* **1998**, 54, 159.
18. Anderson, P. J.; Horlock, R. F.; Oliver, J. F. *Trans. Faraday Soc.* **1965**, 61, 2745.
19. Li, C.; Li, G.; Xin, Qin *J. Phys. Chem*. **1994** 98, 1933.

20. Tretyakov, N. E.; Filimonov, V. N. *J. Phys. Chem. A* **2001** 105, 6443.
21. Knözinger, E.; Jacob, K.-H.; Singh, S.; Hofmann, P. *Surf. Sci.* **1993**, 290, 388.
22. Coluccia, S.; Lavagnino, S.; Marchese, L. *Materials Chemistry and Physics* **1988**, 18, 445.
23. Layman, K. A.; Hemminger, J. C. *J. Cat.* **2004**, 222, 207.
24. Bermudez, V. M., *J. Phys. Chem.*, **1970**, 74, 4160.
25. Morimoto, T. and Suda, Y., *Langmuir*, **1985**, 1, 239.
26. Hoq, M. F.; Nieves, I. and Klabunde, K. J., *J. Catalysis*, **1990**, 123, 349.
27. McCafferty, E. and Wightman, J. P., *Surf. Interface Anal.*, **1998**, 26, 549.
28. Pruett, R. L.; Barr, J. T.; Rapp, K. E.; Bahner, C. T.; Gibson, J. D.; Lafferty, R. H. *J. Am. Chem. Soc.* **1950** 72, 3646.
29. Paris, J. P. *Photochem. Photobiol.* **1965**, 4, 1059.
30. Heller, Carl A.; Fletcher, A. N. *J. Phys. Chem.* **1965**, 69, 3313.
31. Hori, M.; Kimura, K.; Tsubomura, H. *Spectrochimica Acta* **1968**, 24A, 1397.
32. Urry, W. H.; Sheeto, *Photochem. Photobio.* **1965**, 4, 1067.
33. Kuwata, K.; Geske, D. H. *J. Am. Chem. Soc.* **1964**, 86, 2101.
34. Fletcher, A. N.; Heller, Carl A. *J. Phys. Chem.* **1967**, 71, 1507.
35. Orf, H. W.; Dolphin, D. *Proc. Nat. Acad. Sci USA* **1974,** 71, 2649.
36. Adam, W.; Cilento, G. *Chemical and Biological generation of excited state*; Academic Press: New York, 1982; p 229-247.
37. Adam, W. *The Chemistry of Heterocyclic Compounds part 3*, John Wiley and Sons Perss: New York, 1983; p 351.
38. Adam, W. Cilento, G. *Angew. Chem. Int. Ed. Engl.* **1983**, 22, 529.
39. Adam, W.; Rodriguez, O.; Zinner, K. *J. Org. Chem.* **1978**, 43, 4495.
40. Winberg, H. E.; Carnahan, J. E.; Coffman, D. D.; Brown, M. *J. Am. Chem. Soc.* **1965**, 87, 2054.
41. Rewick, R. T.; Schumacher, M. L.; Shapiro, S. L.; Weber, T. B.; Cavalli-Sforza, M. *Anal. Chem.* **1988**, 60, 2095.
42. Hammond, P. R.; Knipe, R. H. *J. Am. Chem. Soc.* **1967**, 89, 6063.
43. Rewick, R. T.; Schumacher, M. L. *Anal.Chem.* **1988**, 60, 2095.
44. Fletcher, A. N. *J. Phys. Chem.* **1969**, 73, 3686.
45. Fletcher, A. N.; Heller, C. A. *J. Cat.* **1966**, 6, 263.
46. Toby, S.; Astheimer, P. A.; Toby, F. S. *J. Photochem. Photobiol. A: Chem.* **1992**, 67, 1.
47. Sato, M.; Kanbayashi, T.; Kobayashi, N.; Shima, Y. *J. Cat.* **1967**, 7, 342.
48. Klabunde, K. J.; Stark, J.; Koper, O.; Mohs, C.; Park, D. G.; Decker, S.; Jiang, Y.; Lagadic, I.; Zhang, D. *J. Phys. Chem.* **1996**, 100, 12142.
49. Itoh, H.; Utamapanya, S.; Stark, J. V.; Klabunde, K. J.; Schlup, J. R. *Chem. Mater.* **1993**, 5, 71.
50. Goodman, A. L.; Bernard, E. T.; Grassian, V. H. *J. Phys. Chem. A* **2001**, 105, 6443.
51. Pokhodnia, K. I.; Papavassiliou, J.; Umek, P.; Omerzu, A.; Mihailovic, D. *J. Chem. Phys*. **1999**, 110, 3606.

52. Tsyganenko, A. A.; Filimonov, V. N. *J. Mol. Str.* **1973**, 19, 579.
53. Coluccia, S.; Marchese, L.; Lavagnino, S.; Anpo, M. *Spectrochimica Acta* **1987**, 43A, 1573.
54. Shido, T.; Asakura, K.; Iwasawa, Y. *J. Chem. Soc., Faraday Trans. 1* **1989**, 85, 441.
55. Chizallet, C.; Costentin, G.; Che, M.; Delbecq, F.; Sautet, P. *J. Am. Chem. Soc.* **2007**, 129, 6442.
56. Bailly, M.-L.; Chizallet, C.; Costentin, G.; Kraft, J.-M.; Lauron-Pernot, H.; Che, M. *J. Cat.* **2005**, 235, 413.
57. Coluccia, S.; Barton, A.; Tench, A. J. *J. Chem. Soc. Faraday Trans. 1* **1981**, 77, 2203.
58. Zecchina, A.; Lofthouse, M. G.; Stone, F. S. *J. Chem. Soc. Faraday Trans. 1* **1975**, 71, 1476.
59. Huang, C.-C.; Hohn, K. L. *Tetrakis(dimethylamino)ethylene Chemiluminescence (TDE CL) Characterization of the CMC and the viscosity of reversed microemulsions*; in preparation.
60. Mukherjee, K.; Moulik, S. P. *Langmuir* **1993**, 9, 1727.
61. Jean, Y.-C.; Ache, H. J. *J. Am. Chem. Soc.* **1978**, 100, 6320.
62. Manoj, K. M.; Jayakumar, R.; Rakshit, S. K. *Langmuir* **1996**, 12, 4068.
63. Majhi, P. R.; Moulik, S. P. *J. Phys. Chem. B* **1999**, 103, 5977.

CHAPTER 5 - Catalytic Reactivity of Surface Isolated Hydroxyls on Aluminum Oxide for Tetrakis(dimethylamino)ethylene Chemiluminescence

5.1 Introduction

Aluminum oxides have been used industrially as catalysts [1,2,3,4] catalyst supports [5,6,7,8] and adsorbents [9]. Due to the widespread use of Al_2O_3 in different fields, the properties, including acid-base properties, reactivity, crystal phases and surface hydroxyls, of Al_2O_3 have been systematically studied [7,10,11,12,13,14,15,16]. Therefore, Al_2O_3 is often chosen when developing a new surface characterization method.

It is well known that the outmost layer of Al_2O_3 is covered by various exterior absorbents, such as molecular water, hydroxyl groups, carbonates and organics with alkyl groups [17,18,19,20]. Hydroxyls and molecular water are the two most abundant species [21,22]. With increasing temperature, the weight loss mostly occurs by the removal of molecular water and hydroxyl groups. Since the interaction between the surface sites (Al^{3+} and O^{2-}) and hydroxyl groups affects the chemical properties (such as reactivity and stretching frequency) of surface hydroxyl groups, an understanding of the surface properties can be derived from the distribution of surface hydroxyl groups. This idea was discussed by Busca *et. al.* [23] who noted that the stretching frequencies of surface hydroxyl groups were associated with the surface structure and the modifications of alumina.

Surface properties of metal oxides have been studied qualitatively by many methods, including FT-IR [24,25], UV-Visible [26,27], photoluminescent spectroscopy [28,29], XRD [25], X-ray photoelectron spectroscopy (XPS) [24], chemical probes [30,31,32] and NMR [33]. However, just a few techniques are suitable for investigating surface properties quantitatively, such as NMR [34], weight loss [35], mass spectrometry [36] and XPS [37]. For example, FT-IR spectroscopy is a powerful methodology widely employed in characterizing surface structure and acid-base properties on metal oxides through the identification of chemisorbed species [13,18].

But to use FT-IR in quantitative analysis, the adsorption coefficients of all adsorbed species have to be determined. [38]

On aluminum oxide, IR bands attributed to hydroxyl groups had been identified in the region from 3800-3000 cm^{-1}. A broad band with lower stretching frequencies in the region from 3600-3000 cm^{-1} is assigned to hydrogen bonded hydroxyls. A few individually sharp bands distributed in the region from 3800-3600 cm^{-1} are ascribed to isolated hydroxyl groups [17,18,19,20]. Klabunde *et. al.* [39] elucidated that the hydroxyl groups concentrated on edge and corner sites are more isolated. Indeed, the ratio of isolated hydroxyl to hydrogen bonded hydroxyl decreases on surfaces with smooth morphologies [39].

The vibrational frequency of an isolated hydroxyl is affected by the coordination of the hydroxyl group and the adjacent aluminum cations (octahedral or tetrahedral) [7,40]. Therefore, the spectral pattern of isolated hydroxyl groups is a spectral fingerprint of the surface and crystal structure of aluminum oxide. A few models have been developed on the configuration of surface hydroxyl groups on alumina [7,13,14,16,23]. Knözinger's model [7] is adopted most frequently. Knözinger noted that there are five possible configurations for isolated hydroxyls and the difference in each configuration is related to the net charge (σ). The difference in the net charge for each configuration is related to the number of adjacent surface sites and the coordination of the cation (Al^{VI} or Al^{IV}). The net charge of isolated hydroxyls in different configurations can be calculated by using **Equation 5- 1** [7,12]. Knözinger *et. al.* also noted that the vibration frequencies and acid-base properties of isolated hydroxyls are functions of the net charge of an isolated hydroxyl. For example, because a Type III isolated hydroxyl bonds to three octahedral aluminum cations, Type III isolated hydroxyls possess the highest net charge (+0.5) and lowest stretching frequency (3680-3590 cm^{-1}) of all isolated hydroxyls. Thus, type III isolated hydroxyls are the most acidic hydroxyl of all isolated hydroxyls on aluminum oxide.

$$C_{Net} = C_{hydrogen} + C_{oxygen} + \frac{C_{cation}}{C_{anion}} \qquad (5\text{- }1)$$

where C_{net} is the net charge of a hydroxyl group. For the hydroxyl group on an aluminum oxide surface, $C_{hydrogen}$, C_{oxygen}, C_{cation} are the charge of hydrogen, oxygen and aluminum and equal +1,

-2 and +3 respectively. n_{anion} represents the number of adjacent anions for the cation (coordination number).

It was shown in our prior studies [41] that the emission of tetrakis(dimethyamino)ethylene chemiluminescence (TDE CL) is catalyzed by isolated hydroxyl groups on MgO. Isolated hydroxyls with lower coordination had higher catalytic reactivity for TDE CL, and 4 coordinated isolated hydroxyls (hydroxyls adsorbed on edges) were concluded to play the largest role in enhancing TDE CL on an eroded MgO surface. This study was undertaken in order to demonstrate the utility of TDE CL as a valuable tool for characterizing the hydroxyl groups on aluminum oxide. Specifically, the surface hydroxyl groups were characterized by TDE CL as the aluminum oxide was pre-treated by several methods, including heat-, acetic acid- and steam-treatment. The impacts of surface hydroxyl in different configurations on TDE CL was evaluated through the interpretation of I_t curve (emission intensity vs. reaction time curve) obtained from the catalyzed TDE CL on aluminum oxide and from infrared spectroscopy data.

5.2 Experimental

5.2.1 Sample Preparation

γ-Alumina oxide (γ- Al_2O_3, Alfa Aesar, 99.97%) with a specific surface area of 70 m^2/g was used without further purification. Heat-treated Al_2O_3 (HT- Al_2O_3) was obtained by heat-treating γ-Al_2O_3 in a channel-type furnace at 900^oC for 3 hours. AA (acetic acid)-treated Al_2O_3 (AAT- Al_2O_3) was derived from the HT- Al_2O_3. To make AAT-Al_2O_3, HT-Al_2O_3 was treated by acetic acid at 80^oC for 8 hour in an AA saturation cell. Before the treatment of acetic acid, HT-Al_2O_3 was pre-treated at 150^oC to remove molecular water adsorbed on surface and transferred from the heat-treatment cell to the AA saturation cell in a nitrogen purged glove box. Steam-treated Al_2O_3 (ST- Al_2O_3) was prepared by following procedure: γ- Al_2O_3 was sealed with water in water saturation cell at 80^oC for 8 hours.

Before the addition of TDE, all aluminum oxide samples were post-treated at 150^oC to avoid the influence of the molecular water or AA on TDE CL. The pre-treatment and post-

treatment of γ-Al_2O_3, heat-treated Al_2O_3, steam-treated Al_2O_3 and AA-treated Al_3O_3 samples were carried out in a sealed cell connected to a nitrogen cylinder and vacuum line. The temperature of the cell was controlled by a cylindrical electric furnace and a temperature controller. The temperature was increased from room temperature to the desired temperature at a rate of 3^oC/minutes. After reaching the desired temperature, the temperature was maintained for 2.5 hours under nitrogen atmosphere. Next, the sample cell was purged by a vacuum line to evacuate the residual gas inside the cell for 0.5 hours.

5.2.2 TDE Synthesis

The synthesis of TDE was carried out by the procedure as described in our early work [41]. Chlorotrifluoroethylene (SynQuest Lab. Inc.) and dimethylamine (Alfa Aesar) were sealed in a high pressure vessel and heated at 56^oC for 10 hours. The product is a bright orange liquid. In order to extract the impurities out in the product, the product was purified by mixing with distilled water. After the purification, the color of the product changed from orange to light yellow.

5.2.3 IR Spectroscopy

All infrared spectra were obtained in a DRIFTS cell (Thermo Nicolet) using a Thermo Nicolet FT-IR spectrometer (Model: Nexus 670). The spectrometer was equipped with a liquid nitrogen-cooled MCT (mercury-cadmium-telluride) detector, KBr beam splitter and tungsten-iodide light source. The scan number and resolution were set as 50 times and 4 cm^{-1} respectively. A helium cylinder was connected to the cell. The flow rate of inlet helium was controlled by a mass flow controller.

5.2.4 Emission Intensity Measurement

The variation of emission intensity with reaction time was collected by a fiber optic spectrometer (StellarNet Inc. EPP2000) and recorded by the SpectraWiz operating software. An apparatus was constructed in which the sample could be monitored while a gas was flowing through the sample. This apparatus consisted of a sample holder, the fiber optic cable, and an

outer glass chamber to which inlet and outlet tubes were connected. The flexible fiber optic cable was positioned below the sample holder. A mixture of 0.15g treated Al_2O_3 sample with 0.3ml TDE was loaded into the sample vial, which was then placed in the sample holder. The chamber was sealed with an O-ring and purged with dry air at 150 ml/min during the reaction. In order to avoid the influence caused by stray light from the surroundings, the outside wall of the glass chamber was covered with aluminum foil.

5.2.5 BET Surface Area and X-ray Powder diffraction Analyses

The surface areas of aluminum oxide samples were determined by the BET dynamic method using a Quantachrome Autosorb-1. Nitrogen was used for the adsorption experiment at liquid nitrogen temperature. X-ray powder (XRD) traces of γ-Al_2O_3 and HT- Al_2O_3 were carried out using a Bruker D8 Advance X-ray diffractometer (40 kV, 40 mA) (Karlsruhe, Germany). The aluminum oxide samples were scanned starting from 2θ=25-70^o with increment of 0.05^o and a scan speed of 1 degree/minute.

5.3 Results

TDE CL was studied in the presence of a number of different aluminum oxide samples, including dehydrated samples, samples treated at high temperatures (900^{o}C), samples exposed to acetic acid, and samples treated with steam. These treatments will change the number of types of surface hydroxyls present, which are believed to be important in TDE CL over metal oxides [41]. In this way, differences in TDE CL can be correlated with the surface chemistry of alumina.

5.3.1 Dehydroxylation of γ-Al_2O_3

Figure 5.1 and **Figure 5.2** show the IR bands of hydroxyl groups and the behavior of the surface hydroxyl groups as a function of temperature in a helium atmosphere on γ-Al_2O_3. The IR spectra of γ-Al_2O_3, as seen in **Figure 5.1**, show an extremely intense band with maxima at 3575 cm^{-1} and three small bands at 3760, 3716 and 3664 cm^{-1} in the region from 3800-3000 cm^{-1}. With increasing temperature, a decrease of the broad band with a maximum at 3575 cm^{-1} is accompanied by increases in the bands at 3760, 3716 and 3664 cm^{-1} (as seen in **Figure 5.2**).

Costa and Shirai *et. al.* [17,42] reported that the bands in the region from 3800-3600 cm^{-1} are attributed to isolated hydroxyl groups and the broad band centered at 3575 cm^{-1} is assigned to hydrogen bonded hydroxyl groups. According to early studies [12,17,19,43], the stretching frequencies of isolated hydroxyls are associated with the coordination number of hydroxyls and the modifications of aluminum cation, such as Al^{IV} and Al^{VI}. The bands in the interval 3790-3750, 3750-3710, and 3700-3590 cm^{-1} are ascribed to type I, II and III isolated hydroxyl groups respectively. Therefore, the bands at 3760, 3716 and 3664 can be assigned as type I, type II and type III isolated hydroxyls, respectively. Out of this region, a band with a maxima at 2908 cm^{-1} is found at lower temperature and disappears at higher temperature. The small bands in the region from 2860-2960 cm^{-1} correspond to C-H stretching and are from the impurities adsorbed on the γ-Al_2O_3 surface [17,44].

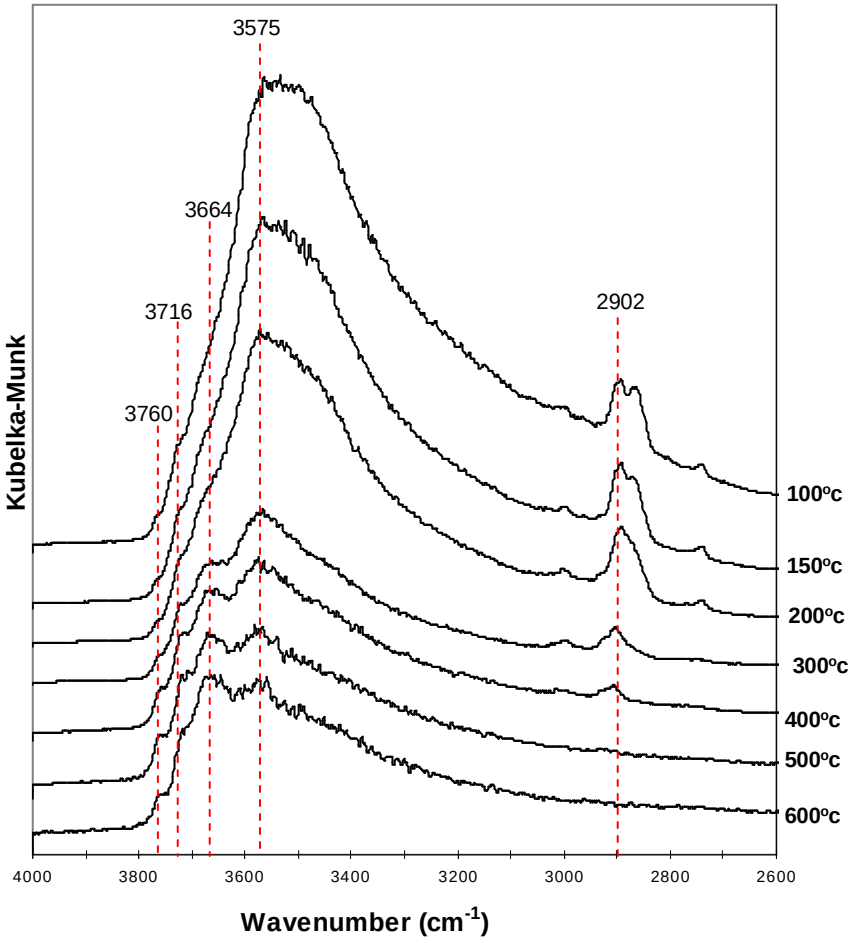

Figure 5.1 The IR spectra of γ-Al_2O_3 at different temperatures.

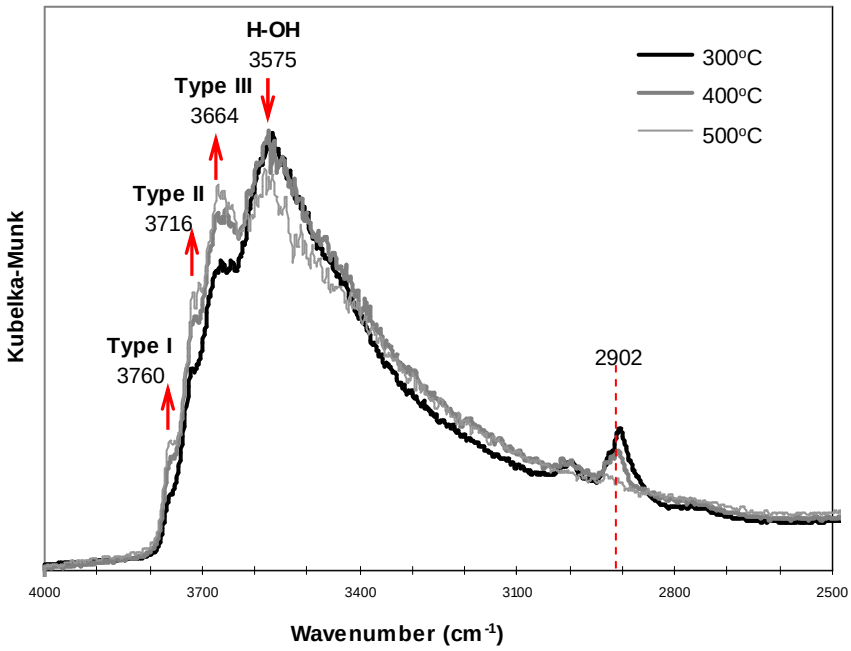

Figure 5.2 IR spectra when γ-Al_2O_3 was dehydrated at 300, 400 and 500°C.

The I_t curves of catalyzed TDE CL shown in **Figure 5.3** were obtained from the mixture of TDE and γ-Al_2O_3 pre-treated at 300°C, 400°C, and 500°C. Before the addition of TDE, the pre-treated γ-Al_2O_3 samples were cooled in a dry nitrogen atmosphere to avoid surface re-hydration. As seen in **Figure 5.3**, the emission intensity of TDE CL changes with pre-treating temperature. Higher emission intensity was found from the mixture of TDE with the γ-Al_2O_3 that was pre-treated at higher temperatures, 400 and 500°C.

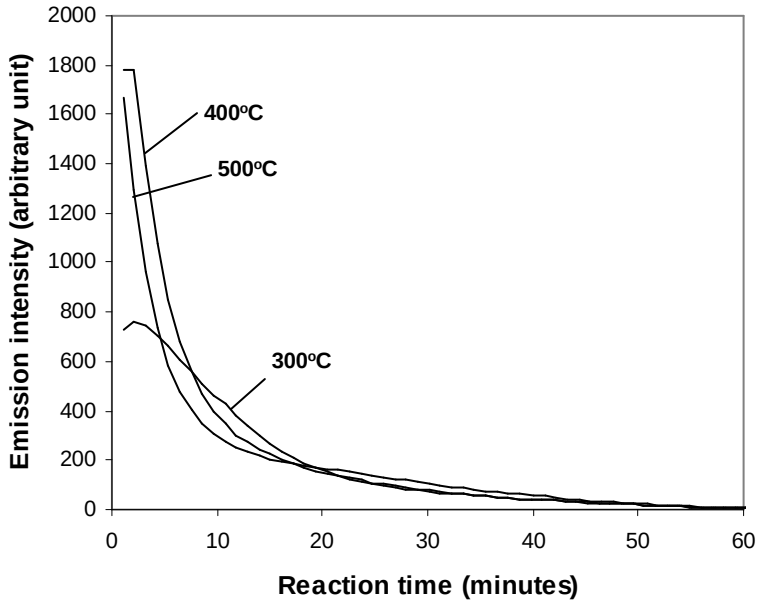

Figure 5.3 I_t curves of TDE CL on γ-Al_2O_3 which was pre-treated at 300, 400 and 500°C.

5.3.2 HT- Al_2O_3

At moderate temperatures (<200°C), the bands of isolated hydroxyl groups closely overlap on γ-Al_2O_3. In order to obtain higher resolution to distinguish the changes in the IR band of isolated hydroxyl following different treatments, γ-Al_2O_3 was treated at high temperature to re-distribute isolated hydroxyl groups. HT- Al_2O_3 was obtained from heat-treating γ-Al_2O_3 at 900°C for 3 hours. After exposing HT- Al_2O_3 to the atmosphere, the decomposition of molecular water on unsaturated active sites, Al^{3+} and O^{2-}, is accompanied by the formation of hydroxyl groups with different configurations. It was found on re-hydrated HT- Al_2O_3 that all isolated hydroxyl bands blue-shift from 3760, 3716 and 3664 to 3770, 3730 and 3694 cm^{-1}, respectively (as seen in **Figure 5.4**). Early studies [12,17,19,43] assigned the bands at 3770, 3730 and 3694 cm^{-1} to type I, II and III isolated hydroxyl groups, respectively. The X-ray diffraction pattern, seen in **Figure 5.5**, of HT- Al_2O_3 shows that a phase transformation occurred after heat-treating γ- Al_2O_3 at 900°C for 3 hours. The XRD pattern is consistent with the formation of δ-Al_2O_3 [45,46].

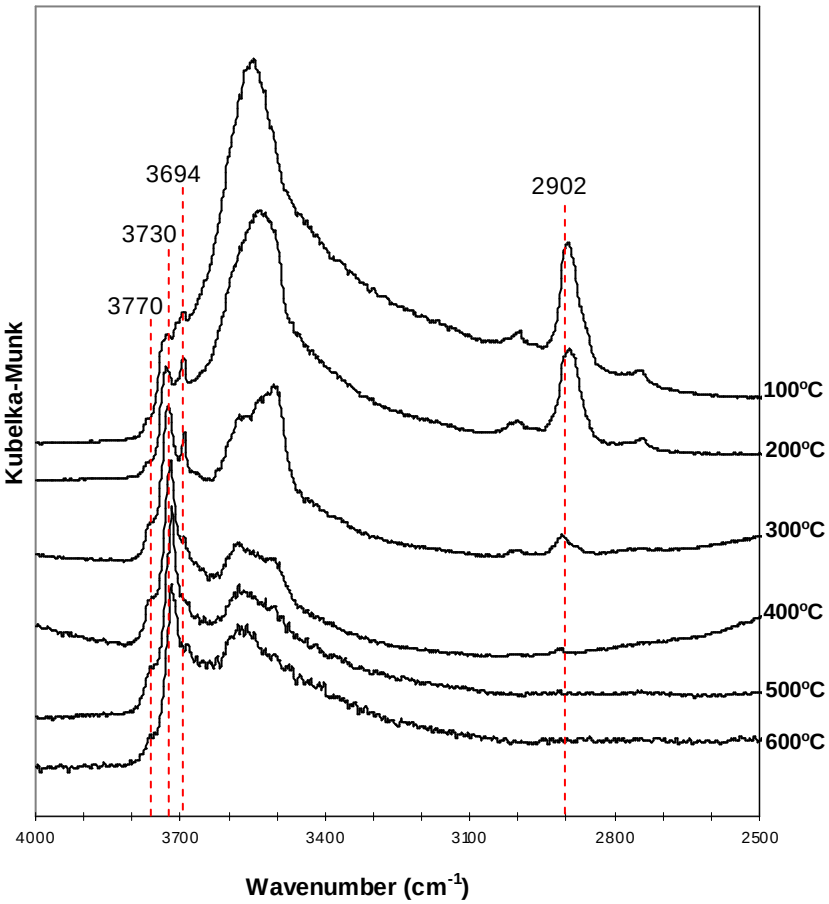

Figure 5.4 IR spectra of heat-treated (850°C) Al_2O_3.

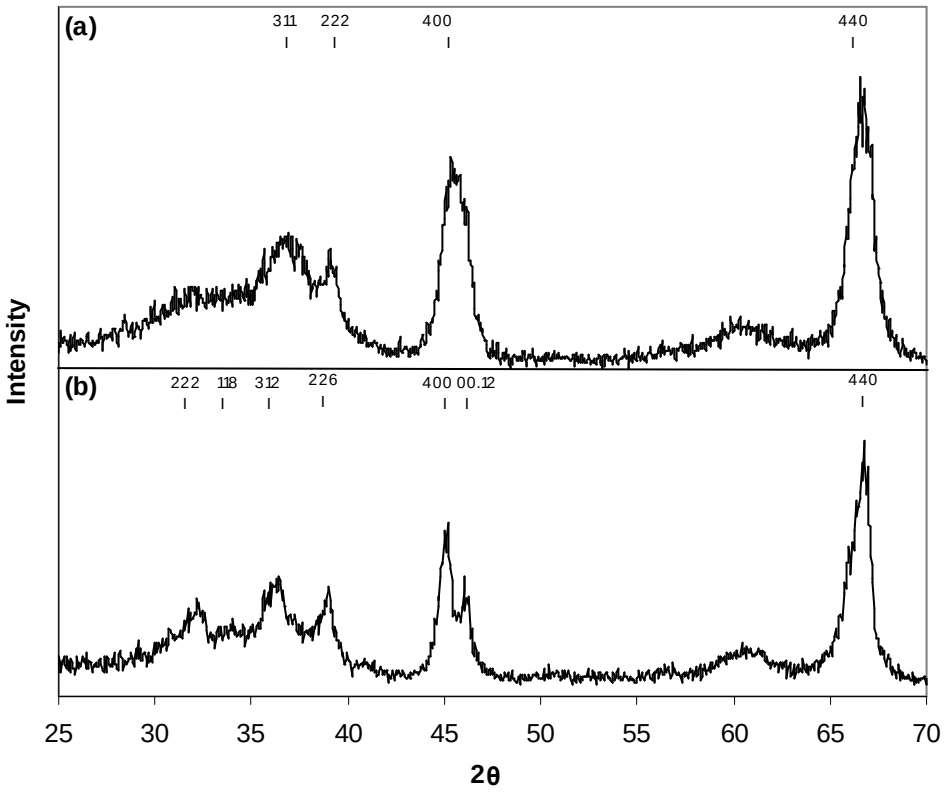

Figure 5.5 X-ray powder diffractometer patterns for γ- Al_2O_3 treated at (a) 150°C for 3 hours; γ- Al_2O_3. (b) 900°C for 3 hours; HT- Al_2O_3 (δ- Al_2O_3).

With increasing temperature, type II isolated hydroxyls have higher thermal stability (**Figure 5.4**) compared with type III isolated hydroxyls. The intensity of type III isolated hydroxyls is higher than that of type II isolated hydroxyls before 300°C. As temperature is increased past 300°C, the band of type II isolated hydroxyl becomes larger than the band of type III isolated hydroxyl. Above 500°C, type III isolated hydroxyls disappear while type II isolated hydroxyls are relatively constant.

5.3.3 AAT- Al_2O_3

TDE CL was also studied on aluminum oxide that was pre-treated by acetic acid (AAT-Al_2O_3). After AA treatment, three new IR bands are observed in the region from 3100-2910 cm^{-1}, as seen in **Figure 5.6**. These three new forming IR bands are ascribed to the formation of acetate

species in different configurations after chemisorption of acetic acid [47,48,49,50,51,52]. The possible configurations of acetate species adsorbed on aluminum oxide is shown in **Figure 5.7**.

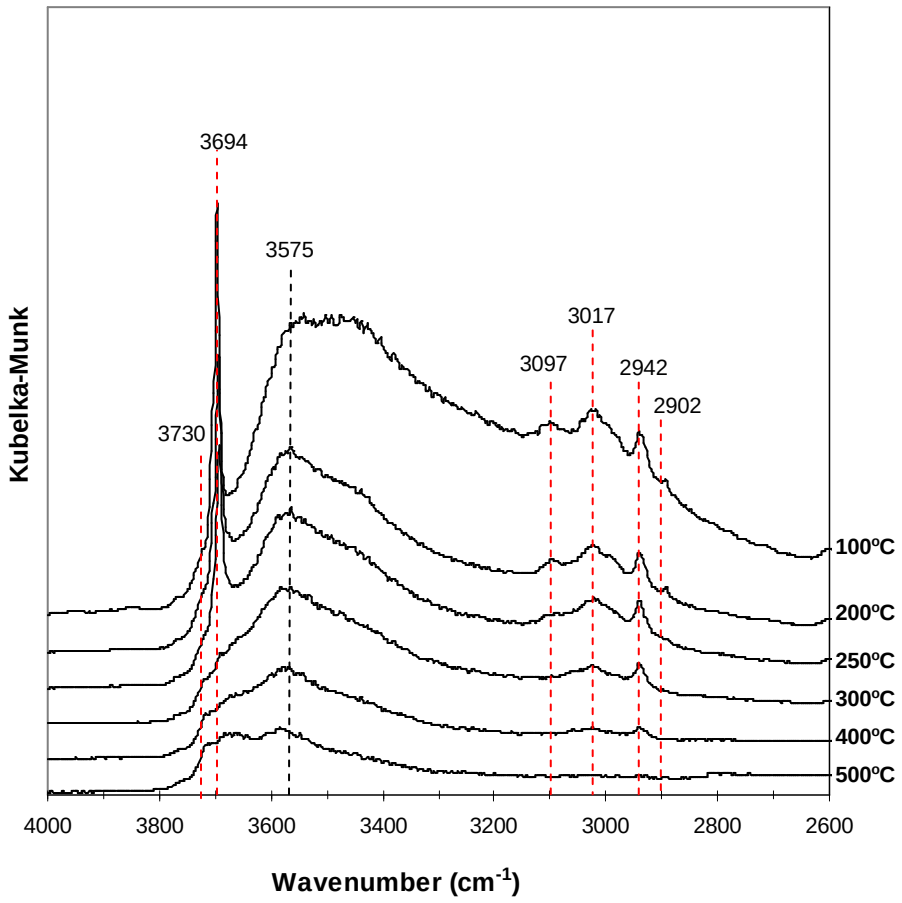

Figure 5.6 IR spectra of AAT- Al_2O_3 AA at 100°C- 500°C.

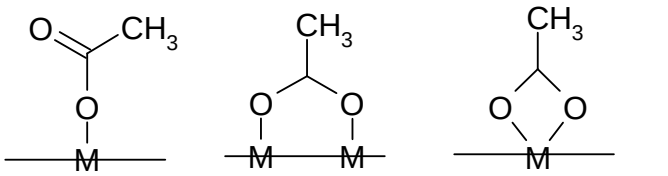

Monodentate *Bidentate Bridging* *Bindentate Chelating*

Figure 5.7. The configurations of acetate species on a metal oxide surface.

In the interval from 3800 to 3500 cm^{-1} in the IR spectrum of AAT-Al_2O_3, the obvious differences on AAT- Al_2O_3 are a decrease in the band of type II isolated hydroxyls (λ= 3730 cm^{-1}) and a dramatic increase in the band of type III isolated hydroxyls (λ= 3694 cm^{-1}), as seen in

Figure 5.8. **Figure 5.8** highlights these differences by contrasting the IR band of hydroxyl groups on AAT- Al_2O_3 with those on HT- Al_2O_3 at 150, 200 and 300^oC. Comparing the IR bands of type III isolated hydroxyl shown in **Figure 5.1**, **Figure 5.4** and **Figure 5.6**, the band of type III isolated hydroxyls (λ= 3694 cm^{-1}) on AAT- Al_2O_3 is more intense compared with the band of type III isolated hydroxyls on HT- Al_2O_3 (λ= 3694 cm^{-1}) and on γ- Al_2O_3 (λ= 3664 cm^{-1}). The results shown in **Figure 5.6** indicate that type III isolated hydroxyls on AAT- Al_2O_3 are thermal unstable as the temperature is increased to 250^oC. Maintaining the temperature at 250^oC, type III isolated hydroxyls were removed gradually with time, as shown in **Figure 5.9**.

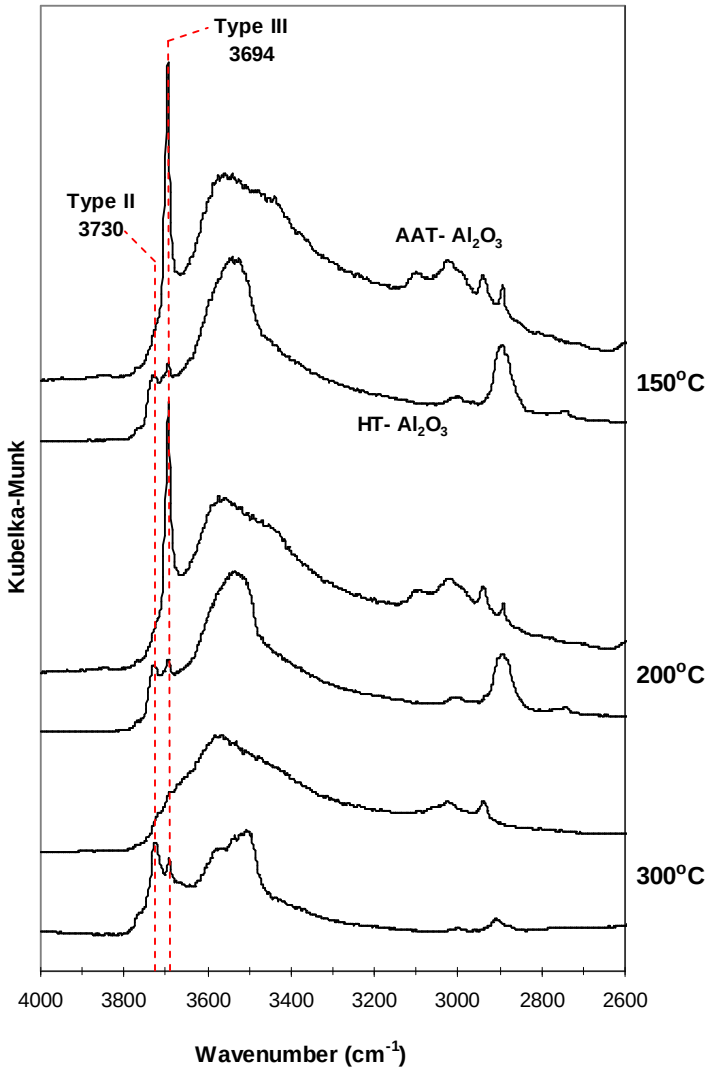

Figure 5.8 The IR spectra of HT-Al_2O_3 and AAT-Al_2O_3 at 150^oC, 200^oC, and 300^oC. For each post-treating temperature, the upper spectrum is from AAT- Al_2O_3 while the lower spectrum is from HT- Al_2O_3.

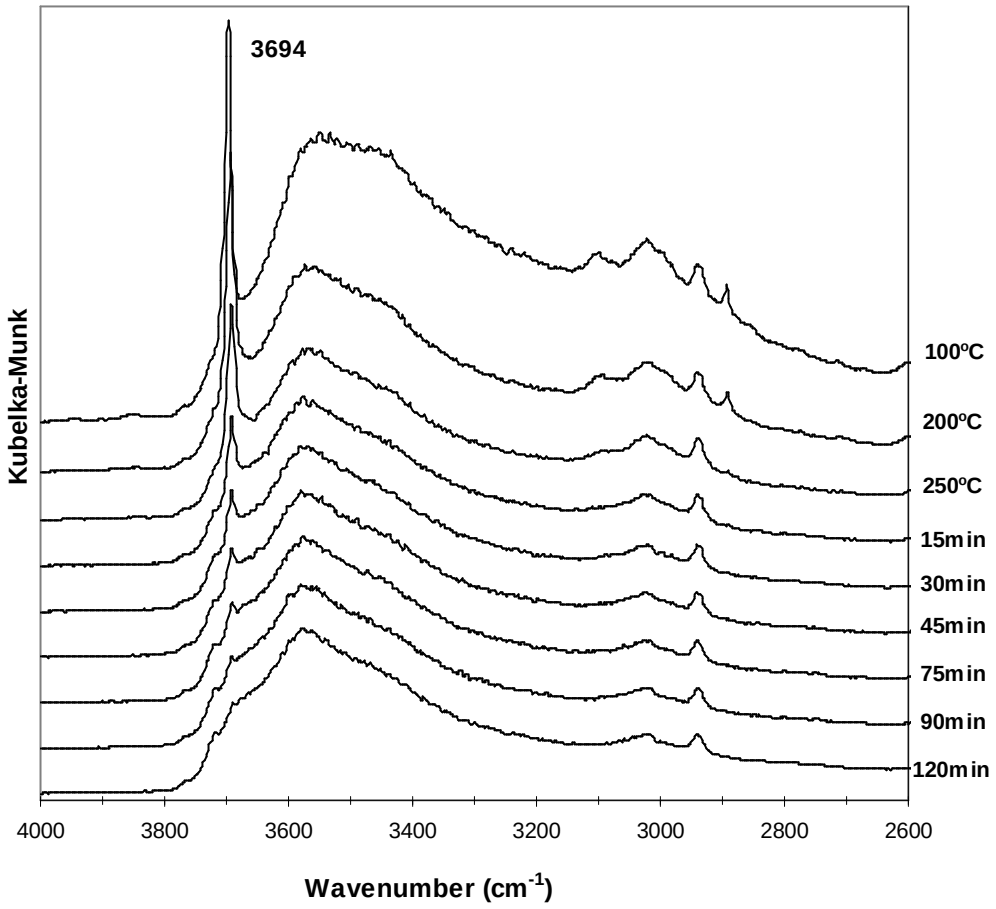

Figure 5.9 IR spectra of AAT- Al_2O_3 from 100°C-250°C. The temperature was maintained at 250°C for 120 minutes after the temperature reached to 250°C.

The I_t curves shown in **Figure 5.10** were obtained from a mixture of TDE and AAT-Al_2O_3 for different post-treatment temperatures. As seen in **Figure 5.10**, the maximum emission intensity on the I_t curves decreased about 52% after HT- Al_2O_3 was treated by AA. A further decrease in the maximum emission intensity of the I_t curve (about 28%) was found when the post-treating temperature was increased to 250°C.

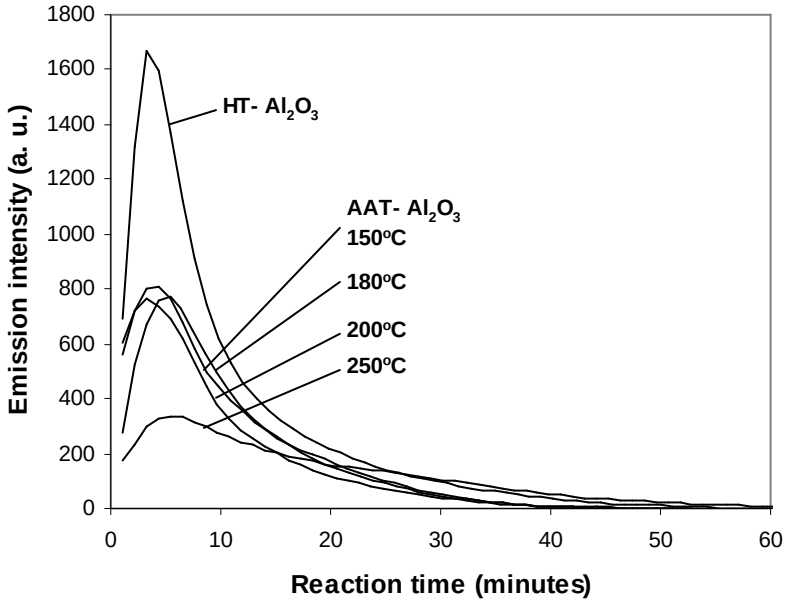

Figure 5.10 The I_t curves of TDE CL on HT- Al_2O_3 and AAT- Al_2O_3 post-treated at 180, 200, and 250°C.

5.3.4 ST- Al_2O_3

ST- Al_2O_3 was obtained by treating γ- Al_2O_3 with steam at 80°C for 8 hours. The IR spectrum of ST-Al_2O_3 showed essentially no difference when compared to that of γ- Al_2O_3 (see **Figure 5.11**). TDE CL on ST- Al_2O_3 gave a similar I_t curve as that obtained from TDE CL on γ-Al_2O_3. This is shown in **Figure 5.12**.

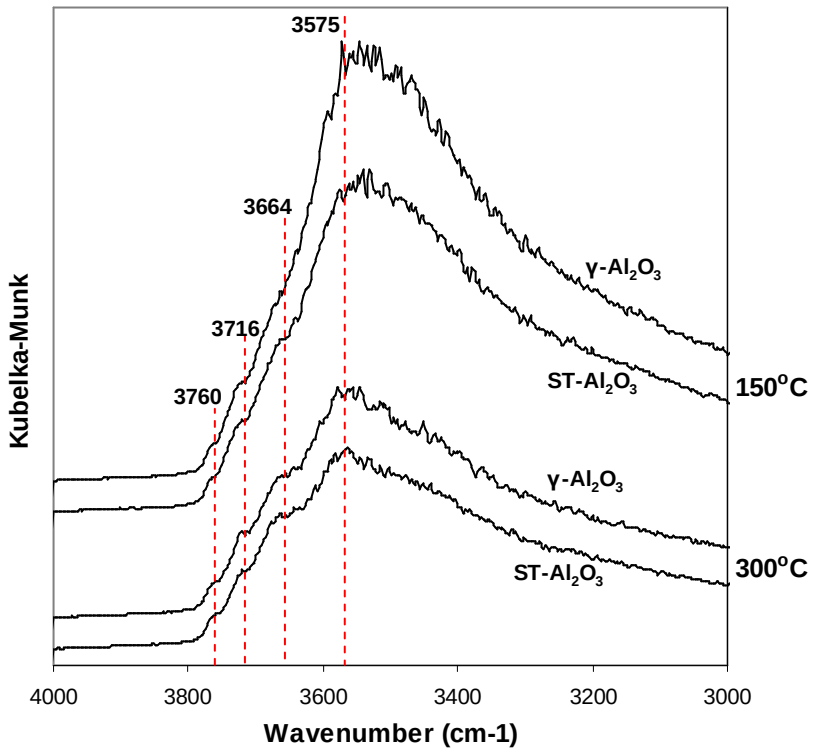

Figure 5.11 IR spectra of γ- Al_2O_3 and ST- Al_2O_3 at 150 and 300°C.

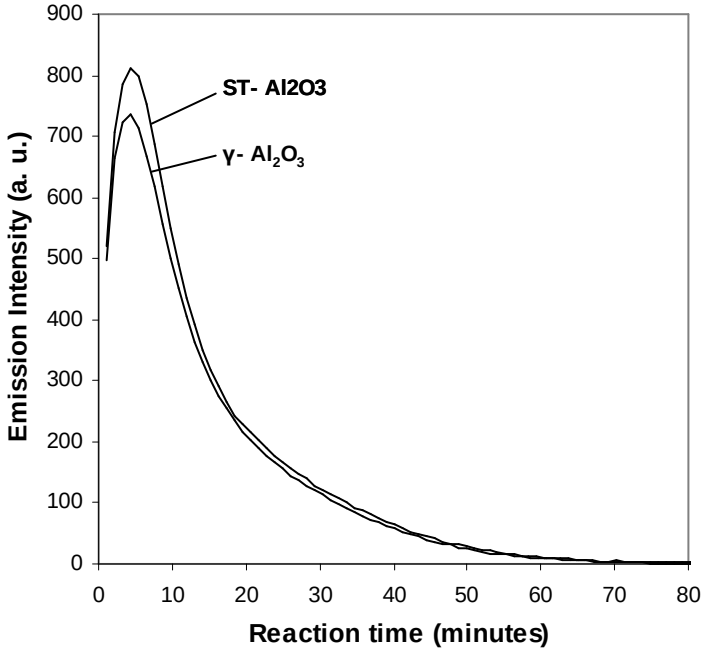

Figure 5.12 The I_t curves of TDE CL on ST-Al_2O_3 and γ-Al_2O_3.

5.4 Discussion

In our prior work [41], it was found that hydroxyl groups on MgO strongly influenced TDE CL. In particular, it was found that the emission intensity of TDE CL was significantly enhanced by the presence of isolated hydroxyls with lower coordination. Quenching species and surface hydroxyls both impact the I_t curves. In this work, our intention was to gain a clearer insight into the connection between the configuration and the catalytic reactivity of surface hydroxyls for TDE CL on aluminum oxide.

5.4.1 Dehydration of γ-Al_2O_3

Heat-treatment was initially used to manipulate the distribution of surface hydroxyl groups. Interestingly, it was found from **Figure 5.2** that isolated hydroxyl groups of all types increased with increasing the pre-treating temperature from 300-500^{o}C. The increase in the number of isolated hydroxyls is thought to be due to the dissociation of hydrogen bonds between neighboring hydroxyl groups (hydrogen bonded hydroxyl), as shown in **Figure 5.13**. This hypothesis agrees with Ballinger *et. al.* [53]. Ballinger *et. al.* noted that thermal dehydration leads to decomposition of the associated hydroxyl (hydrogen bonded hydroxyl) to evolve water and is accompanied by the formation of isolated hydroxyls and unsaturated active sites (Al^{3+} and O^{2-}).

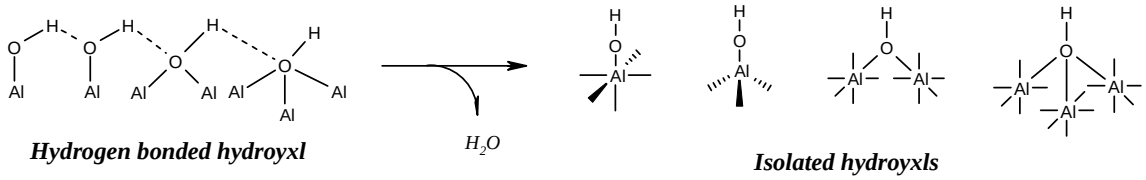

Figure 5.13 The dissociation of the hydrogen bond between neighboring hydroxyls to form isolated hydroxyl groups.

The emission intensity of catalyzed TDE CL appears to be associated with the content of isolated hydroxyls on the aluminum oxide surface, but is not related to amount of hydrogen bonded hydroxyls. The I_t curves, seen in **Figure 5.3**, show a large difference in intensity as the

treatment temperature is increased from 300 to 400°C. This temperature increase results in an increase in isolated hydroxyls and a decrease in hydrogen bonded hydroxyls, as shown in **Figure 5.2**, indicating that the reaction of TDE CL is mainly catalyzed by isolated hydroxyl groups. These results correspond very closely to the results we reported previously [41]. Indeed, isolated hydroxyl groups act in a similar role as hydroxylic additives (such as water and alcohols) in the reaction of TDE CL. The role of hydroxylic additives in TDE CL was reported by Fletcher *et. al.*. Fletcher *et. al.* [54,55,56] indicated that hydroxylic additives act as activators to catalyze the autoxidation reaction between TDE and oxygen. In the environment without protonic activator, pure TDE can not react with oxygen [57,58,59]. The intermediate, tetrakis-dimethylamino-1,2-dioxetane (TDMD), obtained from the autoxidation reaction is the energy source for donation of the required energy for photon emission [54,55,58,59,60,61]. The possible catalytic mechanism is shown in **Figure 5.14**. The production rate of TDMD is likely associated with the emission intensity. Therefore, the emission intensity of TDE CL corresponds to the catalytic ability of the surface.

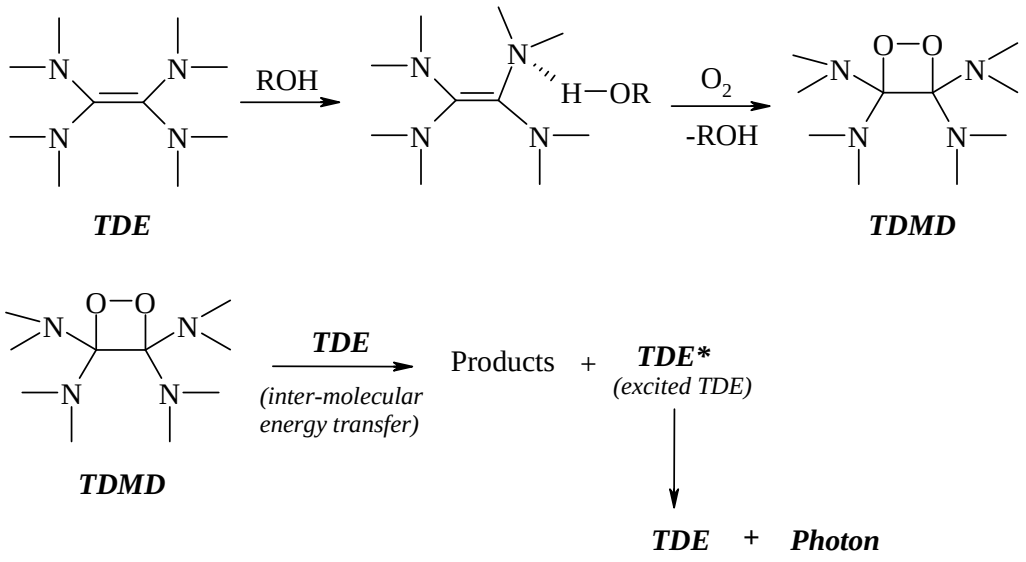

Figure 5.14 The catalytic mechanism of a protonic material (ROH) for the autoxidation reaction of TDE CL.

The IR spectra of dehydrated γ-Al_2O_3, shown in **Figure 5.2**, were taken for γ-Al_2O_3 after different pretreatment temperatures. All types of isolated hydroxyls increased after the temperature was increased from 300 to 400 or 500°C. However, the IR spectra shown in **Figure**

5.4 and **Figure 5.8** indicate that type III isolated hydroxyls have lower thermal stability compared with type I and II isolated hydroxyls. [62] Type III isolated hydroxyls became thermally unstable at 250^{o}C, and were removed from the surface gradually with time. Therefore, the contribution of type III isolated hydroxyls on the enhancement in the catalytic reactivity of dehydrated γ-Al_2O_3 is likely small. It can be assumed that the enhancement in the emission intensity of TDE CL mainly is due to the increase of type I and type II isolated hydroxyls produced from the dissociation of hydrogen bonded hydroxyl.

5.4.2 HT- Al_2O_3

Something interesting was observed in the IR spectrum of HT- Al_2O_3: after heat-treating γ- Al_2O_3 at 900^{o}C and subsequently re-hydrating the sample in atmosphere, all isolated hydroxyl bands blue-shift from 3760, 3716 and 3664 on γ- Al_2O_3 to 3770, 3730 and 3694 cm^{-1} on HT-Al_2O_3 respectively, as seen in **Figure 5.15**. Additionally, the XRD patterns, shown in **Figure 5.5**, offer evidence for the phase transformation of γ- Al_2O_3 after heat-treatment at 900^{o}C. In agreement with Wilson *et. al.* [45,46,63], the XRD pattern given from HT- Al_2O_3 was identified as δ- Al_2O_3. Hence, the blue-shifts of isolated hydroxyl bands are likely caused by the phase transformation.

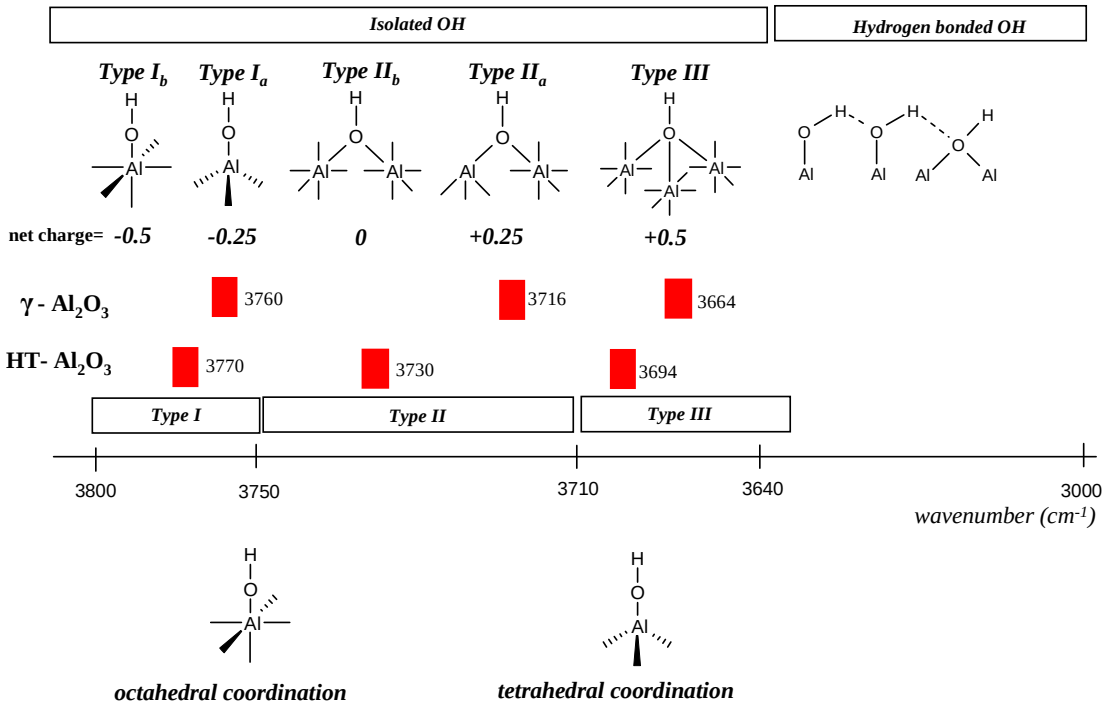

Figure 5.15 Wavenumbers associated with different types of hydroxyl groups and wavenumbers noted in this study for γ- Al_2O_3 and Heat-treated γ- Al_2O_3.

It is well known that tetrahedrally and octahedrally coordinated cations exist simultaneously in transition aluminum oxides (γ-, η-, θ- and δ- Al_2O_3). [23,46] The cation ordering increases with the treatment temperature. γ and η forms are considered low-temperature Al_2O_3 phases, whereas θ and δ forms are regarded as high-temperature Al_2O_3 phases.[12,45] α-Al_2O_3 is derived from the final conversion of transition aluminum oxide. All aluminum cations in α-Al_2O_3 have an octahedral coordination. [63] Morterra *et. al.* [7,12,23] suggested that the isolated hydroxyls on tetrahedral coordinated Al cations, such as Type I_a isolated OH, have lower stretching frequency than that on octahedral coordinated Al cations, such as Type I_b isolated OH. Therefore, the blue-shifts of isolated hydroxyl bands occurring simultaneously with phase transformation from γ to δ can be interpreted to mean that more isolated hydroxyl groups bind to octahedrally coordinated Al cations (Al^{VI}) rather than tetrahedrally coordinated Al cations (Al^{IV}).

The correlation between adjacent cation coordination and the surface catalytic reactivity of isolated hydroxyl was identified on HT- Al_2O_3 by TDE CL. Exposing aluminum oxide to the atmosphere, the surface is covered by a monolayer of hydroxyl with a density of about 1.25×10^{19} OH/m^2 [2,64] HT- Al_2O_3 was derived from heat-treating γ- Al_2O_3 at 900^{o}C. After the treatment, the surface area, measured by BET dynamic method, decreased from 70 m^2/g (γ- Al_2O_3) to 48 m^2/g (HT- Al_2O_3). The decrease in the surface area results in fewer surface hydroxyls participating in the reaction of TDE CL. However, a significant increase in the emission intensity was given from catalyzed TDE CL on HT- Al_2O_3, as seen in **Figure 5.16**. Because the emission intensity responds to the catalytic reactivity of Al_2O_3 surface, it can be proposed that isolated hydroxyl groups on HT- Al_2O_3 have higher catalytic reactivity for TDE CL compared with that on γ- Al_2O_3. These results emphasize again that the catalytic reactivity for TDE CL is independent from the hydrogen bonded hydroxyl, but dependent on the nature of the aluminum cation on which an isolated hydroxyl is located. An isolated hydroxyl with an adjacent Al^{VI} cation appears to have higher catalytic reactivity for TDE CL in contrast with the isolated hydroxyl with an adjacent Al^{IV} cation.

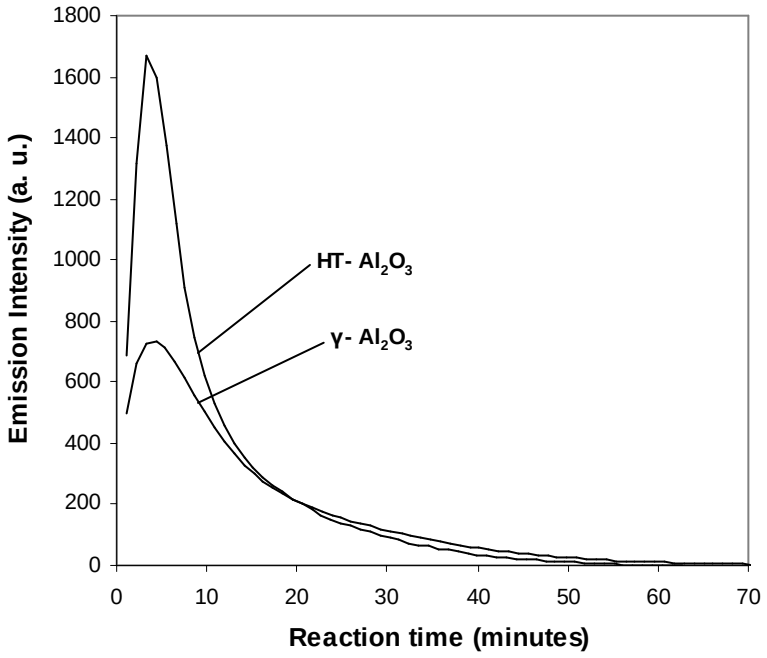

Figure 5.16 The I_t curves of catalyzed TDE CL on HT- Al_2O_3 and γ- Al_2O_3.

5.4.3 AAT- Al_2O_3

Hasan *et. al.* [65] suggested that the isolated hydroxyl groups on aluminum oxide are involved in the reaction with acetic acid. To support this hypothesis, they pointed to the observation of negative adsorption in IR bands with frequencies in the region from 3800-3680 cm^{-1} after treating aluminum oxide by AA for 10 minutes. The results in this work (as shown in **Figure 5.9**) do not perfectly agree with the result reported by Hasan *et. al.*, however. We found that the decrease in the IR band of type II isolated hydroxyls (λ=3730 cm^{-1}) on AAT- Al_2O_3 were accompanied by the significant increase in the IR band of type III isolated hydroxyls (λ=3694 cm^{-1}) when the treatment time was extended from 10 minutes to 8 hours, as seen in **Figure 5.6** and **Figure 5.8**. These differences between this paper and Hansan *et. al.* [65] are likely due to two factors: surface erosion and discrepancies in the reactivity of isolated hydroxyls for AA.

5.4.3.1 Surface Erosion

A wide array of studies have been carried out that investigate the phenomenon of surface erosion caused by small molecules on metal oxides. Zecchina *et. al.* [26,28,66,67] found that an increase in the sites with lower coordination (edge and corner sites) resulted from surface erosion. This agrees with the observation of Foster *et. al.*. Foster *et. al.* [50] inspected the interaction between MgO and a series of small molecules, such as water and AA, by atomic force microscopy (AFM) and subsequently observed that severe topographical change occurred when treating MgO surface by steam and AA. It also was found in our prior work [41] that treating MgO with steam is accompanied by a significant increase in the IR band of isolated hydroxyls with 4 coordination. Because isolated hydroxyls are more concentrated on edge and corner sites [39], the increase in the IR band of isolated hydroxyl groups can be ascribed to formation of sites with lower coordination, such as on edges and corners. As seen in **Figure 5.6** and **Figure 5.9**, a significant increase in the IR band of type III isolated hydroxyls (λ=3730 cm^{-1}) was found on AAT- Al_2O_3. This intense band (λ=3730 cm^{-1}) in the IR spectrum of AAT- Al_2O_3 has similar thermal stability with the IR band at 3730 cm^{-1} on HT- Al_2O_3. Both of these two IR bands become thermally unstable at temperatures higher than 200^oC. Therefore, it is reasonable to assume that AA erodes the surface of HT- Al_2O_3 to give more edge and corner sites.

5.4.3.2 Reactivity of Isolated Hydroxyls for AA

In agreement with the studies of Hasan *et. al.* [68], the involvement of isolated hydroxyls in the reaction of AA also was found in this work, but an obvious decrease was only found for the band of type II isolated hydroxyls (λ=3730 cm^{-1}) after HT- Al_2O_3 was treated by AA (shown in **Figure 5.9**). The band of type I isolated hydroxyls (λ=3770 cm^{-1}) is too small to judge whether type I isolated hydroxyls are involved in the reaction with AA. The consumption of type II isolated hydroxyls by the substitution of acetate species was confirmed by the decrease in the IR band at 3730 cm^{-1} and the formation of the band in the region from 3100-2910 cm^{-1} (attributed to -CH_3 of adsorbed acetate species). In theory, if all isolated hydroxyls are not involved in the reaction of AA, the band of the isolated hydroxyls has to be increased after surface erosion. Instead, only the band of type III isolated hydroxyls was increased after AA treatment. This result suggests that isolated hydroxyls with lower coordination possess higher activity for reaction with AA. Both type I and II isolated hydroxyls are substituted by acetate species on AAT- Al_2O_3.

Hydroxyl groups on Al_2O_3 had been assumed in previous studies to supply protons in certain reactions. [69,70,71,72] Type I isolated hydroxyls are considered the most active group since the restriction from adjacent surface sites is less compared with type II and III isolated hydroxyls. [7,12,19,43] Otherwise, isolated hydroxyls act as Brønsted acid sites and the acid strength follows the order: Type I < Type II < Type III. [7,71] The difference between the acid strength of type I_a and type III isolated hydroxyls is of the order of 10^8. [73] Vigué *et. al.* [19] suggested that type I isolated hydroxyls are the most basic sites. Therefore, it can be assumed that the difference in the reactivity of isolated hydroxyls in the reaction of AA is associated with the acid-base properties of the isolated hydroxyls.

5.4.3.3 Catalytic Reactivity of Isolated Hydroxyls for TDE CL

The systematic change in the post-treatment temperature provides a series of AAT- Al_2O_3 with different catalytic reactivity for TDE CL, as seen in **Figure 5.10**. As seen in **Figure 5.8** and **Figure 5.9**, treating HT- Al_2O_3 by AA was accompanied by the dramatic increase of type III isolated hydroxyls and a loss of type II isolated hydroxyls. Type III isolated hydroxyls have the lowest thermal stability by comparison with type II and I isolated hydroxyls [62]. Type III

isolated hydroxyls were removed gradually with time at 250°C. These changes in the content of isolated hydroxyls corresponded to the change in the intensity of the I_t curves shown in **Figure 5.10**. In **Figure 5.10**, the lowest catalytic activity for TDE CL was found on the AAT- Al_2O_3 which was post-treated at 250°C. Before 250°C, the catalytic ability is independent from post-treating temperature. **Figure 5.17** shows the connection between the maximum emission intensity given from the I_t curves of catalyzed TDE CL and the IR band intensities of type III isolated hydroxyls on AAT- Al_2O_3 which were post-treated at different temperature. An obvious decrease both in maximum emission intensity and IR band intensity occurred when post-treating temperature was increased to 250°C. These results give a good indication that catalytic ability is mainly associated with the content of isolated hydroxyls on aluminum oxide.

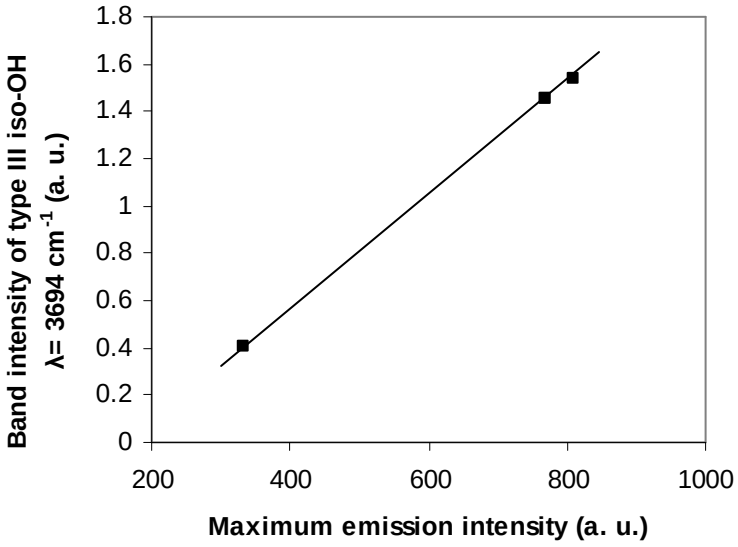

Figure 5.17 The relationship between the IR band intensity of type III isolated hydroxyl (λ= 3694 cm^{-1}) and the maximum emission intensity of TDE CL on AAT- Al_2O_3 when the post-treating temperature was increased from 150°C to 250°C.

A significant difference in the catalytic ability was found between AAT- Al_2O_3 and HT-Al_2O_3. On AAT- Al_2O_3 surface, although more type III isolated hydroxyls are created via surface erosion, the loss of type II isolate hydroxyls by the substitution of acetate species leads to a significant decrease (about 52%) in the catalytic activity of AAT- Al_2O_3 (shown in **Figure 5.10**). Further decrease (about 28%) in the catalytic activity of AAT- Al_2O_3 for TDE CL was found when type III isolated hydroxyl groups were removed at 250°C. This suggests that that the

catalytic ability of type II isolated hydroxyls with respect to TDE CL is much higher than that of type III isolated hydroxyls. It is likely that the catalytic ability of isolated hydroxyls increases with decreasing coordination of the isolated hydroxyls. As can be seen by the data reported above, the emission intensity of TDE CL is associated with the catalytic ability of surface hydroxyl groups.

5.4.4 ST- Al_2O_3

The results shown in **Figure 5.11** indicate that there are no distinct differences in the band of isolated hydroxyls upon treating aluminum oxide by steam. The only difference found on ST- Al_2O_3 is the slight increase in the surface area from 70 (γ- Al_2O_3) to 78 (ST- Al_2O_3) m^2/g. The I_t curve of catalyzed TDE CL on ST- Al_2O_3, shown in **Figure 5.12** has a similar trend as that on γ-Al_2O_3 because the distribution of isolated hydroxyl groups is not changed after steam treatment. The slight difference in the maximum intensity of the I_t curves is likely due to the increase in the surface area.

5.5 Conclusions

The breakage of the hydrogen bond between neighboring hydroxyl groups is accompanied by the creation of isolated hydroxyl groups when dehydrating γ-Al_2O_3 at 400 and 500^{o}C. The catalytic ability of dehydrated γ-Al_2O_3 for TDE CL is enhanced after more isolated hydroxyl groups are formed from the decomposition of hydrogen bonded hydroxyls. This result suggests that isolated hydroxyl groups are the catalysts for the emission of TDE CL.

Upon treating alumina with acetic acid, type II isolated hydroxyl groups were consumed by the substitution of acetate species. The content of type III isolated hydroxyl groups are increased due to surface erosion and lower reaction activity of type III isolated hydroxyls for the reaction with AA. The great decrease (about 52%) in the catalytic reactivity on AAT- Al_2O_3 was found as TDE CL was used to characterize the surface catalytic reactivity. The further decrease (about 28%) in the catalytic reactivity occurred when type III isolated hydroxyls were removed by post-treatment. Because steam did not cause a change in the distribution of isolated hydroxyl, ST- Al_2O_3 had similar catalytic reactivity as γ-Al_2O_3. All of this evidence suggests that the

catalytic ability for TDE CL is associated with the content and the coordination of surface isolated hydroxyls on aluminum oxide. The isolated hydroxyls with lower coordination likely have higher catalytic reactivity for TDE CL.

Heat-treating γ- Al_2O_3 at 900^oC (HT- Al_2O_3) led to a blue-shift in the IR bands of isolated hydroxyls and a phase transformation from the γ to the δ phase. The blue shift of the isolated hydroxyl bands indicates that more isolated hydroxyls are located on octehedrally coordinated Al cations (to Al^{VI}). A great enhancement in the catalytic reactivity was subsequently found on HT-Al_2O_3 for TDE CL. The enhancement in the surface catalytic reactivity is ascribed to the increase in the number of isolated hydroxyls with adjacent Al^{VI} cations. The isolated hydroxyls bound to Al^{VI} cations are thought to have higher catalytic reactivity for TDE CL compared with those on Al^{IV} cations.

5.6 References

1. Knözinger, H., *Adv. Catal.*, **1976**, 25, 184.
2. Rinaldi, R.; Fujiwara, F. Y.; Hölderich, W. and Schuchardt, U., *J. Catalysis*, **2006**, 244, 92.
3. van Vliet, M. C. A.; Mandelli, D.; Arends, W. C. E.; Schuchardt, U. and Sheldon, R. A., *Green Chem.*, **2001**, 3, 243.
4. Silba, J. M. de S; Vinhado, F. S.; Mandelli, D.; Schuchardt, U. and Rinaldi, R., *J. Mol. Catal. A: Chem.*, **2006**, 252, 186.
5. Quigley, W. W. C.; Yamamoto, H. D.; Aegerter, P. A.; Simpson, G. J. and Busseell, M. E., *Langmuir*, **1996**, 12, 1500.
6. Ferri, D.; Diezi, S.; Maciejewski, M. and Baiker, A., *Appl. Catal. A: Gen.*, **2006**, 297, 165.
7. Knözinger, H. and Ratnasamy, P., *Catal. Rev. Sci. Eng.*, **1978**, 17, 31.
8. Szanyi, J.; Kwak, J. H.; Chimentao, R. J. and Peden, C. H. F., *J. Phys. Chem. C*, **2007**, 111, 2661.
9. Lucas, E.; Decker, S.; Khaleel, A.; Seitz, A.; Fultz, S.; Ponce, A.; Li, W.; Carnes, C. and Klabunde, K. J., *Chem. Eur. J.*, **2001**, 7, 2505.
10. Knözinger, H., *Adv. Catal.*, **1976**, 25, 184.
11. Lippens, B. C., and Steggerda, J. J. in *Physical and Chemical Aspects of Adsorbents and Catalysts*; Acadamic Press, Edited by Linsen, B. G., Fortuin, J. M. H., Okkerse, C., and Steggerda, J. J.: New York, **1970.**
12. Morterra, C. and Magnacca, G., *Catal. Today*, **1996**, 27, 497.
13. Peri, J. B., *J. Phys. Chem.*, **1965**, 69, 220.

14. Tsyganenko, A. A. and Filimonov, V. N., *J. Mol. Struct.*, **1973**, 19, 579.
15. Peri, J. B. and Hannan, R. B., *J. Phys. Chem.*, **1960**, 64, 1526.
16. Morterra, C.; Ghiotti, G.; Garrone, E. and Boccuzzi, F., *J. Chem. Soc., Faraday Trans. 1*, **1976**, 72, 2722.
17. Costa, T. M. H.; Gallas, M. R.; Benvenutti, E. V. and da Jornada, J. A. H., *J. Phys. Chem. B*, **1999**, 103, 4278
18. Peri, J. B., *J. Phys. Chem.*, **1965**, 69, 211.
19. Vigué, H.; Quintard, P.; Merle-Méjean, T. and Lorenzelli, V., *J. Eur. Ceram. Soc.*, **1998**, 18, 305.
20. Gadzhieva, N. N. and Gribov, A. A., *J. Appl. Spectr.*, **1998**, 65, 32.
21. Cauwelaer, F. H. V. and Hall, W. K., *Trans. Faraday Soc.*, **1970**, 66, 454.
22. de Boerm, J. H.; Fortuin, J. M. H.; Lippens, B. C. and Meijs, W. H., *J. Catalysis*, **1963**, 2, 1.
23. Busca, G.; Lorenzelli, V.; Escribano, V. S. and Guidetti, R., *J. Catalysis*, **1991**, 131, 167.
24. Kera, Y.; Kamada, M.; Hanada, Y. and Kominami, H., *Compos. Interface.*, **2001**, 8, 109.
25. Henderson, B. and Sibley, W. A., *J. Chem. Phys.*, **1971**, 55, 1276.
26. Zecchina, A.; Lofthouse, M. G. and Stone, F. S., *J. Chem. Soc., Faraday Trans. 1*, **1975**, 71, 1476.
27. Zecchina, A. and Stone, F. S., *J. Chem. Soc., Faraday Trans. 1*, **1976**, 72, 2364.
28. Coluccia, S. and Tench, A. J., *J. Chem. Soc., Faraday Trans. 1*, **1979**, 75, 1769.
29. Anpo, M. and Che, M., *Adv. Catal.*, **2000**, 44, 119.
30. Fouad, N. E.; Thomasson, P. and Knözinger, H., *Appl. Catal. A: Gen.*, **2000**, 194, 213.
31. Chayabutra, S.; Grady, B. V.O' and Larkins, F. P., *Silpakorn University international Journal*, **2003**, 3, 154.
32. Tsyganenko, A. A.; Storozheva, E. N.; Manoilova, O. V.; Lesage, T.; Daturi, M. and Lavalley, J. C., *Catal. Lett.*, **2000**, 70, 159.
33. Ahmed, S. I.-U.; Perry, S. S. and El-Bjeirami, O., *J. Phys. Chem. B*, **2000**, 104, 3343.
34. Bermudez, V. M., *J. Phys. Chem.*, **1970**, 74, 4160.
35. Morimoto, T. and Suda, Y., *Langmuir*, **1985**, 1, 239.
36. Hoq, M. F.; Nieves, I. and Klabunde, K. J., *J. Catalysis*, **1990**, 123, 349.
37. McCafferty, E. and Wightman, J. P., *Surf. Inter. Anal.*, **1998**, 26, 549.
38. Rosenthal, D. J.; White, M. G. and Parks, G. D., *AIChE Journal*, **1987**, 33, 336.
39. Klabunde, K. J.; Stark, J.; Koper, O.; Mohs, C.; Park, D. G.; Decker, S.; Jiang, Y.; Lagadic, I. and Zhang, D., *J. Phys. Chem.*, **1996**, 100, 12142.
40. Nortier, P. and Fourre, P., *Appl. Catal.*, **1990,** 61, 141.
41. Huang, C.-C.; Hohn, K. L. and Schlup, J. R., *J. Phys. Chem. C*, **2009**, 113 (25), 11050.
42. Shirai, T.; Li, J. W.; Matsumaru, K.; Ishizaki, C. and Ishizaki, K., *Sci. Technol. Adv. Mater.*, **2005**, 6, 123.
43. Busca, G.; Lorenzelli, V. and Escribano, V. S., *Chem. Mater.*, **1992**, 4, 595.
44. Morterra, C. and Magnacca, G., *Catal. Today*, **1996**, 27, 497.
45. Wilson, S. J. and McConnell, J. D. C., *J. Solid State Chem.*, **1980**, 34, 315.
46. Paglia, G.; Buckley, C. E.; Rohl, A. L.; Hart, R. D.; Winter, K.; Studer, A. J.; Hunter, B. A. and Hanna, J. V., *Chem. Mater.*, **2004**, 16, 220.
47. Evans, H. E. and Weinberg, W. H., *J. Chem. Phys.*, **1979**, 71, 4789.

48. Xu, C. and Koel, B. E., *J. Chem. Phys.*, **1995**, 102, 8158.
49. Sondag, A. H. M.; Raas, M. C. and van Velzen, P. N. T., *Chem. Phys. Lett.*, **1989**, 155, 503.
50. Foster, M.; Passno, D. and Rudberg, J., *J. Vac. Sci. Technol. A*, **2004**, 22, 1640.
51. Wang, W.; Qiao, X. and Chen, J., *J. Am. Ceram. Soc.*, **2008**, 91, 1697.
52. Petrie, W. T. and Vohs, J. M., *Surf. Sci. Lett.*, **1991**, 259, L750.
53. Ballinger, T. H. and Yates, J. T., *Langmuir*, **1991**, 7, 3041.
54. Fletcher, A. N., *J. Phys. Chem.*, **1969**, 73, 3686.
55. Fletcher, A. N. and Heller, C. A., *J. Catal.*, **1966**, 6, 263.
56. Fletcher, A. N. and Heller, C. A., *Photochem. Photobiol.*, **1965**, 4, 1051
57. Winberg, H. E.; Carnahan, J. E. and Coffman, D. D., *J. Am. Chem. Soc.*, **1965**, 87, 2054.
58. Urry, W. H. and Sheeto, J., *Photochem. Photobiol.*, **1965**, 4, 1067.
59. Paris, J. P., *Photochem. Photobiol.*, **1965**, 4, 1059.
60. Fletcher, A. N. and Heller, C. A., *J. Phys. Chem.*, **1967**, 71, 1057.
61. Toby, S. T.; Astheimer, P. A. and Toby, F. S., *J. Photochem. Photobiol. A: Chem.*, **1992**, 67, 1.
62. Borello, E.; Gatta, G. D.; Fubini, B.; Morterra, C. and Venturello, G., *J. Catalysis*, **1974**, 35, 1.
63. Pecharromán, C.; Sobrados, I.; Iglesias, J. E.; González-Carreño, T. and Sanz, J., *J. Phys. Chem. B*, **1999**, 103, 6160.
64. Cantrell, J. H., *J. Appl. Phys.*, **2004**, 96, 3775.
65. Hasan, M. A.; Zaki, M. I. and Pasupulety, L., *Appl. Catal. A: Gen.*, **2003**, 243, 81.
66. Coluccia, S.; Barton, A. and Tench, A. J., *J. Chem. Soc., Faraday Trans. 1*, **1981**, 77, 2203.
67. Coluccia, S.; Lavagnino, S. and Marchese, L., *Mater. Chem. Phys.*, **1988**, 18, 445.
68. Hasan, M. A.; Zaki, M. I. and Pasupulety, L., *Appl. Catal. A: Gen.*, **2003**, 243, 81.
69. Peri, J. B. and Hannan, R. B., *J. Phys. Chem.*, **1960**, 64, 1526.
70. Rinaldi, R.; Fujiwara, F. Y.; Hölderich, W. and Schuchardt, U., *J. Catalysis*, **2006**, 244, 92.
71. van Vliet, M. C. A.; Mandelli, D.; Arends, W. C. E.; Schuchardt, U. and Sheldon, R. A., *Green Chem.*, **2001**, 3, 243.
72. Silba, J. M. de S; Vinhado, F. S.; Mandelli, D.; Schuchardt, U. and Rinaldi, R., *J. Mol. Catal. A: Chem.*, **2006**, 252, 186.
73. Hiemstra, T.; van Riemsdijk, W. H. and Bolt, G. H., *J. Coll. Int. Sci.*, **1989**, 133, 91.
74. Huang, C.-C. and Hohn, L. K. in Tetrakis(dimethylamino)ethylene Chemiluminescece (TDE CL) Characterization of the CMC and the Viscosity of Reversed Microemulsions, in preparation.

CHAPTER 6 - Characterization of Chemically Grafted Al_2O_3 Surface by Tetrakis(dimethylamino)ethylene Chemiluminescence

6.1 Introduction

Surface modification can be achieved via physical (polishing, mixing and adsorption), chemical (covalent and electrostatic attachment), physicochemical (glow discharge plasma polymerization) or electrochemical (electrochemical activation) methods [1]. For surface modifications on nanoparticles, chemically grafting a functional group on the surface is an efficient manner to alter the surface properties. The early investigations in this area involve the use of grafted ligands for stabilization of nanoparticles in various solutions.[2,3,4,5] Recently, studies have focused on changing the surface behavior of nanoparticles in different reactions by grafting functional ligands on nanoparticles. [6,7]

It is well known that the outmost layer of a metal oxide is substantially covered by hydroxyl groups. [8,9] To bind a functional group on to a metal oxide, surface hydroxyl groups have been widely used as the sites for grafting of organic compounds. [2,10,11] For instance, Matsuno *et. al.* [2] noted that the grafting of nitroxide-mediated initiators on a magnetite surface for following polymerization reactions was due to the interaction between a surface hydroxyl and the phosphoric acid moiety of the initiator. Subsequently, the polymerization of styrene on the surface of magnetite was carried out by heating the mixture of modified magnetite and styrene at 398 K. The inherently hydrophilic magnetite surface was made hydrophobic after the growth of polymer on the surface. A similar reaction mechanism is also applied in grafting functional ligands on magnesium oxide [5] and aluminum oxide [12,13].

To characterize the grafted compounds on nanoparticles, FT-IR [14,15] , XPS [15], NMR [4] usually are used to identify the grafted compound on the surface while the thermal stability and loading of grafted ligands are analyzed by TGA [16,17]. A chemical method also was employed to characterize the loading of a grafted compound. Jeevanandam *et. al.* [5]

checked the effect of grafted compound on the reactivity of surface modified MgO by destructive adsorption of (2-chloroethyl) ethyl sulfide (2-CEES). Research investigating the relationship between the surface properties of the nanoparticle and the loading of the grafted compound is rare.

Our previous studies found that surface hydroxyl groups on MgO and Al_2O_3 significantly impacted TDE CL. [18,19] These surface hydroxyl groups acts as catalysts for TDE CL, substantially increasing the emission intensity. Higher emission intensity was observed when the surface of metal oxide was rich in isolated hydroxyl groups with lower coordination. Klabunde *et. al.* [20,21] suggested that hydroxyl groups concentrated on edge and corner sites are more isolated. The coordination of isolated hydroxyl groups is associated with the topography of metal oxide surfaces. Therefore, it was supposed that TDE CL can be a tool to characterize the acid-base properties, configuration and distribution of surface hydroxyl groups on metal oxides.

For aluminum oxide, it was found in our previous work [18] that the catalytic activity of isolated hydroxyl groups for the emission of TDE CL is related to the coordination of hydroxyl groups and adjacent cations. Isolated hydroxyls with lower coordination and with adjacent aluminum cations with octahedral coordination were the most active sites for the catalysis of TDE CL. Knözinger *et. al.* [22,23] suggested that the acid-base property of an isolated hydroxyl group is related to the coordination of the adjacent Al cations. Because the attachment of an organic ligand to a metal oxide surface results from an acid-base reaction between a surface hydroxyl and the binding terminal end of the grafting ligand, the acid-base property of a hydroxyl group is assumed to play an important role in the loading of a grafted ligand. [2,4,7] TDE CL is considered as a tool for characterizing the reactivity of an aluminum oxide surface for functional ligands since the residual isolated hydroxyl after surface modification can be detected by TDE CL and subsequently reflected in the emission intensity. This study was undertaken in order to understand the potential of using TDE CL for studying the coverage of grafted ligands on aluminum oxide. 2-CEES and hexamethyldisilazane (HMDS) were used as grafting ligands on γ- and δ- Al_2O_3 respectively.

6.2 Experimental

6.2.1 Preparation of Aluminum Oxide Samples

γ- Al_2O_3 with a specific surface area 70 m^2/g was purchased from Alfa Aesar. δ- Al_2O_3 was obtained by heat-treating γ-Al_2O_3 at 900^oC for 3 hours in a channel-type furnace [18]. The surface area, measured by BET method, decreased from 70 m^2/g (on γ- Al_2O_3) to 48 m^2/g (on δ- Al_2O_3) after the heat-treatment. Before the use of γ- and δ- Al_2O_3, aluminum oxide samples were dehydrated at 150^oC.

2-chloroethyl ethyl sulfide (2-CEES, 98%) and hexamethyldisilazane (HMDS, 99+%) were obtained from Sigma-Aldrich and Alfa Aesar, respectively, and used without further purification. To graft 2-CEES and HMDS on the surfaces of γ- and δ- Al_2O_3, a saturation cell was employed. Dehydrated γ- or δ- Al_2O_3 was transferred from the cylindrical cell to the saturation cell with 1.0 ml grafting agent (surface modification agent) in a nitrogen purged glove box. Subsequently, the saturation cell was heated in an oven at 80^oC for 8 hours to allow the evaporation of the grafting agent and chemical deposition of the grafting reagent on dehydrated Al_2O_3. Following grafting, aluminum oxide was treated at 150^oC to remove weakly adsorbed grafting agent.

Both the dehydration of γ-/δ- Al_2O_3 and the post-treatment of the grafted Al_2O_3 were carried out in a cylindrical cell connected to a nitrogen cylinder and vacuum line. After an aluminum oxide sample was loaded in the cell, the cell was heated by an electric furnace to 150^oC at a rate 3^oC/minute and subsequently maintained at 150^oC for 2.5 hours. Next, the cell was purged by a vacuum line at 150^oC for 0.5 hours. TDE was added as the dehydrated or grafted Al_2O_3 sample was cooled down to room temperature in the nitrogen purged glove box.

6.2.2 TDE Synthesis

The synthesis procedure of TDE followed the procedure we reported in earlier work [19]. First, the mixture of chlorotrifluoroethylene (SynQuest Lab. Inc.) and dimethylamine (Alfa Aesar) was sealed in a high pressure vessel. Subsequently, the vessel was heated to 56^oC for 10 hours. Water was further used to remove the impurities in the product.

6.2.3 IR Study

All infrared spectra were obtained in a DRIFT cell (Thermo Nicolet) with a Thermo Nicolet FT-IR spectrometer (Model: Nexus 670) equipped with a liquid nitrogen-cooled MCT detector, KBr beam splitter and tungsten-iodide source. Helium was used as a purging gas to carry compounds eliminated from the aluminum oxide surface out of the cell as the temperature was increased.

6.2.4 Emission Intensity Measurement

The light emission coming out from the TDE CL with and without the presence of aluminum oxide sample was collected by a fiber optic spectrometer (StellarNet Inc. EPP 2000). The reaction was undertaken in a sealed glass chamber. In order to avoid the influence of stray light coming from the environment, the outer wall of the glass chamber was covered by aluminum foil. An air pump and rotameter were connected to the chamber to purge the chamber with dry air. The flow rate of purging gas was regulated by a rotameter at 150 ml/minute.

6.3 Results and Discussion

6.3.1 2-CEES Grafted Al_2O_3

6.3.1.1 IR Studies of 2-CEES Grafted Al_2O_3

It had been reported in our previous work that the IR bands of isolated hydroxyls blue-shifted to higher frequencies as the phase transfer occurred. [18] On γ- Al_2O_3, as seen in **Figure 6.1**, the band 3760, 3710 and 3664 cm^{-1} are ascribed to type I, II and III isolated hydroxyl groups, respectively. [24,25,26,27] These isolated hydroxyl bands were shifted to 3770, 3730 and 3694 cm^{-1} as γ- Al_2O_3 was transferred to δ- Al_2O_3 after heat-treating γ- Al_2O_3 at 900^oC [18], as the IR spectrum shows in **Figure 6.2**. The small band around 2902 cm^{-1} shown in the IR spectra of γ- Al_2O_3 and δ- Al_2O_3 corresponds to C-H stretching of surface impurities. [27,28] 2-CEES was grafted on γ- and δ- Al_2O_3. It can be seen in **Figure 6.1** and **Figure 6.2** that the decrease in the bands of isolated hydroxyls was accompanied with an increase in the band of

hydrogen bonded hydroxyls in the region from 3550-3000 cm^{-1}. Two bands were observed in the region from 3000-2930 cm^{-1}. Kim *et. al.* [29,30,31,32] reported that the bands in this region are due to the symmetrical stretching models of CH_2 and CH_3 moieties of grafted 2-CEES.

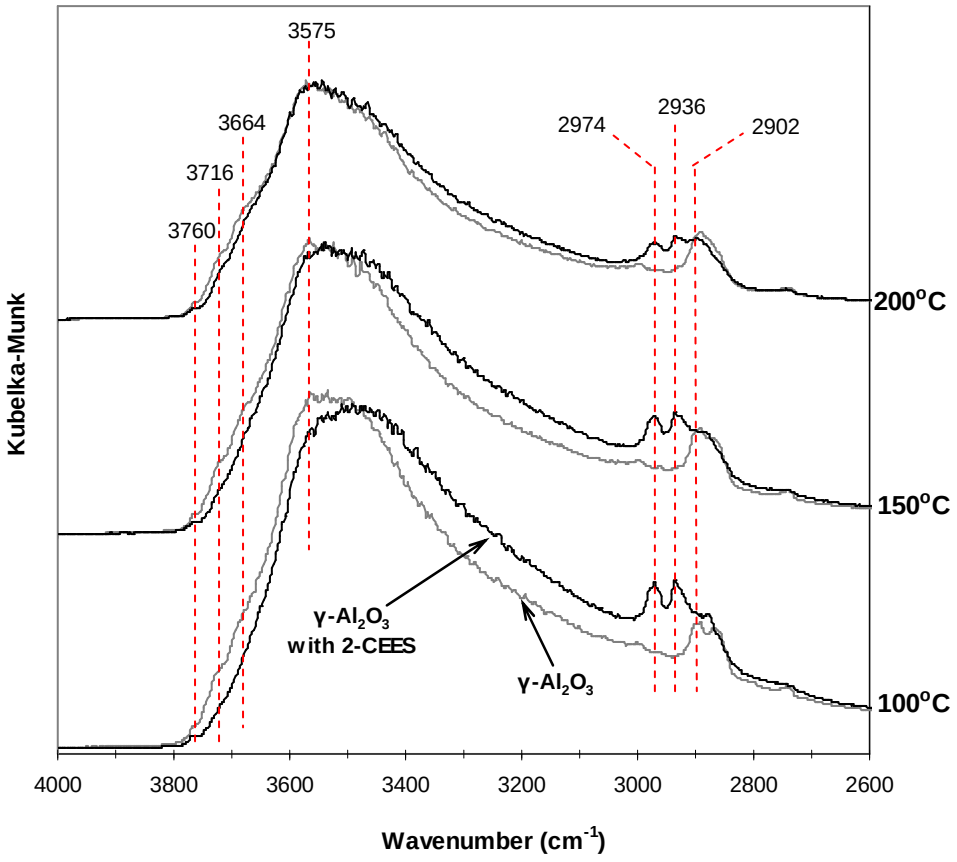

Figure 6.1 The IR spectra of γ- Al_2O_3 and 2-CEES treated γ- Al_2O_3 at 100, 150 and 200°C. The IR spectra of γ- Al_2O_3 is shown by the band with gray color and the spectra of 2-CEES treated of γ- Al_2O_3 is shown by the band with black color.

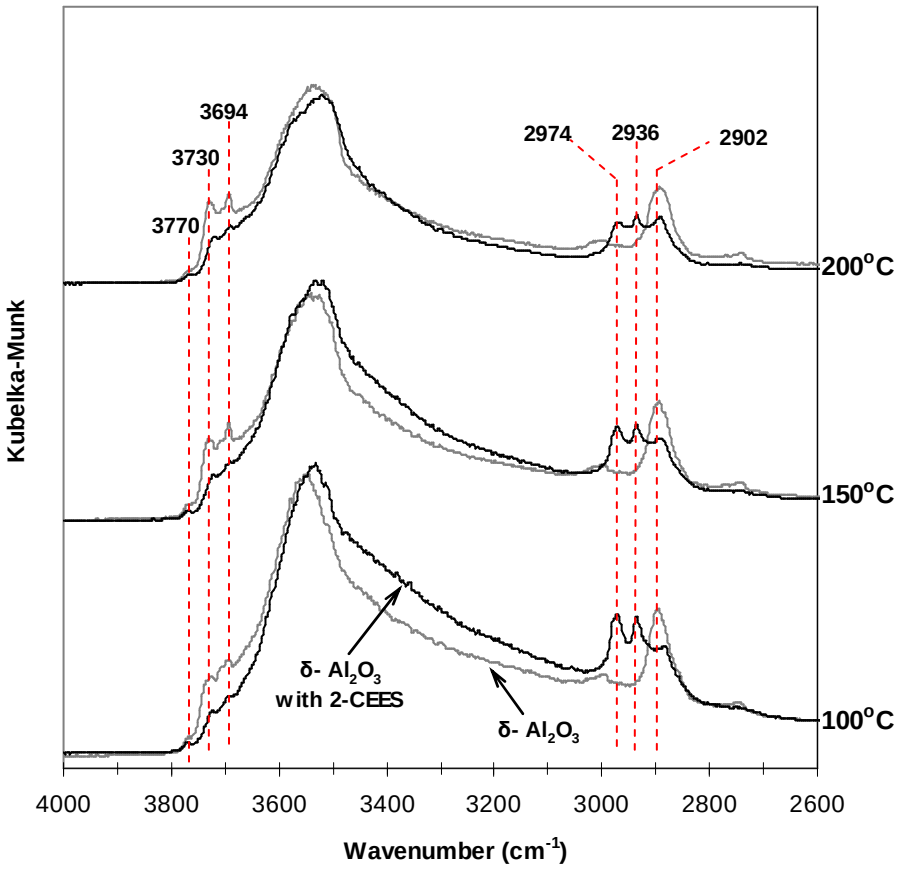

Figure 6.2 The IR spectra of δ- Al_2O_3 and 2-CEES treated δ- Al_2O_3 at 100, 150 and 200°C. The IR spectra of δ- Al_2O_3 is shown by the band with gray color and the spectra of 2-CEES treated of δ- Al_2O_3 is shown by the band with black color.

The grafting of 2-CEES on aluminum oxide involves two sequential processes, as the sketch shows in **Figure 6.3**. [32] At lower temperature, the chlorine terminal of 2-CEES selectively interacts with isolated hydroxyl through hydrogen bonding. The diminution of isolated hydroxyl band is due to the formation of a hydrogen bond between 2-CEES and the isolated hydroxyls. [31,32,33] Isolated hydroxyl groups are eliminated from the surface of aluminum oxide after the 2-CEES bonded to isolated hydroxyl via hydrogen bond is converted to $C_2H_5SC_2H_4$-OAl at higher temperature. This reaction is termed hydrolysis. HCl was liberated from the reaction after the conversion of 2-CEES. Mawhinney *et. al.* suggested that the hydrolysis reaction of adsorbed 2-CEES with isolated hydroxyl group is temperature-dependent. [32,34]

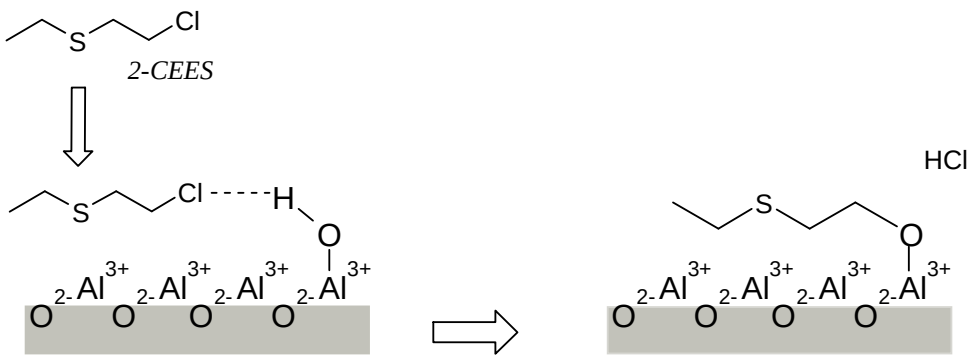

Figure 6.3 Mechanism of the hydrolysis reaction of 2-CEES on the surface of aluminum oxide. In the reaction, 2-CEES specifically bonds to isolated hydroxyl groups. HCl was released in the next step. (from ref. [44])

The same phenomenon was observed in this work. **Figure 6.1** shows the IR bands of surface hydroxyl on 2-CEES grafted γ- Al_2O_3 and γ- Al_2O_3 sample, respectively, at 100, 150 and 200^{o}C. It was found that the band intensity of hydrogen bonded hydroxyl was increased after the adsorption of 2-CEES on γ- Al_2O_3 and δ- Al_2O_3. The increase in the band of hydrogen bonded hydroxyl was accompanied by a decrease in the bands of isolated hydroxyls in the region from 3800-3650 cm^{-1}. Increasing temperature up to 200^{o}C led to a decrease in the band of hydrogen bonded hydroxyls. These results agree with the results reported by Mawhinney *et. al.*. [32] Mawhinney *et. al.* found that the 2-CEES was bonded to surface isolated hydroxyls through a hydrogen bond at 303 K. Further increasing the temperature from 303 K led to hydrolysis of 2-CEES, releasing HCl into the gas phase. Therefore, the decrease in the band of hydrogen bonded hydroxyls can be interpreted as the conversion of bonded 2-CEES over isolated hydroxyls to $C_2H_5SC_2H_4$-OAl.

The change in the bands of the isolated hydroxyl groups was more clear on δ- Al_2O_3 after 2-CEES was grafted on the surface, as seen in **Figure 6.2**. The bands of type II (λ= 3730 cm^{-1}) and III (λ= 3694 cm^{-1}) isolated hydroxyls decrease after δ- Al_2O_3 was treated by 2-CEES. Increasing temperature to 150^{o}C or 200^{o}C causes a decrease in the band intensity of hydrogen bonded hydroxyl groups (λ= 3650-3000 cm^{-1}) but not in the band intensity of isolated hydroxyls. These results reveal the elimination of isolated hydroxyl groups during the transformation from hydrogen bonded 2-CEES over isolated hydroxyls to $C_2H_5SC_2H_4$-OAl species. Otherwise, both

Figure 6.1 and **Figure 6.2** show that the intensity of the bands at 2974 and 2936 cm^{-1} (which are attributed to adsorbed 2-CEES) decrease with increasing temperature. This indicates the removal of residual 2-CEES, weakly-bonded 2-CEES, at the higher temperature before 2-CEES underwent hydrolysis.

6.3.1.2 I_t Curve of Catalyzed TDE CL on 2-CEES Grafted Al_2O_3

TDE was added to characterize the residual isolated hydroxyl groups after 2-CEES was grafted onto γ- and δ- Al_2O_3 surface. The emission intensity vs. reaction time curves (I_t curve) given from TDE CL without catalyst and catalyzed TDE CL in the presence of Al_2O_3 samples are shown in **Figure 6.4** and **Figure 6.5**. As seen in **Figure 6.4**, the emission intensity of TDE CL was enhanced as γ- Al_2O_3 or 2-CEES grafted γ- Al_2O_3 was added. Lower emission intensity was observed after 2-CEES was grafted onto γ- Al_2O_3. The same results also were found in the case of catalyzed TDE CL on 2-CEES grafted δ- Al_2O_3, as shown in **Figure 6.5**. According to the variation of I_{max} (the maximum intensity) in each I_t curve, the grafting of 2-CEES caused about a 75% decrease for grafted γ- and a 39% decrease for δ- Al_2O_3.

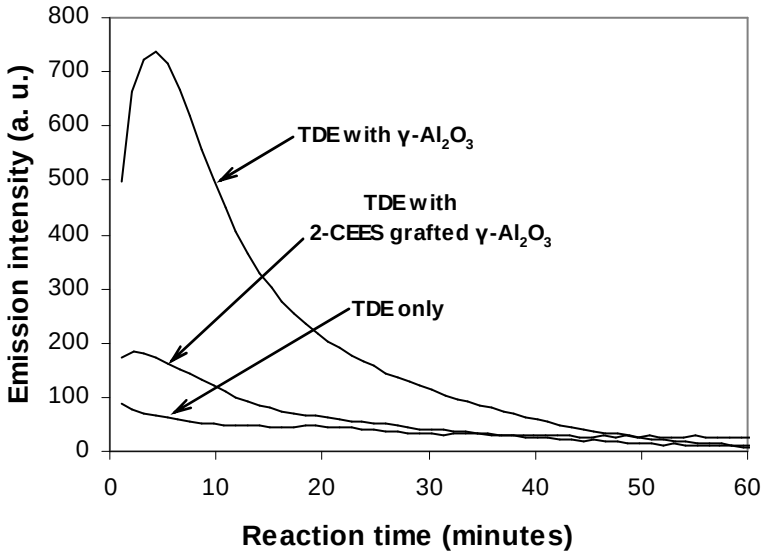

Figure 6.4 Emission intensity as a function of time for TDE CL without catalyst, TDE CL with γ-Al_2O_3 and TDE CL with 2-CEES treated γ- Al_2O_3.

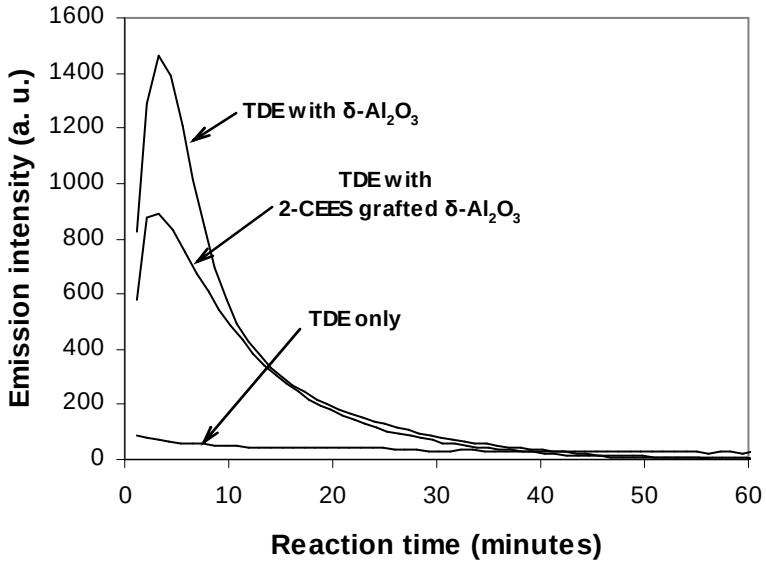

Figure 6.5 Emission intensity as a function of time forTDE CL without catalyst, TDE CL with δ-Al_2O_3 and TDE CL with 2-CEES treated δ- Al_2O_3.

These results can provide information on the types of hydroxyls that are important in catalyzing TDE CL on Al_2O_3, on differences in the surface hydroxyls between δ- Al_2O_3 and γ-Al_2O_3, and differences in how 2-CEES interacts with the two forms of alumina. To interpret these results in terms of the different types of surface hydroxyls present on δ- Al_2O_3 and γ-Al_2O_3, the literature and our prior results [18,19] can provide guidance. Knözinger *et. al.* [35,36] suggested that there are five possible configurations for isolated hydroxyl groups, as shown in **Figure 6.6**. The stretching frequency, net charge, acid-base property, and reaction behavior of each type of isolated hydroxyls are related to the coordination of isolated hydroxyls (1, 2 and 3-coordination) and adjacent cation (octahedral (Al^{VI}) and tetrahedral (Al^{IV}) coordination). Surface hydroxyl groups are Brøsted acid sites. [37] The acidic strength of isolated hydroxyl decreases with increasing net charge of the isolated hydroxyl. [22] Hence, type III isolated hydroxyl are the most acidic isolated hydroxyl. [23] The catalytic reactivity for TDE CL decreases with increasing acidic strength of hydroxyl groups. [18]

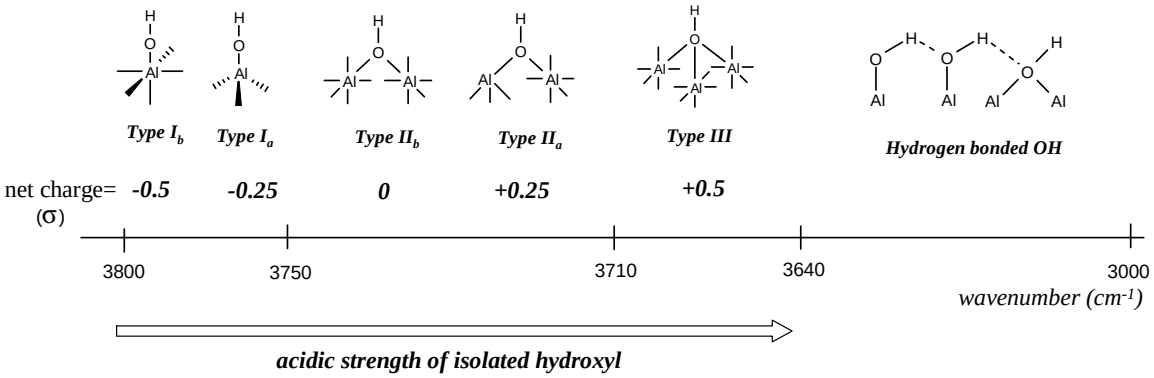

Figure 6.6 Possible configurations of isolated hydroxyl groups on aluminum oxide surface and their corresponding stretching frequencies and net charges (σ).

The IR bands of isolated hydroxyls blue-shift to higher stretching frequencies as the phase of Al_2O_3 was transferred from γ- to δ- phase (see **Figure 6.1** and **Figure 6.2**). The blue-shift of the IR bands of isolated hydroxyls can be interpreted as an indication that more isolated hydroxyls are bonded to Al^{VI} rather than Al^{IV}. [22,24,38] As seen in **Figure 6.4** and **Figure 6.5**, the highest emission intensity is given from catalyzed TDE CL on δ- Al_2O_3. The isolated hydroxyls on δ- Al_2O_3 were proposed to possess higher catalytic reactivity for TDE CL compared with that on γ- Al_2O_3, even though the number of hydroxyl groups participating in the reaction of TDE CL was likely reduced because of the decrease in the surface area from 70 m^2/g on γ- Al_2O_3 to 48 m^2/g on δ- Al_2O_3 [18]. Otherwise, the isolated hydroxyl groups with adjacent cation with octahedral coordination is more basic compared with the isolated hydroxyls with adjacent cation with tetrahedral coordination. [18,22] Therefore, it can be assumed that the isolated hydroxyls on δ- Al_2O_3 are more basic compared with those on γ- Al_2O_3.

The loading of the grafting agent and the binding ability of different isolated hydroxyls for 2-CEES can also be understood from the I_t curves shown in **Figure 6.4** and **Figure 6.5**. The most significant decrease, about 75%, in I_{max} was found after grafting 2-CEES on γ- Al_2O_3. However, the decrease in I_{max} became slight, about 39%, in the case of grafting 2-CEES on δ- Al_2O_3. This result suggests that the isolated hydroxyls on γ- Al_2O_3 have a higher binding ability for 2-CEES: fewer isolated hydroxyls were left after 2-CEES was grafted on γ- Al_2O_3, as evidenced by the lower TDE CL emission intensity. It can be hypothesized that the binding ability of aluminum oxide for 2-CEES is associated with the acidic strength of isolated hydroxyl

groups: the surface with more acidic isolated hydroxyls has higher reactivity for binding 2-CEES. More isolated hydroxyls were eliminated on γ- Al_2O_3 and converted to $C_2H_5SC_2H_4$-OAl after 2-CEES grafting. The threshold for undergoing the hydrolysis reaction of 2-CEES with isolated hydroxyls is lower on γ- Al_2O_3 compared with that on δ- Al_2O_3.

2-CEES grafted δ-Al_2O_3 still maintains relatively higher catalytic reactivity for the emission intensity of TDE CL compared with 2-CEES grafted γ- Al_2O_3. This result indicates that more isolated hydroxyls were left on δ- Al_2O_3 after the 2-CEES grafting. As described in our earlier work [18], catalytic reactivity of the isolated hydroxyls for the emission of TDE CL is associated with the coordination of the isolated hydroxyls. Isolated hydroxyls with lower coordination have higher catalytic reactivity. The elimination of the isolated hydroxyls with lower coordination, such as type I and II isolated hydroxyls, led to a great decrease in the I_{max} (>50%). However, the decrease in I_{max} due to the removal of type III isolated hydroxyls was less than 28%. **Figure 6.5** indicates that the difference in the I_{max} appearing in the I_t curves of catalyzed TDE CL on δ- and grafted δ- Al_2O_3 was about 39%. It can be assumed that 2-CEES mostly are bound to the type III isolated hydroxyls on δ- Al_2O_3. Type I and II isolated hydroxyls on δ- Al_2O_3 likely have lower reactivity for the hydrolysis reaction of 2-CEES. Therefore, 2-CEES grafted δ- Al_2O_3 has higher catalytic activity for the emission of TDE CL. In contrast, the type I and II isolated hydroxyls on γ- Al_2O_3 possess higher reactivity for 2-CEES binding. This is seen in the I_t curve of TDE CL on 2-CEES grafted γ- Al_2O_3 showing lower I_{max} than that on 2-CEES grafted δ- Al_2O_3 because more 2-CEES is bound to the surface and subsequently leads to the elimination of surface isolated hydroxyl groups. Therefore, the I_t curve of TDE CL on 2-CEES grafted γ- Al_2O_3 is close to the I_t curve of TDE CL without Al_2O_3.

6.3.2 HMDS Grafted δ- Al_2O_3

HMDS grafted δ- Al_2O_3 was derived from chemically depositing HMDS on δ- Al_2O_3 at 80^{o}C and subsequently post-treating the sample at 150^{o}C to remove un-reacted HMDS remaining on the surface. The IR spectra shown in **Figure 6.7** was obtained from HMDS grafted δ- Al_2O_3.

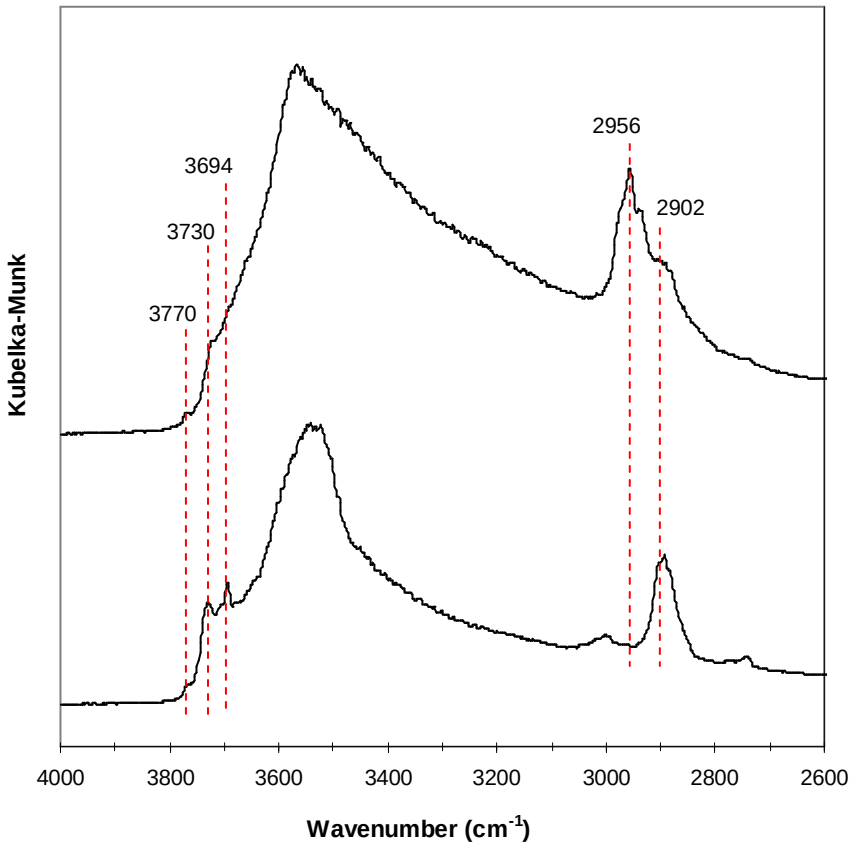

Figure 6.7 IR spectrum given δ- Al_2O_3 (bottom one) and HMDS grafted δ- Al_2O_3 (upper one) at 150°C.

In previous studies, HMDS had been used as a silating agent for investigating the poisoning of catalysts [39] and improving the dispersion ability of metal oxides in non-polar solvents. [12,40,41] The reaction mechanism has been reported, and is sketched in **Figure 6.8**. HMDS selectively reacts with isolated hydroxyl groups and chemically replaces isolated hydroxyls with a silyl ether group, -O-Si$(CH_3)_3$. [39,42,43] Ammonia is liberated after the grafting of HMDS. As seen in **Figure 6.7**, the band with frequency 2902 cm^{-1} is due to the surface impurities, as previously described. The chemical adsorption of HMDS on aluminum oxide was identified by the new formation of bands in the region from 3000-2900 cm^{-1}. These IR bands are ascribed to the stretching modes of the CH_3 moiety, $\nu_{as}(CH_3)$ and $\nu_s(CH_3)$, in the adsorbed silyl ether group. [12] In the region of hydroxyl groups, both bands of type II (λ=3730 cm^{-1}) and III isolated hydroxyls (λ=3694 cm^{-1}) decreased dramatically after HMDS was grafted

onto δ- Al_2O_3. The decrease in the band intensity of type II and III isolated hydroxyl groups can be assumed to be caused by the replacement of isolated hydroxyls by –O-Si$(CH_3)_3$.

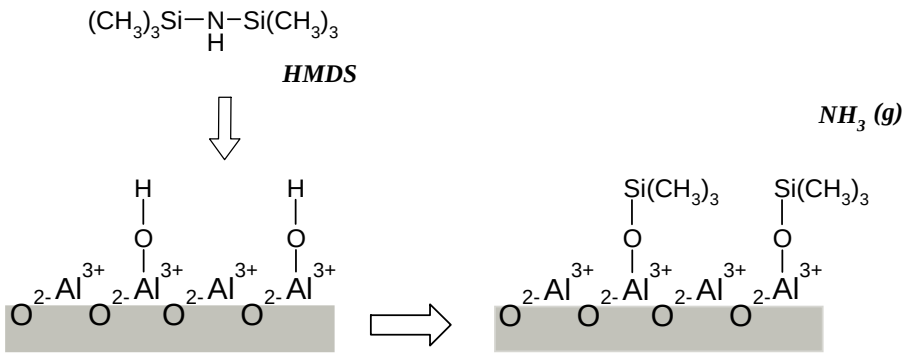

Figure 6.8 HMDS grafting on Al_2O_3 surface.

The I_t curves of catalyzed TDE CL on δ- Al_2O_3 and HMDS grafted δ- Al_2O_3 are shown in **Figure 6.9**. After the grafting of HMDS onto δ- Al_2O_3, the I_{max} decreases by about 68%. The large decrease in the catalytic ability of Al_2O_3 for TDE CL signifies that more isolated hydroxyl groups, especially type I and II isolated hydroxyls, were replaced by –O-Si$(CH_3)_3$. The result emerges that the substitution reaction of silyl ether groups not only occurs over type III isolated hydroxyls, but also occurs over type II and I isolated hydroxyls on δ- Al_2O_3.

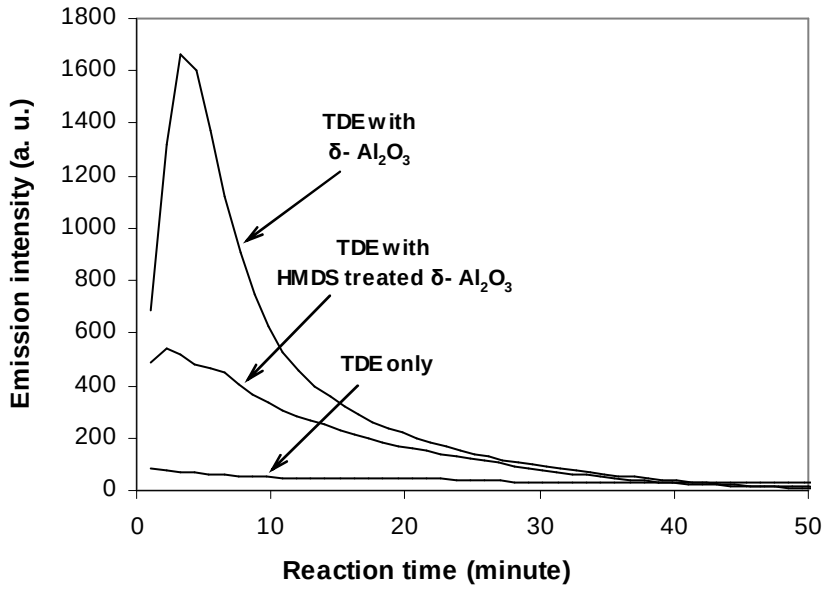

Figure 6.9. The I_t curves of TDE CL without catalyst and catalyzed TDE CL in the presence of δ- Al_2O_3 and HMDS grafted δ- Al_2O_3.

6.4 Conclusions

Surface isolated hydroxyl groups on Al_2O_3 are the active sites for grafting of 2-CEES and HMDS. The reactivity of isolated hydroxyl groups for 2-CEES grafting is associated with the acid-base property of the isolated hydroxyls. Through the difference in the catalytic reactivity of residual isolated hydroxyls after chemical grafting for TDE CL, it was found that more acidic isolated hydroxyl groups have higher reactivity for 2-CEES hydrolysis reaction. Because the isolated hydroxyl groups on γ- Al_2O_3 are more acidic compared with those on δ- Al_2O_3, more isolated hydroxyls were eliminated on γ- Al_2O_3 by the substitution of $C_2H_5SC_2H_4$-OAl after 2-CEES grafting. On γ- Al_2O_3, the isolated hydroxyls with lower acid strengths, such as type I and II isolated hydroxyls, were expected to also participate in the hydrolysis reaction of 2-CEES. The binding of 2-CEES on δ- Al_2O_3 mostly occurred on the sites of type III isolated hydroxyls. In contrast with 2-CEES, the grafting of HMDS is less sensitive to the acid-base properties of isolated hydroxyls. A high percentage of isolated hydroxyl groups on δ- Al_2O_3 were replaced by $–O\text{-}Si(CH_3)_3$ after HMDS grafting. Type I and II isolated hydroxyls were assumed to also be active sites for HMDS grafting.

6.5 References

1. Mottola, H. A. and Steinmetz, J. R. in *Chemically Modified Surfaces*; Elsevier: New York, **1992**.
2. Matsuno, R.; Yamamoto, K.; Otsuka, H. and Takahara, A., *Macromolecules*, **2004**, 37, 2203.
3. Desset, S.; Spalla, O.; Lixon, P. and Cabane, B., *Langmuir*, **2001**, 17, 6408.
4. Gubin, S. P. and Kataeva, N. A., *Russ. J. Coord. Chem.*, **2006**, 32, 849.
5. Jeevanandam, P. and K. J. Klabunde, Langmuir, 2003, 19, 5491.
6. Wight, A. P. and Davis, M. E., *Chem. Rev.*, **2002**, 102, 3589.
7. Kera, Y.; Kamada, M.; Hanada, Y. and Kominami, H., *Compos. Interfac.*, **2001**, 8, 109.
8. Cauwelaer, F. H. V. and Hall, W. K., *Trans. Faraday Soc.*, **1970**, 66, 454.
9. de Boerm, J. H.; Fortuin, J. M. H.; Lippens, B. C. and Meijs, W. H., *J. Catalysis*, **1963**, 2, 1.
10. Yee, C.; Kataby, G.; Ulman, A.; Prozorov, T.; White, H.; King, A.; Rafailovich, M.; Sokolov, J. and Gedanken, A., *Langmuir*, **1999**, 15, 7111.
11. Clark, J. H. and Macquarrie, D. J., *Chem. Commun.*, **1998**, 853.
12. Paul, D. K. and Yates, J. T., *J. Phys. Chem.*, **1991**, 95, 1699.
13. Jacas-Rodríguez, A.; Pérez-Pariente, J.; González-González, C. R.; Díaz-Carretero, I.; Agúndez-Rodriguez, J.; Hernández-Vélez, M., *Materials Letters*, **2005**, 59, 1820.
14. Shen, X.-C.; Fang, X.-Z.; Zhou, Y.-H. and Liang, H., *Chemistry Letters*, **2004**, 33, 1468.
15. Li, H.; Yan, Y.; Liu, B.; Chen, W. and Chen, S., *Powder Technology*, **2007**, 178, 203.
16. Mikhaylova, M.; Kim, D. K.; Berry, C. C.; Zagorodni, A.; Toprak, M.; Curtis, A. S. G. and Muhammed, M., *Chem. Mater.*, **2004**, 16, 2344.
17. Binder, W. H.; Weinstabl, H. and Sachsenhofer, R., *Journal of Nanomaterials*, **2008**, 1.
18. Huang, C.-C. and Hohn, K. L. in Catalytic Reactivity of Surface Isolated Hydroxyl on Aluminum Oxide for Tetrakis(dimethyl amino)ethylene Chemiluminescence, in preparation.
19. Huang, C.-C.; Hohn, K. L. and Schlup, J. R., *J. Phys. Chem. C*, **2009**, 113 (25), 11050.
20. Klabunde, K. J.; Stark, J.; Koper, O.; Mohs, C.; Park, D. G.; Decker, S.; Jiang, Y.; Lagadic, I. and Zhang, D., *J. Phys. Chem.*, **1996**, 100, 12142.
21. Itoh, H.; Utamapanya, S.; Stark, J. V.; Klabunde, K. J. and Schlup, J. R., *Chem. Mater.*, **1993**, 5, 71.
22. Knözinger, H. and Ratnasamy, P., *Catal. Rev. Sci. Eng.*, **1978**, 17, 31.
23. Hiemstra, T.; van Riemsdijk, W. H. and Bolt, G. H., *J. Coll. Int. Sci.*, **1989**, 133, 91.
24. Morterra, C. and Magnacca, G., *Catal. Today*, **1996**, 27, 497.
25. Vigué, H.; Quintard, P.; Merle-Méjean, T. and Lorenzelli, V., *J. Eur. Ceram. Soc.*, **1998**, 18, 305.
26. Busca, G.; Lorenzelli, V. and Escribano, V. S., *Chem. Mater.*, **1992**, 4, 595.
27. Costa, T. M. H.; Gallas, M. R.; Benvenutti, E. V. and da Jornada, J. A. H., *J. Phys. Chem. B*, **1999**, 103, 4278.
28. Morterra, C. and Magnacca, G., *Catal. Today*, **1996**, 27, 497.
29. Panayotov, D. and Yates, J. T., *J. Phys. Chem. B*, **2003,** 107, 10560.
30. Thompson, T. L.; Panayotov, D. A. and Yates, J. T., *J. Phys. Chem. B*, **2004,** 108, 16825.

31. Kim, S.; Byl, O.; Liu, J.-C.; Johnson, J. K. and Yates, J. T., *J. Phys. Chem. B*, **2006**, 110, 9204.
32. Mawhinney, D. B.; Rossin, J. A.; Gerhart, K. and Yates, J. T., *Langmuir*, **1999**, 15, 4789.
33. Mawhinney, D. B.; Rossin, J. A.; Gerhart, K. and Yates, J. T., *Langmuir*, **2000**, 16, 2237.
34. Mawhinney, D. B.; Rossin, J. A.; Gerhart, K. and Yates, J. T., *Langmuir*, **1999**, 15, 4617
35. Knözinger, H. and Ratnasamy, P., *Catal. Rev. Sci. Eng.*, **1978**, 17, 31.
36. Knözinger, H., *Adv. Catal.*, **1976**, 25, 184.
37. Rinaldi, R.; Fujiwara, F. Y.; Hölderich, W. and Schuchardt, U., *J. Catalysis*, **2006**, 244, 92.
38. Busca, G.; Lorenzelli, V.; Escribano, V. S. and Guidetti, R., *J. Catalysis*, **1991**, 131, 167.
39. Rosenthal, D. J.; White, M. G. and Parks, G. D., *AIChE Journal*, **1987**, 33, 336.
40. Armistead, C. G. and Hockey, J. A., *Trans. Faraday Soc.*, **1967**, 63, 2549.
41. Angst, D. L. and Simmons, G. W., *Langmuir*, **1991**, 7, 2236.
42. Hertl, W. and Hair, M. L., *J. Phys. Chem.*, **1971**, 75, 2181.
43. Baraton, M.-I.; Chancel, F. and Merhari, L., *Nanostruct. Mater.*, **1997**, 9, 319.
44. Martin, M. E.; Narske, R. M. and Klabunde, K. J., *Micropor. Mesopor. Mater.*, **2005**, 83, 47.

CHAPTER 7 - Characterization in the Properties of Surface Hydroxyls on Metal Oxides by Tetrakis(dimethylamino)ethylene Chemiluminescence

7.1 Introduction

Metal oxides ($M^{n+}O^{2-}$) have been used frequently as catalysts [1,2,3,4] and supports for functional groups or metals [3,5,6,7,8]. It is well known that the reactivity of metal oxides is strongly associated with surface properties, including surface area, morphology, electronic and acid-base properties. To characterize the surface properties of metal oxides, several spectroscopic techniques have been developed, such as FT-IR [9,10], UV-Visible [11,12], photoluminescent spectroscopy [13,14], NMR [15]. Of these, FT-IR undoubtedly is the most important tool for studying surface properties by identifying the stretching modes of chemisorbed species or the metal oxide itself. However, it is difficult for FT-IR to analyze surface properties quantitatively since the IR adsorption coefficients at each relaxation for the adsorbed groups have to be independently determined. [16]

Surface hydroxyl and molecular water are the most abundant species covering the surface of metal oxides. [17,18] With increasing temperature, most molecular water is removed at temperatures < 200^{o}C [19] while surface hydroxyl groups are eliminated at higher temperatures (from 200 to 1000^{o}C) [20]. The thermal stabilities of surface hydroxyl groups are believed to be related to the interaction between hydroxyl groups and adjacent ions. [21,22,23,24,25] The correlations between the stretching frequencies of surface hydroxyls and their locations have been described by several experimental and theoretically models [13,26,27,28,29].

There are two different categories of surface hydroxyls on metal oxides: hydrogen bonded hydroxyls and isolated hydroxyls. In the IR spectrum, the bands of hydrogen bonded hydroxyls with different coordination overlap each other and appear as a broad band at lower frequency. The individually sharp bands at higher frequencies are ascribed to isolated hydroxyls. Because the stretching frequencies of isolated hydroxyl groups vary with the number and

coordination of adjacent surface ions, [22,30,31] isolated hydroxyls are considered as spectral fingerprints of the surface. [28] The surface reactivity of a metal oxide comes mainly from the unsaturated surface ions (M^{n+} and O^{2-}) and the surface reactivity is developed upon removal of surface species. [17] Therefore, understanding the distribution of surface hydroxyl groups helps to determine and evaluate surface reactivity, acid-base properties, and morphology of a metal oxide.

In our previous studies, it was found that surface hydroxyls on metal oxides act as catalysts for tetrakis(dimethylamino)ethylene (TDE) chemiluminescence (CL). [32,33] The emission of TDE CL was extremely sensitive to the presence of isolated hydroxyl groups. The emission intensity of catalyzed TDE CL was regulated by changing the composition of isolated hydroxyl groups in different configurations via chemical [33,34] or physical [32,33] surface modification. Isolated hydroxyls with lower coordination (with higher stretching frequency) have higher catalytic reactivity for the emission of catalyzed TDE CL.

It has been shown that the nature of surface hydroxyls (i.e. isolated versus hydrogen bonded) depends on the morphology of the metal oxide. For example, Klabunde *et. al.* [24,35] suggested that the hydroxyl groups concentrated on edge and corner sites are more isolated. Since hydroxyls groups cover the active sites of metal oxides, surface reactivity and acid-base property can be interpreted by the types of surface hydroxyls. Ahmed *et. al.* reported that the surface reactivity was associated with intrinsic sites with lower coordination ($M^{n+}{}_{LC}$ and $O^{2-}{}_{LC}$). [15,36,37] The metal oxide with rough surface was thought to feature higher surface reactivity. For the surface acid-base properties, surface hydroxyls and unsaturated ions act as Brønsted and Lewis acid-base sites respectively. The acid- and base- character of metal oxides has been found to play an important role in several acid or base- catalyzed reactions [23,38,39] and the binding capability for grafted functional groups [34]. Consequently, the surface morphology and reactivity of metal oxides can be probed through the emission intensity vs. reaction time (I_t) curve of catalyzed TDE CL because this technique is sensitive to the types and locations of hydroxyl groups.

In this study, the properties of surface hydroxyls on two different forms of MgO (referred to as MgO and MgO^{plus}), two different forms of CaO (referred to as CaO and CaO^{plus}), γ-Al_2O_3, ZnO and TiO_2 were investigated by measuring the I_t curve of catalyzed TDE CL. The catalytic reactivity of surface hydroxyl groups for TDE CL was studied in the context of understanding the types of hydroxyl groups present and their quantities.

7.2 Experimental

7.2.1 BET Surface Area Measurement

MgO^{plus}, MgO, CaO, CaO^{plus}, and TiO_2 were purchased from NanoScale, Inc. (Manhattan, KS.). The differences between MgO^{plus} and MgO, and between CaO and CaO^{plus} were in their particle sizes and surface areas: MgO^{plus} and CaO^{plus} feature smaller particle sizes and higher surface areas compared with MgO and CaO. γ-Al_2O_3 (Al_2O_3) and ZnO were obtained from Alfa Aesar, Inc.. The surface areas of metal oxides were determined by the BET dynamic method using a Quantachrome Autosorb-1. The samples were first outgassed at 150^{o}C. Nitrogen was used for the adsorption experiments at liquid nitrogen temperature.

7.2.2 IR Studies

The surface hydroxyl groups on the metal oxide surfaces were identified by FT-IR (Model: Nexus 670) by using a DRIFTS cell. The FT-IR is equipped with a liquid nitrogen-cooled MCT detector, KBr beam splitter and tungsten-iodide light source. Helium was used as a carrier gas to remove species emitted from the surface when increasing the temperature. The resolution of FT-IR was set at 4 cm^{-1}.

7.2.3 Quantification of Surface Hydroxyl Groups

The method used for measuring the numbers of isolated and hydrogen bonded hydroxyl groups was previously reported. [32] Briefly, this method makes use of a substitution reaction between $AlEt_3$ and the protons of surface hydroxyls. When $AlEt_3$ is added to a metal oxide sample, a substitution reaction between the proton of surface hydroxyls and $AlEt_3$ leads to the production of ethane. In a second step, 1-pentanol was added to react with any un-reacted ethyl groups on metal oxides to produce additional ethane. The ideal gas equation was used to

calculate the number of ethane molecules released in the two steps, from which the number of isolated and hydrogen bonded hydroxyls were obtained. The solubility of ethane in decalin [40] and 1-pentanol [41] was considered in the calculation.

7.2.4 TDE Synthesis

The synthesis processes of TDE has been detailed in our prior work. [32] Dimethylamine (40% in water, Alfa Aesar), first, was purified twice by distillation through a Vigreux column. Then, purified dimethylamine and chlorotrifluoroethylene (SynQuest Laboratories Inc.) were sealed in a high pressure reaction vessel and heated to 56^{o}C for 10 hours. The content of TDE in the product was about 30-40%. After removal of impurities in the product, the remaining light yellow liquid was TDE.

7.2.5 Light Emission Measurement

All metal oxide samples were pre-treated at 150^{o}C for 3 hours to remove molecular water on the metal oxide surface before use. After mixing 0.15 g metal oxide and 0.3 ml TDE in a sample vial, the vial was placed on the sample holder of a sealed chamber. Inlet and outlet tubes allowed the chamber to be purged with dry air. The emission signals were transferred via a flexible fiber optic cable and recorded by a fiber optic spectrometer (StelarNet Inc. EPP2000).

7.3 Results

7.3.1 Surface Hydroxyl Content and Surface Area

The total quantity of hydroxyls and the surface areas for each metal oxide surface were given from $AlEt_3$ titration and BET method, respectively. The results are shown in **Table 7-1**. $AlEt_3$ titration failed to analyze the content of surface hydroxyl groups on TiO_2. This may be due to the high reactivity of surface radicals, $\cdot OH$ and $\cdot O_2$, given from the decomposition of water and oxygen on the TiO_2 surface. [42,43] A distinct difference in the content of surface hydroxyls was found between MgO^{plus} and other metal oxides. The content of surface hydroxyl on MgO^{plus} was 414.76x10^{-5} mole/g while the contents of surface hydroxyl on other metal oxides varied from 210.74 x10^{-5} to 160.95x10^{-5} mole/g.

Sample	Surface area (m^2/g)	Hydroxyl content ($x10^{-5}$ mole/g)	Hydroxyl content (OH number/nm^2)	Average particle size (nm)	Source
MgO^{plus}	614	414.76	4.07	4	NanoScale
MgO	202	192.63	5.74	8	NanoScale
CaO^{plus}	52	210.74	24.41	20	NanoScale
CaO	35	194.62	33.49	40	NanoScale
ZnO	14	160.95	69.24	48	Alfa Aesar
Al_2O_3	70	201.92	17.37	3000	Alfa Aesar
TiO_2	192	-	-	-	NanoScale

Table 7-1 Surface areas and the contents of surface hydroxyl groups on seven metal oxides.

Surface hydroxyls on metal oxide include two types: hydrogen bonded hydroxyls (H-OH) and isolated hydroxyls (iso-OH). The quantity of the two types of surface hydroxyls on each metal oxide was found by $AlEt_3$ and 1-pentanol titration and is shown in **Figure 7.1 A** and **Figure 7.1 B**. **Figure 7.2** shows the percentages of isolated hydroxyl to total hydroxyls on the different metal oxides.

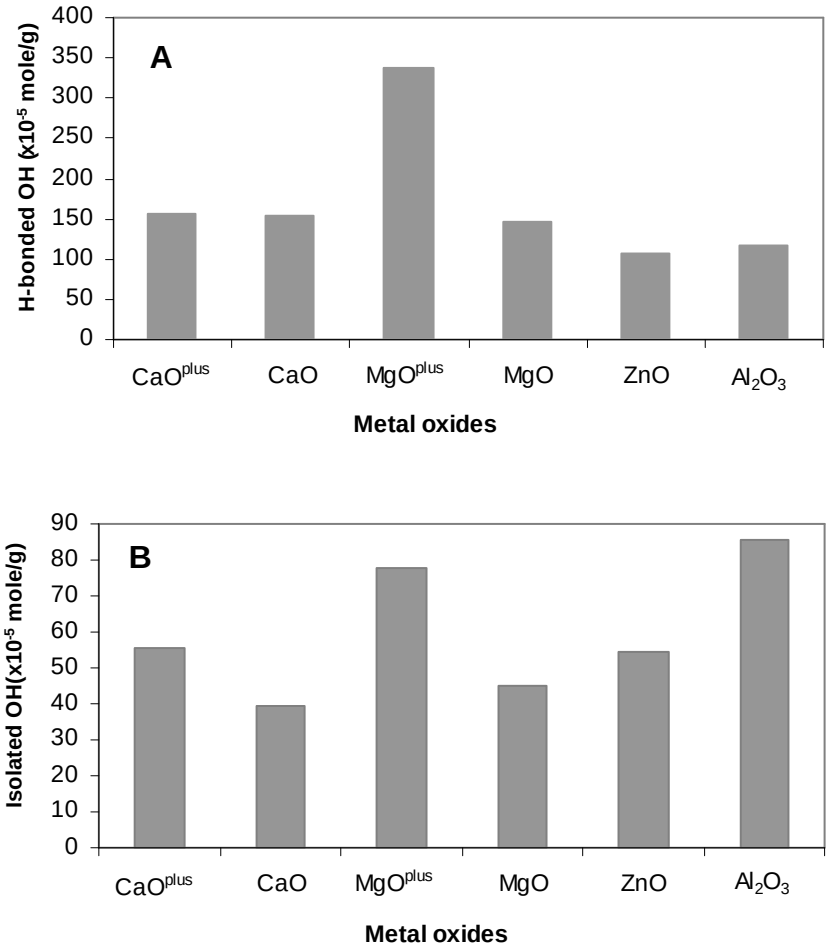

Figure 7.1 The quantities of hydrogen bonded hydroxyls (A) and isolated hydroxyls (B) on metal oxides

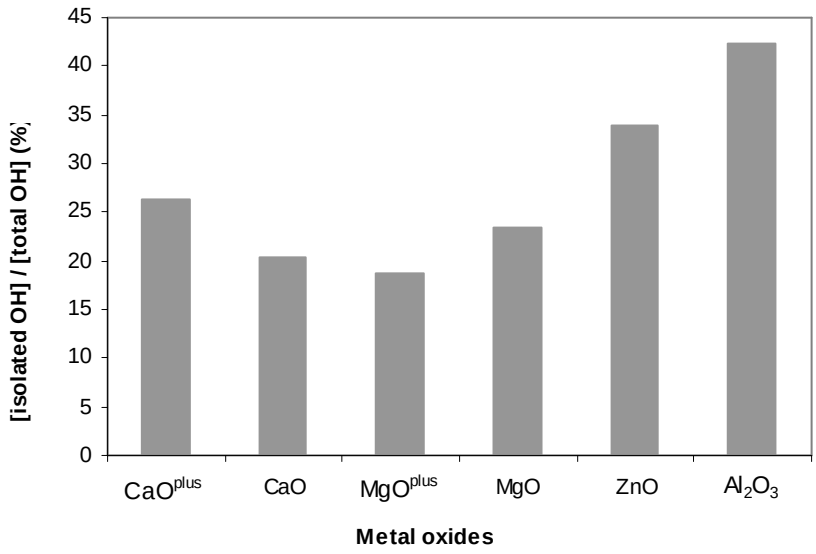

Figure 7.2 The percentages of isolated hydroxyls to total hydroxyls on metal oxides.

As seen in **Figure 7.1**, MgO^{plus} and Al_2O_3 had high contents of isolated hydroxyl groups per unit weight. However, because the content of H-OH on MgO^{plus} was about double of that on other metal oxides, MgO^{plus} had lowest percentage of iso-OH to total OH. The highest percentage of iso-OH to total OH was found on Al_2O_3 surface. About 42 percent of the total hydroxyls were iso-OH. This percentage varied with metal oxide in the following order: Al_2O_3 (42%) > ZnO (34%) > CaO^{plus} (26%) > MgO (24%) > CaO (20%) > MgO^{plus} (19%).

7.3.2 IR Studies of Surface Hydroxyls

The surface hydroxyl groups also were studied by FT-IR. The IR spectra for MgO/MgO^{plus} and CaO/CaO^{plus} are shown in **Figure 7.3 A** and **Figure 7.3 B** respectively. **Figure 7.3 A** reveals two different bands for surface hydroxyls on the MgO surface. The broad band with lower frequency, 3660-3000 cm^{-1}, is attributed to H-OH due to the bonding of hydrogen bond between neighboring hydroxyls. Two bands with higher frequencies (λ=3741 and 3695 cm^{-1}) are assigned to iso-OH. [32] For CaO (see **Figure 7.3 B**), the sharp band at 3639 cm^{-1} is ascribed to iso-OH while the other bands at lower frequencies are due to H-OH. [44] As seen in **Figure 7.3 A** and **Figure 7.3 B**, the hydroxyl bands in the IR spectra for MgO and CaO are also observed in the IR spectra of MgO^{plus} and CaO^{plus}. These results indicate that the type of

surface hydroxyls present is independent from the variations of particle size and surface area: MgO and CaO have the same types of surface hydroxyls as MgO^{plus} and CaO^{plus}. However, the relative amounts of the different types differ for MgO/CaO and MgO^{plus}/CaO^{plus}, as shown in **Table 7-1**, **Figure 7.1** and **Figure 7.2**.

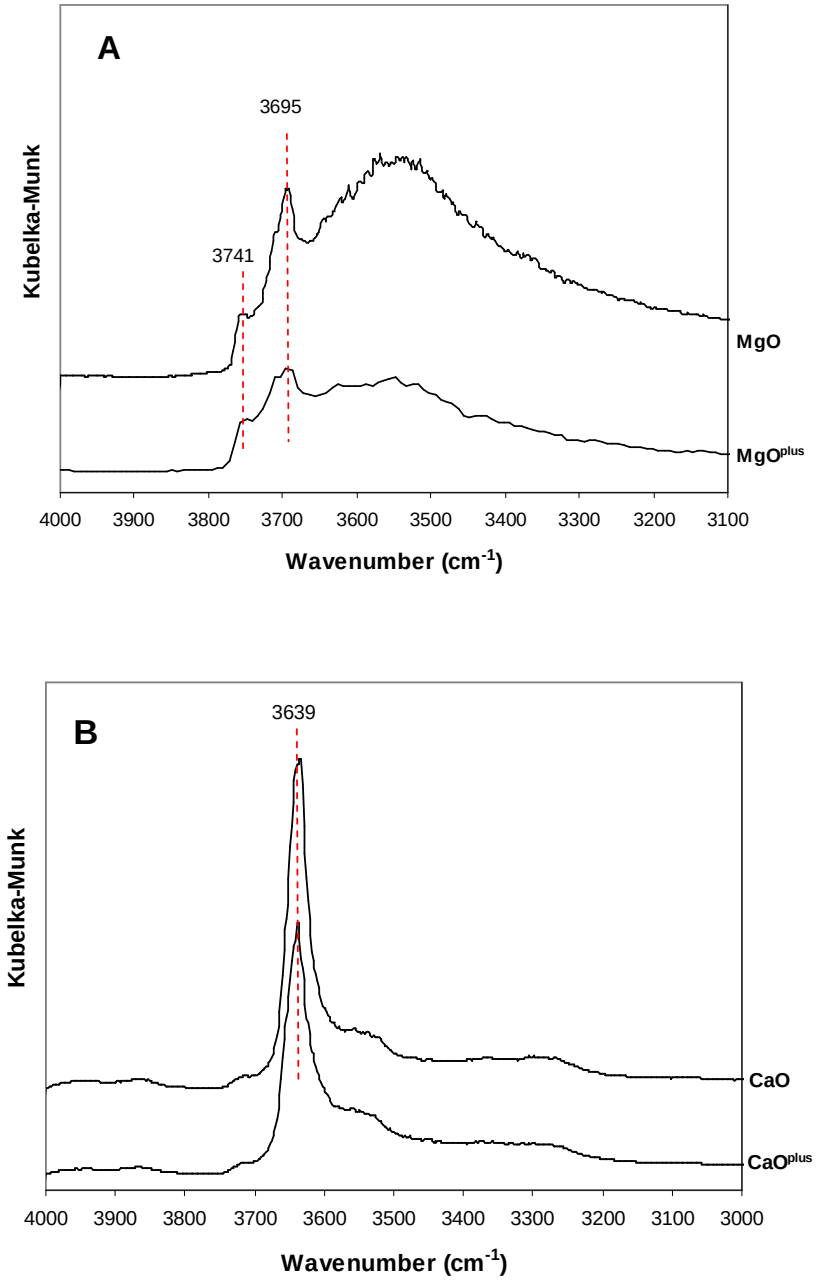

Figure 7.3 IR spectra of surface hydroxyls on (A). MgO/MgO^{plus} and (B) CaO/CaO^{plus} at 150^{o}C.

The IR spectra shown in **Figure 7.4** were obtained for TiO_2, ZnO and Al_2O_3 surfaces. Only one iso-OH band is found in the IR spectrum of TiO_2 and ZnO. The stretching frequency of the iso-OH is 3670 cm^{-1} on TiO_2 and 3673 cm^{-1} on ZnO. [44,45] In contrast, there are three iso-OH bands on Al_2O_3. Their frequencies vary from 3660 to 3760 cm^{-1}. According to Tsyganenko *et. al.* [44], the stretching frequency of iso-OH is associated with the coordination of adjacent ions. The increase in the coordination of adjacent ions causes a downward frequency shift. In the IR spectrum of Al_2O_3, the bands of iso-OH at 3760, 3716 and 3664 cm^{-1} are assigned as the iso-OH bonded to 1, 2 and 3 aluminum ions. [33] As seen in **Figure 7.4**, the iso-OH with higher frequencies (ω=3760 and 3716 cm^{-1}) on Al_2O_3 are more visible at these higher frequencies compared with those on TiO_2 (ω=3670 cm^{-1}) and ZnO (ω= 3673 cm^{-1}).

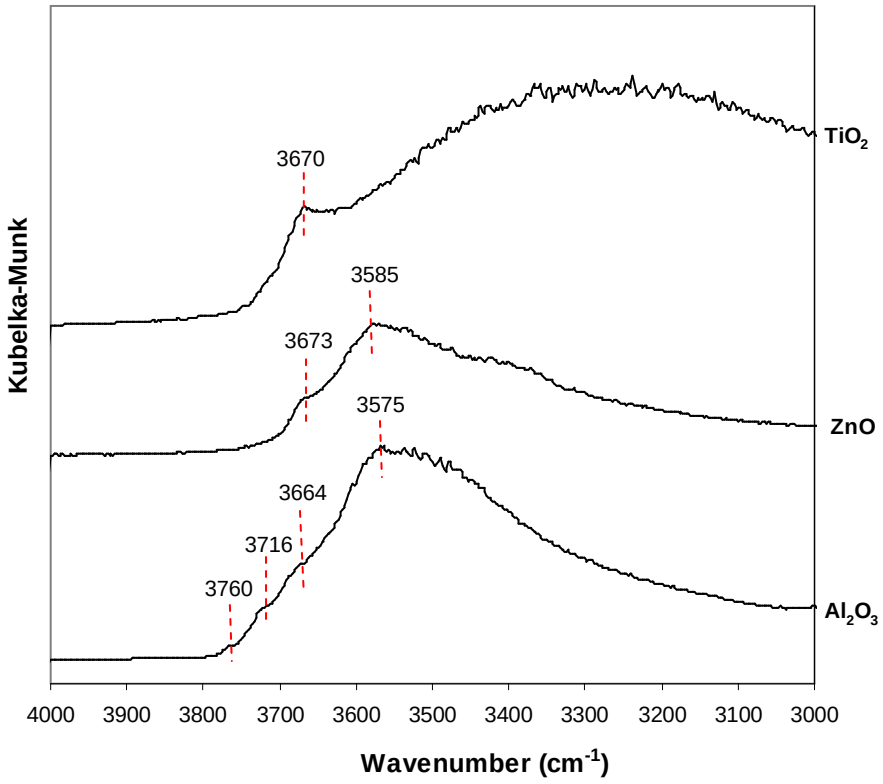

Figure 7.4 IR spectra of surface hydroxyls on Al_2O_3, TiO_2 and ZnO at 150°C.

7.3.3 I_t Curves of Catalyzed TDE CL on Metal Oxide

The emission intensity vs. reaction time (I_t) curves shown in **Figure 7.5** and **Figure 7.6** were obtained for TDE CL on MgO/MgO^{plus} and CaO/CaO^{plus}. As discussed in section 7.3.1, the amount of hydroxyl groups increased as the surface area increased from MgO or CaO to MgO^{plus} or CaO^{plus}. **Figure 7.5** and **Figure 7.6** reveal different trends in the I_t curve when the content of hydroxyl groups was increased for calcium oxide and magnesium oxide. In the case of calcium oxide, the emission was enhanced when the content of hydroxyl groups increased. However, in the case of magnesium oxide, increasing the amount of hydroxyls led to lower emission intensity in the beginning of TDE CL.

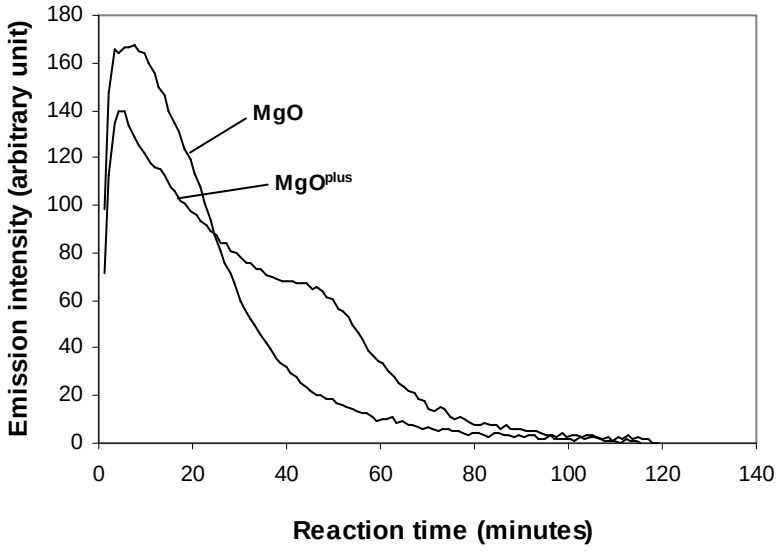

Figure 7.5 I_t curves of catalyzed TDE CL on MgO and MgO^{plus}. MgO^{plus} features higher surface area and lower particle size compared with MgO.

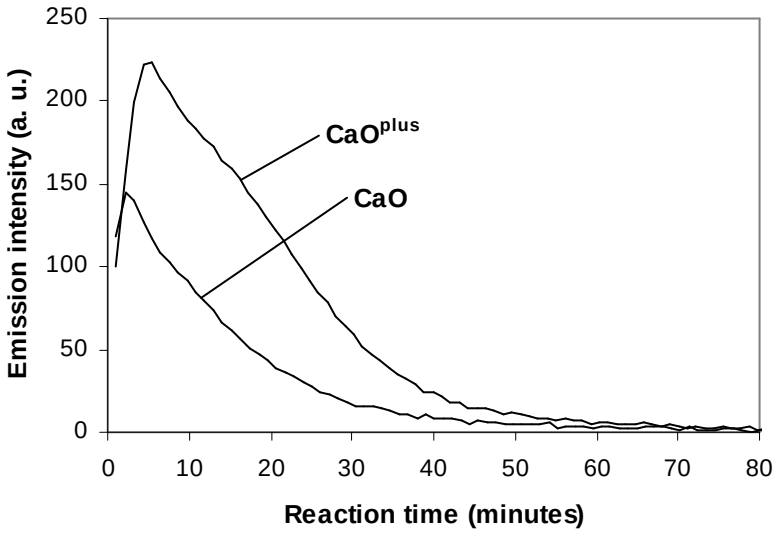

Figure 7.6 I_t curves of catalyzed TDE CL on CaO and CaO^{plus}. CaO^{plus} features higher surface area and lower particle size compared with CaO.

An I_t curve with extremely high emission at the beginning of the reaction was found in the case of catalyzed TDE CL on Al_2O_3, as seen in **Figure 7.7**. The maximum intensity shown in the I_t curve of catalyzed TDE CL on Al_2O_3 was about 4 times of that on MgO and CaO. The lowest emission intensities were obtained in the case of catalyzed TDE CL on TiO_2 and ZnO.

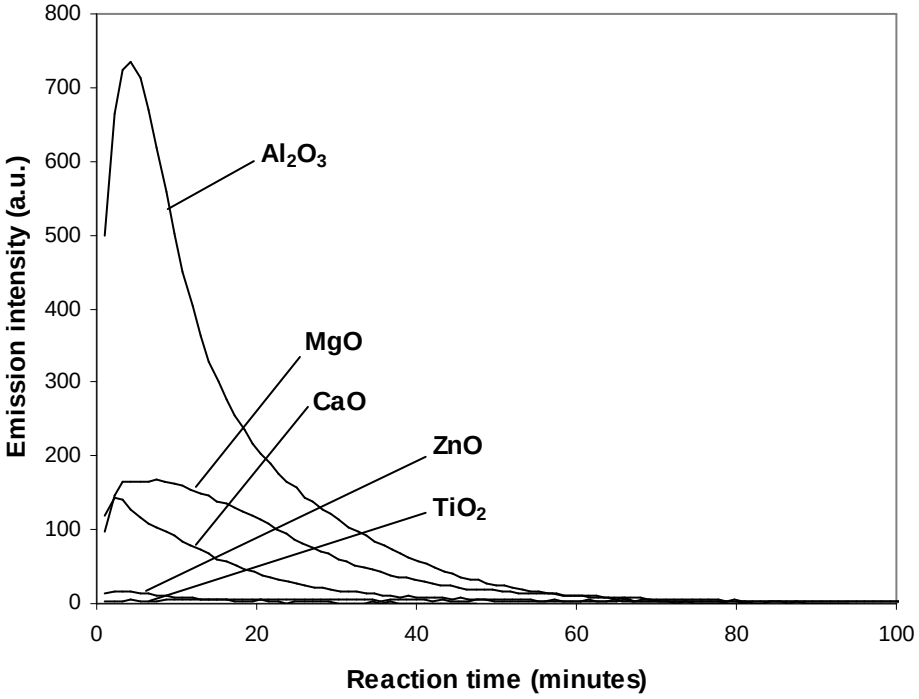

Figure 7.7 I_t curves of catalyzed TDE CL on Al_2O_3, MgO, CaO, ZnO and TiO_2.

7.4 Discussion

7.4.1 Influence of Surface Hydroxyls on I_t Curves

In this study we found that use of a higher surface area form of CaO with more total hydroxyls led to higher emission intensities, while the opposite trend was noted for MgO. This difference can be understood only if the separate roles of isolated and hydrogen-bonded hydroxyls is considered.

As shown in our prior studies [32,33,34] both iso-OH and H-OH increase the production of oxidation products, but only iso-OH enhances the emission intensity of TDE CL. The major product, tetramethylurea, TMU, acts as quenching species for emission of TDE CL, and influences the shape of the I_t curve. [32]

Although the MgO^{plus} surface possesses a higher content of iso-OH groups, MgO^{plus} also features a higher content of H-OH compared with MgO. The lower emission intensity occurring at early reaction times for catalyzed TDE CL on MgO^{plus} is likely due to the high H-OH content. High H-OH content increases the production of quenching species and subsequently leads to diminution in the emission intensity of TDE CL. These ideas agree with prior results that showed that increasing the amount of MgO^{plus} led to decreased emission intensity [32]. Increasing the amount of MgO^{plus} increased the amount of isolated hydroxyls which should catalyze TDE CL, but also increased the amount of H-OH, which ultimately led to lower emission intensity.

For CaO, the opposite trend was noted: the higher amounts of hydroxyls present on CaO^{plus} produced higher emission intensity. This result is due to the lower H-OH content and higher iso-OH to total OH percentage on CaO^{plus} compared with that on MgO^{plus}. There is little H-OH to catalyze reactions that do not emit light or produce quenchers that quench light-emitting reactions.

To explore this idea further, TDE CL was measured when different amounts of Al_2O_3 were used. Al_2O_3 is notable because it has the highest ratio of isolated to total hydroxyls. As seen in **Figure 7.8**, as more Al_2O_3 is used, the emission intensity increases. The increase in iso-OH causes an increase in the rate of TDE oxidation, and therefore increases the emission intensity. The amount of H-OH on Al_2O_3 is, apparently, not sufficient to counteract the effect of iso-OH.

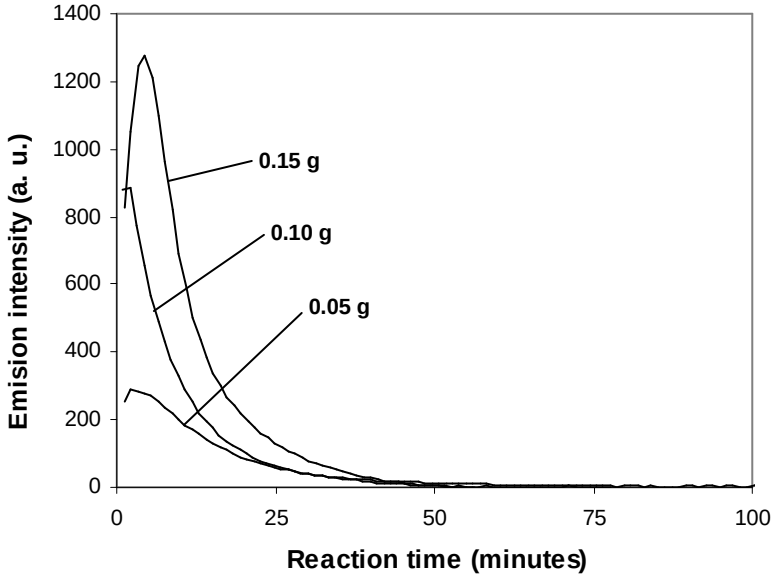

Figure 7.8 The I_t curves of catalyzed TDE CL on Al_2O_3. (ps. Al_2O_3 was purified by heat-treating at 850^{o}C for 2 hours before use)

These results indicate that TDE CL is not a simple function of the total hydroxyls present on a metal oxide surface. Instead, the type of hydroxyl is important. More iso-OH leads to stronger emissions, while increased H-OH can diminish emission intensity.

7.4.2 Isolated Hydroxyls

The properties of iso-OH are associated with the coordination of the oxygen atoms of hydroxyl, and the types of adjacent cations. These differences lead to changes in the stretching frequency of iso-OH. With a decreasing number of adjacent metal ions, the interaction between isolated hydroxyls and metal ions is assumed to be decreased and, subsequently, leads to an increase the binding strength between the proton and oxygen atoms. Therefore, an isolated hydroxyl group with fewer adjacent cations has a higher stretching frequency. [44] This can be seen by looking at the examples of 3, 4 and 5 coordinated (3C, 4C and 5C) iso-OH located on corner, edge and extended plane sites, respectively, on MgO. The binding strength between the proton and oxygen atoms of iso-OH is related to the coordination of the oxygen atom. Thus, stretching frequency of the isolated hydroxyl follows the order: 3C > 4C > 5C iso-OH. [23]

Our prior studies showed that the increase in the stretching frequency of isolated hydroxyls caused an enhancement in the catalytic reactivity of aluminum oxide for the emission intensity of catalyzed TDE CL. [33] A similar result was found on MgO [32] and on chemically modified aluminum oxide [34]. It is natural to propose that the interaction between hydroxyl groups and adjacent cations is associated with the catalytic reactivity of isolated hydroxyls for TDE CL: the lower interaction, the higher catalytic reactivity for the emission of TDE CL. The produce of high energy intermediate, tetrakis-dimethylamino-1,2-dioxetane (TDMD), is dramatically enhanced to support more energy for photon emission when TDE CL is catalyzed by the isolated hydroxyl with higher catalytic reactivity, as seen in **Figure 7.9**. [32]

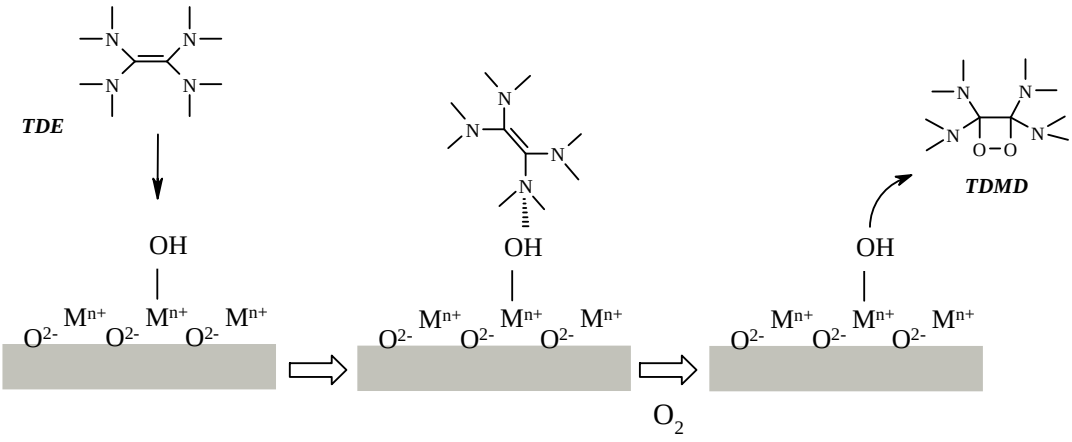

Figure 7.9 Sketch of the catalysis mechanism of isolated hydroxyls in the catalyzed TDE CL. TDMD (tetrakis-dimethylamino-1,2-dioxetane) is the intermediate created from the additional reaction between TDE and oxygen. TDMD also is the necessary energy supporter to excite TDE to an excited state. [47]

As seen in **Figure 7.7**, a great difference in the emission intensity in the I_t curve of catalyzed TDE CL was found in the case of Al_2O_3 and other metal oxides. The maximum emission intensity in the I_t curve of catalyzed TDE CL on Al_2O_3 is about 5 times of that on CaO, and more than 50 times of that on ZnO and TiO_2. The CaO, TiO_2 and ZnO, the surfaces lack iso-OH with adjacent cations with low coordination (high stretching frequency) , as seen in **Figure 7.3** and **Figure 7.4**. Therefore, it can be assumed that the iso-OH with higher stretching frequencies (λ= 3760 and 3716 cm^{-1}) on Al_2O_3 plays a crucially important role to promote the emission intensity of TDE CL.

7.4.3 TDE CL on Metal Oxides with Lower Band Gap Energies

Extremely low emission intensities were found in the case of TDE CL on TiO_2 and ZnO. Comparing with the data reported in our early work [32], the maximum emission intensity derived from the TDE CL on TiO_2 and ZnO were lower than that derived from the TDE CL without the addition of catalyst. Indeed, our prior results showed that even when the surface of a metal oxide lacked iso-OH, the I_t curve had similar emission intensity and trend with the I_t curve of TDE CL without catalyst. [32] The low emission intensity of TDE CL on metal oxides may be due to the lack of the iso-OH with lower interaction with adjacent surface ions, lower content of iso-OH or lower iso-OH to total OH percentage. However, although ZnO had a higher content of iso-OH and higher iso-OH to total OH percentage compared with CaO (shown in **Figure 7.1** and **Figure 7.2**), much higher emission intensity was observed in the I_t curve of catalyzed TDE CL on CaO, as seen in **Figure 7.7**. Therefore, an alternate explanation is needed.

It is known that both ZnO and TiO_2 feature low energy band gaps, about 3.2 eV. [46] This feature enables the creation of two active radicals, $\cdot OH$ and $\cdot O_2$, on the surface. The oxidative ability of the hydroxyl radical was reported to be much higher than those of O_3, H_2O_2 and ClO_2. [42,43] Therefore, the extreme low emission intensity given from TDE CL on TiO_2 and ZnO likely is due to the non-fluorescent decomposition of TDE on the surface of TiO_2 and ZnO via the oxidation reaction of active radicals on the TiO_2 and ZnO surface.

7.5 Conclusions

The emission intensity in the I_t curve of catalyzed TDE CL on metal oxides depends on the hydroxyl groups. Higher emission intensity was derived from the catalyzed TDE CL on metal oxides rich in isolated hydroxyls. Hydrogen bonded hydroxyls also influence the emission intensity but the influence is negative. Because of this, metal oxides with high amounts of hydrogen bonded hydroxyls decrease emission intensity when surface area (and total hydroxyl concentration) is increased, while metal oxides with lower amounts of hydrogen bonded hydroxyls exhibit increased emission intensity when their amount or surface area is increased. The interaction between isolated hydroxyls and adjacent ions plays a crucially important role in

the emission of TDE CL. Isolated hydroxyls with lower interaction with surface ions likely have higher catalytic reactivity for TDE CL. TDE CL was not catalyzed by some metal oxides, such as TiO_2 and ZnO. This result is assumed to be due to the lower band gap energy of these metal oxides and the active oxidant species that can be created on these metal oxides.

7.6 References

1. Menini, C.; Park, C.; Shin, E.-J.; Tavoularis, G. and Keane, M. A., *Catal. Today*, **2000**, 62, 355.
2. Hur, J. M.; Coh, B.-Y. and Lee, H.-I., *Catal. Today*, **2000**, 63, 189.
3. Tanabe, K. and Hölderich, W. F., *Appl. Catal. A: Gen.*, **1999**, 181, 399.
4. Hattori, H. in *Adsorption and Catalysis on Oxide Surfaces*; Elsevier Science Ltd, Edited by Che, M., and Bond, G. C.: New York, **1985**.
5. Giordano, L.; Goniakowski, J. and Pacchioni, G., *Phys. Rev. B*, **2001**, 64, 075417-1.
6. Kurkova, N. S.; Katsobashvili, Ya. R. and Bukhtenko, O. V., *Chem. Tech. Fuels Oils*, **1978**, 14, 9.
7. Matsuno, R.; Yamamoto, K.; Otsuka, H. and Takahara, A., *Macromolecules*, **2004**, 37, 2203.
8. Desset, S.; Spalla, O.; Lixon, P.; and Cabane, B., *Langmuir*, **2001**, 17, 6408.
9. Kera, Y.; Kamada, M.; Hanada, Y. and Kominami, H., *Compos. Interface.*, **2001**, 8, 109.
10. Henderson, B. and Sibley, W. A., *J. Chem. Phys.*, **1971**, 55, 1276.
11. Zecchina, A.; Lofthouse, M. G. and Stone, F. S., *J. Chem. Soc., Faraday Trans. 1*, **1975**, 71, 1476
12. Zecchina, A. and Stone, F. S., *J. Chem. Soc., Faraday Trans. 1*, **1976**, 72, 2364
13. Coluccia, S. and Tench, A. J., *J. Chem. Soc., Faraday Trans. 1*, **1979**, 75, 1769
14. Anpo, M. and Che, M., *Adv. Catal.*, **2000**, 44, 119.
15. Ahmed, S. I.-U.; Perry, S. S. and El-Bjeirami, O., *J. Phys. Chem. B*, **2000**, 104, 3343.
16. Rosenthal, D. J.; White, M. G. and Parks, G. D., *AIChE Journal*, **1987**, 33, 336.
17. Cauwelaer, F. H. V. and Hall, W. K., *Trans. Faraday Soc.*, **1970**, 66, 454.
18. de Boerm, J. H.; Fortuin, J. M. H.; Lippens, B. C. and Meijs, W. H., *J. Catalysis*, **1963**, 2, 1.
19. Borello, E.; Gatta, G. D.; Fubini, B.; Morterra, C. and Venturello, G., *J. Catalysis*, **1974**, 35, 1.
20. Ballinger, T. H. and Yates, J. T., *Langmuir*, **1991**, 7, 3041.
21. Bailly, M.-L.; Costentin, G.; Lauron-Pernot, H.; Krafft, J. M. and Che, M., *J. Phys. Chem. B*, **2005**, 109, 2404.
22. Busca, G.; Lorenzelli, V.; Escribano, V. S. and Guidetti, R., *J. Catalysis*, **1991**, 131, 167.
23. Knözinger, E.; Jacob, K.-H.; Singh, S. and Hofmann, P., *Surf. Sci.*, **1993**, 290, 388.
24. Klabunde, K. J.; Stark, J.; Koper, O.; Mohs, C.; Park, D. G.; Decker, S.; Jiang, Y.; Lagadic, I. and Zhang, D., *J. Phys. Chem.*, **1996**, 100, 12142
25. Itoh, H.; Utamapanya, S.; Stark, J. V.; Klabunde, K. J. and Schlup, J. R., *Chem. Mater.*, **1993**, 5, 71.
26. Knözinger, H. and Ratnasamy, P., *Catal. Rev. Sci. Eng.*, **1978**, 17, 31.

27. Knözinger, H., *Adv. Catal.*, **1976**, 25, 184.
28. Morterra, C. and Magnacca, G., *Catal. Today*, **1996**, 27, 497.
29. Chizalle, C.; Costenitin, G.; Che, M.; Delbecq, F. and Sautet, P., *J. Am. Chem. Soc.*, **2007**, 129, 6442.
30. Goodman, A. L.; Bernard, E. T. and Grassian, V. H., *J. Phys. Chem. A*, **2001**, 105, 6443
31. Li, C.; Li, G. and Xin, Q., *J. Phys. Chem.*, **1994**, 98, 1933.
32. Huang, C.-C.; Hohn, K. L. and Schlup, J. R., *J. Phys. Chem. C*, **2009**, 113 (25), 11050.
33. Huang, C.-C. and Hohn, K. L. in *Catalytic Reactivity of Surface Isolated Hydroxyls on Aluminum Oxide for Tetrakis(dimethyl amino)ethylene Chemiluminescence*, in preparation.
34. Huang, C.-C. and Hohn, K. L. in *Characterization of Chemically Grafting Al_2O_3 Surface by Tetrakis(dimethylamino)ethylene Chemiluminescence*, in preparation.
35. Coluccia, S. and Tench, A. J., *J. Chem. Soc. Faraday Trans. 1*, **1979**, 75, 1769.
36. Mechanism, P.; Boccuzai, F.; Ghiotti, G. and Morterra, C., *J. Chem. Soc., Faraday Trans. 1*, **1982**, 78, 2111.
37. Stirniman, M. J.; Huang, C.; Smith, R. S.; Joyce, S. A. and Day, B. D., *J. Chem. Phys.*, **1996**, 105, 1295.
38. Corma, A., Iborra, S., Primo, J., and Rey, F., *App. Catal. A: Gen.*, **1994**, 114, 215.
39. Di Cosimo, J. I.; Díez, V. K. and Apesteguía, C. R., *Appl. Catal. A: Gen.*, **1996**, 137, 149.
40. Lenoir, J.-Y.; Renault, P. and Renon, H., *J. Chem. Eng. Data.*, **1971**, 16, 340.
41. Yaacobi, M. and Ben-Naim, A., *J. Phys. Chem.*, **1974**, 78, 175.
42. Kubo, W. and Tatsuma, T., *Anal. Sci* , **2004**, 20, 591.
43. Yamakata, A.; Ishibashi, T.-A. and Onishi, H., *J. Phys. Chem.*, **2001**, 105, 7258.
44. Tsyganenko, A. A. and Filimonov, V. N., *J. Mol. Struct.*, **1973**, 19, 579.
45. Maira, A. J.; Coronado, J. M.; Augugliaro, V.; Yeung, K. L.; Conesa, J. C. and Soria, J., J. catalysis, **2001**, 202, 413.
46. Hagfeldt, A. and Grätzel, M., *Chem. Rev.*, **1995**, 95, 49.
47. Orf, H. W. and Dolphin, D., *Proc. Nat. Acad. Sci. USA*, **1974**, 71, 2646.

CHAPTER 8 - Tetrakis(dimethylamino)ethylene Chemiluminescence (TDE CL) Characterization of the CMC and the Viscosity of Reversed Microemulsions

8.1 Introduction

Reverse microemulsions are constructed by the aggregation of amphipathic (surfactant) molecules with the polar heads attracted to interior of micelles while the non-polar tails extend into the bulk non-polar solvent. There are many published articles addressing the main features of normal micelles or oil-in-water microemulsions (O/W) during the past fifty years. [1,2,3,4,5,6,7] However, the properties of reversed microemulsion systems (RMS) have been less frequently analyzed. Due to the nature of surfactants, surfactant molecules can arrange themselves into organized molecular assemblies known as micelles to form a microheterogeneous media (or microemulsion) in solution with oil and aqueous phases. Reversed micelles, or water-in-oil microemulsions (W/O), have attracted much attention recently since they can be used as nano-reactors to synthesize ultra small nanoparticles [8,9,10], or as reaction media for polymerization. [11,12] A few examples include the development of water-in-supercritical carbon dioxide ($scCO_2$) microemulsion systems for synthesizing novel nanosized catalysts and organic compounds and applications in biochemical separation and the food industry. [13,14,15,16,17,18,19] In those studies, $scCO_2$ microemulsions aided in waste minimization and also controlled the reaction environment.

The properties of RMS mainly depend on the type of surfactant used to stabilize the system, the nature of bulk solvent, and the ratio of water-to-surfactant (W_0). The aggregation number, the CMC (critical micellar concentration) and the thermal properties of RMS are typically used to characterize RMS. The CMC is the most important parameter because it identifies when the system starts to possess the full function of a RMS. Before the CMC, the surfactants exist mainly as solvated monomers, while above the CMC, the monomers and micelles exist in dynamic equilibrium. [20] Further increasing the concentration of surfactant in the system will result in aggregation of the surfactants while the concentration of the free

surfactant monomers remains virtually constant in the bulk phase [21]. Otherwise, the thermodynamic properties (free energy , enthalpy, entropy and heat capacity) of a RMS can be obtained if the CMC of a RMS is known. [22,23,24,25,26] The CMC of a RMS is the most important property when the surfactant's architecture is going to be designed for various applications in RMS (especially for application in a water-in-scCO_2 microemulsion). [4,24,27]

The physical properties (such as surface tension, specific heat, conductivity, osmotic pressure, light scattering *et. al.*) of microemulsions will undergo a change when the concentration of surfactant in the bulk phase approaches the CMC. This change could be abrupt or slight. For most normal microemulsion (oil-in-water microemulsion) systems, the determination of the CMC is based on the abrupt change of some physical properties in proximity to the CMC of surfactants. In contrast, the physical properties of water-in-oil microemulsions typically change only slightly in the transition region. Moreover the aggregation number (the number of surfactant monomers involved in the unit aggregation) of reverse micelles typically is small compared to that of normal micelles due to the difference in area occupied by surfactant head and tail. This not only leads to the low CMC of RMS, but also causes difficulties in determining the CMC of RMS by traditional measurements (ex. NMR, UV-Vis, light scattering, surface tension, conductivity *et. al.*) usually used in the characterization of normal microemulsions. [28] A couple of techniques have been developed and employed in the characterization and measuring the CMC of RMS during the past two decades. They include low angle neutron scattering [29], vapor pressure osmometry [30], TCNQ (7,7,8,8-tetracyanoquinodimethane) adsorption [31], calorimetric study [32], positron annihilation techniques [28], fluorescent probe [26,33,34,35,36,37] and ^{1}H NMR [38,39,40]. However these techniques either are limited to a specific RMS, or lead to contradictory conclusions as the RMS is detected by two techniques. A widely applicable and accurate method, thus, is desired to enhance our knowledge of the CMC in RMS.

Methods for characterizing microemulsions involving fluorescent probes have been frequently studied in recent years, and Behera *et. al.* [37,41,42] have published several systematic studies on these methods. There are no published reports of using chemiluminescence, where the release of chemical energy causes the emission of photons rather

than the use of an external light source, for characterization of RMS. Chemiluminescence (CL) has been investigated as a probe in many applications. [43,44,45] The distinct advantage of CL analysis over the method of fluorescent probe is the absence of an external light source, which means that the analytically relevant emission can be measured against a completely dark background. Therefore, the potential interference of light from light scattering can be ignored when CL is used as the detection method. This advantage may allow CL analysis to be used to detect RMS's properties under extreme conditions, such as biochemical systems, when the system is sensitive to irradiation by an externally excited light source, or when the amount of sample is less than the required amount for the analysis using fluorescent probes.

Tetrakis(dimethylamino)ethylene chemiluminescence (TDE CL) has a number of features that make it attractive for study of micelle systems, especially TDE's non-polar molecular structure and autoxidation reaction mechanism. [46,47] In the reaction mechanism of TDE CL, TDE serves as both the excited energy acceptor/emitter during the reaction [48] and reacts with oxygen spontaneously, so addition of fluorescent components (excited energy acceptor and emitter) and reaction inducers are not required. This removes the issues typically associated with fluorescence methods, where the solubility of the emitter and initiators must be considered. In addition, TDE is non-polar while the products of TDE CL are polar. The products, mainly tetramethylurea (TMU) and tetramethyloxamide (TMO), act as quenchers for TDE CL due to their high electron affinities and lower potential energies. [47,49,50,51] TDE CL may provide insights into the properties of RMS because the presence of micelles will effectively isolate the polar quenching species from non-polar TDE, thereby enhancing CL intensity.

Another potential application of TDE CL is as a means for finding the viscosity of a system. Viscometers typically used in the measurement of the viscosity of liquids (ex. capillary, rotation or cone-plate viscometer), have trouble in probing the viscosity of the RMS when contained in a sealed system or the system with small volume, such as bio-RMS used in protein separation or water-in-scCO_2 RMS. [52,53] However the viscosity of RMS is an important parameter. For example, the transport of dissolved components between the continuous non-polar phase and the disperse aqueous phase or the exchange of the contents between reversed micelles is affected by the viscosity of RMS. When RMS is applied in the synthesis of a

nanoparticle with two or more components, the particle size and the coalescence rate of the synthesized nanoparticles are dependent on the interfacial viscosity of the RMS. [54]

The intensity of emission from an excited fluorescent compound depends on whether the excited energy is lost through vibrations and/or collisions. The vibrational dissipation energy of a fluorescent reaction can be limited if the magnitude and the modes of intra-molecular vibration and rotation are limited. Haidekker *et al*. [55,56,57] investigated fluorescent molecular rotors which are constructed of julolidine nitrogen and nitrile groups joined by a vinyl bond. They found that the rotation of groups near the C=C double bond of the fluorescent dyes led to de-excitation and a decrease in emission intensity. However this energy dissipation could be limited in viscous media because of the steric hindrance of intra-molecular rotation. The work of Haidekker *et al.* suggests that TDE CL may aid in identifying the viscosity of RMS because a more viscous media may inhibit the intra-molecular rotation and vibration of di-methyl amino groups bonded to the vinyl center of the TDE molecule. In addition, the migration of quenching species will be affected by solvent viscosity, and could also affect the emission intensity of TDE CL.

This research uses TDE CL to characterize RMS. The CMC was found for three surfactants in multiple solvents. In addition, the use of TDE CL to evaluate the viscosity of a RMS was explored.

8.2 Experimental Section

8.2.1 Tetrakis(dimethylamino)ethylene (TDE)

The probing reagent, TDE, was synthesized by a modification of the method developed by Pruett *et. al.*. [58] The details of the synthesis procedure are described in **Chapter 3**.

8.2.2 Samples

Eight non-polar organic solvents including cyclohexane (Fisher Scientific), benzene (Fisher Scientific), n-heptane (Alfa Aesar), n-octane (Alfa Aesar), iso-octane(Alfa Aesar), n-

decane (Sigma), n-dodecane (Alfa Aesar), and mineral oil (Aqua Solutions, Inc.) were used as received without additional purification. Two anionic surfactants, Dioctyl sulfosuccinatesodium salt (AOT) (Alfa Aesar) and sodium dodecylbenzenesulfonate (NaDDBS) (Sigma), and one nonionic surfactant, Triton X-100 (X-100) (Alfa Aesar), were used as received. The stock solutions were prepared, in advance, by mixing the surfactant and the solvent to give a concentration around 0.45M. The sample solutions were prepared by dilution of the stock solution to give the desired concentration.

8.2.3 Measurement of TDE CL

The I_t (emission intensity vs. reaction time) curves of TDE CL in non-polar organic solvents were collected and recorded with an optic fiber spectrometer (StellarNet Inc. EPP2000) at 25^{o}C. The sample solution (the mixture of non-polar solvent with surfactant in the desired concentration and 1.287M TDE), 0.4ml, was loaded into a sample cuvette that was then placed on the sample holder of the sample chamber. The sample chamber was sealed with an O-ring and purged with dry air at 150 ml/min using a rotameter during the reaction.

8.2.4 Viscosity Measurements

The kinematic viscosity (υ) of the solution was determined by the transit time of the solution (*t*) flowing through the capillary of the cross-arm type viscometers (universal size no. 2 and 4) at 25^{o}C using the equation below (**Equation 8- 1**):

$$\upsilon(cSt) = t \times \theta \qquad (8\text{- }1)$$

where *t* is the efflux time and θ is the constant of the viscometer.

The sample solutions were prepared by mixing cyclohexane and mineral oil in various ratios while the concentrations of AOT in each sample solutions were fixed at 0.43mM. The I_t curve was measured, and the intensity of the local maximum was noted and used to construct a plot of emission intensity as a function of solvent viscosity.

8.3 Results and Discussion

8.3.1 Effect of Quenchers on the I_t Curve of TDE CL

As describing in **Figure 1.1**, the high energy intermediate, Tetrakis-dimethylamino-1,2-dioxetane (TDMD), is produced from TDE autoxidation reaction, and is the excited energy source for TDE CL. [46,51] Because TDMD is unstable at room temperature, TDMD will further decompose immediately into the products of TDE CL, mainly tetramethylurea (TMU, 65 mole %) and tetramethyloxamide (TMO, 18 mole%) [49], and release energy to convert TDE to its excited state, TDE*. TMU and TMO feature higher electron affinity than TDE [49]. On the other hand, TDE is a good electron donor. The high electron donor strength of TDE had been identified by Hammond *et. al.* via the inter-molecular charge-transfer between TDE and π electron acceptors. [50,59] Therefore, the electronically excited energy not only is transferred to un-oxidized TDE but also is transferred to TMO and TMU by molecular collision during the reaction. Winberg *et. al.* found that the emission intensity of TDE CL decreases with increasing the concentration of TMO and TMU [48,60,61]. Fletcher *et. al.* further indicated that TMU and TMO are quenchers for TDE CL. [46,48]

Because TMO is not commercially available, only TMU was studied to understand the effect of quenching species on the emission of TDE CL. **Figure 8.1** shows the effect of TMU on TDE CL. Adding TMU into solution does decrease the intensity of TDE CL; however the trend is not linear. The intensity decreases with increasing TMU concentration, but the slope of this decrease changes at [TMU]=0.383 M. It is hypothesized that the change in the slope is due to the formation of microdroplets of TMU in the bulk phase when TMU reaches its saturation point because droplets become visible when [TMU] is further increased from 0.383 M. After [TMU]=0.383 M, the increase of [TMU] only leads to the increase in the concentration or the size of microdroplet consisting of TMU. In **Figure 8.1**, the difference in the slopes of the lines before and after [TMU]=0.383 M also indicates that the quenching efficiency of dissolved TMU is higher than that of TMU microdroplets.

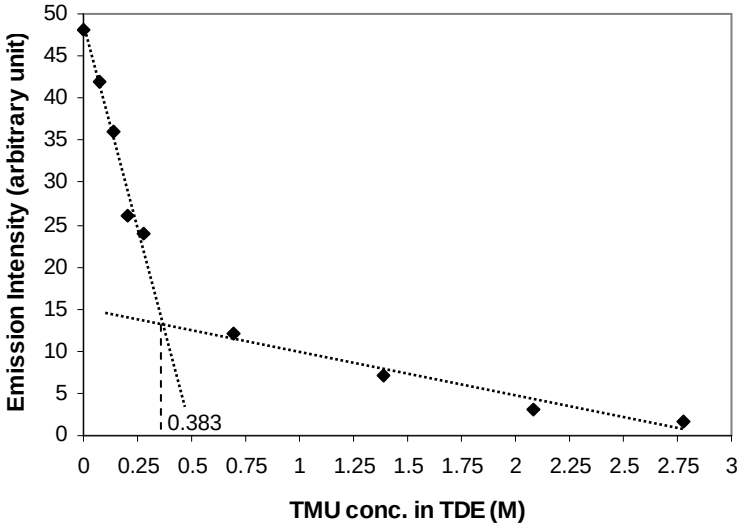

Figure 8.1 The quenching effect caused by TMU in TDE/cyclohexane bulk phase. The dots shown on the figure are the initial emission intensity of TDE CL with TMU concentration. The intersection of two straight lines going through the dots at higher TMU (>0.383M) and lower TMU (<0.383M) concentration indicates the saturation point of TMU in cyclohexane.

TDE CL was considered as a means to measure the CMC of a reversed microemulsion system due to the opposite polarity of TDE and its products, quenchers. Clearly, quenchers affect the emission intensity of TDE CL. However, they can be removed from solution and their effects are minimized because of the differences in the quenchers' polarity compared to TDE. It is well known that the mutual solubility between aqueous phase and oil phase can be enhanced by the addition of surfactant. In this study, it was expected that adding surfactant into the oil phase with TDE can influence the emission intensity since the quenching species are removed from oil phase right after the formation of reversed micelles, as depicted in **Figure 8.2**.

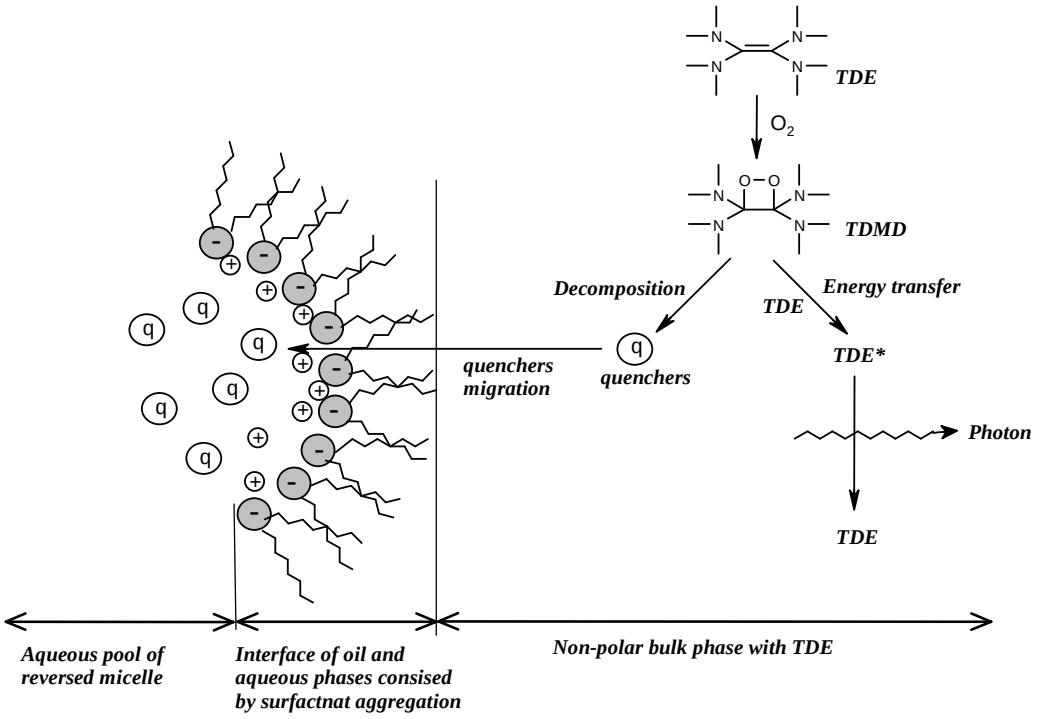

Figure 8.2 Representation of TDE CL in non-polar solvents with AOT micelles when the concentration of [AOT] > CMC.

8.3.2 I_t Curve of TDE CL in RMS

The impact of surfactants on TDE CL was studied by measuring TDE CL in two situations: when a surfactant (AOT) was present in a concentration below the CMC, and when it was present in a concentration above the CMC. **Figure 8.3** shows the results of these experiments. Curve **a** is the I_t curve of TDE CL with lower AOT concentration ([AOT]<CMC) [4,66] while the curve **b** is the I_t curve of TDE CL with higher AOT concentration ([AOT]>CMC) in the AOT/Cyclohexane RMS. For both curves **a** and **b**, the emission intensity decreases with reaction time; however, curve **b** shows a exponentially decreasing trend while curve **a** initially decreases until around 18 minutes, then increases until around 42 minutes before finally decreasing monotonically. The differences seen in **Figure 8.3** are likely due to the formation of reversed micelles that help separate TDE from the quenching species and enhance the emission of TDE CL in the first 20 minutes of the reaction.

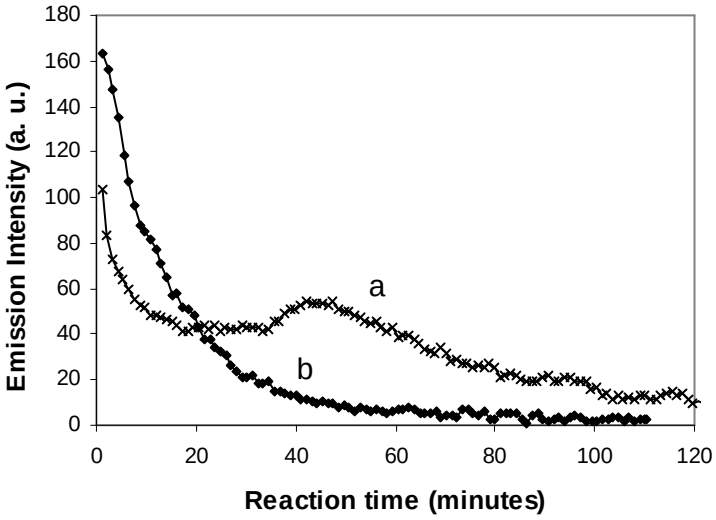

Figure 8.3 I_t curves of TDE CL in AOT/cyclohexane RMS: a. [AOT] = 0.192 mM (< CMC); b. [AOT] = 3.848 mM (>CMC).

The influence of TMU for the I_t curve of TDE CL was studied when the concentration of AOT in the system was adjusted at 3.75 ([AOT]> CMC) [4,66], 0.625 ([AOT]< CMC) and 0 mM respectively, see **Figure 8.4**. In this study, the concentration of additional TMU was fixed at 0.42 mM. Because of quenching phenomenon, the TDE CL gave low emission intensity and shorter life time as AOT was free in the system. Both the emission intensity and life time were enhanced after AOT in moderate amount was added into the solution. This result agrees with the hypothesis shown in **Figure 8.2**. The presence of reversed micellar phase extracts out quenching species from the non-polar bulk phase. This result also reveals pre-micellar phenomena. Although the concentration of AOT was lower than its CMC, a few micelles were present in the solution. Some TMU, subsequently, was enclosed by reversed micelles and higher emission intensity and longer life time was obtained from TDE CL since the collision between excited TDE and quenching species was diminished. This is seen for the I_t curve with [AOT]=0.625 mM in **Figure 8.4**. The effect of pre-micellar phenomenon is further discussed in section 8.3.5.

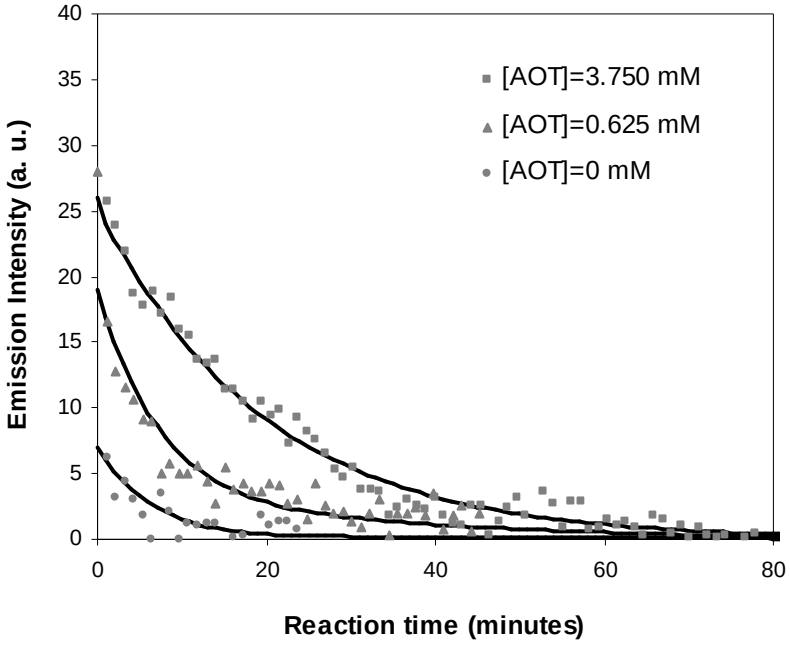

Figure 8.4 I_t curves of TDE CL in AOT/cyclohexane/TMU RMS. The concentration of TMU was fixed at 0.42mM for each curve. The concentration of AOT was adjusted to [AOT]=3.750 mM (> CMC), [AOT]=0.625 mM (< CMC) and [AOT]=0 mM.

8.3.3 Model for TDE CL in a RMS

To understand how the RMS affects the emission intensity of TDE CL, a simple model was constructed to represent the major steps of light emission, while considering the impact of quenchers. This model considers the reaction of TDE and oxygen to produce light and quenching species. To develop this model, we first needed to relate emission intensity with the concentrations of TDE and oxygen. Because the system is continuously purged with air, it can be assumed that the concentration of oxygen is constant with time, and can be lumped into the rate constant. We further assumed that the emission intensity when the concentration of surfactant was high was related only to the concentration of TDE. This essentially assumes that the quenching species are immediately removed from solution, and don't impact the emission intensity. With these assumptions, we can determine the functional relationship between emission intensity and TDE concentration. **Figure 8.5** plots both emission intensity (I) and $\ln(I_0/I)$ vs. reaction time (t). This plot gives a linear relationship, with an R^2 value of 0.99 for the

linear fit of the experimental data, $\ln(I_0/I)$. This indicates that the reaction was first order for TDE concentration and the relationship between emission intensity and TDE concentration could be represented by **Equation 8- 2**.

$$\ln(\frac{[TDE]_0}{[TDE]}) = \ln(\frac{I_0}{I}) = kt \qquad (8\text{- }2)$$

where: $[TDE]_0$ and I_0 are the initial TDE concentration and emission intensity, k is a rate constant for the first-order reaction, and t is reaction time.

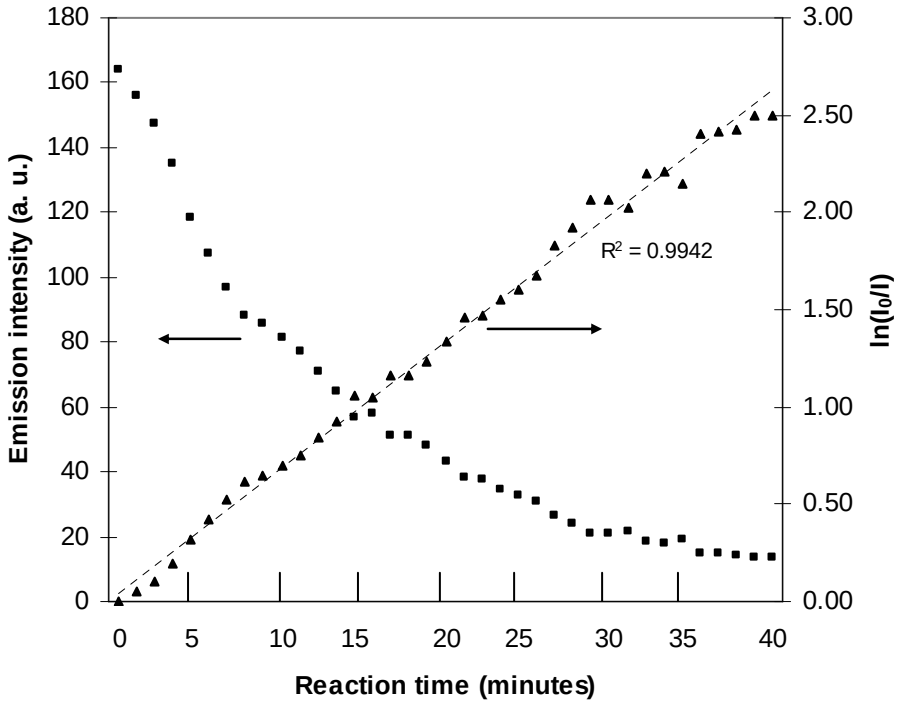

Figure 8.5 Variation of emission intensity of TDE CL in an AOT/cyclohexane reversed microemulsion when [AOT]=3.848 mM (>CMC). The straight line is the result when the curve of emission intensity is fitted by $\ln(I/I_0)$.

The next important consideration in the model is the treatment of quenching species. Quenching species are produced once TDMD is decomposed (as depicted in **Figure 1.1**). It is assumed that two quenching species were formed due to symmetric decomposition of TDMD, so that reaction of one TDE molecule yields two quenching species. Quenching species can, then, be transferred out of bulk solution into a second phase. This second phase could either be a second liquid phase made up of polar products, or could be a micellar phase, depending on how

much surfactant is present. The differential equations giving the concentration of TDE and quenchers over reaction time can, therefore, be written as:

$$\frac{dC_{TDE}}{dt} = -k_1 C_{TDE} \qquad (8\text{- }3)$$

$$\frac{dC_q}{dt} = 2k_1 C_{TDE} - k_{mt} A C_q \qquad (8\text{- }4)$$

where: C_{TDE} and C_q are the concentration of TDE and suspending quenching species in the bulk phase and k_{mt} is the mass transfer coefficient of the quenching species from the bulk phase to the second polar or micellar phase, and A is the area of the interface between the two phases per unit volume of solution.

With the presence of quenching species in the bulk phase, the excited TDE molecules can be de-excited by the collision with quenching species. Therefore, the emission intensity is a function of the concentrations of TDE and quenching species. A second-order reaction is assumed for the quenching reaction. The following equations model TDE concentration, quencher concentration and light emission:

$$C_{TDE} = C_{TDE_0} e^{-k_1 t} \qquad (8\text{- }5)$$

$$C_q = \frac{2k_1 C_{TDE_0}}{k_{mt} - k_1}[\exp(-k_1 t) - \exp(-k_{mt} A t)] \qquad (8\text{- }6)$$

$$I = k_e (k_1 C_{TDE} - k_3 C_{TDE} C_q) \qquad (8\text{- }7)$$

where: k_e is the proportionality constant between the rate of TDE reaction and the photon creation, k_1 and k_3 represent the rate constants for TDE oxidation reaction and bimolecular collisions, respectively, and C_{TDE0} is the initial concentration of TDE in bulk phase.

During the reaction, the collisional quenching and the mass transfer area, A, of quenching species vary with reaction time. Mass transfer area is associated with the interface between the bulk phase and the second polar phase, which can either be a phase made up entirely of quenching species or can be a micellar phase. This area changes with the accumulation of quenching species over time and with the concentration and size of reversed micelles. To adequately model the TDE chemiluminescence process, accurate estimates for the different rate

and proportionality constants must be obtained. In this simple model, we only considered the effect of mass transfer coefficient times area (k_{mt}·A) for the deformation of the I_t curve and assumed that the variation of k_{mt}·A is mainly related to the amount of reversed micelles.

The parameters in the model were adjusted to fit the I_t curve of TDE CL in AOT/cyclohexane with AOT at 3.85 mM (> CMC). This fit is shown in **Figure 8.6** as the mass transfer coefficient times area (k_{mt}·A) is set at 5. Increasing k_{mt}·A from 5 causes only a slight change in the emission intensity of the fitting curve but not in the curve shape since the mass transfer rate of quenching species is higher than the formation rate of quenching species. This result agrees with our assumption that most quenching species are isolated by the surfactant and the effect of quenching species for the emission intensity is minimized when the concentration of surfactant is greater than its CMC. Decreasing the value of k_{mt}·A from 5, the fitting curve shifts to lower emission intensity and, further, a local maxima appears, as seen in **Figure 8.6**. Therefore, it can be assumed that k_{mt}·$A \geq 5$ when the concentration of surfactant is higher or equals to its CMC. The fitting curves with k_{mt}·A= 0.3 and k_{mt}·A= 0.15 represent respectively, that the concentration of surfactant is inside the pre-micellar and out of pre-micellar region.

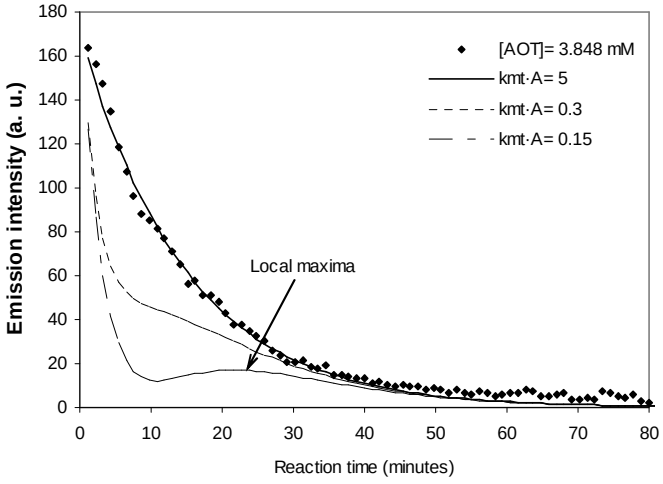

Figure 8.6 Simulated results showing the influence of mass transfer of the quenching species for the emission intensity of TDE CL. The solid dots represent the experiment data collected from the emission intensity of TDE CL in an AOT/cyclohexane reversed microemulsion when [AOT]=3.848 mM (>CMC). The lines from tope to bottom are the simulated results when k_{mt}·A was set to 5, 0.3 and 0.15 respectively.

The presence of a local maxima in **Figure 8.3** is due to the balance between the rate that TDE is oxidized to produce light and the rate at which quenching occurs. Initially, the light emission decreases dramatically both because TDE is consumed and also because the quencher concentration increases, thereby increasing the quenching rate. However, as the quencher concentration increases, the rate of transfer of the quenching species out of the bulk phase is increased. The magnitude of $k_{mt} \cdot A$ drives whether a maximum is seen, and where that maximum is.

Reversed micelles provide a similar function to the microdroplet of quenching species in the bulk phase, but the influence is more significant in the beginning of the reaction. Reversed micelles enhance the mass transfer of quenching species out of bulk phase since the mass transfer area is increased dramatically with the increase of the amount of reversed micelle in the bulk phase. The polar quenching species likely act as glue agents to assemble surfactant monomers. At high $k_{mt} \cdot A$ value, the local maximum is no longer seen because most quenching species are captured by reversed micelles right after the quenching species are produced from the oxidation reaction of TDE. Increased emission intensity is noted at early times due to the capture of quenching species by reversed micelles. Because of the removal of quenching species out of the bulk phase, the decay rate of emission intensity with reaction time is closer to an exponential trend. Under this situation, the decay of emission intensity mainly is related to the concentration of TDE.

8.3.4 Determination of CMC from TDE CL

As depicted in **Figure 8.5**, the oxidation reaction of TDE is first-order in TDE concentration. This assumption agrees with previous studies. [47,70] In this study, a numerical method based on this assumption has been developed to analyze the CMC from TDE CL data. It is proposed that the emission intensity is proportional to the residual TDE in bulk phase (as given in **Equation 8- 2**) when quenching species are isolated by reversed micelles and are free in bulk phase. This situation happens when the concentration of surfactant is higher than its CMC. Therefore, the plot of $-\ln(I_0/I(t))$ vs. reaction time (t) is a linear relationship and the slope equals

the reaction rate constant (*k*) (**Figure 8.5**). However, when the amount of reversed micelle is too low to capture most free quenching species in bulk phase the relationship between $\ln(I_0/I(t))$ and reaction time (t) is not equal to the rate constant. In this situation, the decay of emission intensity not only is influenced by the concentration of TDE in bulk phase (C_{TDE}) but also is associated with the concentration of quenching species in bulk phase (C_q), as seen in **Equation 8- 7**. Subsequently, the value of the apparent rate constant changes with C_q. In this method, and apparent rate constant, *k*, is derived from the fitting curve of **Equation 8- 8** for the emission data of TDE CL. If a local maximum is noted, only the data before that maximum are fit.

$$\ln(\frac{I_0}{I(t)}) = k \cdot t \qquad (8\text{- }8)$$

k is the slope of the fitting curve and represents the decaying rate of emission intensity. When quenching species are present in the bulk phase, they cause the radiationless consumption of excited TDE. This radiationless consumption not only reduces the emission intensity, but also leads to a variation in the value of *k*. The evaluation of the CMC of a reversed microemulsion in this study is based on the variation of *k*.

8.3.4.1 The CMC of AOT/Cyclohexane Reversed Microemulsion

For the reversed microemulsion system consisting of AOT and cyclohexane, the emission intensities over reaction time were collected by fiber optic spectrometer. **Figure 8.7** shows the results of these experiments when the concentration of AOT, [AOT], was changed from 269.36mM to 1.154 mM (**Figure 8.7A**) and from 1.154mM to 0.192 mM (**Figure 8.7B**). When [AOT] is in the high concentration region (**Figure 8.7A**), the curve shifts up to higher emission intensity with decreasing [AOT]. Oppositely, the curve shifts down to lower emission intensity with decreasing [AOT] in bulk phase when [AOT] is in the range 1.154-0.192 mM (**Figure 8.7B**). A local maximum is noted as [AOT] is as low as 0.770 mM (point **a**) and is shifted to longer reaction time as the [AOT] is further decreased from 0.770 to 0.384 mM and 0.192 mM (point **b**).

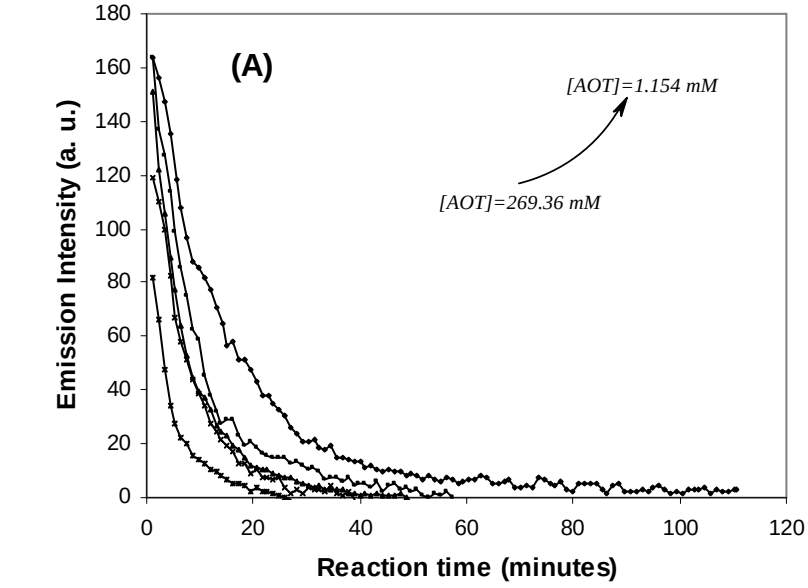

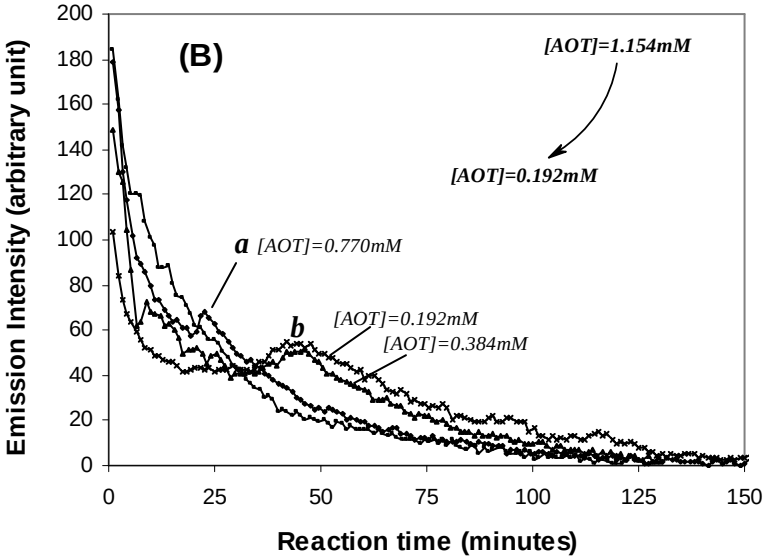

Figure 8.7 The I_t curves of AOT/cyclohexane RMS when (A). [AOT]>CMC; (B). [AOT] is close to the CMC. Point a and b indicate the aggregation of the quenchers in oil bulk phase (cyclohexane) in the region of the pre-micellar concentration (PMC) of AOT (point a) and out of the region of the PMC of AOT (point b) respectively.

Each curve shown in **Figure 8.7A** and **Figure 8.7B** was fit by **Equation 8- 8** to give *k* for each corresponding [AOT]. The different *k* were plotted against the corresponding [AOT] for

determination of the CMC (shown in **Figure 8.8**). As seen in **Figure 8.8**, *k* undergoes two abrupt changes with the increase of [AOT]. The first turning point occurs around [AOT] = 1.80 mM while the second turning point appears around [AOT] = 76.96mM. In high [AOT] region ([AOT] = 230.88-76.96 mM), the value of *k* slightly decreases with increasing [AOT]. Oppositely, the vale of *k* increases with increasing [AOT] when [AOT] is in the region 0-76.96 mM. The increase in the value of *k* is much more significant in the lower [AOT] region, [AOT] = 0-1.80 mM.

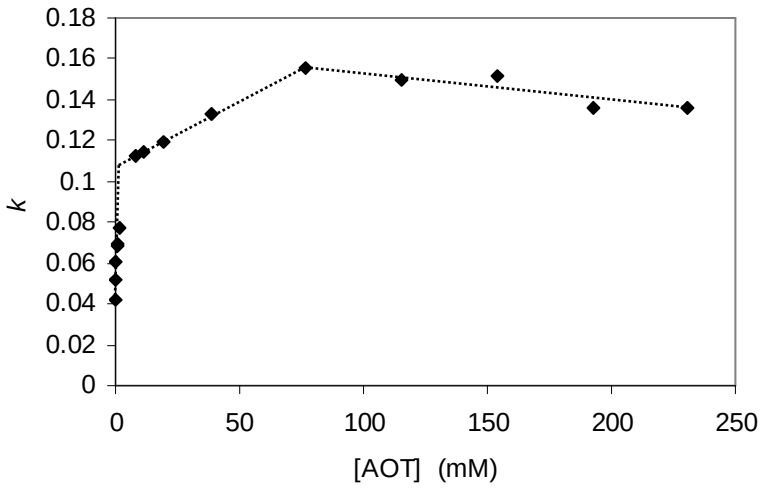

Figure 8.8 The variation of *k* with [AOT] in AOT/cyclohexane reversed microemulsion system.

Figure 8.7B shows that the increase of [AOT] in the lower [AOT] region, 0-1.80 mM, leads to a shift up in the emission intensity of the I_t curve in the first 31 minutes of the reaction. It had been noted previously that the emission intensity of TDE CL is related to the concentration of quenching species. Therefore, it can be assumed that the increase in the emission intensity is due to the removal of quenching species by enclosure in reversed micelles. This assumption agrees with the result showed in **Figure 8.8**. A dramatic increase in the value of *k* is found when [AOT] increases from 0 to 1.8 mM. Because the concentration of quenching species is associated with the enclosing capacity of reversed micelle under low [AOT], [AOT]<CMC, the dramatic increase in the *k* value indicates the increase in the decay rate of emission intensity with reaction time and indicates that the influence of quenching species is reduced.

The increasing magnitude of *k* becomes much slighter when [AOT] is further increased from 1.80 mM to 76.96 mM. (as seen in **Figure 8.8**) These results agree with the modeling results. After the CMC (*kmt·A*= 5), the increase in the value of *kmt·A* causes only a very slight change in the emission intensity of modeled I_t curve. This suggests that collisions between excited TDE and quenching species were minimized when the concentration of surfactant is higher than its CMC. The slight increase in the *k* value may be due to the increase in the trapping rate of reversed micelle for quenching species with the increase in the concentration of reversed micelle. The frequency of radiationless collision between excited TDE and the quenching species is decreased if the trapping rate of reversed micelle for the quenching species is increased. In this study, the CMC is determined by the abrupt change in the *k* value. Therefore, the CMC of AOT/cyclohexane reversed microemulsion is determined to be 1.80 mM.

Figure 8.8 shows that *k* decreases with the increase of [AOT] in very high [AOT] region, [AOT]=76.96-230.88 mM. This suggests that the reversed micelles become the major quenching species when their concentration is large. The decrease in the *k* value is assumed to be due to the collision quenching between excited TDE and reversed micelles and the quenching phenomenon is dominated by the concentration of reversed micelle. The emission intensity is no longer affected by the major products, TMU and TMO, of the TDE oxidation reaction.

8.3.4.2 CMC of AOT/n-decane RMS

Following the procedure described previously, the plot of *k* against [AOT] in AOT/n-decane RMS is shown in **Figure 8.9**. Again, a dramatic increase in the value of *k* with increasing [AOT] is found when [AOT]<1.70 mM. After [AOT]>1.70 mM, the trend of *k* becomes more flat. Thus, the CMC of AOT/n-decane RMS is determined at 1.70 mM.

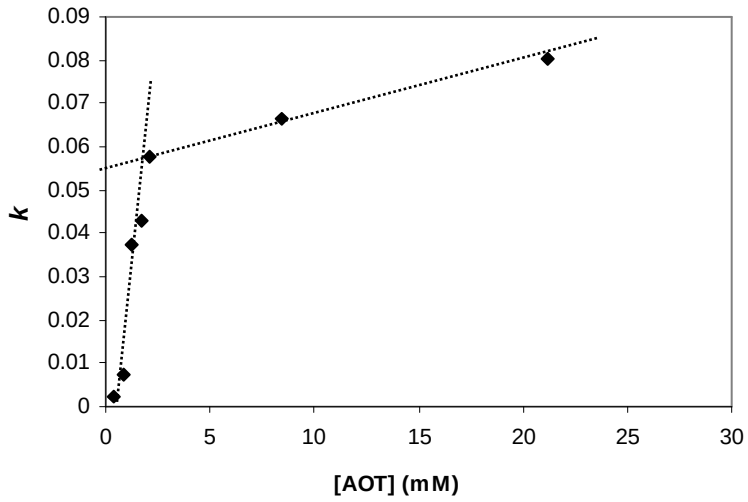

Figure 8.9 The variation of *k* with AOT concentration in the AOT/n-decane reversed microemulsion system.

8.3.4.3 CMC of AOT/Short Carbon Chain Alkane RMS

The I_t curves of TDE CL in AOT/n-dodecane, AOT/iso-octane, AOT/n-octane and AOT/n-heptane reversed microemulsions also had been collected by fiber optic spectrometer. These data were analyzed by variation of k with [AOT] to give the CMC value for each reversed microemulsion system. From these analyses, the CMC of AOT/n-dodecane, AOT/iso-octane, AOT/n-octane and AOT/n-heptane RMS were determined to be at 2.10, 0.79, 0.83 and 0.61mM respectively. Both the CMC data given from the measurement of TDE CL and the CMC data reported in the literature are listed in **Table 8-1**. **Table 8-1** shows that the CMC values vary with the detecting methods. The difference is up to 85% in some cases. The CMC values determined using our method are similar to those detected using other methods.

It is well known that the CMC [32], the solubilization of the water pool [9], the enthalpy of micellization [62] and solvent penetration in the tail region of micelle [63] are influenced by the alkane chain length of the bulk solvent. **Table 8-1** shows that the CMCs of AOT/alkanes RMS vary with the carbon chain length of the solvent: the longer the chain length, the lower the CMC of the AOT/alkane RMS. The polarity of the solvent doesn't appear to make much of a

difference in the CMC. For example, even though iso-octane is more polar than n-octane, the CMC of AOT/n-octane RMS (0.83mM) is close to the CMC of AOT/iso-octane RMS (0.79mM).

Bulk media	CMC determined by TDE CL (mM)	Previously reported CMCs		
		Method	CMC (mM)	Ref.
n-dodecane	2.10	-	-	-
n-decane	1.70	X-ray scattering	0.73	[64]
		Small angle neutron scattering	0.24-1.60	[65]
n-octane	0.83	Calorimeter	1.0	[32]
iso-octane	0.79	Fluorescent probe	1.7	[26]
		Positron annihilation	0.6-0.9	[28]
		Spectrophotometer	1.1	[32]
		Calorimeter	0.84	[32]
		Microcalorimeter 30^{o}C	0.85	[62]
n-heptane	0.61	Spectrophotometer	1.0	[32]
		Calorimeter	1.1	[32]
cyclohexane	1.80	UV spectrum 25^{o}C	0.95-1.1	[4]
		Light scattering	1.35	[66]
		Dye adsorption (iodine)	0.2	[31]

Table 8-1 The CMC reported in early studies and the CMC given from the detection of TDE CL in the reversed microemulsion systems consisting of AOT and non-polar hydrocarbon solvents. (the CMC shown in this table is measured by TDE CL at 25^{o}C)

8.3.4.4 CMC of NaDDBs/Cyclohexane RMS

NaDDBs (sodium dodecylbenzene sulfonate) is an anionic surfactant often utilized to stabilize reversed microemulsion systems. Although NaDDBs has a similar molecular structure as SDS (sodium dodecyl sulfate), we found that NaDDBs can be dissolved into most non-polar solvents and appears to have a higher solubility than SDS. A stable colloid solution forms as NaDDBs is dissolved into a non-polar solvents. The I_t curves of TDE CL in NaDDBs/cyclohexane system also were collected by fiber optic spectrometer when the concentration of NaDDBs was varied. The local maximum appears when the concentration of

NaDDBs is decreased to 0.980mM. An increase in emission intensity was found when the concentration of NaDDBs is increased from 1.226mM to 2.451mM. By the analysis of the *k* values, the CMC of NaDDBs/cyclohexane RMS was found to be 1.90 mM.

8.3.5 Pre-Micellar Concentration Region (RMC region)

RMS are known to have a pre-micellar region prior to the CMC. Manoj *et al.* identified the existence of a pre-micellar concentration region in 1996. [26] In the PMC region, although the concentration of surfactant is lower than the CMC, the surfactant monomers tend to aggregate together. Because of this, the properties of RMS do not change as sharply as normal microemulsions as the CMC is approached.

Figure 8.10 depicts the distribution of AOT monomers when the concentration of AOT approaches the CMC. In the pre-micellar region (shown as b in **Figure 8.10**), both the density of AOT reverse micelles and the solubility of the system for polar species are promoted with increase AOT concentration. This was seen in **Figure 8.8** and **Figure 8.9** as a sharp increase of *k* with increasing AOT concentration.

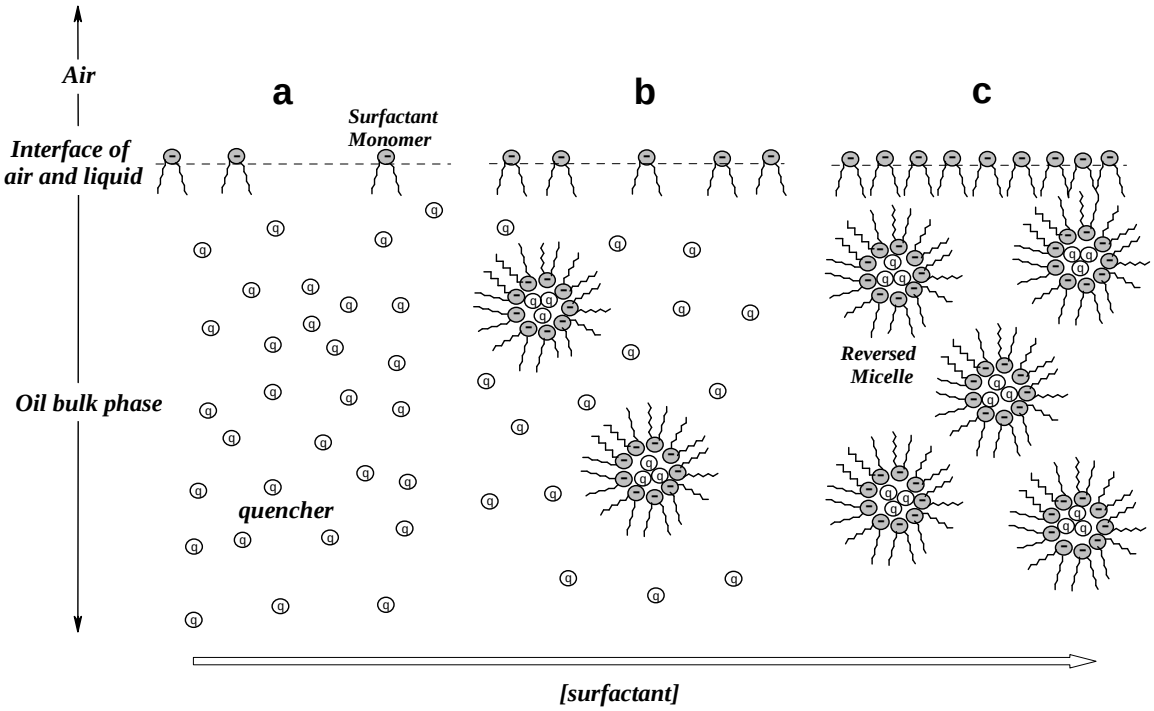

Figure 8.10 Depiction of the pre-micellar concentration (PMC) of AOT (amphipathic molecule with two feet). The concentration of AOT in the oil bulk phase increases from left (a) to right (c). (a) [AOT] is lower than the CMC and out of the PMC region; (b) [AOT] is in PMC region; (c) [AOT] is higher than the CMC.

The location of the local maximum that is observed in **Figure 8.7B** is thought to be related to existence of a pre-micellar region. As seen in **Figure 8.7B**, the local maximum appears for [AOT] between 0.19 and 0.770 mM. As described previously, this local maximum appears because the quenching species begins to be removed from the bulk solution rapidly enough to temporarily increase the emission intensity. Between the concentration of 0.385 and 1.15 mM, the location of the local maximum is shifted to shorter times as the surfactant concentration increases (from point **b** to point **a**). At lower surfactant concentrations, fewer micelles are present, so the rate that the quenchers are removed from solution is lower. The two curves for 0.385 and 0.192 mM are nearly identical in the location of the local maxima. It is thought that this is because 0.385 mM is near the lower limit of the pre-micellar region. Below that concentration, the surfactant molecules are not arranged as micelles, so their concentration

has no effect on TDE CL and the accumulation rate of quenching species in the bulk phase tends to a constant.

8.3.6 Viscosity Determination in Micro-systems

Förster and Hoffman [67] indicated the mathematical relationship between solvent viscosity (υ) and the quantum yield of fluorescence (Φ) as:

$$\log \Phi = \chi \cdot \log \upsilon + C \qquad (8\text{- }9)$$

Because the emission intensity is proportional to the quantum yield, the governing equation could be reworked from **Equation 8- 9** to give equation [68] **Equation 8- 10**:

$$\upsilon = (\xi \cdot I)^n \qquad (8\text{- }10)$$

where C, ξ and n are constants. χ is the slope given from plotting logΦ vs. logυ.

Experiments were run to determine whether the intensity of TDE CL would be fit with **Equation 8- 10**. If so, TDE CL may provide a means to measure solvent viscosity. In this study, the [AOT] was set in its PMC region (0.43 mM). **Figure 8.11** shows the relationship between viscosity and emission intensity. As seen in **Figure 8.11**, there is a linear relationship between *ln(υ)* and *ln(I)*, as predicted by **Equation 8- 10**. The constants ξ and n were found from the linear fit of the data and were calculated to be 0.02627 and 1.70. From this analysis, it emerges that the viscosity can be predicted using TDE CL by using **Equation 8- 11**.

$$\upsilon(cSt) = (0.02627 \cdot I)^{1.70} \qquad (8\text{- }11)$$

where υ is the viscosity of RMS in the unit of *cSt* while I is the emission intensity of TDE CL in the RMS in a arbitrary unit.

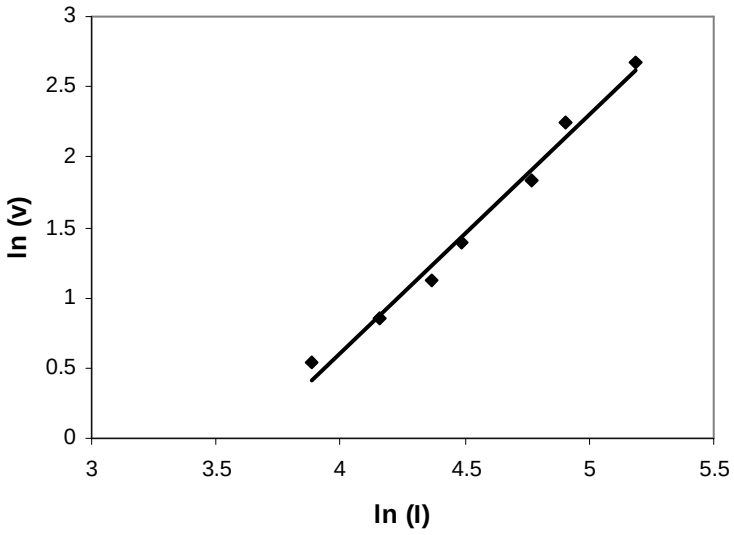

Figure 8.11 The relationship between emission intensity emitted from TDE CL and solvent viscosity.

This equation is only applicable to the specific conditions used in this study (type of surfactant, TDE concentration). However, these results do suggest that TDE CL could be used to estimate the viscosity and overcome the disadvantage of mechanical fluid viscosity measurement methods, such as the limitation in the sample volume and the type of fluid (Newtonian or non-Newtonian fluid).

8.3.7 Limitations of Using TDE CL in Determination of the CMC of RMS

TDE CL fails in detecting the CMC and viscosity of RMS when the surfactant used to stabilize RMS contains hydroxyl group or the organic solvent in continuous phase is an aromatic compound or alcohol. This is because hydroxyl groups can act as catalysts to enhance the reaction rate of TDE CL while aromatic compounds disrupt the transfer of electronically excited energy and leads to the extinction of TDE CL. Both the reaction rate enhancement and the disruption of electronically excited energy will cause inaccuracies in the identifications of the CMC and viscosity of RMS when TDE CL is employed in the characterization of RMS.

8.3.7.1 Surfactant with Hydroxyl Group

Triton X-100 can demonstrate the influence of a surfactant with hydroxyl group on TDE CL. The molecular structure of Triton X-100 is similar to that of NaDDBs. The hydrophilic terminal of X-100 contains a hydroxyl group while the hydrophilic terminal of NaDDBs is a sodium sulfate group. Based on the procedure described previous, the CMC of X-100/cyclohexane RMS is identified around 60mM through the determination of *k* values. Obviously 60mM deviates far from the published values, 0.22-0.24mM. [69] The over-estimation of the CMC value detected by TDE CL also occurred when a co-surfactant, alcohols with short carbon chains, was added into the system. These over-estimations in the CMC are due to the disturbance for TDE CL caused by the hydroxyl group of X-100 since it had been identified that the compound containing a hydroxyl group, such as water and alcohols, acts as catalyst for TDE CL. [47,70,71,72]

8.3.7.2 Solvent Effects

Aromatic compounds usually are the backbone of fluorescent dyes due to their conjugated and rigid molecular structure. For instance, benzene has six delocalized π electrons over all six C-C bonds and an unsaturated electron structure. Thus, benzene acts as an electron pool to donate or accept electrons when an electron donor or acceptor substituent is bonded to benzene. The enlargement of conjugated system (addition of an adjacent benzene ring or bonding an extra substituent) will lead to lower T (triple state) to S_0 (ground single state) and S_1^* (first excited single state) to S_0 transitions and increase the quantum yield. For instance, the quantum yield increases from benzene, 0.007, to anthracene, 0.36, in cyclohexane solution. [73]

When benzene is used as the non-polar solvent in the bulk phase of RMS, the emission of TDE CL becomes dim. The extinction of the emission of TDE CL is due to the termination of excited energy transfer from TDMD to TDE while benzene is the bulk solvent. Because of the big energy gap between the S_0 state and S_1* state of benzene, both the adsorption and emission maxima of benzene are in the UV region. However, the adsorption maximum , λ_{ex}=436nm, and the emission maximum, λ_{em}=494nm, of TDE are in visible region. It is hypothesized that the

energy released from the decomposition of TDMD is less than the excited energy for benzene. The excited energy transfer from TDMD to benzene, thus, leads to the extinction of TDE CL.

8.4 Conclusion

The results reported in this chapter show that TDE CL is a powerful technique in characterizing the properties of RMS, including the CMC, pre-micelle concentration (PMC) and viscosity. TDE CL allows the CMC and PMC to be probed due to the mass transfer of quenching species from the TDE bulk solution to micelles. This process gets more efficient when micelles form, so TDE CL emission intensity is markedly different when there are micelles. The CMC of two different RMS systems with various solvents were estimated using TDE CL, and the values were similar to reported literature values. It was also found that the intensity of TDE CL varied with the viscosity of the solvent, providing a potential new way to find viscosity for RMS.

8.5 References

1. Elworthy, P. H.; Florence, A. T. and Macfarlane, C. B. *Solubilization by suface active abents and its applications in Chemistry and the Biological Sciences*; Chapman & Hall: London, **1968**.
2. Mukerjee, P. and Mysels, K. J. *Critical Micelle Concentrations of Aqueous Surfactant Systems*; NSRDS-NBS 36. Superintendent of Documents, U.S. Gov. Printing Office: Washington, D.C., **1971**.
3. Shinoda, K.; Nakagawa, T.; Tamamushi, B. and Isemura, T. *Colloidal Surfactants: Some Physio-Chemical Properties*; Academic Press: New York, **1963**.
4. Fendler, J. H. and Fendler, E. J. *Catalysis in Micellar and Macromolecular Systems*; Academic Press: New York, **1975**.
5. Warisnoicharoen, W.; Lansley, A. B. and Lawrence, M. J. *AAPS Pharmsci*, **2000,** article 12, 2(2).
6. Jaye, A. A.; Hunt, N. T. and Meech, S. R. *Langmuir*, **2005,** 21, 1238.
7. Gunaseelan, K.; Umlong, I. M.; Mukhim, T. and Ismail, K. *Langmuir*, **2003,** 19, 7276.
8. Eriksson, S.; Nylén, U.; Rojas, S. and Boutonnet, M. *Appl. Catal. A: Gen.*, **2004,** 265, 207.
9. Chew, C. H. and Gan, L. M. *J. Disp. Sci. Technol.*, **1990,** 11, 593.
10. Paul, B. K. and Moulik, S. P. *Curr. Sci.*, **2001,** 80, 990.
11. Hernández-Barajas, J. and Hunkeler, D., *Polymer*, **1997,** 38, 5623.
12. Candau, F.; Leong, Y. S.; Pouyet, F. and Candau, S. *J. Coll. Int. Sci.*, **1984,** 101, 167.
13. Clarke, M. J.; Harrison, K. L.; Johnston, K. P. and Howdle, S. M. *J. Am. Chem. Soc.*, **1997,** 119, 6399.

14. Ohde, H.; Ohde, M.; Bailey, F.; Kim, H. and Wai, C. M. *Nano Lett.*, **2002,** 2, 721.
15. Liu, J.; Ikushima, Y. and Shervani, Z. *Curr. Opin. Solid State Mat. Sci.*, **2003,** 7, 255.
16. Holmes, J. D.; Bhargava, P. A.; Korgel, B. A.; Johnston, K. P. *Langmuir*, **1999,** 15, 6613.
17. Ohde, H.; Hunt, F. and Wai, C. M. *Chem. Mater.*, **2001,** 13, 4130.
18. Lee, C. T.; Psathas, P. A.; Johnston, K. P. *Langmuir* **1999,** 15, 6781.
19. Jacobson, F. B.; Lee, C. T. and Johnston, K. P. *J. Org. Chem.*, **1999,** 64, 1201.
20. Domínguez, A.; Fernández, A.; González, N.; Iglesias, E. and Montenegro, L. *J. Chem. Edu.*, **1997,** 74, 1227.
21. Fendler, J. H. *Acc. Chem. Res.*, **1976,** 9, 153.
22. Mukerjee, P. *Adv. Coll. Int. Sci.*, **1967,** 1, 241.
23. Jayakumar, R.; Jeevan, R. G. and Mandal, A. B. *J. Chem. Soc. Faraday Trans.*, **1994,** 90, 2725.
24. da Rocha, S. R. P. and Johnston, K. P. *Langmuir*, **2000,** 16, 3690.
25. Majhi, P. R.; Mukherjee, K. and Moulik, S. P. *Langmuir*, **1997,** 13, 3284.
26. Manoj, K. M.; Jayakumar, R. and Rakshit, S. K. *Langmuir*, **1996,** 12, 4068.
27. Bharatwaj, B. and Rocha, S. R. P. *Briazilian J. Chem. Eng.*, **2006,** 23, 183.
28. Jean, Y.-C. and Ache, H. J. *J. Am. Chem. Soc.*, **1978,** 100:20, 6320.
29. Kotlarchyk, M. and Huang, J. S. *J. Phys. Chem.*, **1985,** 89, 4382.
30. Ueda, M. and Schelly, Z. A. *Langmuir*, **1988,** 4, 653.
31. Muto, S. and Meguro, K. *Bull. Chem. Soc. Jap.*, **1973,** 46, 1316.
32. Mukherjee, K. and Moulik, S. P. *Langmuir*, **1993,** 9, 1727.
33. Herrmann, U. and Schelly, Z. A. *J. Am. Chem. Soc.*, **1979,** 101, 2665.
34. Brennecke, J. F. and Eckert, C. A. *ACS Symp. Ser.*, **1989,** 406, 14.
35. Tomasko, D. L.; Knutson, B. L.; Coppom, J. M.; Windsor, W.; West, B. and Eckert, C. A. *ACS Symp. Ser.*, **1993,** 514, 220.
36. Alvarez, J.; Lissi, E. A. and Encinas, M. V. *Langmuir*, **1996,** 12, 1738.
37. da Miguel, M. G. *Adv. Coll. Int. Sci.*, **2001,** 89, 1.
38. Fendler, J. H.; Fendler, E. J.; Medary, R. T. and El Seoud, O. A. *J. Chem. Soc., Faraday Trans.*, **1973,** 2, 69.
39. Fendler, E. J.; Constien, V. G. and Fendler, J. H. *J. Phys. Chem.*, **1975,** 79, 917.
40. Heatley, F. *J. Chem. Soc., Faraday Trans. 1*, **1987,** 83, 517.
41. Behera G. B., Mishra, B. K., Behera, P. K., and Panda, M., *Adv. Coll. Int. Sci.*, **1999**, 82, 1.
42. Silber, J. J., Biasutti, A., Abuin, E., and Lissi, E., *Adv. Coll. Int. Sci.*, **1999**, 82, 189.
43. Adam, W. and Cilento, G. *Chemical and Biological Generation of Excited States*; Academic Press: New York, **1982**.
44. Gold, V. and Bethell, D. *Advance in Physical Organic Chemistry V18*; Academic Press: New York, **1982**.
45. Gundermann, K.-D. and McCapra, F. *Chemiluminescence in Organic Chemistry*; Springer Verlag: New York, **1987**.
46. Fletcher, A. N. and Heller, C. A. *J. Phys. Chem.*, **1967,** 71, 1507.
47. Urry, W. H. and Sheeto, J. *Photo. and Photobio.*, **1965,** 4, 1067.

48. Winberg, H. E.; Carnahan, J. E. and Coffman, D. D. *J. Am. Chem. Soc.*, **1965,** 87, 2054.
49. Rewick, R. T.; Schumacher, M. L.; Shapiro, S. L.; Weber, T. B. and Cavalli-Sforza, M. *Anal. Chem.*, **1988,** 60, 2095.
50. Hammond, P. R. and Knipe, R. H. *J. Am. Chem. Soc.*, **1967,** 89, 6063.
51. Orf, H. W. and Dolphin, D. *Proc. Nat. Acad. Sci. USA*, **1974,** 71, 2646.
52. Berg, R. F. and Moldover, M. R. *J. Chem. Phys.*, **1987**, 87, 3687,.
53. Gómez-Díaz, D. Mejuto, J. C. and Navaza, J. M. *J. Chem. Eng. Data*, **2006,** 51, 409.
54. Shah, D. O.; Bagwe, R. P. and Parmar, B. S. *Mater. Res. Soc. Symp. Proc.*, **2002,** 704, 327.
55. Law, K. Y. *Chem. Phys. Lett.*, **1980,** 75, 545.
56. Haidekker, M. A. and Theodorakis, E. A. *Org. Biomol. Chem.*, **2007,** 5, 1669.
57. Haidekker, M. A.; Akers, W.; Lichlyter, Darcy; Brady, T. P. and Theodorakis, E. A. *Sensor Lett.*, **2005,** 3, 42.
58. Pruett, R. L.; Barr, J. T.; Rapp, K. E.; Bahner, C. T.; Gibson, J. D. and Lafferty, R. H. *J. Am. Chem. Soc.*, **1950,** 72, 3646.
59. Hori, M.; Kimura, K. and Tsubonura, H. *Spectrochimica Acta*, **1968**, 24A, 1397.
60. Winberg, W. E., *US. Paten 3,264,221*, **1960**.
61. Heller, C. A. and Fletcher, A. *J. Phys. Chem.*, **1965**, 69, 3313.
62. Majhi, P. R. and Moulik, S. P. *J. Phys. Chem. B*, **1999,** 103, 5977,.
63. García-Río, L.; Godoy, A. and Rodríguez-Dafonte, P. *Eur. J. Org. Chem.*, **2006,** 15, 3364.
64. Assih, T.; Larche, F. and Delord, P. *J. Coll. Int. Sci.*, **1982,** 89, 35.
65. Gorski, N. and Ostanevich, Y. M. *Coll. Polym. Sci.*, **1993,** 93, 256.
66. Kitahara, A.; Kobayashi, T. and Tachibana, T. *J. Phys. Chem.*, **1962,** 66, 363.
67. Förster, T. and Hoffmann, G. Z. *J. Phys. Chem.*, **1971,** 75, 63.
68. Akers, W. and Haidekker, M. A. *J. Biomech. Eng.*, **2004,** 126, 340.
69. Wang, H.; Zhou, W.; Ho, D. L.; Winey, K. I.; Fischer, J. E.; Glinka, C. J. and Hobbie, E. K. *Nano Lett.*, **2004,** 4, 1789.
70. Huang. C.-C.; Hohn, K. L. and Schlup, J. R. in *The Influence of Surface Hydroxyls on Catalyzed Tetrakis(dimethylamino)ethylene Chemiluminescence, J. Phys. Chem. C*, **2009**, 113 (25), 11050.
71. Fletcher, A. N. and Heller, C. A. *J. Catalysis*, **1966,** 6, 263.
72. Toby, S.; Astheimer, P. A. and Toby, F. S. *J. Photochem. Photobiol.* A: *Chem.*, **1992,** 67, 1.
73. Krasovitskii, B. M. and Bolotin, B. M. *Organic Luminescent Materials*; VCH: New York, **1988**.

CHAPTER 9 - Conclusions and Future Work

9.1 Conclusions

The potential to use TDE CL in characterizing the surface properties of metal oxides and identifying the critical micellar concentrations (CMC) of surfactants in reversed microemulsion systems has been studied. Both the surface properties of metal oxides and the formation of reversed micelle were determined through the trend of the emission intensity vs. reaction time (I_t) curve of TDE CL. The CMCs were evaluated by TDE CL in different non-polar solvents (alkanes, cyclohexane and mineral oil) with non-ionic and ionic surfactants. For surface characterization, several surface modifying methods, including steam-treatment, grafting agent and heat-treatment, were employed to regulate the distribution of surface hydroxyl. The influence of surface hydroxyls in different configurations on the emission intensity of TDE CL was studied.

The results elucidated that isolated hydroxyls speed up the oxidation reaction of TDE. Obvious enhancement in the emission intensity was found when the surface of metal oxide abounds in isolated hydroxyl groups. Metal oxide surfaces lose their catalytic ability for enhancing the emission intensity of TDE CL when most isolated hydroxyl groups were removed at high temperature.

The catalytic reactivity for the emission of TDE CL is associated with the local environment of the isolated hydroxyl groups on metal oxides. Treating γ- Al_2O_3 at high temperature, 900^oC, led to a transformation of the crystalline phase. It was found that the stretching frequencies of isolated hydroxyl shifts upward after phase transformation occurred. Subsequently, higher emission intensity was detected as TDE CL was catalyzed by the treated Al_2O_3. In contrast, a dramatic decrease in the emission intensity of TDE CL was observed as the isolated hydroxyl groups at higher frequencies were substituted by grafting agents. Moreover, treating the surface oxide surface by steam or acetic acid created more defects on the surface. More isolated hydroxyl groups with lower coordination are created after steam treatment, since the hydroxyl groups with lower coordination are isolated hydroxyls adsorbed on edge and corner

sites. The steam treated metal oxide was proven to have higher catalytic reactivity for TDE CL. Lower catalytic reactivity for the emission of TDE CL was found on acetic acid treated metal oxide since acetic acid also participates in the substitution reaction of the isolated hydroxyls with higher stretching frequencies.

The influence of quenching species formed during TDE oxidation was used to investigate reversed micelle systems. It was proposed in this study that the quenching magnitude is diminished after the formation of reversed micelle because the quenching species were extracted out from the bulk phase and isolated in the water pool of reversed micelles. Therefore, the decaying rate of emission intensity varied with the concentration of micelles in bulk phase. It was found that the decay rate increased linearly with increasing surfactant concentration, but there was a point where the slope of the trend changed dramatically. The concentration of surfactant at this transition point was determined as the CMC. All CMC values for different reversed microemulsion systems given by TDE CL characterization are close to the CMC values evaluated by spectrometric methods reported in prior studies. It was found that the CMC value decreases with decreasing carbon number of the alkane. Otherwise, it also was demonstrated that the emission intensity of TDE CL was proportional to the viscosity of the bulk phase. This feature enables TDE CL to be a molecular rotor for detecting the viscosity of reversed microemulsion systems.

In previous studies, tetrakis(dimethylamino)ethylene (TDE) was mostly used as a reducing agent in different reactions. For the determination of metal oxides' surface properties and the characterization of reversed microemulsion systems, a lot of techniques have been developed and employed in laboratories and industrials, but the potential of TDE Chemiluminescence (CL) as a tool for such characterizations is presented for the first time in this work. The method of TDE CL is different from other techniques applied in characterizing surface properties of metal oxides in that TDE CL analyzes surface chemistries via the catalytic reactivity of surface hydroxyl groups (which are the most abundant species adsorbed on metal oxide surfaces). This important feature enables the analysis to proceed at room temperature with no need for the extreme high temperatures required to remove surface adsorbents before other analysis techniques can be implemented. It is well known that metal oxide surface properties

change at high temperatures because of the migration of surface ions, so the ability to analyze the surfaces at room temperature is a significant advantage over other techniques.

The excited energy for TDE CL is supplied by the reaction intermediate, “tetrakis-dimethylamino-1,2-dioxetane” (TDMD). This allows TDE CL to be used to characterize reversed microemulsion systems without the need for irradiation by an excited laser beam. Even for systems which tolerate excitation by laser beam, TDE CL has the advantages of eliminating the light source device’s installation, warm-up, and the potential for interference from light scattering. As for the disadvantages of using TDE CL in characterizing the properties of reversed microemulsion systems and metal oxide surfaces, this work showed that unusual results were obtained when the probing target is a metal oxide with very low potential, or a reversed microemulsion system containing aromatic or alcoholic compounds.

9.2 Future work

Reversed microemulsions have been widely applied in synthesizing nano-catalysts or nano-metal particles. [1,2] In the synthesis procedure of nanoparticles, the exchange of ions contained inside reversed micelles via diffusion and re-dispersion processes is a crucial step. [3] Prior studies indicated that the change in temperature and composition of reversed microemulsion systems (RMS) facilitate the interaction between reversed micelles by mass transfer. [4,5,6,7,8,9] The aggregation and clustering of particles are ascribed to the increase in the transportation of the ions between reversed micelles. Temperature- or water-induced percolation regulate the diffusion and re-dispersion of the precursors of metal particles in reversed microemulsion systems. The occurrence of temperature- or water-induced percolation is due to changes in the packing parameter and the curvature of surfactant aggregation (described in section 2.3). In early studies, percolation phenomenon mostly were monitored by various spectroscopes, such as NMR. Research applying CL reactions in detecting the phenomenon of temperature- or water-percolation has not been reported. TDE CL is considered as a probe in detecting the occurrence of percolation at a specific temperature and W_0 (surfactant-to-water ratio) since the occurrence of percolation is hypothesized to increase the quenching collision between excited TDE and quenching species and subsequently cause a decrease in the emission of TDE CL.

Otherwise, it can be envisioned that TDE CL can be applied as a characterization method under some specific conditions because the method of TDE CL features the absence of an external excited source and no limitation in sample amount compared with present fluorescent method. For example, the irradiation by a laser beam is necessary for the probing of a fluorescer. However, bio-systems usually are sensitive to this irradiation.

9.3 References

1. Eriksson, S.; Nylén, U.; Rojas, S. and Boutonnet, M., *Applied Catalysis A: General*, **2004**, 265, 207.
2. Ohde, H.; Ohde, M.; Bailey, F.; Kim, H. and Wai, C. M., *Nano Lett.*, **2002**, 2, 721.
3. Hirai, T.; Sato, H. and Komasawa, I., *Ind. Eng. Chem. Res.*, **1994**, 33, 3262.
4. Ray, S.; Paul, S. and Moulik, S. P., *J. Colloid Interface Sci.*, **1996**, 183, 6.
5. García-Río, L.; Godoy, A. and Rodríguez-Dafonte, P., *Eur. J. Org. Chem.*, **2006**, 3364.
6. Hou, M. J.; Kim, M. and Shah, D. O., *J. Colloid Interface Sci.*, **1988**, 123, 398.
7. Jada, A.; Lang, J. and Zana, R., *J. Phys. Chem.*, **1989,** 93, 10-12.
8. Jada, A.; Lang, J. and Zana, R., *J. Phys. Chem.*, **1990**, 94, 381.
9. Alexandridis, P.; Holzwarth, J. F. and Hatton, T. A., *J. Phys. Chem.*, **1995**, 99, 8222. Toby, S. T., Astheimer, P. A., and Toby, F. S.